A&MS
Atomic and Mass Spectrometry

ISOTOPIC ANALYSIS OF MERCURY (Hg) *VIA* MULTI-COLLECTOR ICP-MASS SPECTROMETRY (MC-ICP-MS) – METHOD DEVELOPMENT & APPLICATIONS

Ana María Rua Ibarz 2018

Ana María Rua Ibarz

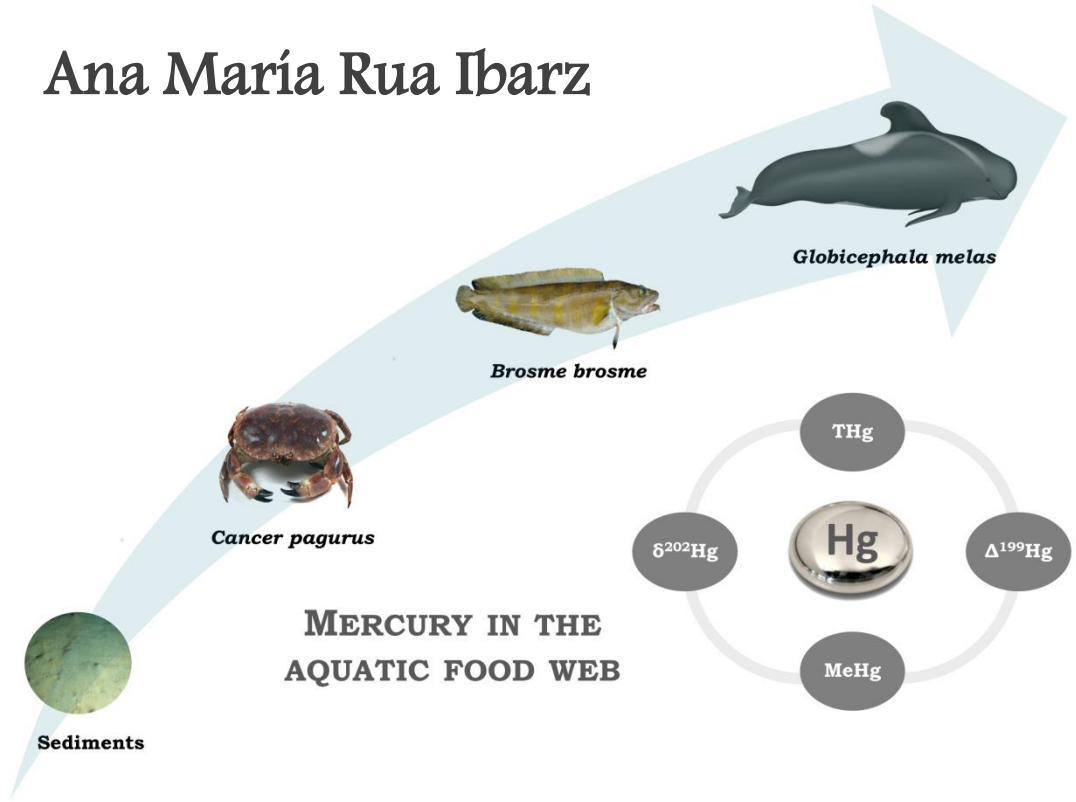

GHENT UNIVERSITY

FACULTY OF SCIENCES

SUPERVISORS:

Prof. Dr. Frank Vanhaecke

Prof. Dr. Martín Resano

FACULTY OF SCIENCES

DEPARTMENT OF CHEMISTRY
ATOMIC AND MASS SPECTROMETRY (A&MS)

Isotopic analysis of mercury (Hg) *via* multi-collector ICP-mass spectrometry (MC-ICP-MS) – Method development & Applications

.

Ana María Rua Ibarz
Student number: 01209886

Supervisors: Prof. Dr. Frank Vanhaecke and Prof. Dr. Martín Resano

A dissertation submitted to Ghent University in partial fulfilment of the requirements for the degree of Doctor of Science: Chemistry

Academic year: 2017 – 2018

GHENT UNIVERSITY

Para mi familia

y

Para Edu

Table of contents

List of abbreviations

AC	alternate current
AE	assimilation efficiency
A&MS	atomic and mass spectrometry unit
ANOVA	analysis of variance
ASGM	artisanal and small-scale gold mining
B	magnetic field
BCR CRM	Community Bureau of Reference Certified Reference Material
CAIS	common analyte internal standardization
CRC	collision-reaction-cell
CVG	cold vapor generation
CVG-MC-ICP-MS	cold vapor generation multi-collector inductively coupled plasma-mass spectrometry
CRM	certified reference material
CRMs	certified reference materials
ERM CE	certified reference materials European Reference Material European Commission
DC	direct current
DGHg	dissolved gaseous Hg
DMHg	dimethyl mercury
DOC	dissolved organic carbon

DOM	dissolved organic matter
E	electrical field
EFSA	European Food Safety Authority
EMRP	European Metrology Research Programme of EURAMET
EU	European Union
EURAMET	European Association of National Metrology Institutes
F	fraction of MeHg remaining after photodegradation
FAO	Food and Agriculture Organization
GC	gas chromatography
GC-ICP-MS	gas chromatography inductively coupled plasma-mass spectrometry
GEM	gaseous elemental mercury
GLS	gas liquid separator
GTA	gold trap amalgamation
HG	hydride generation
Hg-col	colloidal Hg
HgP	particulate mercury
HgR	reactive Hg dissolved in water
HR	high resolution
HR-SF-ICP-MS	high resolution sector field inductively coupled plasma-mass spectrometry
ICP	inductively coupled plasma-mass spectrometry

ICP-MS	inductively coupled plasma-mass spectrometry
IHg	inorganic mercury
IS	internal standard
JECFA	Joint FAO/WHO Expert Committee on Food Additives
Ld	Landegode
Lf	Lofoten
LR	low resolution
Lt	Lusterfjord(en)
MC-ICP-MS	multi-collector inductively coupled plasma-mass spectrometry
MDF	mass dependent fractionation
MeHg	methylmercury
MerA	mercuric reductasa
MerB	organomercuric lyasa
MIE	magnetic isotope effect
MIF	mass independent fractionation
MMHg	monomethyl mercury
MR	medium resolution
MT	metallothionein
MW	microwave
m/z	mass-to-charge ratio
NIFES	National Institute of Nutrition and Seafood Research

NIST	National Institute of Standards and Technology
NMIs	National Metrology Institutes
nmi	nautic miles
NOM	natural organic matter
Ny	Nordøyan
NRC-CNRC	National Research Council Canada - Conseil national de recherches Canada
NRCC NIMS-1	National Research Council Canada mercury isotopic reference material
NVE	nuclear volume effect
p	p-value, calculated probabiblity
PHg	particulate-bond Hg
PN	pneumatic nebulization
PN-MC-ICP-MS	pneumatic nebulization multi-collector inductively coupled plasma-mass spectrometry
PTFE	polytetrafluoroethylene
PTWI	provisional tolerable weekly intake
Q	quadrupole mass filter
Q-ICP-MS	quadrupole based – inductively coupled plasma-mass Spectrometry
ρ	Spearman's correlation coefficient
RF	radio frequency
RGM	reactive gaseous mercury

RMs	reference materials
ROV	remote operated vehicle
RSD	relative standard deviation
RSE	relative standard error
Ry	Ryvingen fyr
S	slope
SC-SF-ICP-MS	single-collector sector-field – inductively coupled plasma-mass spectrometry
SD	standard deviation
Sf	Sørfjord
SF	sector field
SF-ICP-MS	sector-field – inductively coupled plasma-mass spectrometry
SRB	sulfate reducing bacteria
SRM	standard reference material
SSB	sample standard bracketing
St	Steinstøberget
t_{crit}	t-student critical
t_{exp}	t-student experimental
TDS	total dissolved solids
THg	total mercury
TIMS	thermal ionization mass spectrometry
ToF	time of flight

TWI	tolerable weekly intake
UGent	Ghent University
UNEP	United Nations Environment Program
US	United States
WHO	World Health Organization
w.w.	wet weight
WWII	World War II

Outlook and goals

Mercury (Hg) is one of the most important global pollutants. It can travel long distances through the atmosphere, be persistent in the environment and be accumulated along the food web. The toxicity of Hg strongly depends on its chemical form, methylmercury (MeHg) being the most toxic Hg species. Since the Minamata disaster in 1956, there is a rising concern about the potential risk of this highly toxic heavy metal and its related compounds. Hg occurs in the environment as a result of both natural and anthropogenic sources. Atmospheric Hg is abundantly deposited in the oceans, one of the major reservoirs of Hg on Earth, and fish consumption is considered as the main source of human MeHg exposure. Thus, the development of novel tools aiming to evaluate the risks associated with Hg in aquatic ecosystems is of the utmost importance. Next to elemental (total Hg quantification) and speciation (inorganic *versus* organic Hg) analysis, isotopic analysis of Hg has been revealed as a key tool to study the complex biogeochemical Hg cycle in nature and to evaluate the risks associated with the presence of and exposure to Hg.

However, Hg isotopic analysis still poses important analytical challenges, such as (*i*) the high precision required to see the small natural variations in the isotopic composition of Hg and/or (*ii*) the low Hg concentrations present in most of the samples of interest. Multi-collector ICP-mass spectrometry (MC-ICP-MS) is the technique of choice for high-precision isotopic analysis of Hg. This technique enables accurate and precise isotope ratio measurements, although at the cost of a relatively poor sensitivity and a laborious and time-consuming sample preparation (*e.g.*, isolation of the target analyte from the sample matrix). In the case of Hg, cold vapor generation (CVG) coupled to MC-ICP-MS can be used for sample introduction; Hg^{2+} is selectively converted into Hg^0 (gas) *via* reaction with $SnCl_2$ and can be transported out of the reaction cell and into the ICP *via* an Ar carrier gas. In this way, spectral interferences and/or matrix effects can be avoided, while the sensitivity can be increased significantly. Hg isotopic analysis *via* CVG-MC-ICP-MS is, however, still affected by instrumental mass discrimination, a phenomenon resulting in a measured isotope ratio different from the true one. Therefore, this instrumental mass bias needs to be adequately corrected for.

The main goals of this PhD were the development, optimization and validation of a robust analytical method for accurate and precise Hg isotopic analysis and its subsequent application in the context of real-life situations of high environmental relevance.

The first chapter of this PhD thesis provides a description of the importance of Hg as a global environmental pollutant. This includes a summary of its chemical characteristics, most common sources, toxicity, exposure pathways, health implications, and a general overview of the complex biogeochemical Hg cycle. In addition, the capabilities of high-precision Hg isotopic analysis as a means to study the occurrence of Hg in the environment has been described into some detail. For this purpose, the general principles of Hg isotope fractionation, the extent of this fractionation in different environmental processes, and a general overview of the Hg isotopic signatures reported for several environmental matrices, are provided.

Chapter 2 summarizes the basic operating principles of multi-collector ICP-MS (MC-ICP-MS), the technique of choice for Hg isotopic analysis. In this chapter, the setup used during this PhD, comprising a cold-vapor generation (CVG) system for sample introduction and a multi-collector ICP-MS instrument, is briefly described. Finally, the last part of this chapter is devoted to instrumental mass discrimination, a phenomenon strongly affecting MC-ICP-MS measurement results. This section discusses the origin of instrumental mass discrimination, the most widely applied approaches used for mass bias correction within the scientific community, and a more in-depth description of the correction approach selected in this PhD research project for Hg isotopic analysis.

In chapter 3, an in-depth evaluation of Hg isotopic analysis *via* the use of two different sample introduction systems, pneumatic nebulization and cold vapor generation, is provided. This work has been carried out in the context of the SIB-09 “Elements” project, funded by the EMRP (European Metrology Research Programme of EURAMET). The aim of this work was to provide National Metrology Institutes (NMIs) with sufficient information as to which approach to use in the characterization of future Hg isotopic reference materials. This study comprises (*i*) an optimization of the instrument settings and acquisition parameters, (*ii*) an assessment of the effect of Hg and Tl (analyte and internal standard, respectively) concentrations, and (*iii*) an evaluation of the applicability of different mass bias correction approaches. Additionally, the extent and stability of mass bias and short-

and long-term precision of Hg isotopic analysis were documented, as well as the effect of the matrix composition. Finally, the methodology selected has been used for the determination of the Hg isotopic composition of several reference materials (RMs) with environmentally relevant matrices.

After the development, optimization and validation of a reliable protocol for high-precision Hg isotopic analysis, it has been applied to different sample types and in different studies of high environmental relevance. As indicated above, fish consumption is considered the major source of MeHg for humans. Therefore, several marine species from different levels within the trophic chain were analyzed for their Hg isotope ratios.

In this context, Chapter 4 describes a research project carried out in collaboration with the Norwegian National Institute of Nutrition and Seafood Research (NIFES). The goal of this work was to assess the effect of the introduction of a large amount of metallic Hg leaking from a submarine wreck on the local food web. The U-864 submarine was torpedoed and sunk during WWII close to the Norwegian coast and in the immediate proximity of Fedje island. The U-864 was carrying approximately 70 tons of metallic Hg in its keel, and a large fraction of this metallic Hg was introduced in the marine ecosystem. In this work, the information provided by THg quantification, MeHg speciation, and Hg isotopic analysis of different sample types has been combined, aiming to evaluate the potential impact of the U-864 Hg. The isotopic signature of metallic Hg salvaged from the sunken submarine was compared to those obtained for sediments from the immediate vicinity of the wreck location, and those for different tissues of crabs (*Cancer pagurus*) from the wreck location, 4 nautic miles north and 4 nautic miles south of this location.

Based on the hypotheses and tentative conclusions provided in Chapter 4, Chapter 5 describes a subsequent study, going one step further by analyzing a fish species located at a higher level within the food web. For this work, liver and muscle tissues of tusks (*Brosme brosme*) have been analyzed for their THg and MeHg concentrations and Hg isotopic signatures for tracing Hg pollution along the Norwegian coast, and for evaluating the possibility of using tusk as a fish species in future Hg monitoring programs. Tusks from eight coastal locations, including fjords, have been analyzed and the results have been complemented with those obtained upon quantification of other environmentally relevant metals (As, Cd, Cu, Cr, Ni, Pb and Zn) in order to elucidate the origin and fate of Hg.

Finally, Chapter 6 deals with the study of Hg in a marine mammal (located at the top of a marine trophic chain), an issue of great concern in terms of seafood safety, and of special relevance owing to the similarities these species may show with humans in terms of metabolic pathways. A cooperation with the University of Aberdeen (Scotland, UK) was established and, in the context of this work, different sample types of long-finned pilot whales (*Globicephala melas*), stranded on a beach between Ansturther and Pittenween in Scotland (UK) on the 12th of September 2012, were studied. In this work, different tissue types (liver, kidney and muscle) and biological fluids (blood and milk) of these stranded long-finned pilot whales have been analyzed for their THg and MeHg concentrations, and Hg isotope ratios, aiming at obtaining a more profound insight into the metabolic pathways that Hg undergoes in this type of animal.

Situering en doelstellingen

Kwik (Hg) is wereldwijd één van de belangrijkste verontreinigende stoffen. Het kan grote afstanden afleggen doorheen de atmosfeer, is niet afbreekbaar en vertoont biomagnificatie in de voedselketen. De toxiciteit van Hg is sterk afhankelijk van de chemische vorm, waarbij methylkwik (MeHg) beschouwd wordt als de meest toxische Hg-species. Sinds de Minamata-ramp in 1956 is er een groeiende bezorgdheid over het potentiële risico van dit zeer giftige zware metaal en zijn verbindingen. Hg komt in de omgeving voor als gevolg van zowel natuurlijke als antropogene bronnen. Atmosferisch Hg wordt overvloedig afgezet in de oceanen, één van de belangrijkste reservoirs van Hg op aarde. De consumptie van vis en schaaldieren wordt beschouwd als de belangrijkste bron van menselijke blootstelling aan MeHg. Bijgevolg is de ontwikkeling van nieuwe methodes om de risico's van Hg in aquatische ecosystemen te evalueren van het grootste belang. Naast elementanalyse (voor de kwantitatieve bepaling van het totale Hg-gehalte) en speciatie-analyse (waarbij onderscheid kan gemaakt worden tussen anorganisch en organisch Hg), wordt isotopenanalyse van Hg gezien als een belangrijk middel om de complexe biogeochemische Hg-cyclus in de natuur te bestuderen en de risico's die samenhangen met de aanwezigheid van en blootstelling aan Hg te evalueren.

Hg-isotopenanalyse kent nog steeds belangrijke analytische uitdagingen, zoals (i) de hoge precisie die vereist is om de kleine natuurlijke variaties in de isotopensamenstelling van Hg te detecteren en kwantificeren en (ii) de lage Hg-concentraties die aanwezig zijn in de meeste van de relevante monsters. Multi-collector ICP-massaspectrometrie (MC-ICP-MS) is de techniek bij uitstek voor isotopenanalyse van Hg met hoge precisie. Deze techniek maakt een accurate en precieze meting van isotopenverhoudingen mogelijk, weliswaar met een relatief beperkte gevoeligheid en vaak is een omslachtige en tijdrovende monstervoorbereiding vereist (bijvoorbeeld isolatie van het analietelement uit de monstermatrix). In het geval van Hg kan de koude-damp-methode (Cold Vapour Generation of CVG) gebruikt worden voor monsterintroductie in MC-ICP-MS. Bij deze methode wordt Hg^{2+} selectief gereduceerd tot Hg^0 (gas) via reactie met $SnCl_2$, waarna de Hg-damp via Ar-draaggas uit de reactiecel kan verwijderd worden en naar het ICP worden getransporteerd. Op deze manier kunnen spectrale interferenties en/of matrixeffecten worden vermeden, terwijl de gevoeligheid

aanzienlijk kan worden verhoogd. Hg isotopenanalyse via CVG-MC-ICP-MS wordt echter nog steeds beïnvloed door instrumentele massadiscriminatie, een fenomeen dat resulteert in een gemeten isotopenverhouding die verschilt van de ware. Daarom moet voor deze instrumentele afwijking adequaat worden gecorrigeerd.

De belangrijkste doelen van dit doctoraat waren de ontwikkeling, optimalisatie en validatie van een robuuste analytische methode voor accurate en precieze Hg-isotopenanalyse en de daaropvolgende toepassing ervan in actuele contexten met een hoge milieurelevantie.

Het eerste hoofdstuk van dit proefschrift beschrijft het belang van Hg als een wereldwijd milieuverontreinigende stof. Dit omvat een samenvatting van de chemische kenmerken, meest voorkomende bronnen, toxiciteit, blootstellingsroutes, gezondheidsimplicaties en een algemeen overzicht van de complexe biogeochemische Hg-cyclus. Bovendien zijn de mogelijkheden van hoge-precisie Hg-isotopenanalyse als middel om het in de omgeving aanwezige Hg te bestuderen tot in detail beschreven. Voor dit doel worden de algemene principes van Hg-isotopenfractionactie, de omvang van deze fractionatie in verschillende omgevingsprocessen en een algemeen overzicht van de isotopische samenstellingen van Hg die voor verschillende omgevingsmatrices zijn gerapporteerd, verstrekt.

Hoofdstuk 2 vat de basisprincipes van multi-collector ICP-MS (MC-ICP-MS) samen, de voorkeursmethode voor hoog-precieze Hg-isotopenanalyse. In dit hoofdstuk wordt de opstelling beschreven die tijdens dit doctoraat werd gebruikt, bestaande uit een koude damp systeem (CVG) voor monsterintroductie en een multi-collector ICP-MS-instrument. Ten slotte is het laatste deel van dit hoofdstuk gewijd aan instrumentele massadiscriminatie, een fenomeen dat de meetresultaten met MC-ICP-MS sterk beïnvloedt. Deze paragraaf bespreekt de oorsprong van instrumentele massadiscriminatie, de meest toegepaste benaderingen gebruikt voor correctie, en een meer diepgaande beschrijving van de correctie-aanpak die in dit werk werd geselecteerd.

Hoofdstuk 3 beschrijft de resultaten van een grondige evaluatie van MC-ICP-MS Hg-isotopenanalyse via het gebruik van twee verschillende monsterintroductiesystemen, nl. pneumatische verstuiving en koude dampgeneratie. Dit werk werd uitgevoerd in het kader van het SIB-09 "Elements" project, gefinancierd door het EMRP (European Metrology Research Program of

EURAMET). Het doel van dit werk was om Nationale Metrologische Instituten (NMI's) voldoende informatie te verschaffen over de te gebruiken aanpak bij de karakterisering van toekomstige Hg-isotopische referentiematerialen. Deze studie omvat (i) een optimalisatie van de instrumentinstellingen en acquisitieparameters, (ii) een beoordeling van het effect van de Hg- en Tl-concentratie (als respectievelijk analiet en interne standaard), en (iii) een evaluatie van de toepasbaarheid van verschillende methodes om te corrigeren voor massadiscriminatie. Bovendien werd de stabiliteit van de instrumentele massadiscriminatie en de korte- en lange-termijn precisie van Hg-isotopenanalyse gedocumenteerd, evenals het effect van de matrixsamenstelling. Ten slotte werd de gekozen methode gevalideerd via de bepaling van de isotopische samenstelling van Hg van verschillende referentiematerialen (RM's) met voor het milieu relevante matrices.

Na de ontwikkeling, optimalisatie en validatie van een betrouwbaar protocol voor hoge-precisie Hg isotopenanalyse, werd dit ingezet in verschillende studies met een hoge milieurelevantie. Zoals hierboven aangegeven, wordt de consumptie van vis en schaaldieren beschouwd als de belangrijkste bron van MeHg voor mensen. Daarom werden mariene species van verschillende niveaus binnen de trofische keten geanalyseerd op hun Hg-isotopenverhoudingen.

In dit verband beschrijft hoofdstuk 4 een onderzoeksproject dat werd uitgevoerd in samenwerking met het Noorse National Institute for Nutrition and Seafood Research (NIFES). Het doel van dit werk was om het effect van de introductie van een grote hoeveelheid metallisch Hg dat lekt uit een onderzeeërwrak op de lokale voedselketen te beoordelen. De U-864-onderzeeër werd tijdens de Tweede Wereldoorlog getorpedeerd en tot zinken gebracht dicht bij de Noorse kust en in de onmiddellijke nabijheid van het eiland Fedje. De U-864 vervoerde ongeveer 70 ton metallisch Hg in zijn kiel en een groot deel daarvan werd geïntroduceerd in het mariene ecosysteem. In dit werk werd de informatie, bekomen op basis van kwantificering van het totale Hg-gehalte, MeHg-bepaling en Hg-isotopenanalyse van verschillende monstertypes, gecombineerd om de potentiële impact van het U-864 Hg te evalueren. De isotopische samenstelling van metallisch Hg bemonsterd in de gezonken onderzeeër werd daarbij vergeleken met deze verkregen voor sedimenten uit de onmiddellijke nabijheid van de locatie van het wrak, en die voor verschillende weefsels van krabben (*Cancer pagurus*) bemonsterd op de locatie van het wrak en 4 zeemijlen ten noorden en ten zuiden van deze locatie.

Hoofdstuk 5 beschrijft een vervolgstudie, die een stap verder gaat door het analyseren van een vissoort die zich op een hoger niveau in de voedselketen bevindt. Voor dit werk zijn lever- en spierweefsels van de Lom (*Brosme brosme*) geanalyseerd op hun THg- en MeHg-concentraties en de isotopische samenstelling van het aanwezige Hg voor het opsporen van Hg-vervuiling langs de Noorse kust, en voor het evalueren van de mogelijkheid om Lom in de toekomst als vissoort te gebruiken voor het monitoren van Hg-vervuiling. Vissen afkomstig van acht kustlocaties, waaronder fjorden, werden geanalyseerd en de resultaten zijn aangevuld met de concentraties bepaald voor andere voor het milieu relevante metalen (As, Cd, Cu, Cr, Ni, Pb en Zn) om de oorsprong van het aanwezige Hg te onderzoeken en de processen waaraan het deelneemt te documenteren.

Tot slot behandelt hoofdstuk 6 de studie van Hg in een zeezoogdier (gesitueerd aan de top van een mariene trofische keten). Dit omwille van het grote belang van de voedselveiligheid van predatorspecies, en de relevantie wegens de overeenkomsten die deze soorten kunnen vertonen met mensen wat betreft de metabole routes. Hiervoor werd een samenwerking opgezet met de Universiteit van Aberdeen (Schotland, VK), waarbij verschillende monstertypes werden bestudeerd afkomstig van grienden (*Globicephala melas*), die strandden op een strand tussen Ansturther en Pittenween in Schotland (VK) op 12 september 2012. In dit werk werden verschillende weefseltypes (lever, nieren en spieren) en biologische vloeistoffen (bloed en melk) van deze gestrande grienden onderzocht op hun THg- en MeHg-concentraties en Hg-isotopenverhoudingen, met als doel een grondiger inzicht te verkrijgen in de metabole omzettingen die Hg bij dit type dier ondergaat.

Scientific outcome

1. List of peer-reviewed scientific publications

1.1. Publications in peer-reviewed international journals included in this PhD thesis

1.1.1. Ana Rua-Ibarz, Eduardo Bolea-Fernandez, Frank Vanhaecke. An in-depth evaluation of accuracy and precision in Hg isotopic analysis *via* pneumatic nebulization and cold vapor generation multi-collector ICP-mass spectrometry. Analytical Bioanalytical Chemistry, 408 (2016) 417 – 429. Q1, IF: 3.431. (Chapter 3)

1.1.2. Ana Rua-Ibarz, Eduardo Bolea-Fernandez, Amund Maage, Sylvia Frantzen, Stig Valdersnes, Frank Vanhaecke. Assessment of Hg pollution released from a WWII submarine wreck (U-864) by Hg isotopic analysis of sediments and *Cancer pagurus* tissues. Environmental Science & Technology, 50 (2016) 10361 – 10369. Q1, IF: 6.198. (Chapter 4)

1.2. Additional manuscripts including in this PhD thesis intended for publication in peer-reviewed international journals

1.2.1. Ana Rua-Ibarz, Eduardo Bolea-Fernandez, Amund Maage, Sylvia Frantzen, Frank Vanhaecke. Tracing mercury pollution along the Norwegian coast *via* elemental and isotopic analysis of deep-water marine fish (*Brosme brosme*). Submitted to Environmental Science & Technology. Q1, IF: 6.198. (Chapter 5)

1.2.2. Ana Rua-Ibarz, Eduardo Bolea-Fernandez, Eva M. Krupp, Jörg Feldmann, Frank Vanhaecke. Unraveling Hg exposure of long-finned pilot whales (Globicephala melas) *via* isotopic analysis with multi-collector ICP-mass spectrometry. Intended for submission to Nature. Q1, IF: 40.137. (Chapter 6)

1.3. Other peer-reviewed scientific publications in international journals

1.3.1. Eduardo Bolea-Fernandez, Diego Leite, Ana Rua-Ibarz, Lieve Balcaen, Maite Aramendía, Martín Resano, Frank Vanhaecke. Characterization of SiO_2 nanoparticles by single particle-inductively coupled plasma-tandem mass spectrometry (SP-ICP-MS/MS). Journal of Analytical Atomic Spectrometry, 32 (2017) 2140 - 2152. Q1, IF: 3.379.

2. Conference proceedings

2.1. Presentations on international conferences by the author

2.1.1. Ana Rua-Ibarz, Frank Vanhaecke. Mercury isotopic analysis *via* cold vapor generation multi-collector ICP-MS: mass bias correction and application to environmental samples. *2015 European Winter Conference on Plasma Spectrochemistry*. 22 – 26 February 2013. Münster, Germany. Poster presentation.

2.1.2. Ana Rua-Ibarz, Frank Vanhaecke, Amund Maage, Stig Valdersnes. Mercury isotopic analysis *via* cold vapor generation multi-collector ICP-MS: mass bias correction and provenancing of Hg pollution. *12th International Conference of Mercury as a Global Pollutant*. 14 – 19 June 2015. Jeju, South Korea. Oral presentation.

2.1.3. Ana Rua-Ibarz, Eduardo Bolea-Fernandez, Amund Maage, Sylvia Frantzen, Stig Valdersnes, Frank Vanhaecke. Mercury isotopic analysis *via* cold vapor generation – multi- collector – ICP-mass Spectrometry as a key tool for evaluating pollution in marine ecosystems. *18th International Conference on Heavy Metals in the Environment*. 12 – 15 September 2016, Ghent, Belgium. Oral presentation.

2.2. Presentation on international conferences by other co-authors

2.2.1. Frank Vanhaecke, Lieve Balcaen, Eduardo Bolea-Fernandez, Patrick Degryse, Veerle Devulder, Axel Gerdes, Lara Lobo, Amund Maage, Martín Resano, Ana Rua-Ibarz. Extending the application range of provenance determination based on isotopic analysis. *Pacifichem 2015 International Chemical Congress of Pacific Basin Societies.* 15 – 20 December 2015, Honolulu, Hawaii. Invited lecture.

2.2.2. Frank Vanhaecke, Yulia Anoshkina, Lieve Balcaen, Stepan Chernonozhkin, Marta Costas-Rodriguez, Maria Florez-Garcia, Sara Lauwens, Ana Rua-Ibarz, Steven Goderis, Philip Claeys, Joris Delanghe, Hans Van Vlierberghe, Amund Maage. From outer space to within the human body: natural isotope ratios as proxies. *2016 Winter Conference on Plasma Spectrochemistry*. 10 – 16 January 2016. Tucson, Arizona, US. Invited lecture..

2.2.3. Frank Vanhaecke, Andrea Bazzano, Marco Grotti, Ana Rua-Ibarz, Eduardo Bolea-Fernandez, Amund Maage. Improved insight into environmental issues via high-precision isotopic analysis by means of multi-collector ICP-MS (MC-ICP-MS). *ISEAC39 – International Conference on Environmental & Food Monitoring*. 19 – 22 July 2016 Hamburg, Germany. Invited lecture.

2.2.4. Diego Pereira Leite, Eduardo Bolea-Fernandez, Ana Rua-Ibarz, Martin Resano, Frank Vanhaecke, Maite Aramendia. Characterization of SiO_2 Nanoparticles by Single Particle - Inductively Coupled Plasma - Tandem Mass Spectrometry. *Colloquium Spectroscopicum Internationale XL IX Euro-Mediterranean Symposium on LIBS*. 11 - 16 June 2017, Pisa, Italy.

2.2.5. Maite Aramendia, Eduardo Bolea-Fernandez, Diego Leite, Ana Rua-Ibarz, Lieve Balcaen, Martin Resano, Frank Vanhaecke. Characterization of SiO_2 Nanoparticles by Single Particle - Inductively Coupled Plasma -

tandem mass spectrometry (SP-ICP-MS/MS). *SCIX 2017 - The Great Scientific Exchange*. 8 - 13 October 2017, Reno, Nevada, USA. Invited lecture.

2.2.6. Eduardo Bolea-Fernandez, Ana Rua-Ibarz, Amund Maage, Sylvia Frantzen, Jorg Feldmann, Eva M. Krupp, Frank Vanhaecke. Tracing mercury pollution in and unraveling exposure pathways for marine species via high-precision isotopic analysis with multi-collector ICP-mass spectrometry. *SCIX 2017 - The Great Scientific Exchange*. 8 - 13 October 2017, Reno, Nevada, USA. Invited lecture.

2.2.7. Frank Vanhaecke, Eduardo Bolea-Fernandez, Ana Rua-Ibarz, Amund Maage, Eva Krupp, Joerg Feldmann. High-precision mercury isotopic analysis via multi-collector ICP-MS for obtaining an enhanced insight in environmental case studies. *2018 Winter Conference on Plasma Spectrochemistry*. 8 -13 January 2018, Amelia Island, Florida, USA. Invited lecture

2.3. Presentations on other conferences by the author

2.3.1. Ana Rua-Ibarz, Eduardo Bolea-Fernandez, Amund Maage, Sylvia Frantzen, Stig Valdernes, Frank Vanhaecke. Assessment of Hg pollution released from a WWII submarine wreck by Hg isotopic analysis of sediments and Cancer pagurus tissues via cold vapor generation – multi collector ICP-mass spectrometry (CVG-MC-ICP-MS). *2016 Doctoraatssymposium*. 17 March 2016, Gent, Belgium. Poster presentation.

2.3.2. Ana Rua-Ibarz, Eduardo Bolea-Fernandez, Amund Maage, Sylvia Frantzen, Stig Valdersnes, Frank Vanhaecke. Tracking mercury pollution in marine ecosystems. *Voorjaarsbijeenkomst Werkgroep Atoomspectrometrie*. 19 May 2016, Werkendam, Netherland. Invited lecture.

2.4. Presentations on other conferences by other co-authors

2.4.1. Frank Vanhaecke, Yulia Anoshkina, Lieve Balcaen, Marta Costas-Rodriguez, Eduardo Bolea-Fernandez, Ana Rua-Ibarz, Stijn Van Malderen. *Mass Spectrometry in Food and Feed II*, 15 September 2015, Ghent, Belgium.

2.4.2. Eduardo Bolea-Fernandez, Yulia Anoshkina, Lieve Balcaen, Marta Costas-Rodriguez, Sara Lauwens, Ana Rua-Ibarz, Frank Vanhaecke. ICP - mass spectrometry as a versatile tool for the determination of ultra-trace amounts and isotopic analysis of metals and metalloids. *2016 Doctoraatssymposium*. 17 March 2016, Gent, Belgium. Oral presentation.

2.4.3. Lieve Balcaen, Eduardo Bolea-Fernandez, Ana Rua-Ibarz, Stijn Van Malderen, Frank Vanhaecke. Development and refinement of analytical methods based on ICP-mass spectrometry to meet the needs of contemporary chemical research. *Chemical Research in Flanders Symposium*. 24 – 26 October 2016, Blankenberge, Belgium. Invited lecture.

2.4.4. Eduardo Bolea-Fernandez, Diego Leite, Ana Rua-Ibarz, Lieve Balcaen, Maite Aramendia, Martin Resano, Frank Vanhaecke. Exploring the limits of ICP- tandem mass spectrometry: Single Particle (SP) ICP-MS/MS for characterizing SiO2 Nanoparticles. *SETAC Europe 27th Annual Meeting (Agilent Lunch Seminar)*. 7 - 11 May 2017, Brussels, Belgium. Invited lecture.

2.4.5. Eduardo Bolea-Fernandez, Diego Leite, Ana Rua-Ibarz, Lieve Balcaen, Maite Aramendia, Martin Resano, Frank Vanhaecke. ICP-MS/MS for the determination of elements at ultra-trace level in dissolved and nanoparticulate form. *Agilent Atomic Spectroscopy User's day*. May 31st and June 1st. Barneveld, The Netherlands. Invited lecture.

3. Teaching activities

3.1. Supervision of Alexander Timm. Master thesis student during 1 academic year (2014 – 2015). *Investigation of mercury distribution in a polluted marine ecosystem based on isotopic analysis using MC-ICP-MS*

3.2. Guidance of a group of three Bachelor students during a 1 month project (2015). *Elemental and isotopic analysis of Hg in fish samples to evaluate the environmental risk and track the possible contamination sources.*

3.3. Supervision of Arnout Laureys. Master thesis student during 1 academic year (2016 – 2017). *Unraveling Hg exposure of long-finned pilot whales (Globicephala melas) via isotopic analysis with multi-collector ICP-mass spectrometry.*

Chapter 1

Mercury in the Environment

1.1. Mercury as a global pollutant

Mercury (Hg) occurs in the environment as a result of natural and anthropogenic sources, and both wildlife and humans are exposed to the harmful effects of this highly toxic heavy metal and its compounds. Since the Minamata disaster in 1956, the risks associated with Hg are widely recognized and there is increasing concern about the rising levels of Hg around the world.**[1]** As a result, the United Nations Environment Program (UNEP) mandated to study the impacts of Hg and to provide legal instruments as to address the Hg issue. In 2013, the Minamata Convention on Mercury was signed, which aims to protect human health and the environment from anthropogenic emissions and releases of Hg and Hg compounds. Nowadays, Hg is recognized as one of the most important global pollutants because it can travel long distances through the atmosphere, be persistent in the environment, be accumulated in the food web, and cause severe adverse effects on human and ecosystem health.**[2]**

This chapter aims at giving a general overview, thus providing a basic understanding of the chemistry of Hg, its toxicity and the risks associated with Hg exposure, the most important Hg sources and exposure pathways, the complexity of the Hg cycle, and the role of isotopic analysis of Hg as a key tool for unraveling the biogeochemistry of Hg in nature.

1.1.1. Chemistry of mercury

Mercury (Hg) is the only metal that is liquid at room temperature, a reason why it was commonly known as “quicksilver” or “liquid silver”. The symbol “Hg” is coming from the Latin term “*hydrargyrum*”. The atomic number of Hg is 80 and its atomic weight is 200.6025 amu. As a result of its electronic configuration, with completely full f and d orbitals ($[Xe]4f^{14}5d^{10}6s^2$), Hg shows a similar stability as the noble gas elements. Due to its unique physicochemical properties, *i.e.* melting point of -38.87 °C, boiling point of 356.7 °C, density of 13.534 g cm^{-3}, vapor pressure of 1.22 x 10^{-3} mmHg at 20°C and solubility of 5.6 x 10^{-7} g L^{-1} in water at 25 °C,**[3, 4]** Hg has been used by humans since ancient times. Hg occurs in the environment in three main oxidation states: Hg(0) (elemental or metallic), Hg(I) (mercurous) and Hg(II) (mercuric). However, Hg(I) is metastable and is typically an intermediate in the

oxidation of Hg (0) to Hg (II). In the atmosphere, Hg(0) comprises approximately 95% of the total Hg, while Hg(II) is the most common oxidation state in aquatic and terrestrial ecosystems. In addition, both Hg(I) and Hg(II) can form inorganic and organic chemical compounds.**[5]** Hg(II) is commonly present in water, soils and sediments under the form of sulfides, chlorides, selenides and tellurides, while the organic compound monomethylmercury (MMHg or MeHg) is the dominant Hg species in biota.**[6]**

Some fractions of Hg present in the environment have been classified as "operationally defined fractions" instead of specific compounds, depending on how they can be collected and how elemental Hg can be released from them (see **Figure 1-1**). However, there is still some controversy regarding the names and definitions of some of those fractions, such as DGHg (dissolved gaseous Hg), HgR (reactive Hg dissolved in water), Hg(II) (dissolved Hg, used to quantify bio-available Hg), Hg-Col (colloidal Hg), RGM (reactive gaseous mercury) and PHg (particulate-bound Hg).**[7-10]**

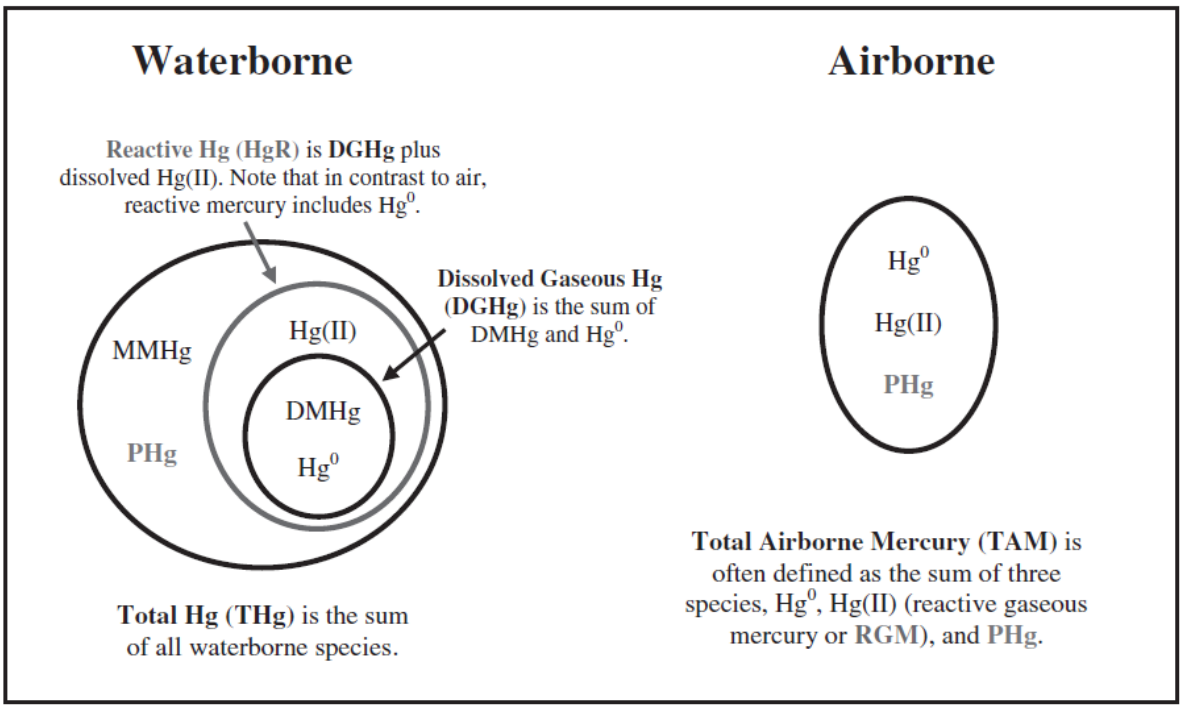

Figure 1-1. Diagram representing the major chemical forms of Hg found in water and air.**[10]**

1.1.2. Mercury sources

Mercury is a naturally occurring element in the Earth's crust that can enter the environment as a result of natural and anthropogenic processes, and it can be re-emitted or re-mobilized after its introduction. The main natural sources of Hg are volcanoes, forest fires, cinnabar (ore) and fossil fuels, such as coal, petroleum and natural gas deposits. Cinnabar (HgS) is considered the main mineral source of Hg, however, intermetallic alloys, halides, sulfides, arsenides, selenides, antimonides, tellurides, sulfosalts, oxides, carbonates and sulfates are also considered as Hg mineral sources. They occur in magmatic, hydrothermal, evaporitic and surface weathering environments.**[11]** Therefore, the "pure" natural processes that can emit Hg into the atmosphere may include volcanic eruptions, geothermal vents and Hg emission from terrestrial enriched soils,**[10]** with gaseous elemental mercury (GEM) as the predominant form of Hg from natural emissions (> 99%).**[12]** Some models of the flow of Hg through the environment suggest that natural sources account for about 10% of the estimated amount of Hg emitted and re-emitted into the atmosphere (see **Figure 1-2**).**[13]**

Human activities have increased the mobilization of Hg from deep mineral reservoirs into the environment, raising the Hg levels in the atmosphere, soils, fresh waters and oceans. The main anthropogenic Hg sources are fossil fuel combustion, gold production, non-ferrous metal smelting (mainly of lead and zinc), cement production, caustic soda manufacturing, chlor-alkali production, iron and steel production and waste incineration. Other activities involving the use of considerable amounts of Hg, such as the production of batteries, measuring and control instruments, electrical lighting, wiring devices and electrical switches can also contribute to the release of Hg into the environment, as well as dental amalgams, medicinal waste incinerators and landfills.**[10, 14]** Similarly to natural emissions, anthropogenic Hg is mainly released to the atmosphere as GEM (~61%), although also reactive gaseous mercury (RGM, ~ 32%) and particulate Hg (PHg, ~ 7%) occur.**[14]**

Therefore, in the case of both natural and anthropogenic sources, the atmosphere plays a major role in the global transport of Hg. GEM can be transported over long distances from the point source owing to its high atmospheric residence time, ranging from several months to one year. Hg(0) can be oxidized in the atmosphere

and be removed by particle and gas-phase dry deposition or by scavenging by precipitation. RGM and PHg have shorter residence times in the atmosphere in comparison with GEM, therefore they are typically deposited locally or regionally, relatively close to the point source.**[2]** Atmospheric deposition can occur in a terrestrial and/or in an aquatic ecosystem, in which Hg can subsequently follow different pathways (see section 1.1.4.)

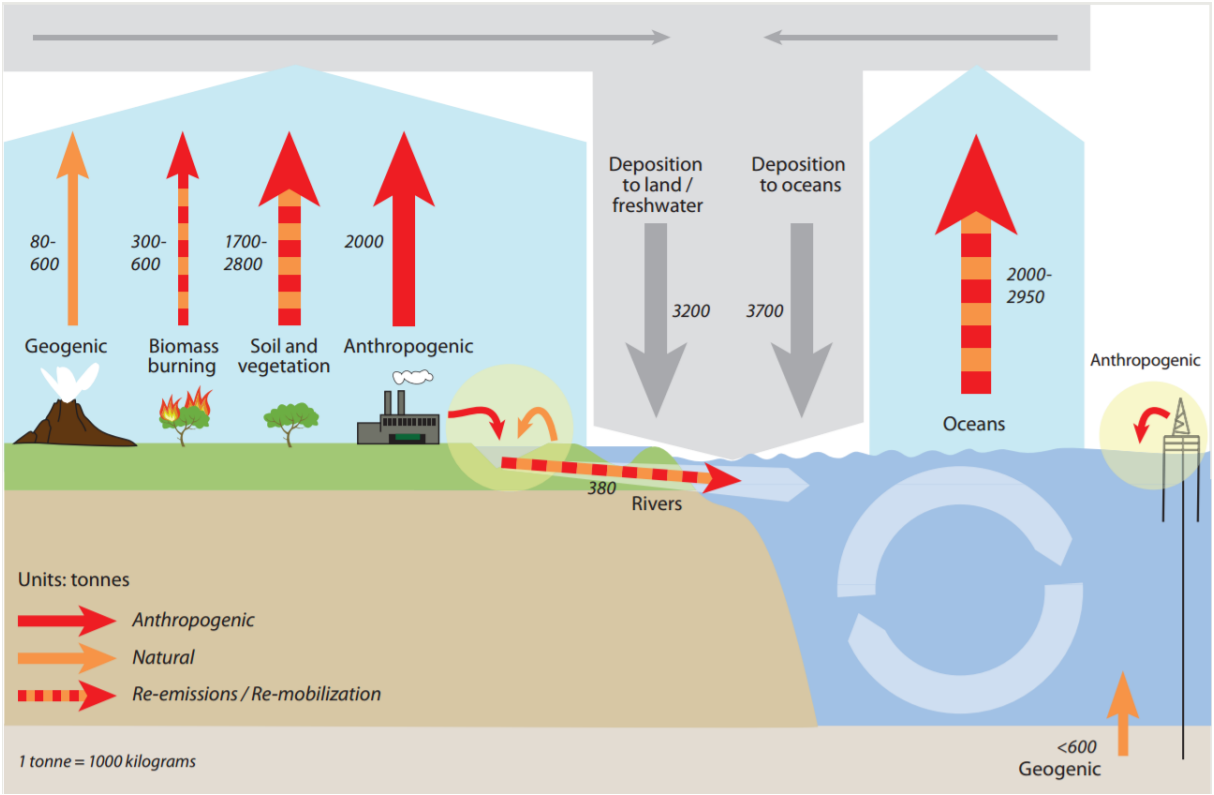

Figure 1-2. Global Hg budgets, based on models, of the main environmental compartments including natural sources, anthropogenic sources, as well as re-emissions of Hg previously deposited.**[13]**

1.1.3. Toxicity, exposure and health implications

Mercury is a toxic heavy metal, but its toxicity strongly depends on its chemical form. Inorganic mercury compounds are elemental mercury (Hg^0), which can be in metallic or gaseous form, and mercurous (Hg_2^{2+}) or mercuric (Hg^{2+}) salts. Organic mercury compounds contain carbon-containing structures, such as (a) methyl, ethyl or phenyl group(s) bound to Hg. The most typical organic Hg compounds are

methyl mercury (CH_3Hg^+) and dimethyl mercury $(CH_3)_2Hg$, which are the most toxic mercury species.

In liquid state, elemental Hg is minimally absorbed by humans, but the problem arises when the elemental Hg is in its gaseous form. After inhalation, GEM is readily absorbed in the lungs and is able to enter the blood stream, from where it is distributed to all tissues within the body.**[15]** It can pass though the blood-brain barrier, where it can cause severe damage to the central nervous system,**[16]** and also the placenta barrier, settling down in the fetal brain.**[17]** Other organs or tissues that can also be affected by the deposition of metallic Hg include the kidneys, liver, pancreas, lungs, muscles, thyroid gland, myocardium, salivary glands, prostate, testes and breasts.**[18]** The biological half-life of absorbed Hg vapor in blood is approximately two to four days, while part of the Hg vapor is oxidized to Hg^{2+}, the rest is excreted *via* urine and feces.**[19]** Elemental Hg exposure is normally divided into occupational and non-occupational exposure. Occupational exposure occurs as a result of activities that produce Hg vapor, such as the manufacturing of chlor-alkali compounds, the production of lighting or Hg-containing devices, and mining activities. In addition to Hg mining itself, one of the other mining activities of special concern is the artisanal and small-scale gold mining (ASGM) in developing regions, where also children participate in the gold extraction under “unsafe” conditions. For the extraction of Au, Hg is added to the gold-containing ore, aiming at producing an amalgam between gold and mercury (AuHg). Subsequently, the Hg from this amalgam is burned off to obtain pure gold. Of course, this leads to the release of Hg in gaseous form.**[20]** Occupational exposure can induce both short-term and chronic effects, including dyspnea, paroxysmal cough, chest pain, pulmonary infiltration, chills, nausea, vomiting, tremor, psychological disturbances, *erethism* (psychotic symptoms), gingivitis, stomatitis and severe kidney damage associated with the nephrotic syndrome.**[21]** The most important non-occupational Hg exposure occurs through amalgam dental fillings. The majority of these filling consist of about 50% of metallic Hg mixed with other metals, typically silver, copper, tin and zinc. The Hg present in these dental fillings can be continuously released from the surface into the oral cavity by chewing, eating, brushing and drinking hot liquids.**[22]** The research community has published several studies investigating the relation between the number of Hg-containing dental fillings with some symptoms, diseases or elevated Hg levels in the

body.**[23-25]** Nowadays, alternative materials are investigated and used for dental fillings. However, up to date it is not possible to provide a clear solution to this problem.**[26, 27]**

Mercurous Hg salt mainly occurs under the form of Hg_2Cl_2 (calomel), and due to its low solubility, it is poorly absorbed. However, once inside the body, it undergoes disproportionation, leading to Hg^0 and Hg^{2+}, which are more absorbable Hg forms. Major pathways of exposure to this Hg compound was *via* the use of teething powders, deworming products and laxative preparations until the mid-20th century, sometimes causing acrodynia or "pink desease", which is characterized by a pink discoloration of the hands and feet, photophobia, irritability and polyneuritis.**[28]**

The most typical mercuric salt, cinnabar (HgS), shows an extremely low solubility in water, and therefore, its toxicity is relatively low. However, mercury chloride ($HgCl_2$), also called sublimate, is readily soluble in water, and consequently, its toxicity is much higher.**[29]** This compound was typically used as a component of some skin creams, as preservative and for the devolvement of photographic films. Its ingestion in a sufficient dose can cause extensive corrosive damage in the gastrointestinal tract, complete collapse of the kidney function, and indirectly, also cardiovascular collapse.**[30]** The patients surviving such intoxication commonly develop renal tubular necrosis with anuria.**[31]** Although the kidneys are the main organ affected by mercuric salts, they can also cause dermatitis, immune dysfunctions, asthma, stomatitis and gastroenteritis.**[32]** Nowadays, poisoning with mercury salts is rare, and the most common form of occupational exposure is to Hg vapor. Mercuric Hg cannot cross the blood-brain barrier as efficiently as elemental Hg, but it can be accumulated in the placenta, fetal tissues and amniotic fluid.**[33]** The free Hg^{2+} ions show an extremely high affinity to compounds containing functional sulfhydryl (–SH) groups, such as amino acids, peptides and proteins, allowing Hg accumulation in the red blood cells, brain, liver, kidney and other tissues. This can produce an inhibition of the activity of the corresponding cells, leading to damage in their cell membranes, a denaturalization of proteins, causing severe problems in the immune system and in the central nervous system.**[15, 21]**

The most common organic Hg species are monomethyl-, dimethyl-, ethyl- and phenyl-mercury compounds. Among these, the last two are rapidly converted into inorganic Hg, resulting in similar toxic effects as those of mercuric compounds, although they are more efficiently absorbed into the body. These compounds have

been used and are – to a lower extent – still used as preservative antibacterial agents in vaccines, *e.g.,* thimerosal (ethylmercury thiosalicylate), and they were widely used as components of latex paints before the 1990s.**[21]** On the other hand, the two methylmercury compounds are considered potent neurotoxins. Other organic Hg compounds can enter the environment from anthropogenic sources because of their presence in some products, such as fungicides, slimicides and paints, although nowadays their use has declined.**[34]** The main source of methylmercury compounds, however, is their production from inorganic Hg species by microorganisms in natural waters and/or at sediment-water interfaces, or *via* the decomposition of other organomercurial compounds.**[10]** The microorganisms convert the mercuric species into methylated species as a protective mechanism, because for them MeHg is less toxic than Hg^{2+}. Sulfate-reducing bacteria are considered the main responsible for this methylation process in aquatic ecosystems (see section 1.1.4.). DMHg is a volatile Hg compound with a short lifetime in the atmosphere because it is easily degraded by chemical or photochemical reactions. In aquatic ecosystems, it is rarely present in surface waters, and it is slowly accumulated in deep open ocean waters below the thermocline, because its rate of formation is of the same order as its decay rate.**[7]** MeHg is the most stable organic Hg compound, is one of the most abundant Hg species in the environment, is highly toxic and has been stated as the major source of human Hg exposure; therefore, it is considered the Hg species of greatest interest and most studies have focused on it.**[35, 36]** In terrestrial environments, the MeHg bioaccumulation is relatively low. However, the effect of Hg on plant growth and its transfer into food products of plant origin have been studied because of the use of some organomercurial compounds in agriculture. Exceptionally high levels of MeHg intake from a food source occurred upon consumption of rice originating from some mining regions in China. The particular characteristics of rice cultivation involving the flooding of the paddies were demonstrated to enhance the microbial activity, favoring the production of MeHg from inorganic Hg. This newly generated MeHg can be easily taken up by the rice plant, and subsequently accumulated in the rice grains, which are consumed in high amounts in these areas.**[37, 38]** In aquatic environments, on the other hand, the bioaccumulation of MeHg is extremely high, thus making the consumption of fish and seafood the most important source of human MeHg exposure. Once MeHg is produced, it can be easily bioaccumulated and biomagnified across the aquatic food web, reaching the highest levels in the top fish

predators, marine mammals and aquatic birds which are important sources of food for humans around the world. The most vulnerable populations are those for which fish consumption is the major source of proteins. Self-evidently, this vulnerability can be increased if the population lives close to a local Hg pollution source.**[39]** Approximately 95% of the MeHg ingested *via* the diet, mainly *via* fish consumption, is absorbed in the intestine and transferred to the blood stream. There, it mainly adheres to sulfhydryl groups, particularly to those of cysteine, and is distributed to all the body tissues, while only the 5% of the absorbed dose remains in the blood compartment.**[21]** The main target organ of MeHg is the brain and the nervous system, causing cell membrane damage, free radical generation, neurotransmitter disruption and stimulation of neural excitoxins. These damages result in sensory disturbance, constriction of the visual field, deafness, mental disorders, and motoric aberrations, such as ataxia, dysarthria, cramps, tremors and paralysis.**[30, 40]** An important subject of study is the adverse effects that MeHg can cause in neonates, infants and children. MeHg can pass the placenta barrier, inhibiting the fetal brain development, resulting in severe cerebral palsy-like symptoms in the infants, although the mother has no manifestation of any such symptom.**[35]** Some studies of children exposed *in-utero* to MeHg have documented different symptoms and signs such as mental retardation, cerebellar ataxia, primitive reflexes, dysarthria, strabismus, hyper-salivation, epileptic attacks, chrorea and athetosis, growth disorders and hyperkinesias.**[41, 42]** In addition to the brain and nervous system, MeHg can also affect the reproduction system and cause severe damage in the immune and cardiovascular systems, although the data obtained in these studies are still studied to evaluate a possible association between MeHg exposure and the symptoms observed.**[35]**

1.1.4. Biogeochemical mercury cycle

The global biogeochemical Hg cycle comprises the different transformations that Hg can undergo in the atmosphere, land and aquatic ecosystems, as well as its transport between the different compartments.

In the atmosphere, Hg can be present under three main forms: gaseous elemental Hg (Hg(0)), divalent Hg or reactive gaseous mercury (Hg(II) or RGM) and particulate Hg (PHg or Hg(P)). Hg(0) is the most abundant form of Hg in the atmosphere (~95

%). It has a long lifetime in the atmosphere (up to 1 year) because of its relatively low deposition velocity and high vapor pressure.**[43]** These characteristics enable Hg to be globally distributed. The most common divalent mercury form in the atmosphere is $HgCl_2$, and both RGM and PHg are shorter-lived and only constitute ~ 5 % of the THg present.**[44]** These both forms are more soluble in water than Hg(0), and they are deposited into terrestrial or aquatic ecosystems through wet and dry deposition. In addition to divalent Hg, Hg can also be present as organic compounds, such as MeHg and DMHg, although they are considered negligible in comparison with the inorganic forms because they tend to be converted into elemental or RGM due to their high instability.**[45, 46]** The atmospheric chemistry of Hg has to be explained in terms of the conversion processes (see **Figure 1-3**) between the different Hg forms in the atmosphere, Hg deposition and evasion to/from other ecosystems (terrestrial and aquatic). The conversion between different Hg species in the atmosphere comprises redox reactions. The main redox reaction that occurs in the atmosphere is the oxidation of Hg(0) to Hg(II) or to Hg(P). It was stated that this reaction principally occurs due to the presence of oxidants such as OH, O_3 and molecular halogens, although further observations indicate that the oxidation process must be mainly produced by photochemical reactions involving halogens or other radicals, principally Br and OH.**[47]** The occurrence of a reduction process producing Hg(0) has been demonstrated to occur in the atmosphere and also in power plant plumes.**[48, 49]** Hg deposition occurs through wet or dry deposition. Wet deposition involves scavenging of RGM and PHg, and it is more efficient by cold precipitation and snow, respectively. In both cases, the deposition rate can vary seasonally.**[50]** On the other hand, dry deposition involves surface uptake of Hg(0) and Hg(II). Although few measurements have been carried out and the mechanisms have only been poorly characterized, it could be even more important than wet deposition.**[51]** Finally, the evasion of Hg from other environmental compartments into the atmosphere can also be taken into account. This evasion is produced by the reduction of Hg(II) into Hg(0) or *via* desorption processes. At the water-atmosphere interface, this reaction mainly occurs *via* photoreduction, and to a lesser extent, *via* biotic processes. However, also oxidation occurs, and at similar rates as reduction, causing an equilibrium between the two processes.**[52]** The evasion of Hg from soil surfaces to the atmosphere is considered an important source of atmospheric Hg, and the extent to which it occurs depends on the Hg species present, the soil pH, its content of organic matter, the

temperature, wind speed and turbulence, the vegetative cover, microbial activity, barometric pressure and particularly, the amount of solar irradiation.**[53]** Therefore, the terrestrial cycling is extremely closely related with the atmospheric one, because the Hg deposited from the atmosphere has been shown to preferentially re-volatilize (between 5 – 60 %), a process called "prompt recycling".**[54]** Within terrestrial ecosystems, vegetation plays an important role in the absorption and release of Hg, although the chemical processes involved in this exchange require further experiments for clarification.**[55]** In the terrestrial ecosystem, the majority of absorbed Hg resides in the soil, associated with the thiol groups of natural organic matter (NOM), although in places with direct deposition of Hg from industrial or mining processes, Hg has also be found in other mineral forms, such as HgO, $HgCl_2$, Hg_2OCl, $Hg_3Cl_3O_2H$, $Hg_3S_2Cl_2$ and $Hg_3O_2SO_4$.**[56]** The other part of the absorbed Hg which is in solution can be runoff into a watershed or undergo methylation.

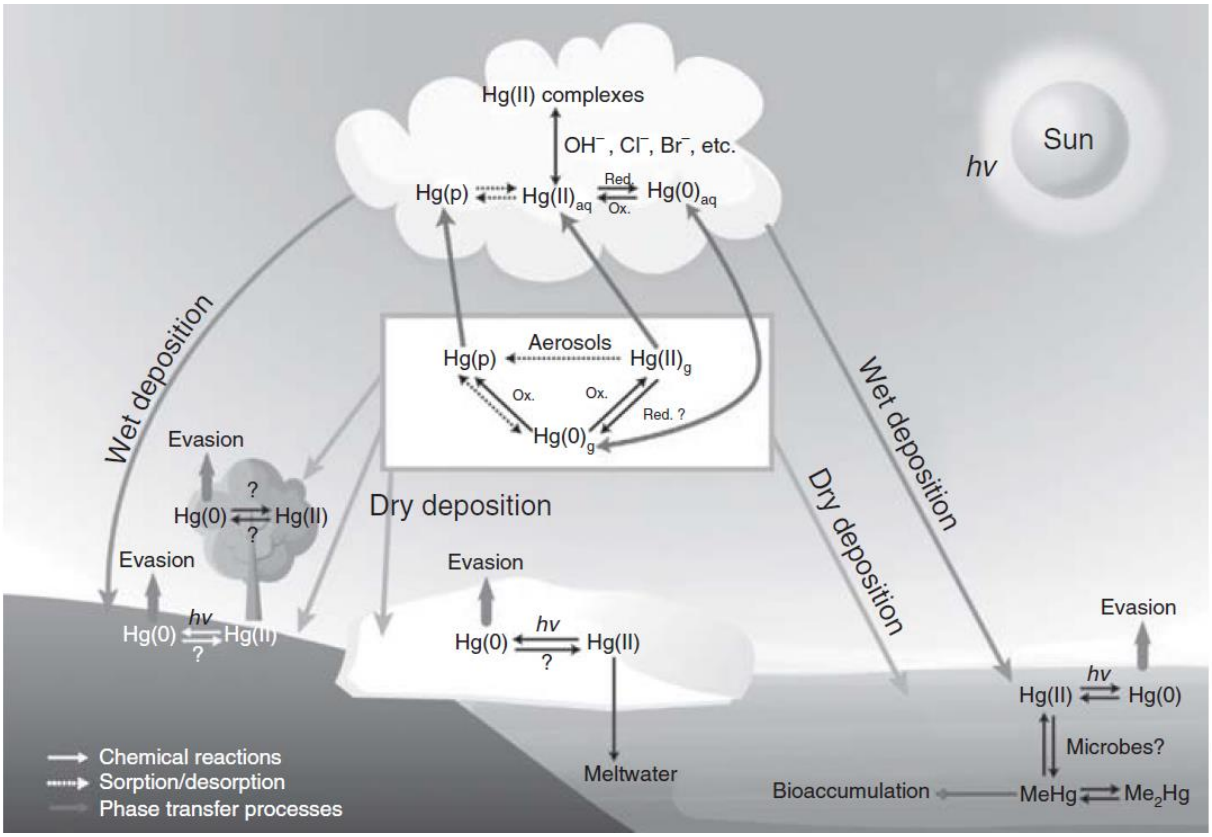

Figure 1-3. Schematic representation of the chemical processes of Hg in the atmosphere and at the interface of the different environmental compartments.**[57]**

The aquatic ecosystems are considered of high relevance within the biogeochemical Hg cycle because of the MeHg formation, bioaccumulation across the food web and subsequent human MeHg exposure *via* fish consumption. Different aquatic ecosystems exist: freshwater, marine and oceanic systems. The freshwater systems include watersheds, lakes, ponds and reservoirs, and the marine systems include estuaries and coastal waters. The Hg cycle in the aquatic ecosystems mainly comprises redox reactions, and methylation/demethylation processes (see **Figure 1-4**). The inorganic Hg (II) species can be photochemically or biotically reduced to Hg(0), which can then volatilize into the atmosphere. At the same time, the Hg(0) or the PHg can be oxidized into soluble or insoluble Hg(II) species, such as HgS, which can precipitate and accumulate in the sediments, although remobilization of the HgS from the sediments has also been observed.**[58]**

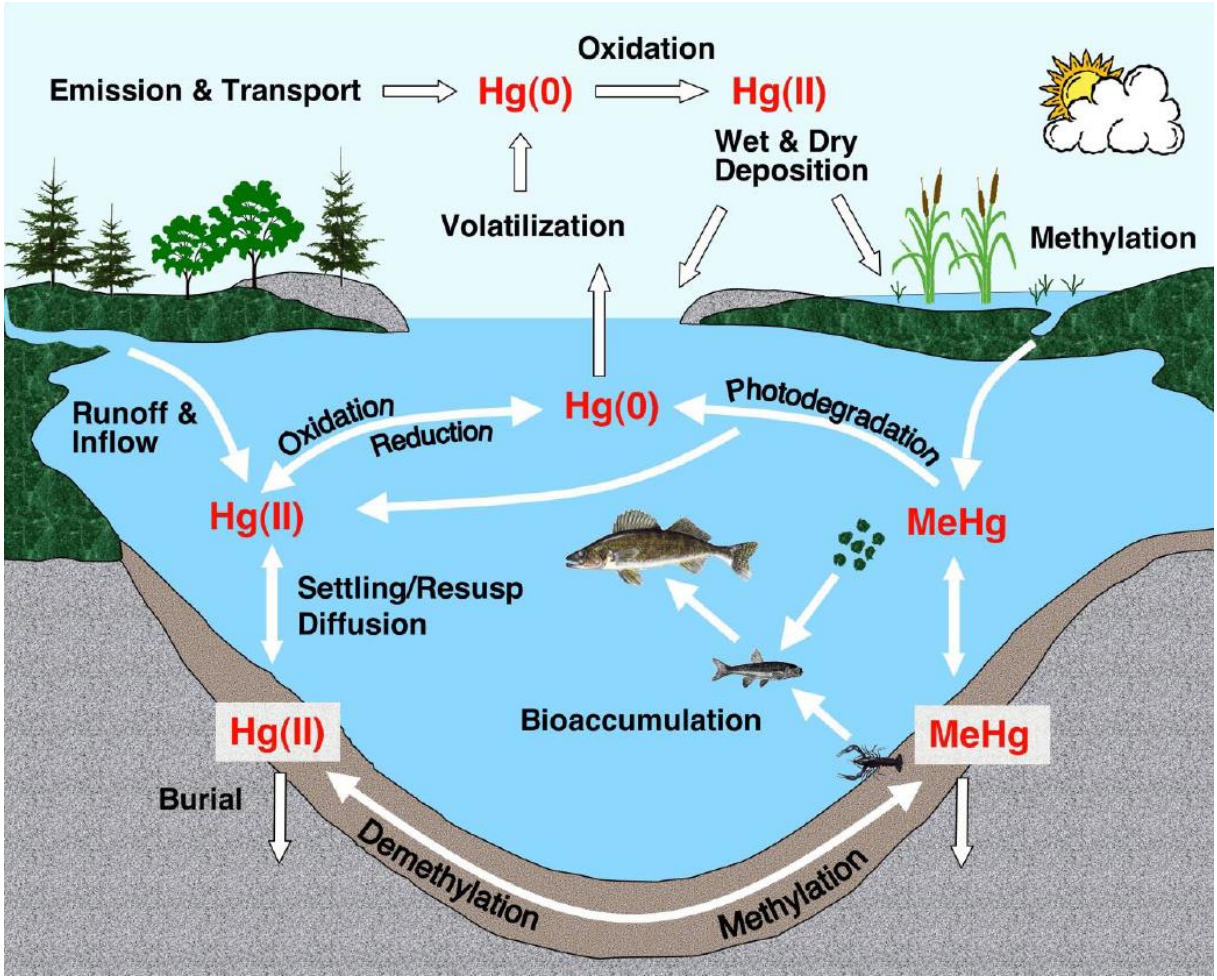

Figure 1-4. Mercury cycling in a lake and its watershed.**[59]**

The methylation and demethylation processes have been widely studied over the years because they directly affect the net amount of MeHg, which is available for the aquatic organisms. Microbial Hg methylation is the main source of MeHg in aquatic ecosystems, although abiotic Hg methylation can also occur in humic substances.**[60]** Microbial methylation occurs mainly in anoxic environments mediated by sulfate-reducing bacteria (SRB), and to a lesser extent by iron-reducing bacteria.**[61, 62]** Different parameters can affect the extent of methylation and among these, dissolved organic matter (DOM) plays a pivotal role.**[63, 64]** The main difference between the aquatic ecosystems is that in open oceans, a deficit of oxygen is not a prerequisite for MeHg formation, while the methylation process can also produce DMHg.**[65]** MeHg degradation can occur *via* photodemethylation or *via* a microbially mediated process. The photodegradation of MeHg is caused by ultraviolet radiation and enhanced by the presence of organic ligands. The extent to which this process occurs, is lower in seawater than in freshwater, although also high rates have also been observed in marine surface waters.**[66]** The biotic demethylation in the water column and in sediments can proceed under aerobic and anaerobic conditions, and oxidative or reductive pathways have been described. The oxidative mechanism is still unclear, although it has been stated to be the major pathway for degradation of MeHg in the environment. Reductive demethylation involves the organomercury lyase enzyme of the microbial *mer* operon (*vide infra*) and leads to the degradation of MeHg into Hg (II) and methane.**[67, 68]**

In summary, the biogeochemical Hg cycle comprises a large number of pathways and transformation (see **Figure 1-5**). An enhanced insight into this biogeochemical cycle is required to finally mitigate the adverse health effects that this toxic heavy metal can produce in humans and wildlife. Along the years, different approaches have been developed for this purpose, and efforts were especially directed at quantification and speciation analysis of Hg. More recently, Hg isotopic analysis has been introduced as it was deemed a powerful tool, capable of shedding more light onto the complex biogeochemical cycle by identifying important Hg sources and unraveling the pathways that Hg follows in the environment.

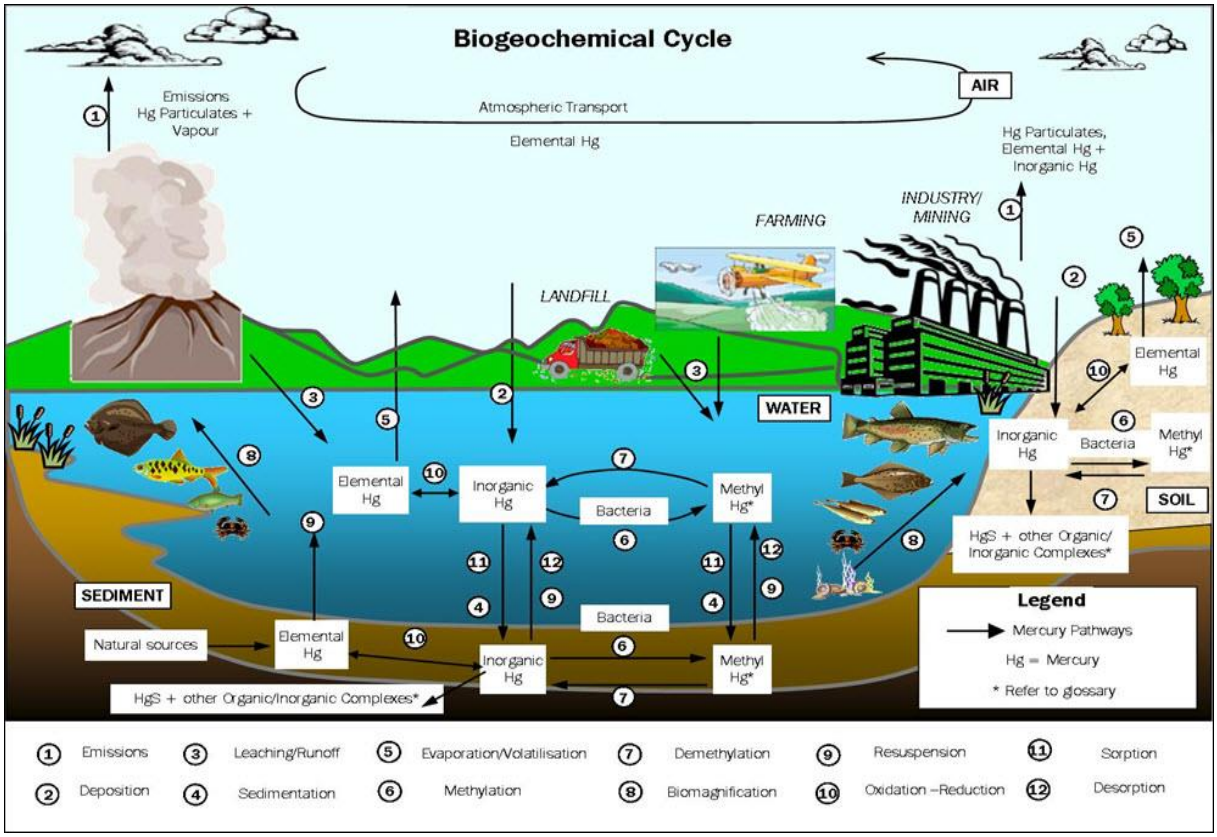

Figure1-5. Schematic representation of the environmental processes that Hg can undergo in the environment.**[69]**

1.2. Mercury isotope fractionation in the environment

1.2.1. Principles of mercury isotope fractionation

The isotopic compositions of the elements are sometimes assumed to be constant in nature, but, some variations occur, mainly as a result of the decay of naturally occurring and long-lived radionuclides and/or natural isotope fractionation effects. The latter is the most common process affecting the isotopic composition of the elements, including Hg. It occurs because different isotopes of the same element can show small differences in their physicochemical behavior, and therefore they can take part to a slightly different extent in physical processes or (bio)chemical reactions.**[70]** However, the natural variations in the isotopic composition of the elements tend to be very small and therefore, high-precision isotope ratio measurement is required to reveal and quantify these small variations, and the use of delta notation in per mil (δ, ‰) has been established to report the deviations relative to a reference standard.

Mercury has seven stable isotopes ^{196}Hg, ^{198}Hg, ^{199}Hg, ^{200}Hg, ^{201}Hg, ^{202}Hg and ^{204}Hg with natural abundances of 0.155, 10.04, 16.94, 23.14, 13.17, 29.73 and 6.83 % respectively.**[71]** However, due to the low abundance of ^{196}Hg and the isobaric interference of ^{204}Hg with ^{204}Pb, these Hg isotopes are typically not measured. The entire scientific community tends to use the ^{198}Hg isotope as the denominator for reporting Hg isotope ratios, following the convention in stable isotope geochemistry that the isotope with the lower mass is used as denominator.**[72]** The reference material NIST SRM 3133 is commonly used as Hg reference standard for calculating δ^{xxx}Hg values.**[71]**

$$\partial^{xxx}Hg\ (‰) = \left(\frac{\left(^{xxx}Hg/^{198}Hg\right)_{sample}}{\left(^{xxx}Hg/^{198}Hg\right)_{NIST\ SRM\ 3133}} - 1 \right) * 1000$$

where xxx = 199, 200, 201 or 202.

Mercury is one of the few elements that can undergo different types of isotope fractionation effects, *i.e.* mass-dependent and mass-independent fractionation (MDF and MIF). MDF is a fractionation effect observed to occur in many thermodynamically or kinetically controlled processes and is governed by the differences between the masses of the nuclei, which affect the frequencies of molecular vibrations.**[73]** For Hg isotopic analysis, MDF is typically reported as δ^{202}Hg and it affects all isotopes of Hg. It has been experimentally observed during evaporation, volatilization, adsorption, leaching, diffusion, reduction, complexation with thiol resins, methylation and demethylation. The effect of MDF allows one to discern between different processes, allowing us to identify the Hg transformations in the environment. A more detailed description of each process is provided in the next section.

MIF is governed by other properties of the nuclei than their mass, such as nuclear spin and charge density. This specific type of fractionation occurs for specific reactions only, thus providing interesting information on them. Most of the studies on Hg isotopic composition in environmental samples testify of MIF affecting the odd-numbered Hg isotopes only. Additionally, recent studies of samples of atmospheric origin have also reported MIF affecting the even-numbered isotopes of Hg, although the mechanisms involved have not been unraveled yet.**[74-76]** The extent of MIF is provided as the difference between a measured δ^{xxx}Hg value and the one predicted assuming pure kinetically controlled MDF.**[71]**

$$\Delta^{199}Hg = \partial^{199}Hg - \left(\partial^{202}Hg * 0.2520\right)$$

$$\Delta^{200}Hg = \partial^{200}Hg - \left(\partial^{202}Hg * 0.5024\right)$$

$$\Delta^{201}Hg = \partial^{201}Hg - \left(\partial^{202}Hg * 0.7520\right)$$

The constant values have been calculated applying the exponential law:

$$\boldsymbol{slope}\left(\frac{\boldsymbol{\delta_{a/b}}}{\boldsymbol{\delta_{c/b}}}\right) = \frac{\ln \boldsymbol{m_a/m_b}}{\ln \boldsymbol{m_c/m_b}}$$

$$\frac{\delta_{199/198}Hg}{\delta_{202/198}Hg} = \frac{\ln 198.968/197.9667}{\ln 201.971/197.9667} = 0.2519$$

$$\frac{\delta'_{200/198}Hg}{\delta'_{202/198}Hg} = \frac{\ln 199.968/197.9667}{\ln 201.971/197.9667} = 0.5023$$

$$\frac{\delta'_{201/198}Hg}{\delta'_{202/198}Hg} = \frac{\ln 200.97/197.9667}{\ln 201.971/197.9667} = 0.7519$$

Two different mechanisms have been proposed as responsible for the odd-MIF, the nuclear volume effect (NVE) and the magnetic isotope effect (MIE). These mechanisms can be distinguish based on the $\Delta^{199}Hg/\Delta^{201}Hg$ ratio. The NVE is controlled by the nuclear radius of the isotopes.**[77]** For the even isotopes, the nuclear radius correlates with mass, but for the odd isotopes this correlation disappears, leading to a smaller size than expected. The resulting higher nuclear charge density and its effect on the surrounding electron cloud results in weaker chemical bonds for the odd-numbered Hg isotopes.**[78]** It has been observed that the NVE occurs mainly during reactions resulting in an equilibrium, such as equilibrium evaporation. The MIE is a kinetically controlled isotope fractionation, mainly accompanying radical reactions and it is caused by the hyperfine interaction between nuclear and electron spins.**[79]** The odd-numbered Hg isotopes have unpaired nuclear spins and thus are subject to spin-selective separation from the even-numbered Hg isotopes during radical reactions.**[80]** The MIE has been observed for aquatic Hg photoreactions, *i.e.* photoreduction of Hg (II) and photodegradation of MeHg. Between the two different mechanisms explaining the MIF, the MIE is considered the predominant effect due to the low magnitude of NVE.

1.2.2. Mercury isotope fractionation in environmental processes

As was explained in the previous section, Hg isotopic analysis can be used to identify the different transformations that Hg can undergo in the environment. This

section attempts to summarize the isotope fractionation effects (MDF and MIF) observed for the different environmental processes that Hg can be involved in (see **Figure 1-6**).

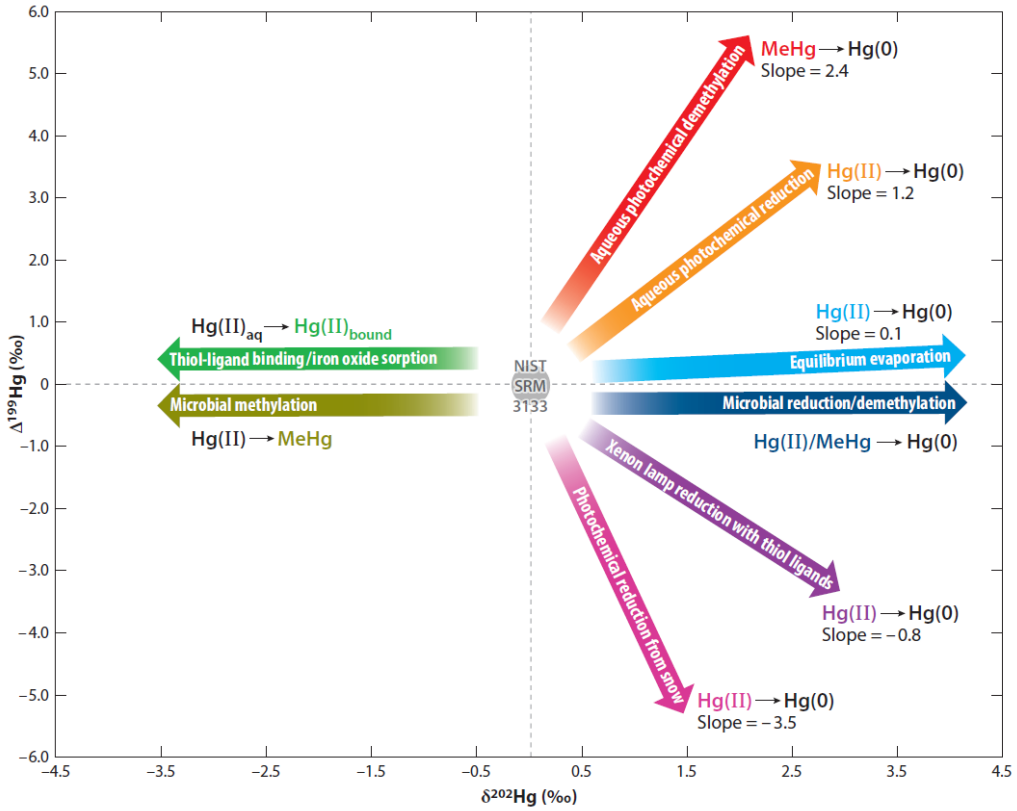

Figure 1-6. Overview of the general patterns in Hg isotope fractionation observed experimentally.**[81]**

1.2.2.1. Physical processes

Volatilization of Hg(0) dissolved in water, producing Hg(0) vapor is accompanied by MDF, with an enrichment of the lighter Hg isotopes in the gas phase.**[82]** The same fractionation effect has been observed to accompany evaporation of metallic Hg(0) into Hg(0) vapor, where the vapor phase is enriched in the lighter isotopes relative to the liquid metal. Additionally, also a small degree of MIF has been observed in these evaporation processes, with condensed Hg vapor being enriched in the odd-numbered Hg isotopes, thus leading to slightly positive Δ^{199}Hg and Δ^{201}Hg values. Based on the ratio obtained in some studies between the MIF values of the two odd Hg isotopes (Δ^{199}Hg/Δ^{201}Hg ~ 1.6), it has been stated that this small MIF is caused by the NVE.**[83, 84]**

It is well known that Hg shows strong affinity for the thiol groups of dissolved organic matter (DOM).**[85]** Therefore, the complexation of Hg(II) by thiol ligands mobilizes Hg from soil and sediments, which makes Hg more available for further important transformations, *e.g.,* methylation.**[86]** Additionally, in soils and sediments with low organic matter contents, the adsorption of Hg to mineral phases, such as iron or other metal oxides, can decrease the mobility of Hg, and thus its transport and bioavailability.**[87]** In both cases, the dissolved Hg(II), *i.e.* the most mobile and bioavailable form of Hg, is enriched in the heavy Hg isotopes, while the Hg sequestered in the mineral or organic matter is isotopically lighter. The same pattern of MDF has also been found in leaching processes, where the water-soluble and $(NH_4)_2S_2O_3$-extractable Hg species were enriched in the heavier isotopes relative to the total Hg in the soil samples.**[88]** Small MIF effects were observed to accompany the complexation with organic matter *via* the thiol groups, and they were attributed to the NVE, produced by shifts in electron density during ligand exchange. However, for adsorption onto minerals and leaching, MIF was observed to be insignificant.

The last physical process that has been recently studied in relation with Hg isotope fractionation is Hg diffusion in air. The MDF accompanying this diffusion can be modeled using a Rayleigh distillation model, with the lighter isotopes diffusing faster than the heavier ones.**[89]**

1.2.2.2. Methylation

The methylation process is of the utmost importance because of the production of the most dangerous of the Hg species. Methylation can occur *via* biotic processes and under abiotic conditions. The methylation process most studied is the biotic methylation mediated by sulfate-reducing bacteria (SRB) under anaerobic conditions. Despite the importance of this reaction, the isotope fractionation accompanying this process has not been widely investigated due to the challenges associated with isotope ratio measurements of the MeHg thus produced, such as the necessity of using organic solvents and of handling highly toxic MeHg-containing solutions. Chromatographic separation coupled on-line to an MC-ICP-MS unit has been preferred over off-line extraction followed by digestion prior to MC-ICP-MS measurement in this context.**[90-92]** Off-line approaches are based on

multiple sequential extraction steps, a process that is tedious and time-consuming, while the resulting MeHg has to be converted into the oxidized Hg^{2+} species prior to CVG-MC-ICP-MS. In the case of on-line approaches, the main issues are degradation of the Hg isotope ratio precision owing to the necessity of dealing with short transient signals (*e.g.*, those produced using GC and/or HPLC), also requiring a more complex and less straightforward data evaluation. Methylation under abiotic conditions in aquatic environments has recently been studied using methylcobalamin as methyl donor compound under dark and visible light conditions.**[93]** In both cases, under biotic and abiotic conditions, MDF has been observed with preferential methylation of the lighter Hg isotopes leading to positive δ-values in the remaining Hg(II) substrate and negative δ-values in the MeHg formed. In addition, MIF has only been observed under abiotic conditions with irradiation.

1.2.2.3. Reduction of Hg (II) and MeHg (demethylation)

As is the case for methylation, also the reduction process can proceed *via* a biotic or abiotic pathway. The importance of the reduction of Hg(II) and MeHg into Hg(0) is linked to the limited bioavailability of Hg(II), which is rather susceptible to methylation than to release of Hg(0) into the atmosphere.

Biotic Hg(II) and MeHg reduction are carried out by micro-organisms, mainly by Hg-resistant aerobic bacteria expressing the *mer* operon, although other anaerobic bacteria are also able to produce the reduction. The *mer* operon is a naturally occurring cluster of genes that confers mercury resistance to bacterial cells. The structure of the *mer* operons vary and are constituted by genes that encode the functional proteins for regulation (*mer*R), transport (*mer*T, *mer*P and/or *mer*C, *mer*F) and reduction (*mer*A and/or *mer*B).**[94]** Most often, bacteria capable of expressing the mercuric reductasa (merA) enzyme are involved in biotic Hg(II) reduction. The complete process comprises the diffusion of Hg(II) across the outer cell membrane, the transport of Hg(II) by merP – merT through the periplasm and inner membrane into the cytoplasm, and the final reduction by MerA. This process leads to a net MDF favoring the reduction of the light Hg isotopes following the Rayleigh fractionation law. Therefore, the Hg(0) produced is enriched in the light isotopes, resulting in negative δ^{xxx}Hg values with respect to the remaining substrate of

Hg(II).**[95, 96]** Biotic MeHg reduction can proceed according to two different pathways, oxidative or reductive. The oxidative pathway has been associated with methanogenic and SRB leading to Hg(II) and CO_2, although little is known about this pathway. The reductive pathway has been studied more intensively and it has also been associated with the mer system. This process also comprises different steps including the breakage of the Hg – C bond by the organomercuial-lyase MerB to produce Hg(II) and its subsequent reduction by *mer*A to Hg(0).**[97]** It is important to point out that the biotic Hg(II) and MeHg reduction are not accompanied by MIF.

Abiotic Hg(II) and MeHg reduction have been described to be typically initiated by DOC, and it can proceed under dark or light conditions. It has been demonstrated that the reduction under sunlight, *i.e.* photochemical pathway, is one of the most important mechanisms to produce Hg(0) in aquatic ecosystems. The main characteristic of the photochemical reduction is that it is accompanied by MIF in addition to the common MDF due to the radical character of the reaction. Depending on the mechanistic conditions, the MIF can be positive or negative. Laboratory experiments were carried out at a high Hg/DOC ratio and under exposure to sunlight. The reduced Hg(0) shows enrichment in the lighter Hg isotopes in comparison with the remaining Hg(II) or MeHg species (higher δ^{202}Hg values) and negative Δ-values due to the MIE. This means that the remaining Hg(II) or MeHg in the solution are significantly enriched in the odd-numbered Hg isotopes (positive MDF and MIF). Also the photoreduction of Hg (II) and MeHg can be differentiated on the basis of the Δ^{201}Hg/δ^{202}Hg and the Δ^{199}Hg/Δ^{201}Hg ratio. The Δ^{201}Hg/δ^{202}Hg ratio was observed to be ~1.5 and ~3.0 for Hg(II) and MeHg photoreduction, respectively. Additionally, the Δ^{199}Hg and Δ^{201}Hg values are linearly correlated leading to a slope of 1.00 for Hg(II) photoreduction and 1.36 for MeHg photoreduction.**[98]** The different slopes observed for the two different photoreductions allow the differentiation of the two processes when applied to real environmental samples. It has been demonstrated that the Hg/DOC ratio in natural waters, the total level of dissolved solids (TDS), the pH of the water and the presence of substances that can act as radical scavengers affect the degree of MIF accompanying photochemical reduction.**[99]** The Hg/DOC ratio also has an important impact on the slope between the Δ-values for MeHg photoreduction, varying between 1.31 for a high Hg/DOC ratio and 1.19 at lower ratios, which agree better with the actual values in natural waters.**[100]** Further experiments were

carried out to evaluate the isotopic effects produced by specific functional groups present in low molecular-weight organic compounds. It was stated that when Hg binds with O/N functional groups, the fractionation is similar to that observed in previous works, however, in the presence of reduced sulfur groups the fractionation is following an opposite MIF trend, with the remaining Hg(II) depleted in the odd-numbered isotopes (negative MIF).**[80]** The same patterns of MIF have been observed in the reduction of Hg(II) associated with halogens in surface snow in the Artic.**[101]** As was mentioned before, also non-photochemical abiotic reduction can occur, although it is not the dominant pathway in the presence of light. The reduction of Hg(II) by $SnCl_2$ and $NaBH_4$ was investigated and the reactant tends to be enriched in the heavier isotopes, while the Hg(0) formed is enriched in the lighter ones, but MIF for the odd-numbered Hg isotopes during the reduction process was found to be insignificant.**[102]** However, in a later work also investigating the abiotic reduction of Hg(II) in the absence of light by DOM and $SnCl_2$, the same trend for MDF was reported, but also significant MIF anomalies were observed. These MIF anomalies were found to enrich the final product in the odd-numbered Hg isotopes and this observation was attributed to the contribution of the NVE rather than that of the MIE.**[103]**

1.2.3. Mercury isotopic composition in environmental matrices

The study of the Hg isotope fractionation occurring during different environmentally relevant Hg transformations (previous section) in combination with the measurement of the isotopic composition of Hg in actual environmental samples can contribute to a better understanding and quantification of the sources and processes involved in the complex global biogeochemical Hg cycle. Many studies have already determined the Hg isotope composition in natural samples of different origin, *e.g.*, geogenic reservoirs, surface soils and sediments, the hydrosphere and atmosphere. A large variability in the Hg isotopic composition of the different natural samples has been observed, but the samples can be grouped in order to obtain a general overview about how the Hg isotopic composition is affected in nature. The Hg isotopic composition of different sample types, expressed as $\delta^{202}Hg$ (MDF) and $\Delta^{199}Hg$ (MIF), is shown in **Figure 1-7**. Generally speaking, the Hg isotopic composition shows an important variability of ~7 ‰ for $\delta^{202}Hg$ and of ~10 ‰ for

Δ^{199}Hg for the complete set of samples. However, it is necessary to point out that the main variability in Δ^{199}Hg values needs to be attributed to the differences between snow samples and/or aquatic organisms, while larger differences have been observed in the case of δ^{202}Hg values. This variability in δ^{202}Hg between different groups is to be expected, because most of the physical and (bio)chemical processes are accompanied by MDF, and the extent of this MDF strongly depends on the characteristics of the specific ecosystem. In addition to the differences between groups, also high variations in δ^{202}Hg values have been found in the case of samples from the same group, *e.g.,* sediments samples can show different δ^{202}Hg values depending of the site where they were sampled, the temperature, organic content, pH, etc. On the other side, the relatively small variability of the Δ^{199}Hg values between most of the samples is a result of the fact that MIF occurs for some specific reactions only. Additionally, the two mechanisms hypothetically at the basis of MIF, *i.e.* the NVE and the MIE produce different extents of MIF, with the resulting Δ-values significantly higher for the MIE than for the NVE. The two exceptional MIF anomalies (snow and aquatic organisms) can be tentatively explained because this MIF is occurring in photochemical reactions, accompanied with different extents of the MIE occurring, depending on the ligand with which Hg is binding, *i.e.* with or without thiol groups, resulting in a preferential release of the odd or the even Hg isotopes, respectively, as was explained in the previous section.**[80, 98, 99]**

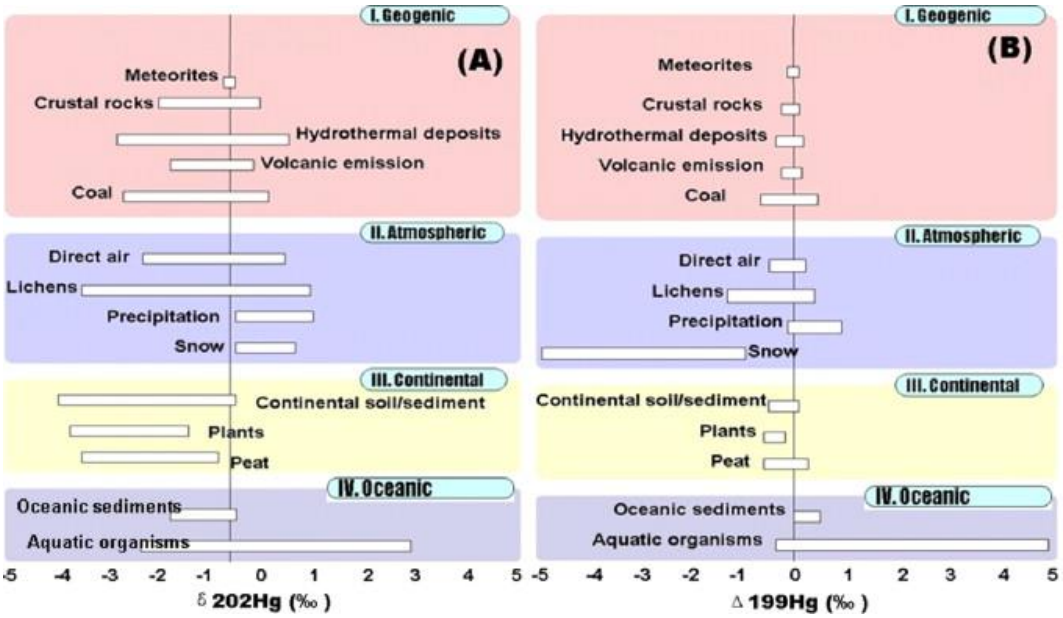

Figure 1-7. Summary of published Hg isotope ratio data in natural samples (A: δ^{202}Hg; B: Δ^{199}Hg).**[104]**

References

[1] C.H. Lamborg, C.R. Hammerschmidt, K.L. Bowman, G.J. Swarr, K.M. Munson, D.C. Ohnemus, P.J. Lam, L.-E. Heimbürger, M.J.A. Rijkenberg, M.A. Saito, Nature, 512 (2014) 65 - 68.

[2] C.T. Driscoll, R.P. Mason, H.M. Chan, D.J. Jacob, N. Pirrone, Environ. Sci. Technol., 47 (2013) 4967 - 4983.

[3] D.C. Adriano, Trace elements in terrestrial environments. New York, Springer-Verlag., (2001).

[4] F. Beckers, J. Rinklebe, Crit. Rev. Environ. Sci. Technol., 47 (2017) 693 - 794.

[5] Y. Zheng, A.D. Jensen, C. Windelin, F. Jensen, Prog. Energ. Combust., 38 (2012) 599 - 629.

[6] J.D. Blum, M.W. Johnson, Rev. Mineral. Geochem., 82 (2017) 733 - 757.

[7] R.P. Mason, K.R. Rolfhus, W.F. Fitzgerald, Mar. Chem., 61 (1998) 37 - 53.

[8] M.S. Landis, R.K. Stevens, F. Schaedlich, E.M. Prestbo, Environ. Sci. Technol., 36 (2002) 3000 - 3009.

[9] W.F. Fitzgerald, C.H. Lamborg, C.R. Hammerschmidt, Chem. Rev., 107 (2007) 641 - 662.

[10] P. Swartzendruber, D. Jaffe, Sources and Transport. A Global Issue. In Mercury in the environment. Pattern and process, M. S. Bank, Ed. University of California press, Berkeley, Los Angeles, London, (2012) 3 - 18.

[11] R.M. Hazen, J. Golden, R.T. Downs, G. Hystad, E.S. Grew, D. Azzolini, D.A. Sverjensky, Am. Mineral., 97 (2012) 1013 - 1042.

[12] G. Liu, Y. Cai, N. O'Driscoll, X. Feng, G. Jiang, Overview of Mercury in the environment. In Environmental Chemistry and Toxicology of Mercury. Ed. John Wiley & Sons, Hoboken, New Jersey, (2012).

[13] UNEP, United Nations Environment Programme. Global Mercury Assessment 2013. Sources, Emissions, Releases and Environmental Transport, (2013).

[14] E.G. Pacyna, J.M. Pacyna, J. Fudala, E. Strzelecka-Jastrzab, S. Hlawiczka, D. Panasiuk, Sci. Total Environ., 370 (2006) 147 - 156.

[15] R.A. Bernhoft, J. Environ. Public Health, (2012) 1 - 10.

[16] G.F. Nordberg, F. Serenius, Acta Pharmacol. Toxicol., 27 (1969) 269 - 283.

[17] T.W. Clarkson, L. Magos, M.R. Greenwood, Biol. Neonate, 21 (1972) 239 - 244.

[18] M. Berlin, R.K. Zalups, B.A. Fowler, Mercury. In Handbook on the Toxicology of Metals. Forth Edition. Ed. Elservier, New York, USA, (2014) 1013 - 1077.

[19] M. Sakamoto, K. Murata, A. Kakita, M. Sasaki, A review of mercury toxicity with special reference to methylmercury. In Environmental Chemistry and Toxicology of Mercury. Ed. John Wiley & Sons, Hoboken, New Jersey, (2012).

[20] H. Gibb, K.G. O'Leary, Environ. Health Perspect. , 122 (2014) 667 - 672.

[21] T.W. Clarkson, L. Magos, Crit. Rev. Toxicol. , 36 (2006) 609 - 662.

[22] S.M.J. Mortazavi, M. Neghab, S.M.H. Anoosheh, N. Bahaeddini, G. Mortazavi, P. Neghab, A. Rajaeifard, Int. J. Occup. Environ. Med., 5 (2016) 101 - 105.

[23] L. Palkovicova, M. Ursinyova, V. Masanova, Z. Yu, I. Hertz-Picciotto, J. Exposure Sci. Environ. Epidemiol., 18 (2008) 326 - 331.

[24] G. Guzzi, M. Grandi, C. Cattaneo, S. Calza, C. Minoia, A. Ronchi, Am. J. Forensic Med. Pathol. , 7 (2006) 42 - 45.

[25] G.M. Richardson, R. Wilson, D. Allard, C. Purtill, S. Douma, J. Gravière, Sci. Total Environ., 409 (2011) 4257 - 4268.

[26] E. Rodríguez-Farre, E. Testai, E. Bruzell, W.D. Jong, G. Schmalz, M. Thomsen, A. Hensten, Regul. Toxicol. Pharmacol., 79 (2016) 108 - 109.

[27] U.G. Bengtsson, L.D. Hylander, Biometals, 30 (2017) 277 - 283.

[28] J. Warkany, D.M. Hubbard, J. Pediatr., 42 (1953) 365 - 386.

[29] B.K. Lasorsa, G.A. Gill, M. Horvat, Analytical Methods for Measuring Mercury in Water, Sediment, and Biota. In Mercury in the Environment. Pattern and process, M. S. Bank, Ed. University of California press, Berkeley, Los Angeles, London, (2012) 3 - 18.

[30] M. Horvat, D. Gibičar, Speciation of Mercury: Environement, Food, Clinical, and Occupational Health. In Handbook of Elemental Speciation II: Species in the Environment, Food, Medicine & Occupational Health. Ed. John Wiley & Sons, Chichester, England, (2005) 281 - 304.

[31] L. Barnes, E.M. McDowell, J.S. McNeil, Virchows Archiv. Abteilung B Cell Pathology, 32 (1980) 233 - 260.

[32] G. De Vos, S. Abotaga, Z. Liao, E. Jerschow, D. Rosenstreich, Immunopharmacol. Immunotoxicol, 29 (2007) 537 - 548.

[33] T. Suzuki, T.I. Takemoto, S. Shishido, K. Kani, Scand. J. Work, Environ. Health, 3 (1977) 32 - 35.

[34] UNEP/IOMC, Global Mercury Assessment, UNEP Chemicals, Geneva, (2002).

[35] D. Mergler, H.A. Anderson, L.H.M. Chan, K.R. Maheffey, M. Murray, M. Sakamoto, A.H. Stern, Ambio, 36 (2007) 3 - 11.

[36] C.C. Bridges, R.K. Zalups, J. Toxicol. Environ. Health, Part B, 13 (2010) 385 - 410.

[37] M. Horvat, N. Nolde, V. Fajon, V. Jereb, M. Logar, S. Lojen, R. Jacimovic, I. Falnoga, L.Y. Qu, J. Faganeli, D. Drobne, Sci. Total Environ., 304 (2003) 231 - 256.

[38] H. Zhang, X. Feng, T. Larssen, L. Shang, P. Li, Environ. Sci. Technol., 44 (2010) 4499 - 4504.

[39] FAO/WHO, Report of the Joint FAO/WHO Expert Consultation on the Risks and Benefits of Fish Consumption, Rome, (2011).

[40] T.W. Clarckson, L. Magos, G.J. Myers, N. Engl. J. Med., 349 (2003) 1731 - 1737.

[41] M. Harada, Crit. Rev. Toxicol., 25 (1995) 1 - 24.

[42] M. Harada, S. Nakachi, T. Cheu, H. Hamada, Y. Ono, T. Tsuda, K. Yanagida, T. Kizaki, H. Ohno, Sci. Total Environ., 227 (1999) 249 - 256.

[43] E.D. Stein, Y. Cohen, A.M. Winer, Environ. Sci. Technol., 26 (1996) 1 - 43.

[44] C.-J. Lin, P. Pongprueksa, S.E. Lindberg, S.O. Pehkonen, D. Byun, C. Jang, Atmos. Environ., 40 (2006) 2911 - 2928.

[45] C.J. Lin, S.O. Pehkonen, Atmos. Environ., 33 (1999) 2067 - 2079.

[46] C.R. Hammerschmidt, C.H. Lamborg, W.F. Fitzgerald, Atmos. Environ., 41 (2007) 1663 - 1668.

[47] N.E. Selin, D.J. Jacob, R.J. Park, R.M. Yantosca, S. Strode, L. Jaeglé, D. Jaffe, J. Geophys. Res., 112 (2007) D02308.

[48] H.M. Amos, D.J. Jacob, C.D. Holmes, J.A. Fisher, Q. Wang, R.M. Yantosca, E.S. Corbit, E. Galarneau, A.P. Rutter, M.S. Gustin, A. Steffen, J.J. Schauer, J.A. Graydon, V.L.S. Louis, R.W. Talbot, E.S. Edgerton, Y. Zhang, E.M. Sunderland, Atmos. Chem. Phys., 12 (2012) 591 - 603.

[49] K.P. Vijayaraghavan, P. Karamchandani, C. Seigneur, R. Balmori, S.-H. Chen, J. Geophys. Res., 113 (2008) D24305.

[50] X. Wang, L. Zhang, M.D. Moran, Atmos. Chem. Phys. Discuss., 11 (2011) 11859 - 11866.

[51] L. Zhang, L.P. Wright, P. Blanchard, Atmos. Environ., 43 (2009) 5853 - 5864.

[52] L. Whalin, E.-H. Kim, R. Mason, Mar. Chem., 107 (2007) 278 - 294.

[53] D.W. Johnson, J.A. Benesch, M.S. Gustin, D.S. Schorran, S.E. Lindberg, J.S. Coleman, Sci. Total Environ., 304 (2003) 175 - 184.

[54] N.J. Selin, D.J. Jacob, R.M. Yantosca, S. Strode, L. Jaegle, E.M. Sunderland, Global Biogeochem. Cycles, 22 (2008) GB2011.

[55] J.A. Graydon, V.L.S. Louis, S.E. Lindberg, H. Hintelmann, D.P. Krabbenhoft, Environ. Sci. Technol., 40 (2006) 4680 - 4688.

[56] C.S. Kim, G.E.B. Jr, J.J. Rytuba, Sci. Total Environ., 261 (2000) 157 - 168.

[57] C.-J. Lin, P. Singhasuk, S.O. Pehkonen, Atmospheric Chemistry of Mercury. In Envionmental Chemistry and toxicology of Mercury. Ed. John Wiley & Sons, Hoboken, New Jersey, (2012) 113 - 153.

[58] A. Iverfeldt, O. Lindqvist, The transfer of mercury at the air/water intarface. In Gas Transfer at Water Surfaces. Ed. Springer, Dordrecht, (1984).

[59] D.R. Engstrom, PNAS, 104 (2007) 16394 - 16395.

[60] S.D. Siciliano, N.J. O'Driscoll, R. Tordon, J. Hill, S. Beauchamp, D.R. Lean, Envion. Sci. Technol., 39 (2005) 1071 - 1077.

[61] E.J. Kerin, C.C. Gilmour, E. Roden, M.T. Suzuki, J.D. Coates, R.P. Mason, Appl. Environ. Microbiol., 72 (2006) 7919 - 7921.

[62] C.C. Gilmour, E.A. Henry, R. Mitchell, Envion. Sci. Technol., 26 (1992) 2281 - 2287.

[63] B.M. Miskimmin, Bull. Environ. Contam. and Toxicol., 47 (1991) 743 - 750.

[64] G.R. Aiken, C.C. Gilmour, D.P. Kabbenhoft, W. Orem, Envion. Sci. Technol., 41 (2011) 217 - 248.

[65] R.P. Mason, A.L. Choi, W.F. Fitzgerald, C.R. Hammerschmidt, C.H. Lamborg, A.L. Soerensen, E.M. Sunderland, Environ. Res., 119 (2012) 101 - 117.

[66] M. Monperrus, A. Tessier, D. Amouroux, A. Leynaert, P. Huonnic, O.F.X. Donard, Mar. Chem. , 107 (2007) 46 - 63.

[67] M.C. Marvin-Dipasquale, J. Agee, C. McGowan, R.S. Oremland, M. Thomas, D. Krabbenhoft, C.C. Gilmour, Environ. Sci. Technol., 34 (2000) 4908 - 4917.

[68] J.K. Schaefer, J. Yagi, J.R. Reinfelder, T. Cardona, K.M. Ellickson, S. Tel-Or, T. Barkay, Environ. Sci. Technol., 38 (2004) 4304 - 4311.

[69] L. Chrystall, A. Rumsby, Mercury Inventory for New Zealand 2008. Pattle Delamore Partners Limited, (2009).

[70] F. Vanhaecke, L. Balcaen, D. Malinovsky, J. Anal. At. Spectrom., 24 (2009) 863 - 886.

[71] J.D. Blum, B.A. Bergquist, Anal. Bioanal. Chem., 388 (2007) 353 - 359.

[72] T.B. Coplen, Rapid Commun. Mass Spectrom., 25 (2011) 2538 - 2560.

[73] E.D. Young, A. Galy, H. Nagahara, Geochim. Cosmochim. Acta, 66 (2002) 1095 - 1104.

[74] L.E. Gratz, G.J. Keeler, J.D. Blum, L.S. Sherman, Environ. Sci. Technol., 44 (2010) 7764 - 7770.

[75] J. Chen, H. Hintelmann, X. Feng, B. Dimock, Geochim. Cosmochim. Acta, 90 (2012) 33 - 46.

[76] Z. Wang, J. Chen, X. Feng, H. Hintelmann, S. Yuan, H. Cai, Q. Huang, S. Wang, C. R. Geosci., 347 (2015) 358 - 367.

[77] J. Bigeleisen, J. Am. Chem. Soc., 118 (1996) 3676 - 3680.

[78] E. Schauble, Geochim. Cosmochim. Acta, 71 (2007) 2170 - 2189.

[79] A.L. Buchachenko, J. Phys. Chem. A, 105 (2001) 9995 - 10011.

[80] W. Zheng, H. Hintelmann, J. Phys. Chem. A, 114 (2010) 4246 - 4253.

[81] J.D. Blum, L.S. Sherman, M.W. Johnson, Annu. Rev. Earth Planet. Sci., 42 (2014) 249 - 269.

[82] W. Zheng, D. Foucher, H. Hintelmann, J. Anal. At. Spectrom., 22 (2007) 1097 - 1104.

[83] N. Estrade, J. Carignan, J.E. Sonke, O.F.X. Donard, Geochim. Cosmochim. Acta, 73 (2009) 2693 - 2711.

[84] S. Ghosh, E.A. Schauble, G.L. Couloume, J.D. Blum, B.A. Bergquist, Chem. Geol., 336 (2013) 5 - 12.

[85] U. Skyllberg, P. Bloom, J. Qian, C. Lin, W. Bleam, Environ. Sci. Technol., 40 (2006) 4174 - 4180.

[86] J.G. Wiederhold, C.J. Cramer, K. Daniel, I. Infante, B. Bourdon, R. Kretzschmar, Environ. Sci. Technol., 44 (2010) 4191 - 4197.

[87] M. Jiskra, J.G. Wiederhold, B. Bourdon, R. Kretzschmar, Environ. Sci. Technol., 46 (2012) 6654 - 6662.

[88] R. Yin, X. Feng, J. Wang, Z. Bao, B. Yu, J. Chen, Chem. Geol., 336 (2013) 80 - 86.

[89] P.G.K.van Groos, B.K. Esser, R.W. Williams, J.R. Hunt, Environ. Sci. Technol., 48 (2014) 227 - 233.

[90] T.A. Jackson, D.M. Whittle, M.S. Evans, D.C.G. Muir, Appl. Geochem., 23 (2008) 547 - 571.

[91] M. Dzurko, D. Foucher, H. Hintelmann, Anal. Bioanal. Chem., 393 (2009) 345 - 355.

[92] P. Rogríguez-González, V.N. Epov, R. Bridou, E. Tessier, R. Guyoneaud, M. Monperrus, D. Amouroux, Environ. Sci. Technol., 43 (2009) 9183 - 9188.

[93] M. Jiménez-Moreno, V. Perrot, V.N. Epov, M. Monperrus, D. Amouroux, Chem. Geol., 336 (2013) 26 - 36.

[94] A.M.A. Nascimento, E. Chartone-Souza, Genet. Mol. Res., 2 (2003) 92 - 101.

[95] K. Kritee, J.D. Blum, M.W. Johnson, B.A. Bergquist, T. Barkay, Environ. Sci. Technol., 41 (2007) 1889 - 1895.

[96] K. Kritee, J.D. Blum, T. Barkay, Environ. Sci. Technol., 42 (2008) 9171 - 9177.

[97] K. Kritee, T. Barkay, J.D. Blum, Geochim. Cosmochim. Acta, 73 (2009) 1285 - 1296.

[98] B.A. Bergquist, J.D. Blum, Science, 318 (2007) 417 - 420.

[99] D. Malinovsky, K. Latruwe, L. Moens, F. Vanhaecke, J. Anal. At. Spectrom., 25 (2010) 950 - 956.

[100] W. Zheng, H. Hintelmann, Geochim. Cosmochim. Acta, 73 (2009) 6704 - 6715.

[101] L.S. Sherman, J.D. Blum, K.P. Johnson, G.J. Keeler, J.A. Barres, T.A. Douglas, Nat. Geosci., 3 (2010) 173 - 177.

[102] L. Yang, R.E. Sturgeon, Anal. Bioanal. Chem., 393 (2009) 377 - 385.

[103] W. Zheng, H. Hintelmann, J. Phys. Che. A, 114 (2010) 4238 - 4245.

[104] R. Yin, X. Feng, X. Li, B. Yu, B. Du, Trends Environ. Anal. Chem., 2 (2014) 1 - 10.

Chapter 2

Mercury isotopic analysis *via* cold vapor generation multi-collector inductively coupled plasma-mass spectrometry (CVG-MC-ICP-MS)

2.1. Basic principles of (multi-collector) ICP-MS

Inductively coupled plasma-mass spectrometry (ICP-MS) is considered one of the most powerful analytical techniques for elemental and isotopic analysis of metals and metalloids in a large variety of sample matrices. The main advantages of ICP-MS are the low limits of detection attainable, its multi-element capabilities, a wide linear dynamic range, relatively simple spectra, high sample throughput, and the ease of combination with different introduction systems and with chromatographic separation techniques. Self-evidently, the technique also has disadvantages, the most important being the occurrence of spectral interferences. An ICP-mass spectrometer has three main parts, the ion source, the mass analyzer and the detection system, and other additional, but no less important parts, such as the sample introduction system and the interface (see **Figure 2-1**). The samples are introduced *via* the introduction system into the ion source. This ion source is an argon inductively coupled plasma (ICP), which can reach very high temperatures, thus allowing the formation of atomic ions (M^+). The ions thus formed are extracted *via* an interface and separated from one another depending on their mass-to-charge (m/z) ratio in the mass analyzer. Finally, the resulting ion beam is converted into an electrical signal in the detection system.

The main components of an ICP-MS unit are briefly described here in general terms. This technique has been widely described in literature, where more detailed information can be found. During this PhD research project, mercury quantification was done *via* single-collector sector field ICP-MS (SC-SF-ICP-MS) and Hg isotopic analysis has been carried out using multi-collector ICP-MS (MC-ICP-MS), which will be described in more detail in the next section.

ICP-MS is primarily designed for the analysis of liquid samples (solutions). The conventional introduction system comprises the nebulizer and the spray chamber. The main objective of the nebulizer is to form the primary aerosol, while the spray chamber is used to smooth the pulses created by the peristaltic pump and to select the smallest droplets of the aerosol formed in order to allow an efficient production of M^+ ions in the ion source. Different types of nebulizers and spray chambers have been developed over the years. Both pneumatic and ultrasonic nebulizers exist, and within the “pneumatic category”, different types can be distinguished, such as concentric, micro-concentric and cross-flow nebulizers. The two more common

designs of spray chambers are the Scott-type double-pass and cyclonic spray chambers, although the combination of both designs is also used and is typically called dual spray chamber. The main disadvantages of the standard sample introduction system are the low introduction efficiency (approximately 1 – 2%), which can compromise the sensitivity, and the limitation to liquid samples (solutions). Other introduction strategies that can be used in ICP-MS include laser ablation, electrothermal vaporization and cold vapor or hydride generation. In this research project, both conventional pneumatic nebulization and cold vapor generation have been used. Special attention has been paid to the hyphenation of a cold vapor generation system to a MC-ICP-MS unit and a more detailed description is included in section 2.2.2.

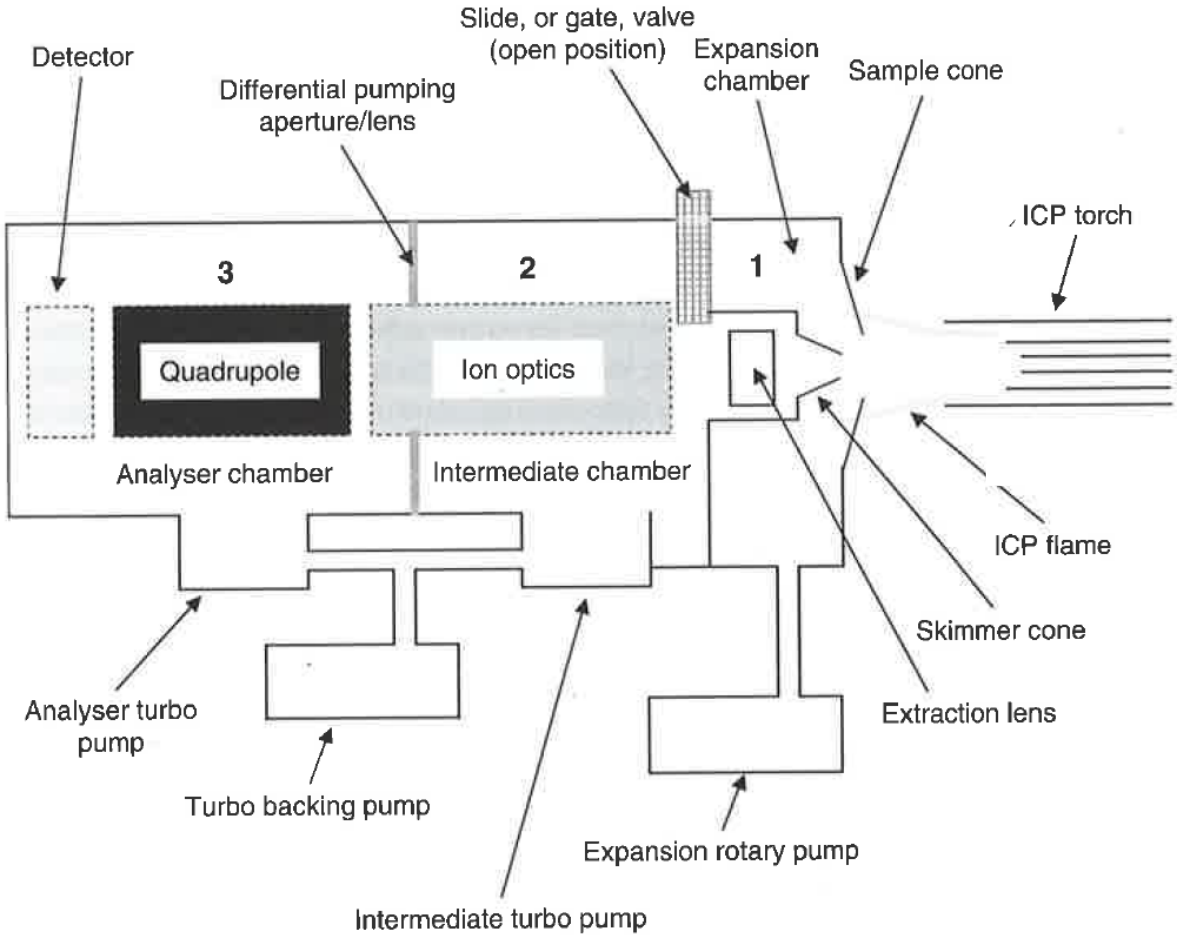

Figure 2-1. Schematic representation of the different parts of an ICP-MS (Q-ICP-MS) unit.**[1]**

As mentioned before, the aerosol produced in the introduction system is transported into the ion source. The plasma ion source is formed at the end of a torch, surrounded by an RF coil, fed by the RF supply. The ion source is an argon plasma, initially formed by an electrical discharge and is further maintained by energy that is transferred from a radio frequency (RF) generator by inductive coupling. The temperature of the plasma varies depending on the location and is between 6000K to 10000K. At that temperature, the sample aerosol is desolvated, the salt particles vaporized, the molecules thus formed atomized and the atoms thus generated finally ionized. The ionization process relies on electron impact ionization, charge transfer ionization and/or Penning ionization and the ionization efficiency depends on the first ionization energy of the element.

The introduction system and the ICP ion source are operated under atmospheric pressure (10^5 Pa), while the mass spectrometer should be under high vacuum conditions ($\leq 10^{-2}$ Pa). Therefore, an interface between these two instrument compartments is required to extract the ions formed in the ICP and transport them to the mass spectrometer. The interface consists of two consecutive water-cooled metal cones, sampler and skimmer, typically made of Ni or Pt, with a small orifice (0.8 – 1.2 and 0.4 – 0.8 mm, respectively). Between the two cones, an intermediate vacuum of ~ 10^2 Pa is maintained *via* the use of a fore-vacuum pump. The ions extracted by the interface are guided to the mass spectrometer by an ion optic system, which also selects the positive ions, rejecting the electrons, the negatively charged and the neutral species.

The ion beam focused by the ion optic system enters into the mass spectrometer where the ions are separated according to their m/z ratio. Three main types of mass spectrometer used in commercially available ICP-MS instrumentation: the quadrupole mass filter (Q), sector field mass spectrometer (SF) and time-of-flight (ToF) analyzer, although the latter is less conventional. All of them have advantages and disadvantages, but two main characteristics that have to be taken into account are mass resolution and abundance sensitivity.**[2]** Mass resolution is defined as the capability of the mass spectrometer to distinguish two neighboring spectral peaks, and two approaches are used to calculate it. One is based on the width at 5% of the experimentally observed spectral peak, while the other considers the valley between two peaks of equal intensity that are considered as separated when the valley intensity does not exceed the 10 % of the peak heights:**[3]**

$$R = \frac{m}{\Delta m_{5\%}} \approx \frac{\left(\frac{m_1 + m_2}{2}\right)}{m_2 - m_1} \qquad \textbf{Equation 2 - 1}$$

Abundance sensitivity expresses the contribution of the tail of a neighboring peak to the signal intensity of the target analyte.

Here, a brief comparison between Q-ICP-MS and SF-ICP-MS instrumentation will be made. A quadrupole filter consists of four parallel cylindrical or hyperbolic rods to which a combination of a direct current (DC) and an alternate current (AC) potential is applied to select ions within a narrow m/z window only (see **Figure 2-2**). The opposite rods are electrically connected, forming two electrode pairs, and the voltage applied to these pairs is the same in magnitude but different in sign. The main advantages of a Q-ICP-MS instrument are its technical simplicity and low cost, while the main disadvantage is the lower mass resolution (m/Δm = 300). With the introduction of the collision/reaction cell (CRC) technology, the capabilities for resolving spectral interferences improved considerably.

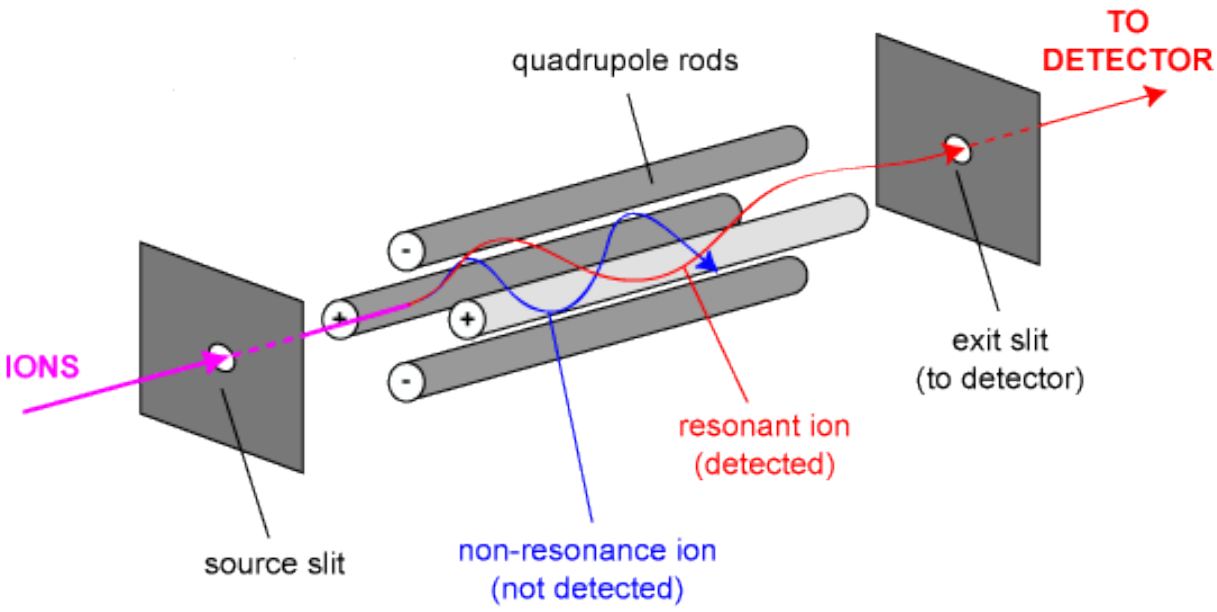

Figure 2-2. Schematic representation of a quadrupole mass spectrometer.**[4]**

A double-focusing sector field mass spectrometer consists of a combination of an electrostatic sector, used as energy filter, and a magnetic sector, used to separate the ion beams according to their m/z ratio. Sector field mass anayzers are characterized by a high mass resolution (up to 10,000 in ICP-MS), low abundance sensitivity, high ion transmission efficiency and the ability to generate flat-topped peaks with trapezoidal shape at low mass resolution. The ThermoScientific Element XR SF-ICP-MS instrument used in this work allows one to work in three different resolution modes: low resolution (LR, R = 300), medium resolution (MR, R = 4000) and high resolution (HR, R = 10,000), but the sensitivity is decreasing roughly 10-fold when increasing the mass resolution setting from LR to MR and from MR to HR.**[5]**

When the ions accelerated by the ion optics enter into the magnetic field they are focused to move along a circular path with a specific radius depending on the m/z ratio by the Lorentz force. The radius of the trajectory depends on the acceleration voltage (V) and the strength of the magnetic field (B):

$$F = \frac{mv^2}{r} = zvB \;\rightarrow\; r = \frac{mv}{zB} = \frac{\sqrt{2Vm}}{B\sqrt{z}} \qquad \textbf{Equation 2 - 2}$$

The electrostatic sector improves the mass resolution by dispersing the ions according to their energy before introducing them into the magnetic sector. For this purpose, the ions are forced to follow a circular path in an electrostatic field created between a positively charged and negatively charged bent plate. The centripetal force required is provided by the electrical field (E), and the radius of the trajectory depends on the kinetic energy of the ion:

$$F = \frac{mv^2}{r} = zE \;\rightarrow\; r = \frac{mv^2}{zE} = \frac{2E_{Kin}}{zE} \qquad \textbf{Equation 2 - 3}$$

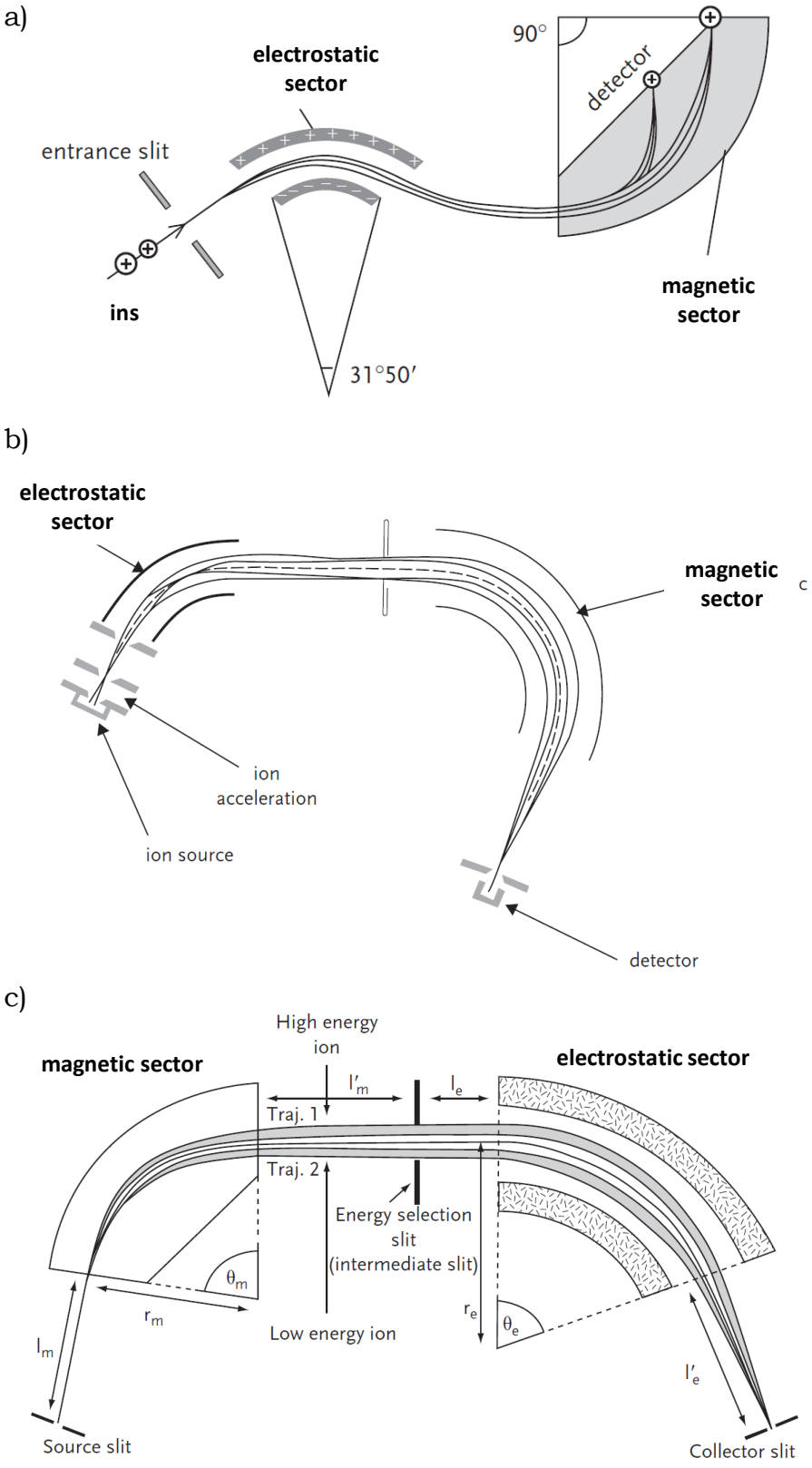

Figure 2-3. Representation of the different double focusing setups. a) Mattauch-Herzog, b) Nier-Johnson, and c) reversed Nier-Johnson.**[2, 3]**

Three main double-focusing geometries have been developed (see **Figure 2-3**): (i) the Nier-Johnson geometry, where a 90° electrostatic sector is followed by a 90° magnetic sector, (ii) the reverse Nier-Johnson geometry; this geometry is opposite to the previous, *i.e.* the 90° magnetic sector is located first and is followed by the 90° electrostatic sector, and (iii) the Mattauch-Herzog geometry that comprises a 30°50' electrostatic sector followed by a curved 90° magnetic sector. The latter allows a simultaneous monitoring of the entire mass spectrum because the focal points of all ion beams are located in one focal plane. In the reverse Nier-Johnson geometry, only for one m/z ratio, the ion beam can be focused. Therefore, the signals have to be measured in dynamic mode, the so-called peak-hopping mode. However, the Nier-Johnson geometry allows a simultaneous separation and monitoring of different ion beams, and it is this geometry that is used in MC-ICP-MS instrumentation for isotopic analysis (see next section).

The final part of an ICP-MS unit is the detection system, where the ion beam coming from the mass analyzer is converted into electrical pulses to be counted by an integrated measurement circuitry or into an amplified electrical current that can be measured and correlated with the amount of analyte in the sample *via* the use of proper calibration approaches. Two types of detector are commonly used in the modern ICP-MS instruments: the electron multiplier and the Faraday cup. An electron multiplier can consist of one continuous dynode or of several discrete dynodes and is typically working in pulse counting mode. The ions collide with the surface made of a semiconducting material, which releases electrons. These electrons are accelerated to the backside of the detector and on their way, they can continue to collide with the surface, liberating more electrons, thus leading to an intense pulse for each incoming ion. The time required to treat the pulses is the detector dead time and it should be taken into account to obtain the correct signal. The electron multiplier can also work in analog mode at higher count rates to extend the lifetime of the detector. The other type of detector is the Faraday cup. It consists of a metallic cup collecting the ions coming from the mass analyzer. These ions are neutralized by electrons from ground, and thus, a potential difference over a high-ohmic resistor is induced. The amplifiers currently used show a resistance of 10^{10}, 10^{11}, 10^{12} or 10^{13} Ω. The Faraday cup is extremely robust, provides an accurate and linear response, and has a long lifetime. However, it has lower sensitivity and shows a slower response than an electron multiplier.

2.2. Mercury isotopic analysis

For a long time, thermal ionization mass spectrometry (TIMS) was considered the technique of choice for isotopic analysis of a wide range of metallic and metalloid elements due to the high precision attainable. However, TIMS also has some important drawbacks, the requirement of laborious sample preparation, the mono-element capabilities, the low sample throughput, and the limitation to elements with low ionization potential (< 7.5 eV). ICP-MS can be seen as a viable alternative because it can avoid some of the drawbacks associated with TIMS. Unfortunately, the use of quadrupole-based ICP-MS (Q-ICP-MS) and single-collector sector field ICP-MS (SC-SF-ICP-MS) are limited to a few types of applications owing to the improved isotope ratio precision (down to ~ 0.05% RSD under ideal circumstances) in comparison with TIMS.**[5]** The introduction of multi-collector ICP-MS (MC-ICP-MS) instrumentation allowed to measure all the isotopes of a target element simultaneously, improving the isotope ratio precision down to 0.002 % RSD.**[6]** At that point, MC-ICP-MS became to the technique of choice for isotopic analysis of the majority of metals and metalloids.

2.2.1. Multi-collector ICP-MS (MC-ICP-MS)

Multi-collector ICP-MS instruments are typically based on a double-focusing sector field mass analyzer with Nier-Johnson geometry followed by an array of Faraday cups as detection system, which allows simultaneous detection of several ion beams. Faraday cups are preferred over ion counters for their linearity, robustness and accuracy, and they also do not suffer from dead time effects. However, some ion counters can also be pre-installed for selected isotope systems.

As was mentioned in Chapter 1, determination of an element isotopic composition provides relevant information on the natural changes produced by different processes in the context of geo- and cosmochemical, environmental, and biomedical applications. Isotope ratio measurement by MC-ICP-MS was demonstrated to reach the accuracy and precision similar to those attainable with TIMS.**[7]** Moreover, the ICP ion source allows the efficient ionization of elements with high ionization energy, which are not accessible *via* TIMS, as is the case for Hg. Therefore, the use of MC-ICP-MS is in many cases the preferred technique for isotopic analysis due to

the higher sample throughput, the wider application range and the more robust character of the ion source, operated at atmospheric pressure.

For the specific case of Hg, its high first ionization energy (10.437 eV) and its high volatility do not allow the measurement of the Hg isotopic composition by TIMS because, this technique is limited to elements with ionization energies below 7.5 eV. Additionally, the natural isotopic composition of Hg is affected by natural isotope fractionation only, which causes only subtle variations in its isotopic composition, such that the precision attainable with Q-ICP-MS or SF-ICP-MS instruments is not sufficient to reveal these small variations. Therefore, MC-ICP-MS is the only technique which can provide sufficiently accurate and precise Hg isotope ratio measurements. One of the main drawbacks of MC-ICP-MS is that it suffers from mass discrimination, which needs to be corrected for in order to obtain accurate isotope ratio results (see section 2.3)

The MC-ICP-MS instrument used during this PhD research project is a ThermoScientific Neptune (Bremen, Germany) installed at the Atomic and Mass Spectrometry unit (A&MS) of the Department of Chemistry at Ghent University (UGent). This instrument is equipped with nine movable Faraday cups connected to 10^{10} (2), 10^{11} (6) and 10^{12} Ω (3) amplifiers. The cup configuration used for Hg isotopic analysis comprises the use of seven Faraday cups, five for different Hg isotopes (^{198}Hg, ^{199}Hg, ^{200}Hg, ^{201}Hg and ^{202}Hg), and two more for the monitoring of the two isotopes of thallium (^{203}Tl and ^{205}Tl) used for mass discrimination correction purposes. For the less abundant ^{198}Hg isotope, a 10^{12} Ω amplifier was used.

Cup configuration							
Isotope	^{198}Hg	^{199}Hg	^{200}Hg	^{201}Hg	^{202}Hg	^{203}Tl	^{205}Tl
Cup name	L3	L2	L1	C	H1	H2	H3
Amplifier (Ω)	10^{12}	10^{11}	10^{11}	10^{11}	10^{11}	10^{11}	10^{11}

2.2.2. Cold vapor generation system (CVG)

As was indicated in the first section of this chapter, ICP-MS is typically used for liquid samples (solutions). One important drawback of the standard sample introduction system (nebulizer + spray chamber) is the low introduction efficiency, compromising the sensitivity of the method. In the case of Hg isotopic analysis, this is of the utmost importance due to the low concentration of Hg in most environment samples. Therefore, alternative introduction systems aiming to improve the Hg introduction efficiency have been under study over the years. Due to the special chemical properties of Hg, the generation of Hg vapor was proposed as the preferred method for Hg introduction. The use of hydride generation (HG) was extensively used for the determination of elements that can form volatile hydrides, such as arsenic, antimony and selenium *via* their reaction with sodium borohydride ($NaBH_4$).**[8, 9]** An extensive description of the corresponding setup for As introduction was provided by Klaue and Blum (1999),**[10]** and it was further improved over the next years. This approach has also been used for the production of Hg vapor for Hg isotopic analysis of cinnabar ores, as described by Hintelmann and Lu (2003).**[11]** Later on, the use of tin chloride ($SnCl_2$) was preferred over $NaBH_4$ due to its specificity for Hg, avoiding hydride formation of other elements.**[12, 13]** Nowadays, it is the preferred introduction system for Hg isotopic analysis applications, although also other introduction systems are used, such as gold trap amalgamation (GTA) and gas chromatography (GC).**[14]** The main advantages of the cold vapor generation (CVG) of Hg over the other approaches are the generation of a continuous stable signal, instead of a transient signal, while the sample throughput is improved. A picture and schematic diagram of the commercially available cold vapor generation and hydride generation system used in this work (HGX-200 from Teledyne Cetac Technologies, US) is shown in **Figure 2-4**.

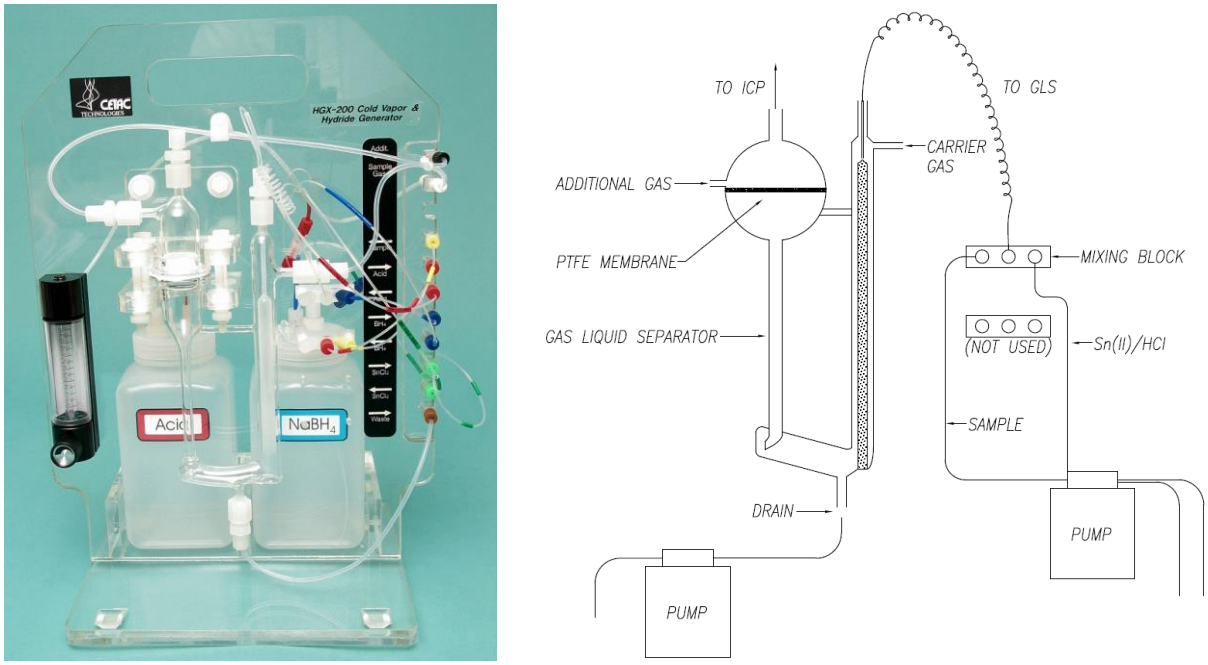

Figure 2-4. HGX-200 Cold Vapor & Hydride Generator from Teledyne Cetac Technologies (US).**[15]**

The cold vapor generation of Hg is based on the production of Hg^0 vapor *via* the reduction of Hg^{2+} to Hg (0) by the use of $SnCl_2$, as follows:

$$Hg^{2+} + Sn^{2+} \rightarrow Hg^0 + Sn^{4+} \quad \textbf{Equation 2-4}$$

It is important to point out that all the Hg present in the liquid sample should be present as Hg^{2+}, therefore pre-oxidation can be carried out prior to CVG if necessary. The liquid sample containing the Hg^{2+} is introduced and mixed with a solution of $SnCl_2$ in a mixing block prior to the introduction in the gas liquid separator (GLS) with a "frosted tip" design, which enhances the efficiency of the gas/liquid phase exchange. The Hg^0 generated is flushed out of the liquid phase with Ar carrier gas. The U-shape of the HGX-200 in combination with the PTFE membrane located after the GLS allows to reduce the signal noise and to achieve a complete gas/liquid separation. Also, an additional current of Ar gas is introduced

after the PTFE membrane to further minimize signal noise and reduce washout time, as well as to improve the stability of the signal.

An in-depth evaluation of the CVG system and comparison with the conventional pneumatic nebulization sample introduction system for Hg isotopic analysis has been carried out in the context of this PhD research project and is summarized in Chapter 3.

2.3. Instrumental mass discrimination

As was previously mentioned, the main drawback of isotopic analysis via ICP-MS is that the raw measurement data are affected by instrumental mass discrimination. This phenomenon produces a bias between the measured isotope ratio and the corresponding true value. Therefore, this phenomenon needs to be corrected for to obtain accurate isotope ratio results. In this section, a brief explanation of this phenomenon, as well as the different correction approaches enabling mass discrimination to be addressed will be described.

2.3.1. Origin of mass discrimination

Instrumental mass discrimination (also called mass bias) in ICP-MS leads to a non-stoichiometric detection of the ions with respect to the original sample, due to a more efficient transport of the ions of a heavier than of a lighter isotope of the analyte. This deviation is typically of the order of 1% per mass unit, but it can be significantly higher for light elements (*e.g.*, up to 25% for lithium **[16]**), and it is much larger than the bias introduced by fractionation in TIMS. Additionally, the mass fractionation observed in TIMS and the mass discrimination produced in ICP-MS are profoundly different.

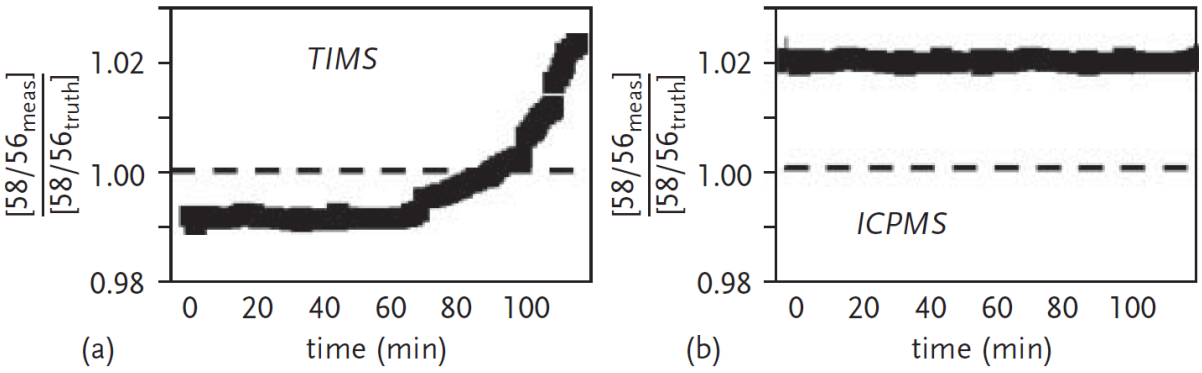

Figure 2-5. Comparison of mass fractionation in TIMS (a) and ICP-MS (b).**[3]**

In TIMS, the mass fractionation is time-dependent, while the mass discrimination in ICP-MS remains essentially stable (see **Figure 2-5**). This difference arises because in TIMS, the preferential ionization/vaporization of the lighter isotopes is at the origin of the phenomenon, while in ICP-MS the ion beam is continuously enriched in the heavier isotopes. The causes of this phenomenon in ICP-MS are not completely understood yet, but have been related with different processes occurring in the plasma source and in the interface region. It is considered mainly as a mass-dependent phenomenon, although cases of mass-independent instrumental mass discrimination have also been reported when using a high sensitivity interface (Jet interface) in the ThermoScientific Neptune, and they have been associated to oxide ion formation.**[17]** The most important contribution has been associated with the space-charge effects, which cause the lighter ions to be displaced out of the center of the ion beam, such that the heavier ions are more efficiently transported to the detector.**[18, 19]** In addition, it has also been partly attributed to the supersonic expansion occurring in the interface region between the sampler and skimmer cone, which leads to a more efficient extraction of the heavier ions as a result of the so-called nozzle effect.**[20, 21]**

It has been demonstrated that the target element concentration and the concomitant matrix have an important effect on the extent of mass discrimination.**[22]** Therefore, isolation of the target element prior the MC-ICP-MS measurements is typically done in order to minimize the effect of the matrix while all sample and standard solutions are concentration-matched.**[23]**

2.3.2. Mass discrimination correction approaches

In order to obtain accurate isotope ratio results *via* ICP-MS, it is necessary to correct for instrumental mass discrimination. Several correction approaches have been proposed over the years and they are basically based on the use of external or internal standardization, or a combination of both.**[24]** However, this terminology is considered ambiguous because no clear consensus exists as to their exact meaning.

External standardization is referring to the measurement of an isotopic standard of the target element with known isotopic composition and comparison of the measured isotope ratio(s) to the corresponding true value(s) to calculate the deviation produced by mass discrimination. As such, a correction factor which should also be applied to the sample can be obtained. The typical way to apply external standardization is in a sample-standard bracketing approach (SSB), in which the sample is measured between "brackets", *i.e.* the measurement of each sample is preceded and followed by a measurement of the isotopic standard. With this approach, it is assumed that mass discrimination evolves linearly with time and that the external standard and the samples are affected equally by mass discrimination. Therefore, it is of the utmost importance that the target analyte is isolated from the concomitant matrix or that a "matrix matched" standard is used, and that the concentration of the target element in both the sample and the external standard match within ± 30%.**[23]** SSB is often the preferred choice for mass discrimination correction due to its simplicity.

Internal standardization can be performed in two different ways, by the use of a pair of isotopes of the analyte that is considered sufficiently constant, or by the use of a pair of isotopes of another element, which is admixed to the sample as internal standard. These two possibilities can be called intra-element or inter-element internal standardization.**[25]** The intra-element standardization can correct for both mass discrimination and natural mass-dependent isotope fractionation of the target analyte, thus allowing to reveal mass-independent contributions. However, this approach has limited applicability, almost exclusively for some analytes with radiogenic isotopes. Therefore, the inter-element internal standardization approach is the most common. The internal standard selected should has at least two isotopes, show a mass number similar to that of the analyte and have a known isotopic composition (preferably certified isotopic composition). Several models have

been proposed over the years, depending on the assumption that the mass discrimination varies according to a linear, power-law or exponential function as a function of the difference in mass between the two isotopes (Δm).**[26]** Nowadays, the so-called exponential Russell's law still remains the most widely used approach for MC-ICP-MS, and here, the mass discrimination factor (f) is assumed to rather vary with the mass of the isotopes instead of with the mass difference between them:**[27]**

$$R_{true} = R_{exp}\left(\frac{m_i}{m_j}\right)^f \quad \textbf{Equation 2 - 5}$$

$$f = \frac{ln\left(R_{true}/R_{exp}\right)}{\ln\left(m_i/m_j\right)} \quad \textbf{Equation 2 - 6}$$

First, the mass discrimination correction factor is calculated for the internal standard. This correction factor can then be subsequently applied for mass discrimination correction for the analyte. It is assumed that both elements display the same behavior ($f_{analyte} = f_{IS}$). However, this assumption could be risky, and further refinements were introduced, based on linear relationships between the correction factors for analyte and internal standard ("Woodhead approach").**[28]**

An alternative approach relies on plotting the natural logarithms of the measured ratios obtained for standard solutions of analyte and internal standard against one another ("Baxter approach").**[29]**

$$\ln R_{analyte,RM} = a + b * \ln R_{IS,RM} \quad \textbf{Equation 2 - 7}$$

where $R_{analyte,RM}$ and $R_{IS,RM}$ are the measured ratios of the analyte and the internal standard for the reference materials, respectively. Also, a and b correspond with the intercept and slope of the regression line obtained. Therefore, the corrected isotope ratio for the sample ($R_{smpl,correct}$) can be calculated as:

$$R_{smpl,correct} = r_{smpl,meas} * \frac{R_{analyte,RM}}{e^{a} * \left(r_{IS,meas}\right)^{b}} \quad \textbf{Equation 2 - 8}$$

where $r_{smpl,meas}$ and $r_{IS,meas}$ are the measured ratios for the analyte and the internal standard in the sample, respectively, with a and b the previously calculated intercept and slope.

These two approaches are currently those most often used for mass discrimination correction in MC-ICP-MS, although the common analyte internal standardization (CAIS approach) has also been evaluated. In this approach, the raw isotope ratios for the analyte and the internal standard of the reference solutions are plotted versus one another and the best fitting straight line is traced through the data points.**[30]**

$$R_{analyte,RM} = a + b * R_{IS,RM} \quad \textbf{Equation 2 - 9}$$

$$R_{analyte,interpolated} = a + b * R_{IS,meas} \quad \textbf{Equation 2 - 10}$$

$$R_{smpl,correct} = r_{smpl,meas} * \frac{R_{analyte,interpolated}}{R_{analyte,ref.meas}} \quad \textbf{Equation 2 - 11}$$

Additionally, the use of the double spike approach has also been used for mass discrimination correction purposes. In this approach the sample is spiked with a standard solution of the analyte enriched in two of its isotopes with known isotope ratio. It can provide accurate and precise isotope ratio data and allows to correct for sample loss during sample preparation. However, it is necessary that the analyte has at least four isotopes, while the isotopically enriched materials are expensive, the sample throughput is low and memory effects may occur.**[31-33]**

The selection of the mass discrimination correction approach should be evaluated for each specific case due to the influence of different factors, such as analyte and matrix. For a large number of applications, the use of a combination of internal and external standardization has been proposed.

For the specific case of Hg, an in-depth evaluation has been done as is presented in chapter 3. However, the final approach selected for mass discrimination correction in all the applications summarized in this thesis is the combination of the "Baxter approach" and the SSB approach as is explained below.

Double mass discrimination correction approach (Baxter + SSB) for the accurate and precise isotopic analysis of Hg

The double mass bias correction approach (Baxter + SSB) is based on both internal and external standardization. First, the internal standard (NIST SRM 997 – Tl – in this case) is added to all solutions: the external standard, i.e. an isotopic reference material of the analyte element (NIST SRM 3133 – Hg – in this case), and the sample solutions. Then, the isotope ratios for analyte element and internal standard are measured in a "bracketing" sequence (standard – sample – standard). After the measurements, the natural logarithm of the raw ratios obtained for the analyte element in the external standard solution (NIST SRM 3133 – Hg) are plotted *versus* the natural logarithm of the raw ratios obtained for the internal standard selected (NIST SRM 997 – Tl). The best-fitting straight line is traced through these data points and its intercept (a) and slope (b) are determined. Correction of the Hg isotope ratios according to the Baxter approach (with Tl as internal standard) uses these values of a and b as shown below.

$$\left(\frac{^{xxx}Hg}{^{198}Hg}\right)_{smpl,correct(Baxter)} = \left(\frac{^{xxx}Hg}{^{198}Hg}\right)_{smpe,meas} * \frac{\left(\frac{^{xxx}Hg}{^{198}Hg}\right)_{NIST\ SRM\ 3133,recomm}}{e^{a} * \left(\frac{^{205}Tl}{^{203}Tl}\right)^{b}} \quad \textbf{Equation 2 – 12}$$

Once the isotope ratios of the analyte element – Hg – have been corrected for mass bias as explained above, additional external correction is applied, based on the corresponding isotope ratios measured for the external standard (NIST SRM 3133 – Hg) solutions measured immediately before and after the sample considered. The

results for the double mass bias correction approach can be presented as (i) isotope ratios and/or (ii) delta values δ (‰), as follows:

$$\left(\frac{^{xxx}Hg}{^{198}Hg}\right)_{smpl,correc\ (Baxter+SSB)} = \left(\frac{\left(\frac{^{xxx}Hg}{^{198}Hg}\right)_{smpl,correct(Baxter)}}{\frac{\left(\frac{^{xxx}Hg}{^{198}Hg}\right)_{NIST\ SRM\ 3133-1,meas} + \left(\frac{^{xxx}Hg}{^{198}Hg}\right)_{NIST\ SRM\ 3133,meas}}{2}}\right) * \left(\frac{^{xxx}Hg}{^{198}Hg}\right)_{NIST\ SRM3133,recomm}$$

Equation 2-13

$$\partial^{xxx}Hg\ (‰)_{(Baxter+SSB)} = \left(\frac{\left(^{xxx}Hg/^{198}Hg\right)_{smpl,correct(Baxter)}}{\frac{\left(\frac{^{xxx}Hg}{^{198}Hg}\right)_{NIST\ SRM\ 3133-1,meas} + \left(\frac{^{xxx}Hg}{^{198}Hg}\right)_{NIST\ SRM\ 3133+1,meas}}{2}} - 1\right) * 1000$$

Equation 2-14

References

[1] S.J. Hill, A. Fisher, M. Liezers, Plasma Generation, Ion Sampling and Focusing. In ICP Mass Spectrometry Handbook. Ed. S. M. Nelms. Blackwell Publising. CRC Press, (2005) 1 - 25.

[2] P.J. Turner, D.J. Mills, E. Schröder, G. Lapitajs, L.A. Iacone, D.A. Haydar, A. Montaser, Instrumentation for low-and high-resolution ICP MS. In Inductively Coupled Plasma Mass Spectrometry. Ed. Wiley-VCH Verlag GmBH, Weinheim, (1998).

[3] F. Vanhaecke, Single-Collector Inductively Coupled Plasma Mass Spectrometry. In Isotopic Analysis. Fundamentals and Applications Using ICP-MS. Ed. Wiley-VCH Verlag GmbH. Weinheim, Germany. (2012) 31 - 75.

[4] P. Gates, Chromatography Mass Spectrometry (GC/MS) at http://www.bris.ac.uk/nerclsmsf/techniques/gcms.html (Last accessed on 30 November 2017), University of Bristol, (2017).

[5] F. Vanhaecke, L. Balcaen, D. Malinovsky, J. Ana. At. Spectrom., 24 (2009) 863 - 886.

[6] M.E. Wieser, J.B. Schwieters, Int. J. Mass Spectrom., 242 (2005) 97 - 115.

[7] A.J. Walder, P.A. Freedman, J. Ana. At. Spectrom., 7 (1992) 571 - 575.

[8] C. Haraldsson, M. Pollak, P. Öhman, J. Ana. At. Spectrom., 7 (1992) 1183 - 1186.

[9] S.T. Anderson, R.V.D. Robért, H.N. Farrer, J. Ana. At. Spectrom., 9 (1994) 1107 - 1110.

[10] B. Klaue, J.D. Blum, Anal. Chem., 71 (1999) 7408 - 1414.

[11] H. Hintelmann, S.Y. Lu, Analyst, 128 (2003) 635 - 639.

[12] D. Foucher, H. Hintelmann, Anal. Bioanal. Chem., 384 (2006) 1470 - 1478.

[13] T.A. Jackson, D.C.G. Muir, Environ. Sci. Technol., 38 (2004) 2813 - 2821.

[14] R. Yin, X. Feng, X. Li, B. Yu, B. Du, Trends Environ. Anal. Chem., 2 (2014) 1 - 10.

[15] Teledyne Cetac Technologies, HGX-200 Advanced Membrane Cold-Vapor and Hydride Generation System Operator's Manual, (2008).

[16] R. Millot, C. Guerrot, N. Vigier, Geostand. Geoanal. Res., 28 (2004) 153 - 159.

[17] K. Newman, P.A. Freedman, J. Williams, N.S. Belshaw, A.N. Halliday, J. Anal. At. Spectrom., 24 (2009) 742 - 751.

[18] S.D. Tanner, Spectrochi. Acta Part B, 47 (1992) 809 - 823.

[19] N. Kivel, I. Günther-Leopold, F. Vanhaecke, D. Günther, Spectrochim. Acta Part B, 76 (2012) 126 - 132.

[20] H. Andrén, I. Rodushkin, A. Stenberg, D. Malinovsky, J. Anal. At. Spectrom., 19 (2004) 1217 - 1224.

[21] F. Albarède, E. Albalat, P. Télouk, J. Anal. At. Spectrom., 30 (2015) 1736 - 1742.

[22] J. Barling, D. Weis, J. Anal. At. Spectrom., 27 (2012) 653 - 662.

[23] F. Albarède, B. Beard, Rev. Mineral. Geochem, 55 (2004) 113 - 152.

[24] L. Yang, Mass Spectrom. Rev., 28 (2009) 990 - 1011.

[25] M. Horsky, J. Irrgeher, T. Prohaska, Anal. Bioanal. Chem., 408 (2016) 351 - 367.

[26] L. Yang, R. Sturgeon, J. Anal. At. Spectrom., 18 (2003) 1452 - 1457.

[27] W.A. Russell, D.A. Papanastassiou, T.A. Tombrello, Geochim. Cosmochim. Acta, 42 (1978) 1075 - 1090.

[28] J. Woodhead, J. Anal. At. Spectrom., 17 (2002) 1381 - 1385.

[29] D.C. Baxter, I. Rodushkin, E. Engström, D. Malinovsky, J. Anal. At. Spectrom., 21 (2006) 427 - 430.

[30] V. Devulder, L. Lobo, K.Van Hoecke, P. Degryse, F. Vanhaecke, Spectrochim. Acta Part B, 89 (2013) 20 - 29.

[31] C. Mead, T.M. Johnson, Anal. Bioanal. Chem., 397 (2010) 1529 - 1538.

[32] S.J.G. Galer, Chem. Geol., 157 (1999) 255 - 274.

[33] J.G. Konter, A.J. Pietruszka, B.B. Hanan, Am. Geophys. Union, (2008) A2102.

Chapter 3

An in-depth evaluation of accuracy and precision in Hg isotopic analysis *via* pneumatic nebulization and cold vapor generation multi-collector ICP-mass spectrometry

Adapted from Rua-Ibarz et. al., Anal. Bioanal. Chem., 408 (2016) 417 - 429

3.1. Introduction

Due to its toxicity, its various natural and anthropogenic sources and its transport over long distances, Mercury (Hg) is one of the most important global pollutants.**[1, 2]** The toxicity of Hg strongly depends on its chemical form, with methyl-Hg compounds being more toxic than inorganic Hg.**[3-5]** Elemental Hg, on the other hand, is volatile, persistent in the atmosphere, prone to long-range atmospheric transport and deposition far from the original source.**[6]** The remarkable behavior of Hg results in a challenge for the scientific community, as new approaches for obtaining a more profound insight into the biogeochemistry of this element are required. The determination of the isotopic composition of Hg is an elegant approach to identify Hg sources and to improve the understanding of its transport pathways, conversions and/or deposition mechanisms.**[7-10]**

However, Hg isotopic analysis is not free from challenges, mainly due to the high precision required to reveal the slight differences in the isotopic composition of Hg between different sources or samples and the very low concentrations at which Hg occurs in some matrices. The isotopic composition of Hg shows natural variation as a result of mass-dependent isotope fractionation (MDF),**[11, 12]** accompanying physical processes and/or bio-chemical reactions.**[13]** These variations are usually reported as per mil deviation (δ^{xxx}Hg ‰) with respect to an isotopic reference material (NIST SRM 3133), as indicated in **equation 3-1**.

$$\partial^{xxx}Hg\ (‰) = \left(\frac{\left(^{xxx}Hg/^{198}Hg\right)_{sample}}{\left(^{xxx}Hg/^{198}Hg\right)_{NIST\ SRM\ 3133}} - 1 \right) * 1000 \qquad \textbf{Equation 3 - 1}$$

where xxx can be 199, 200, 201, 202 or 204. Among the Hg isotopes, ^{204}Hg is less frequently measured due to its lower abundance, the limitation in the number of Faraday cups available and/or potential ^{204}Pb interference.

In addition, the isotopic composition of Hg can also be affected by mass-independent fractionation (MIF), typically exhibited by the odd-numbered isotopes. “Odd-MIF” can be tentatively explained *via* hyperfine coupling between the nuclear spin and the electron cloud of these odd-numbered isotopes and/or by the nuclear field shift effect.**[14, 15]** The latter effect stems from the fact that the nuclei of the

odd-numbered Hg isotopes are smaller than those of their even-numbered "neighbors", as a result of which also the electron cloud surrounding the nucleus is affected differently. Recently, MIF has also been reported for ^{200}Hg. The origin of this "even-MIF" is still unclear, although tentatively related with the photo-initiated oxidation of Hg^0 in the tropopause.**[16, 17]** The 'capital delta' (Δ) has been widely accepted as a suitable way to report MIF, as done previously for sulfur and oxygen.**[18, 19]** Δ^{xxx}Hg is calculated as the difference between the experimentally observed δ^{xxx}value and the corresponding "predicted" value when assuming mass-dependent kinetic fractionation only, as derived from the $\delta^{202}Hg/^{198}Hg$ value, as is exemplified in **equations 3-2, 3-3 and 3-4**.

$$\Delta^{199}Hg = \partial^{199}Hg - \left(\partial^{202}Hg * 0.2520\right) \qquad \textbf{Equation 3-2}$$

$$\Delta^{200}Hg = \partial^{200}Hg - \left(\partial^{202}Hg * 0.5024\right) \qquad \textbf{Equation 3-3}$$

$$\Delta^{201}Hg = \partial^{201}Hg - \left(\partial^{202}Hg * 0.7520\right) \qquad \textbf{Equation 3-4}$$

As the extent of MDF tends to decrease significantly with the increase of the atomic mass, or more accurately with a decreasing relative difference between the masses of the isotopes considered, high-precision mass spectrometry is required for Hg isotopic analysis. However, due to the high volatility and ionization energy of Hg, thermal ionization mass spectrometry (TIMS) does not allow for Hg isotopic analysis. It was only with the introduction of multi-collector inductively coupled plasma-mass spectrometry (MC-ICP-MS) that high-precision isotopic analysis of Hg was enabled, and several works to date have reported on environmental applications relying on isotopic analysis of Hg.**[20-24]** However, even with MC-ICP-MS, Hg isotopic analysis is not self-evident, and a number of pitfalls need to be avoided.

MC-ICP-MS suffers from instrumental mass discrimination,**[25, 26]** resulting in a measured isotope ratio different from the corresponding true value (typically by approx. 1% per amu mass difference between the isotopes). This phenomenon is not completely understood yet, but different processes occurring in the plasma source and in the interface region have been identified as contributions. These include collisional scattering and space-charge effects.**[27, 28]** Also, matrix effects have

been widely reported.**[29, 30]** Different correction approaches to correct for these mass discrimination effects relying on the use of an external and/or an internal standard are used within the scientific community.**[11, 26, 27, 31-33]** External correction is based on the use of an isotopic standard of the analyte element with known isotopic composition and is preferably carried out in a sample-standard bracketing (SSB) approach, *i.e.* the external standard is measured immediately before and after every sample. In this case, mass discrimination is assumed to evolve linearly with time and the interpolated relative difference between the measurement result and the true value for the external isotopic standard is assumed to be valid for the sample as well.**[33]** Also, an internal standard, *i.e.*, typically a pair of isotopes of an admixed element with an atomic mass similar to that of the analyte element,**[34, 35]** can be selected for mass discrimination correction purposes. In this case, a mass bias correction factor can be obtained *via* comparison of the measured and the true values for the internal standard isotope ratio. Several mass bias correction models have been used (*e.g.*, linear law, power law, exponential law, Russell law) depending on how the mass discrimination is assumed to vary as a function of the mass difference between the analyte element isotopes or as a function of the analyte element nuclide masses.**[31, 32]** The Russell law is one of the most widely used approaches in MC-ICP-MS.**[36]** In the original Russell law, it is assumed that the mass bias correction factors for the analyte element and the internal standard are identical, although later studies have demonstrated that this assumption needs to be refined.**[37, 38]** In further improvements of the Russell law, a relationship between the mass bias correction factors for analyte element and internal standard is established using standard solutions, such that later on, the mass bias correction factor obtained for the internal standard admixed to the sample can be converted into a correction factor applicable to the analyte element. For that purpose, the mass bias correction factors (Woodhead approach),**[39]** the ln(raw isotope ratio) values (Baxter approach),**[40]** or the raw isotope ratio values themselves (CAIS approach) **[33]** for analyte element and internal standard are plotted *versus* one another, and the best fitting straight line is traced through the experimental data points. Also other approaches, such as the generalized power law **[41]** or the double spike approach,**[42]** for mass bias correction have been developed.

In addition to the problems arising from mass discrimination, Hg isotopic analysis *via* MC-ICP-MS at low level concentrations of Hg (*e.g.*, biological samples) is not an easy task. Different approaches to overcome the challenge posed by these low concentrations have been proposed in the literature. For instance, sample combustion and subsequent trapping of the Hg on a gold trap can be used as a means of pre-concentration.**[43-45]** However, the sample throughput is strongly reduced with this approach, and the necessity of dealing with transient signals can jeopardize the precision of the results. Meanwhile, several researchers have adapted cold vapor generation (CVG) as the preferred sample introduction strategy for the accurate and precise isotopic analysis of Hg at low concentrations. First, Hg vapor was created *via* reaction of Hg^{2+} with sodium borohydride ($NaBH_4$),**[46]** but later on, stannous chloride ($SnCl_2$) was selected as a more specific reductant for Hg,**[47]** among other to avoid potential interference from ^{204}Pb. As the analyte introduction efficiency with CVG is much higher (theoretically 100%) than with pneumatic PN (from 1–2 % for a 1 mL min^{-1} concentric nebulizer to several % for a microconcentric version **[48]**), the corresponding enhancement in Hg^+ signal intensity allows one to measure at lower concentrations, at which other approaches have failed. A very important additional advantage of CVG over other introduction systems, is the fact that Hg is efficiently separated from the concomitant matrix, such that chromatographic isolation of Hg prior to MC-ICP-MS analysis, as required with PN, can be avoided. Of course, also in the case of sample introduction with CVG, instrumental mass discrimination needs to be corrected for. An external standard in an SSB approach is typically used for this purpose, but also the use of Tl as internal standard for mass bias correction has been reported on.**[49-51]** In this approach, a Tl standard solution with known isotopic composition is nebulized and the corresponding aerosol is desolvated before it is admixed to the Hg-containing carrier gas stream from the CVG unit. In both configurations, dry plasma conditions are obtained, which can sometimes give rise to a lower plasma robustness and to plasma instability.**[52]**

Several papers to date have reported on the use of CVG for the isotopic analysis of Hg in a variety of applications. However, no systematic comparison between or in-depth evaluation of Hg isotopic analysis *via* PN-ICP-MS and CVG-MC-ICP-MS can be found in the literature. Therefore, in the context of the SIB-09 "Elements" project, funded by EMRP (European Metrology Research Programme of EURAMET),

we have carried out an extensive study, aiming to provide National Metrology Institutes (NMIs) with sufficient information as to which approach to use in the characterization of future Hg isotopic reference materials. The effect of several experimental parameters with sample introduction *via* PN and *via* CVG on the figures of merit have been assessed and the capabilities and limitations of various approaches to correct for mass discrimination in the context of Hg isotopic analysis have been compared. This systematic study also involved a comparison of PN and a dual introduction system based on the combination of CVG for Hg introduction and PN for Tl, the internal standard selected for correction for mass discrimination (simply called CVG henceforth). In the latter case, wet plasma conditions are obtained *via* the introduction of an aqueous solution – also containing Tl isotopic standard – into the Hg vapor containing carrier gas coming from the CVG unit. These are expected to provide higher plasma robustness than dry plasma conditions.**[52]** Hg isotopic analysis *via* the final PN-MC-ICP-MS and CVG-MC-ICP-MS protocols was assessed using the metallic Hg reference material UM-Almaden, and the results thus obtained were compared with literature values available for this reference material. Additionally, various reference materials (RMs) with different matrix compositions were analyzed *via* CVG-MC-ICP-MS for their Hg isotopic composition. While older RMs were used for validation purposes, novel Hg isotopic data are provided for the latest generations of some biological RMs.

3.2. Experimental

3.2.1. Instrumentation and sample introduction system

The isotope ratio measurements were performed using a ThermoScientific Neptune (Germany) multi-collector ICP-MS instrument, equipped with nine Faraday collectors. Two different introduction systems were evaluated: (i) conventional PN for the introduction of Hg – as analyte element – and Tl – as an admixed internal standard to correct for mass discrimination effects – as a wet aerosol produced by a concentric nebulizer (100 μL min^{-1}) fitted onto a dual spray chamber, consisting of a cyclonic and a Scott-type sub-unit, and (ii) the combination of CVG for Hg introduction using a HGX-200 Cold Vapor & Hydride Generation unit (Teledyne Cetac Technologies, US) and PN for Tl introduction.**[52, 53]** The latter combination will be simply referred to as 'CVG' in the further text. In the HGX-200 unit, Hg^{2+}

was reduced with $SnCl_2$ into Hg(0), which was transported using Ar carrier gas into the ICP ion source. The wet aerosol containing Tl is mixed with the Hg vapor coming from the HGX-200 unit *via* a "T piece". **Figure 3-1** provides a schematic representation of both introduction systems and, in **Table 3-1**, the operating conditions for each configuration have been summarized. Both setups were studied and the figures of merit thus obtained will be documented throughout this chapter.

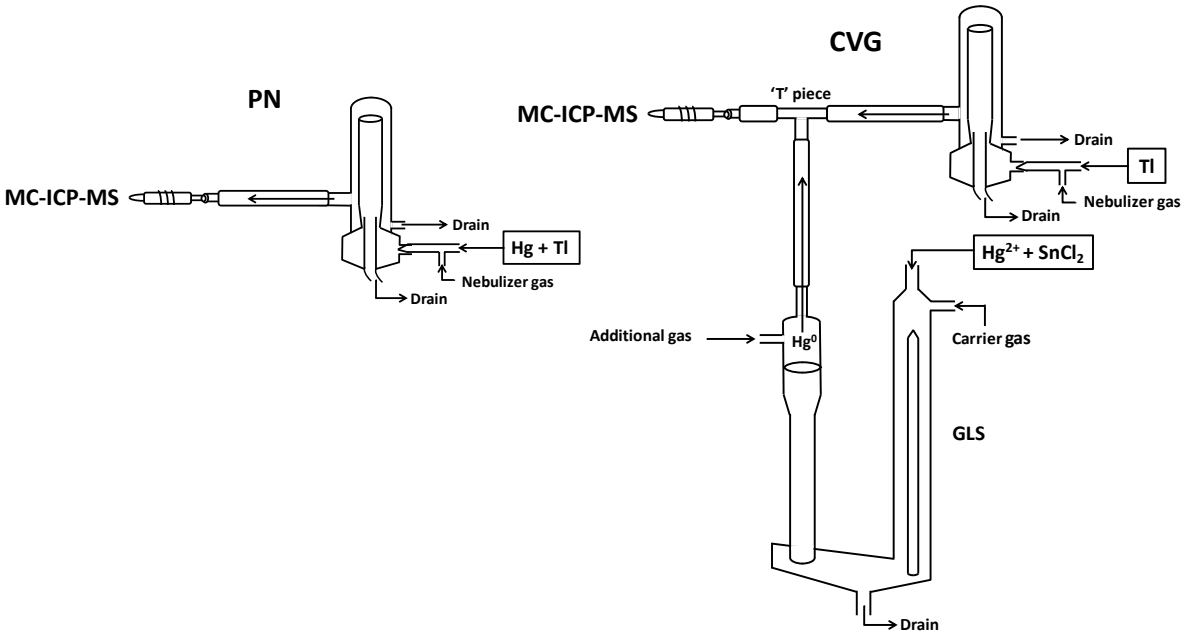

Figure 3-1. Schematic representation of both sample introduction systems evaluated in this study: pneumatic nebulization (PN) and the dual introduction system for the simultaneous introduction of gaseous elemental Hg – using a cold vapor generation unit – and Tl – by pneumatic nebulization – *via* mixing in a "T piece" (CVG).

Table 3-1. Instrument settings and data acquisition parameters for the Neptune MC-ICP-MS unit.

Neptune MC-ICP-MS						
Cup configuration						
L3	L2	L1	C	H1	H2	H3
^{198}Hg	^{199}Hg	^{200}Hg	^{201}Hg	^{202}Hg	^{203}Tl	^{205}Tl
Instrument settings						
RF power (W)	1250 – 1300					
Cool gas flow rate (L min^{-1})	13					
Auxiliary gas flow rate (L min^{-1})	0.70					
Nebulizer gas flow rate (L min^{-1})	0.70 – 0.75					
Carrier gas flow rate (L min^{-1})	0.19 – 0.21					
Additional gas flow rate (L min^{-1})	0.03 – 0.04					
Uptake rate sample – Hg (mL min^{-1})	0.7					
Uptake rate Tl (mL min^{-1})	0.17					
Uptake rate $SnCl_2$ (mL min^{-1})	0.7					
Uptake time (s)	100					
Wash time (s)	180					
Sensitivity ^{202}Hg (µg L^{-1}) mV	120 - 190					
Sampler cone	Ni Thermo Scientific					
Skimmer cone	Ni, H-type Thermo Scientific					
Resolution	Low resolution					
Mode	Static mode					
Data acquisition parameters						
Integration time (s)	4					
Blocks	5					
Cycles/block	10					
Total cycles	50					

A Thermo Element XR single-collector sector-field ICP-MS instrument was used for quantitative Hg determination. The introduction system comprises a 100 µL min^{-1} concentric nebulizer and a cyclonic spray chamber. The selected instrument settings for elemental assay are provided in **Table 3-2**.

Table 3-2. Instrument settings and data acquisition parameters for the Element XR SF-ICP-MS unit (quantitative Hg determination).

Element XR SF-ICP-MS	
Instrument settings	
RF power (W)	1250
Cool gas flow rate (L min^{-1})	15
Auxiliary gas flow rate (L min^{-1})	0.85
Nebulizer gas flow rate (L min^{-1})	0.97 – 1.05
Resolution	Low resolution
Scan type	EScan
Data acquisition parameters	
Mass window (%)	150
Search window (%)	150
Integration window (%)	80
Sample time (s)	0.01
Samples/peak	30
Total analysis time/sample (s)	90
Nuclides monitored	^{103}Rh, ^{202}Hg

3.2.2. Reagents and standards

High-purity water (resistivity > 18.2 MΩ.cm) was obtained from a Milli-Q Element water purification system (Millipore, France). Pro-analysis 14 M HNO_3 and 12 M HCl (ChemLab, Belgium), further purified by sub-boiling distillation, and 9.8 M H_2O_2 (Fluka, Belgium) were selected for the purpose of sample digestion and dilution. Pro-analysis $SnCl_2.2H_2O$ (3% $SnCl_2$ in 1.2 M HCl) was used for Hg^{2+} reduction in the CVG unit. When PN was used, $KBrO_3$ (0.01 mM $KBrO_3$ in 0.12 M HCl) was added to all sample and wash solutions (0.35 M HNO_3) to avoid Hg volatilization and reduce memory effects. Both solutions were made fresh every day and the $SnCl_2$ solution was bubbled with purified Ar during 30 min in order to avoid possible Hg contamination.

Two standard solutions of Hg – one based on the isotopic reference material NIST SRM 3133 and an in-house standard solution (Inorganic Ventures, The Netherlands, Lot: F2-HG02105) – and a standard solution of Tl – based on the isotopic reference material NIST SRM 997 – were appropriately diluted (with 0.35 M HNO_3 for PN, while for CVG, 0.35 and 0.7 M HNO_3 was used for Tl and Hg solutions, respectively) and used throughout the work for optimization, method development and validation purposes. Appropriate dilutions of single-element standard solutions (1 g L^{-1}; Instrument Solutions, The Netherlands) were used in the quantification of the analyte element Hg (with Rh as internal standard) and for evaluation of the effect of concomitant elements – Ba, Ce, Cl, Cs, Na and Sb – on Hg isotope ratio results.

3.2.3 Samples and sample preparation

The reference material UM-Almaden was selected for further evaluation of the accuracy and precision attainable in Hg isotopic analysis, using both introduction systems (PN and CVG). Seven reference materials – NIST SRM 2704 (Buffalo River sediment), NRC-CNRC DORM-1, DORM-2 and DORM-4 (Fish protein), NRC-CNRC TORT-2 and TORT-3 (Lobster hepatopancreas), and BCR CRM 464 (Tuna fish) – were analyzed *via* CVG-MC-ICP-MS and, when possible, the experimentally determined Hg isotope ratio results were compared to the corresponding values reported in the literature (see **Table 3-7**).

Digestion of the samples analyzed was accomplished *via* acid digestion in closed Teflon® Savillex beakers, which were pre-cleaned with HNO_3 and HCl and subsequently rinsed with Milli-Q water. The selected protocol consists of digestion of approx. 0.2 - 1 g of sample with 3 mL of 14 M HNO_3 and 1 mL of 9.8 M H_2O_2. To complete the procedure, the samples were heated on a hot plate at 110 °C overnight. The resulting solutions were appropriately diluted to 5 µg/L of Hg for elemental and isotopic analysis.

3.3. Results and discussion

3.3.1. Effect of instrument settings and acquisition parameters

In order to obtain the best analytical performance for the isotopic analysis of Hg *via* MC-ICP-MS using either PN or CVG as introduction system, the influence of the most important instrument settings and data acquisition parameters was evaluated.

First, the effect of the combination of RF power and different gas flow rates – of nebulizer gas for PN and of carrier, nebulizer and additional gases for CVG (see a diagram of the setup in **Figure 3-1**) – was tested as these are the most important parameters affecting the intensity and stability of the Hg^+ signal. The complete sets of results are shown in **Figure 3-2** and the conditions finally selected in **Table 3-1**. An approximately 20-fold increase in the Hg^+ signal intensity was achieved with CVG in comparison to PN. There was no significant effect on the precision at equal signal intensities > 0.5 V (see also section 3.2). Thus, according to the results shown in section 3.2 and aiming at identifying optimum conditions in further experiments, the concentration of Hg was selected to be 200 μg L^{-1} and 10 μg L^{-1} for PN and CVG, respectively.

Once the optimum instrument settings were selected for each configuration, the data acquisition parameters – integration time and number of cycles – were optimized in order to reach an internal precision ≤0.002% RSE, without compromising the measurement time to values strongly affecting the sample throughput.

Integration times in the range of 1 – 16 s were evaluated, with the number of cycles fixed at 50, and the results obtained for each configuration are summarized for the $^{202}Hg/^{198}Hg$ isotope ratio in **Figure 3-3A**. An important degradation of the internal precision was observed for integration times < 4 s, while for integration times > 4 s the precision was only slightly better than at 4 s.

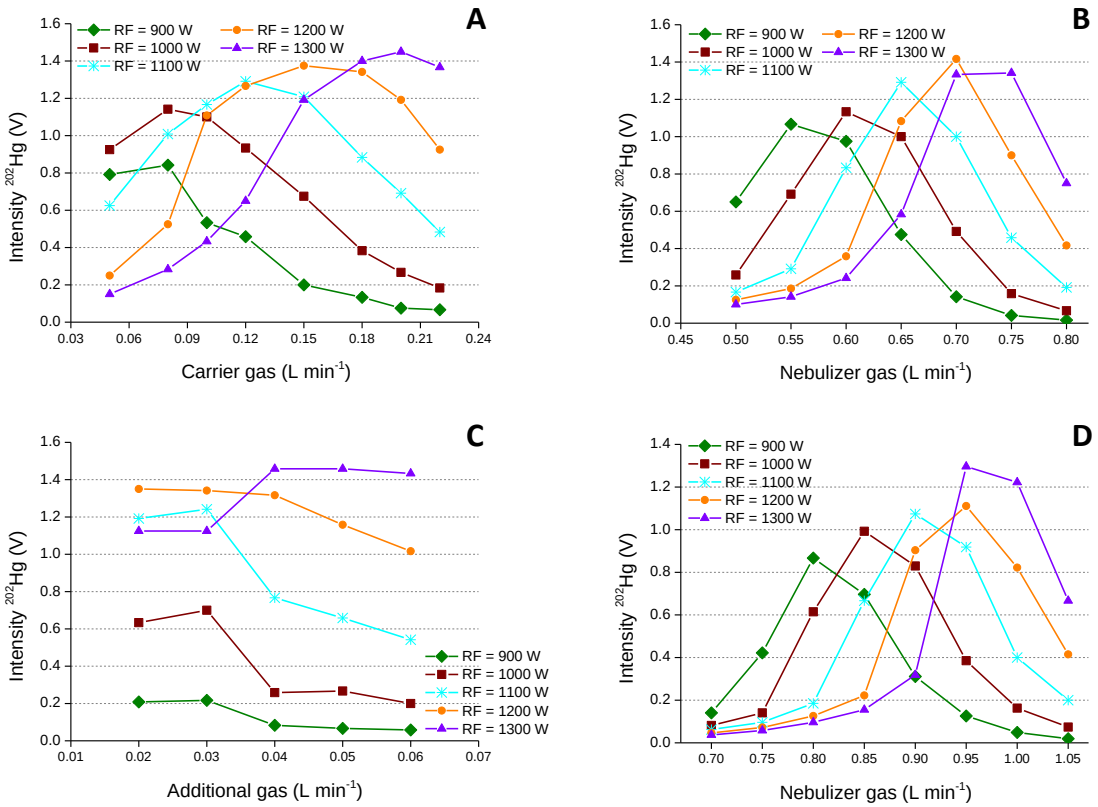

Figure 3-2. Effect of the RF power on the signal intensity for ^{202}Hg using different gas flow rates for CVG (A, B and C) and PN (D) using 10 µg L^{-1} and 200 µg L^{-1} of Hg, respectively. For A, nebulizer and additional gas flow rates were fixed at 0.735 and 0.04 L min^{-1}, respectively. For B, carrier and additional gas flow rates were fixed at 0.2 and 0.04 L min^{-1}, respectively. For C, nebulizer and carrier gas flow rates were fixed at 0.735 and 0.2 L min^{-1}, respectively. See **Figure 3-1** for a better understanding of the different gas flows.

A similar tendency was found for both PN and CVG, and thus, a compromise between precision and measurement time was achieved at 4 s, which was selected as the optimum integration time and this value was used throughout further work. With the integration time fixed at 4 s, optimization of the number of cycles was carried out. MC-ICP-MS software allows one to divide a cycle into a number of blocks, however, Hintelmann *et al.***[46]** have demonstrated that only the final number of cycles (regardless of how the cycles are divided into blocks) affects the accuracy and precision of the isotope ratio measurements. Therefore, the number of cycles was studied in the range of 10 to 300. As can be seen in **Figure 3-3B**, 50

cycles provided suitable precision without resulting in an excessively long total acquisition time.

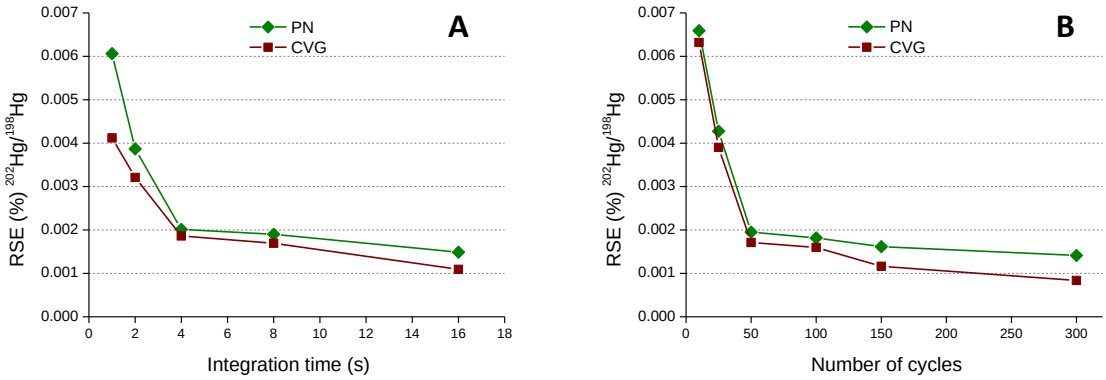

Figure 3-3. Effect of the integration time and number of cycles on the internal precision for the raw $^{202}Hg/^{198}Hg$ isotope ratio values using both introduction systems, PN (200 µg L^{-1} Hg) and CVG (10 µg L^{-1} Hg) for approximately the same $^{202}Hg^{+}$ signal intensity (1.1 – 1.3 V).

3.3.2. Optimization of the concentrations of Hg and Tl

It is well known that the concentrations of analyte and internal standard have an important effect on the accuracy and precision of isotope ratio results.**[11]** This is often even more relevant in the case of Hg, because of its typically low concentrations in real samples, while as a result of important memory effects, excessively high concentrations of Hg also need to be avoided. As this study was focused onto providing National Metrology Institutes (NMIs) with sufficient information as to which approach to use in the characterization of future Hg isotopic reference materials, also the optimum analyte element concentration could be evaluated. Self-evidently, in real-life applications the Hg concentration in the sample is often the limiting factor. For evaluating the capabilities and limitations of the approaches studied, and in order to establish the optimum concentrations of analyte element and internal standard, several experiments were conducted for both introduction systems, PN and CVG, using NIST SRM 3133 for Hg and NIST SRM 997 for Tl. The results obtained were corrected for mass discrimination using the Baxter approach followed by SSB, which was selected as the approach of choice, as is explained in the next section.

First, the effect of the Hg concentration was evaluated by fixing the concentration of Tl at 20 µg L^{-1}, while the concentration of Hg was varied in the range of 50 to 500 µg L^{-1} and 1 to 20 µg L^{-1} for PN and CVG, respectively. These concentrations were selected such that accuracy and precision (n = 15) obtained using both introduction systems could be compared at similar Hg^+ signal intensities. As the same conclusion was obtained for all the Hg isotope ratios studied, only an example of such results is shown in **Figure 3-4A**, which represents the variation in the $^{202}Hg/^{198}Hg$ isotope ratio results and the accompanying RSD (%) – left y-axis – and the $\delta^{202}Hg$ (‰) and accompanying SD – right y axis – as a function of the signal intensity of ^{202}Hg. As can be seen, the concentration does not seem to exert a clear influence on the accuracy of the isotope ratio results using either of the two introduction systems studied. However, with CVG, the precision seems to be strongly affected by the Hg^+ signal intensity (0.004 – 0.024 % RSD), while with PN, the impact of the Hg concentration on the precision seems to be less pronounced (0.004 – 0.007 % RSD). It was verified that this observation was reproducible. The reason for this different effect on the precision attainable at equal signal intensities is not clear to us. Based on these results, it can be concluded that in the case of CVG, at signal intensities below ca. 0.5 V ($^{202}Hg^+$ signal intensity), the precision is substantially deteriorated, while in the case of PN, the degradation in precision is less outspoken. However, at signal intensities > 0.5 V, no significant differences were found between the precision obtained using both introduction systems, in spite of the considerable differences in concentration, and thus, 200 µg L^{-1} and 10 µg L^{-1} were selected as suitable Hg concentrations for further experiments with PN and CVG, respectively.

Once the effect of the concentration of Hg was evaluated and an appropriate analyte element concentration was selected as explained above, the effect of different concentrations of Tl (10 - 30 µg L^{-1}) – used as internal standard to correct for the mass bias using the Baxter approach followed by external correction in an SSB approach – was studied, and an example of the results thus obtained is shown in **Figure 3-4B**, which represents the $^{202}Hg/^{198}Hg$ isotope ratio results and the accompanying RSD (%) – left y-axis – and the $\delta^{202}Hg$ (‰) and accompanying SD – right y axis – as a function of the ^{205}Tl signal intensity (n = 15). As with the concentration of Hg, there is no clear effect of the Tl concentration on the accuracy of the results. With CVG, there is also no important effect on the precision (0.005 –

0.009 % RSD). However, a strong effect on the precision is seen for PN (0.005 – 0.026 % RSD), especially at ^{205}Tl signal intensities lower than ca. 1.5V. This difference in response towards variation in the Tl concentration between both introduction systems at similar Tl signal intensities was verified to be reproducible and was tentatively attributed to the analyte element / internal standard ratio. Therefore, a compromise concentration of 20 µg L^{-1} Tl was selected for both configurations and used throughout the further work.

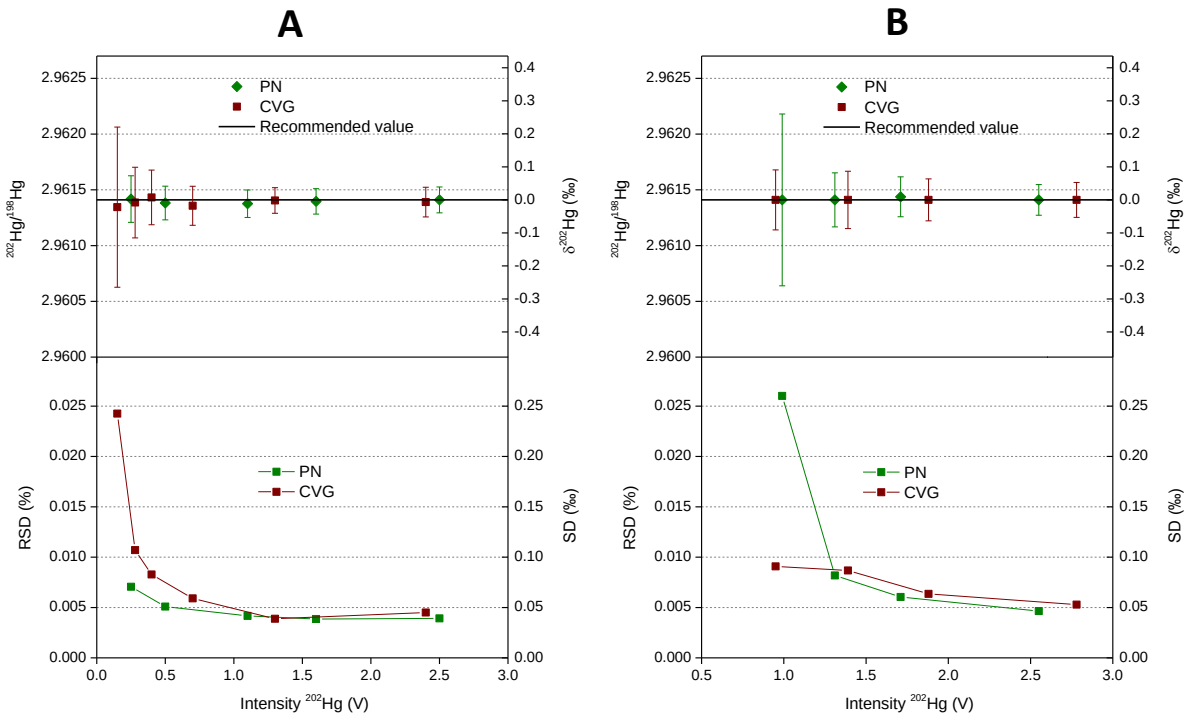

Figure 3-4. Effect of the signal intensity for Hg (A) and Tl (B) on the accuracy and precision of the ^{202}Hg/^{198}Hg isotope ratio results reported as the ^{202}Hg/^{198}Hg isotope ratio and RSD (%) – left y-axis – and δ^{202}Hg (‰) and SD (‰) – right y-axis – for n = 15 using both introduction systems: PN (green) and CVG (red). For Fig. 3-4A, the concentration of Tl was selected to be 20 µg L^{-1}, while the concentration of Hg was in the range of 50 – 500 µg L^{-1} and 1 – 20 µg L^{-1} for PN and CVG, respectively. For Fig. 3-4B, the concentration of Hg was fixed at 200 and 10 µg L^{-1} for PN and CVG, respectively, while the concentration of Tl was in the range of 5 – 30 µg L^{-1}.

3.3.3. Evaluation of different mass bias correction approaches

As has been described in the introduction, all types of ICP-MS instrumentation, and thus also MC-ICP-MS, suffer from instrumental mass discrimination, resulting in an isotope ratio that is biased with respect to the true value. For that reason, the selection of an adequate mass bias correction approach is an important prerequisite for successful isotopic analysis. Using the optimum measuring conditions detailed above, several approaches for mass bias correction were evaluated using an in-house standard solution of Hg. After the evaluation, the reference material UM-Almaden was used to further validate the accuracy and precision attainable with the finally selected approach. The Hg isotopic reference material NIST SRM 3133 was used as an external standard to correct for mass bias in a sample – standard bracketing approach (SSB) and the Tl isotopic reference material NIST SRM 997 was selected as internal standard. External correction was done in an SSB approach,**[33]** and combinations of this approach with different strategies for internal correction were tested for their capability to accurately and precisely correct for mass discrimination using both introduction systems, PN and CVG. The analyte element concentration in the external standard was always matched within ± 10% with that of the sample.

Table 3-3 shows the comparison of the isotope ratio results for the in-house standard solution of Hg (n = 50) expressed in delta notation (δ^{xxx}Hg, ‰) and in capital delta (Δ^{xxx}Hg ‰) obtained for 200 µg L^{-1} or 10 µg L^{-1} of Hg in the case of PN and CVG, respectively, and 20 µg L^{-1} of Tl (for both approaches). For internal correction, we relied on the Russell law,**[36]** and some refined approaches based on the Russell law and a linear relationship between (i) the mass bias correction factors for analyte element and internal standard (Woodhead approach),**[39]** (ii) the ln(raw isotope ratio) values for analyte element and internal standard (Baxter approach) **[40]** or (iii) the raw isotope ratio results for analyte element and internal standard (CAIS).**[33]** ANOVA indicated that there are no significant differences between the different mass bias correction approaches for each δ^{xxx}Hg value ($F_{experimental}$ = 0.070 – 0.19 (PN), 0.20 – 0.53 (CVG) < $F_{critical}$ = 2.41), nor between both introduction systems ($F_{experimental}$ = 0.64 – 1.18 < $F_{critical}$ = 1.90).

The results suggest that the dual CVG (Hg) – PN (Tl) sample introduction system allows for the accurate and precise measurement of the isotopic composition of Hg without the introduction of additional fractionation, and that the introduction of Tl solution as a wet aerosol to a current of Hg vapor can be successfully applied to correct for mass discrimination effects. Moreover, the analyte introduction efficiency with this approach is approximately a factor of 20 higher than that of PN, thus allowing sample solutions with lower Hg concentration to be successfully analyzed for their Hg isotopic composition.

In order to further validate the accuracy and precision of the approaches using PN and CVG, the Hg isotopic composition of the reference material UM-Almaden was determined. As the mass bias correction methods evaluated above performed equally, a combination of the Baxter approach followed by SSB was selected and used throughout the further work, except for that part of the work described in section 3.5, in which also the use of SSB only was considered of interest when evaluating matrix effects. **Table 3-4** shows the comparison of the experimental δ^{xxx}Hg (‰) and Δ^{xxx}Hg ‰ values obtained in this work (n = 15) using both approaches to literature values for the isotopic composition of Hg in UM-Almaden. At a 95% level of significance, no differences were found between the results obtained using both PN and CVG ($t_{experimental}$ = 0.11 – 1.23 < $t_{critical}$ = 2.05). Additionally, no significant differences were found between the results obtained in this work and the literature values ($t_{experimental}$ = 0.42 – 2.06 < $t_{critical}$ = 2.14), which is a further proof of the capabilities of the approaches evaluated for the accurate and precise measurement of the Hg isotopic composition.

Table 3-3. Comparison of different mass bias correction approaches for an in-house standard solution of Hg (n = 50) using both introduction systems, PN (200 µg L^{-1} Hg) and CVG (10 µg L^{-1} Hg), reported as δ^{xxx}Hg (‰) values against NIST SRM 3133. For completeness, also the Δ^{199}Hg (‰) values have been added

		In-house standard solution													
		PN							CVG						
		δ^{199}Hg	δ^{200}Hg	δ^{201}Hg	δ^{202}Hg	Δ^{199}Hg	Δ^{200}Hg	Δ^{201}Hg	δ^{199}Hg	δ^{200}Hg	δ^{201}Hg	δ^{202}Hg	Δ^{199}Hg	Δ^{200}Hg	Δ^{201}Hg
SSB	**Average**	-0.15	-0.29	-0.47	-0.59	0.00	0.01	-0.02	-0.14	-0.30	-0.45	-0.59	0.01	0.00	-0.01
	2SD	0.11	0.12	0.14	0.13	0.01	0.01	0.02	0.09	0.12	0.12	0.15	0.01	0.01	0.01
Russell + SSB	**Average**	-0.15	-0.28	-0.46	-0.60	0.00	0.02	0.00	-0.14	-0.30	-0.45	-0.59	0.01	0.00	-0.01
	2SD	0.11	0.12	0.14	0.12	0.02	0.01	0.02	0.09	0.10	0.12	0.11	0.01	0.01	0.01
Baxter + SSB	**Average**	-0.15	-0.28	-0.46	-0.60	0.00	0.02	-0.01	-0.13	-0.29	-0.44	-0.58	0.01	0.00	-0.01
	2SD	0.11	0.12	0.14	0.12	0.02	0.01	0.02	0.08	0.10	0.12	0.12	0.01	0.01	0.01
Woodhead + SSB	**Average**	-0.15	-0.28	-0.45	-0.60	0.00	0.02	0.00	-0.13	-0.29	-0.44	-0.58	0.01	0.00	0.00
	2SD	0.11	0.12	0.14	0.12	0.02	0.01	0.02	0.08	0.10	0.12	0.12	0.01	0.01	0.01
CAIS + SSB	**Average**	-0.15	-0.28	-0.46	-0.60	0.00	0.02	-0.01	-0.13	-0.30	-0.44	-0.59	0.02	0.00	0.00
	2SD	0.11	0.12	0.14	0.12	0.02	0.01	0.02	0.08	0.10	0.12	0.12	0.01	0.01	0.01

Table 3-4. Comparison of the isotope ratio data obtained for Hg – expressed as δ^{xxx}Hg (‰) and Δ^{xxx}Hg (‰) – in UM-Almaden in this work (n = 15), using both introduction systems (200 μg L^{-1} and 10 μg L^{-1} of Hg for PN and CVG, respectively) and corrected for mass bias using the Baxter approach (Tl) followed by SSB, with the corresponding literature values.

Literature values		**UM-Almaden**			
		δ^{199}Hg	**δ^{200}Hg**	**δ^{201}Hg**	**δ^{202}Hg**
Blum *et al.*	**Average**	-0.14	-0.27	-0.44	-0.54
	2SD	0.06	0.04	0.07	0.08
Mead *et al.*	**Average**	-0.15	-0.29	-0.44	-0.58
	2SD	0.06	0.06	0.08	0.08

This work		**PN**							**CVG**						
		δ^{199}Hg	**δ^{200}Hg**	**δ^{201}Hg**	**δ^{202}Hg**	**Δ^{199}Hg**	**Δ^{200}Hg**	**Δ^{201}Hg**	**δ^{199}Hg**	**δ^{200}Hg**	**δ^{201}Hg**	**δ^{202}Hg**	**Δ^{199}Hg**	**Δ^{200}Hg**	**Δ^{201}Hg**
Baxter + SSB	**Average**	-0.15	-0.28	-0.45	-0.57	-0.01	0.00	-0.02	-0.14	-0.29	-0.45	-0.58	0.01	0.01	-0.01
	2SD	0.04	0.07	0.07	0.12	0.01	0.01	0.03	0.05	0.05	0.07	0.08	0.01	0.01	0.01

3.3.4. Assessment of extent and stability of mass bias and long-term precision of Hg isotopic analysis

In order to better assess the extent and stability of the mass bias, Hg isotope ratio data for NIST SRM 3133 (Hg) and NIST SRM 997 (Tl) were collected during a period of 18 months (n = 250) for each introduction system. An example of the raw $^{202}Hg/^{198}Hg$ and $^{205}Tl/^{203}Tl$ isotope ratios is given in **Figure 3-5**.

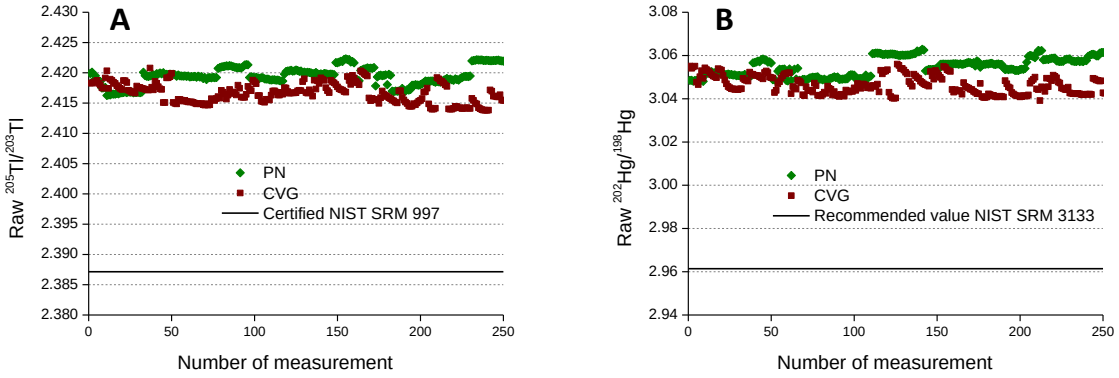

Figure 3-5. Comparison of the raw $^{205}Tl/^{203}Tl$ (A) and $^{202}Hg/^{198}Hg$ (B) isotope ratio values for PN (200 µg L^{-1} Hg) and CVG (10 µg L^{-1} Hg) using 20 µg L^{-1} of Tl for both configurations

For both configurations, the raw ratios of Hg were clearly biased in favor of the heavier of the two isotopes considered, but the extent of bias was slightly lower with CVG than with PN. The same tendency was observed in the raw $^{205}Tl/^{203}Tl$ results, which supports the conclusion that the admixed Tl – introduced as a wet aerosol – can be properly used to correct for mass discrimination in the isotopic analysis of Hg. Additionally, when plotting the raw isotope ratios for Hg divided by the corresponding true ratios as a function of the nuclide mass of the isotope indicated in the nominator, a linear relationship is obtained for both configurations (R^2 = 0.9998 and 0.9994, PN and CVG, respectively), indicating that no instrumental mass-independent fractionation could be observed within the level of precision attained (see **Figure 3-6**), despite the claim of some authors that this effect can occur in MC-ICP-MS instrumentation.**[54]**

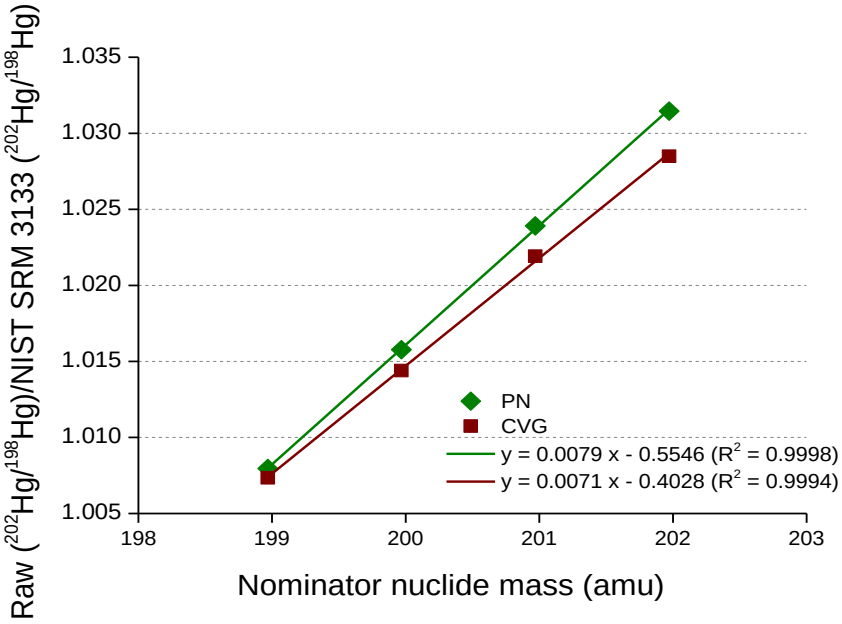

Figure 3-6. Evidence for the absence of mass-independent instrumental mass fractionation: raw isotope ratios for Hg divided by the corresponding recommended value plotted as a function of the nominator nuclide mass using results in a straight line for both configurations, PN (200 µg L^{-1} Hg) and CVG (10 µg L^{-1} Hg).

For evaluating the accuracy after mass discrimination correction, the parameter "Bias (B, ‰)" was defined as indicated in **equation 3-5**. The results are shown in **Table 3-5** and **Figure 3-7** and provide a view on the stability of this parameter over the entire period of measurements, showing a random distribution, which proves the robustness of the approaches developed for the isotopic analysis of Hg. Additionally, F-tests indicate no significant differences between both introduction systems in terms of precision ($F_{experimental} < F_{critical}$), except for the B^{199}Hg, for which a slight significant difference was observed ($F_{experimental} = 1.43 > F_{critical} = 1.23$).

$$\textbf{Bias } (\boldsymbol{B})^{\textbf{xxx}}\textbf{Hg } (‰) = \left(\frac{\left(\frac{^{xxx}Hg}{^{198}Hg}\right)_{corrected}}{\left(\frac{^{xxx}Hg}{^{198}Hg}\right)_{true}} - \mathbf{1} \right) * \mathbf{1000} \qquad \textbf{Equation } \mathbf{3-5}$$

Table 3-5. Evaluation of the accuracy and precision during a long-term study (n = 250, 18 months) for NIST SRM 3133 (Hg) using both, PN (200 μg L^{-1} Hg) and CVG (10 μg L^{-1} Hg) as an introduction systems and correcting for mass bias using the Baxter approach followed by SSB.

	PN				CVG			
Accuracy – Bias (‰)								
	$B^{199}Hg$	$B^{200}Hg$	$B^{201}Hg$	$B^{202}Hg$	$B^{199}Hg$	$B^{200}Hg$	$B^{201}Hg$	$B^{202}Hg$
Average	-0.001	0.000	0.003	0.004	0.000	-0.002	-0.002	0.002
2SD	0.087	0.093	0.120	0.109	0.104	0.095	0.123	0.115
Max	0.156	0.171	0.168	0.141	0.196	0.131	0.145	0.128
Min	-0.149	-0.162	-0.241	-0.129	-0.176	-0.156	-0.160	-0.134
Range	0.305	0.333	0.409	0.270	0.372	0.287	0.305	0.262
Long-term precision								
	$^{199}Hg/^{198}Hg$	$^{200}Hg/^{198}Hg$	$^{201}Hg/^{198}Hg$	$^{202}Hg/^{198}Hg$	$^{199}Hg/^{198}Hg$	$^{200}Hg/^{198}Hg$	$^{201}Hg/^{198}Hg$	$^{202}Hg/^{198}Hg$
Average	1.68721	2.30468	1.31210	2.96142	1.68721	2.30468	1.31209	2.96141
2SD	0.00014	0.00018	0.00014	0.00028	0.00018	0.00022	0.00016	0.00034
RSD%	0.004	0.004	0.005	0.005	0.005	0.005	0.006	0.006

Recommended value NIST SRM 3133				
	$^{199}Hg/^{198}Hg$	$^{200}Hg/^{198}Hg$	$^{201}Hg/^{198}Hg$	$^{202}Hg/^{198}Hg$
Average	1.68721	2.30468	1.31209	2.96141
2SD	0.00007	0.00013	0.00010	0.00031
Certified value NRCC NIMS-1				
	$^{199}Hg/^{198}Hg$	$^{200}Hg/^{198}Hg$	$^{201}Hg/^{198}Hg$	$^{202}Hg/^{198}Hg$
Average	1.6873	2.3050	1.3120	2.9629
U*	0.0011	0.0024	0.0024	0.0039

*Precision expressed as expanded uncertainty with a coverage factor of two.

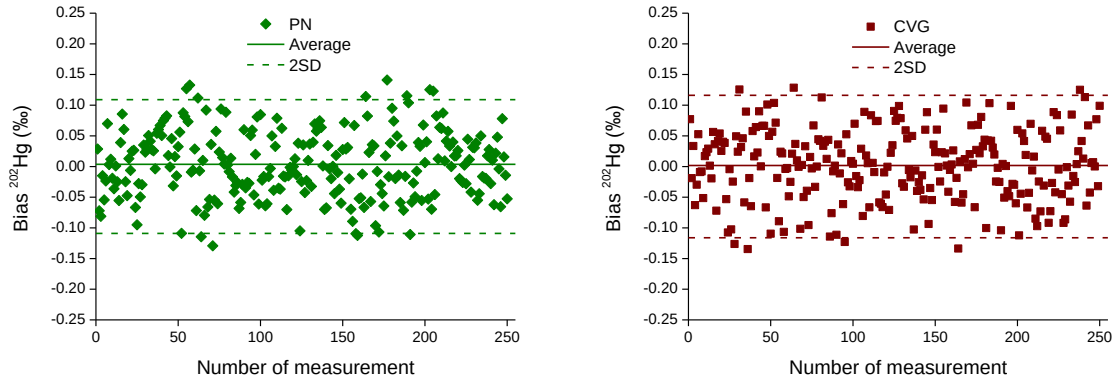

Figure 3-7. Representation of the accuracy and long-term precision attainable for NIST SRM 3133 after mass bias correction – expressed as the bias with respect to the recommended value B^{202}Hg (‰) – during a period of 18 months (n = 250) for both introduction systems, PN (200 µg L^{-1} Hg, left, green) and CVG (10 µg L^{-1} Hg, right, red).

Furthermore, **Table 3-5** shows the comparison between the isotope ratios for NIST SRM 3133 obtained in this work and the recommended values, extracted from the work of Blum *et al.*,**[55]** and with the certified values for NRCC NIMS-1 (a dilution of NIST SRM 3133).**[56]** In addition, **Table 3-6** shows the capital delta – Δ^{xxx}Hg ‰ – values obtained for the NIST SRM 3133 in this work. It can be clearly seen that no significant differences from Δ^{xxx}Hg = 0 were found. In terms of precision, values around 0.004 – 0.006 % RSD were obtained (n = 250), without differences between PN and CVG. Such precision values are sufficient for studying natural variation in the isotopic analysis of Hg.**[55]**

Table 3-6. Capital delta values – Δ^{xxx}Hg (‰) – obtained for NIST SRM 3133 (long term study, n = 250, 18 months) using both introduction systems, PN (200 μg L^{-1} Hg) and CVG (10 μg L^{-1} Hg), and corrected for mass bias using the double correction approach – Baxter + SSB. See **Table 3-4** for the corresponding δ^{xxx}Hg (‰) values.

		NIST SRM 3133					
		PN			CVG		
		Δ^{199}Hg	**Δ^{200}Hg**	**Δ^{201}Hg**	**Δ^{199}Hg**	**Δ^{200}Hg**	**Δ^{201}Hg**
Baxter + SSB	**Average**	0.00	0.00	0.00	0.00	0.00	0.00
	2SD	0.08	0.07	0.08	0.11	0.11	0.13

3.3.5. Effect of matrix composition

In MC-ICP-MS, the matrix composition affects the ionization and transmission efficiencies of the analyte nuclides,**[57, 58]** which can jeopardize the accuracy and precision of the isotope ratio results. For that reason, typically the analyte element is chemically isolated prior to MC-ICP-MS isotopic analysis. Due to the matrix removal *via* the use of CVG, this effect is expected to be removed. However, the presence of concomitant elements at relatively high concentrations may induce changes in the chemical reaction taking place in the CVG unit, thus potentially introducing additional fractionation. In this section, experiments permitting one to evaluate the presence or absence of matrix effects using both introduction systems and to assess whether the application of SSB and the double mass bias correction – Baxter and SSB approach – still provide accurate results under these conditions are reported on.

It has been described in literature **[29, 59, 60]** that a few elements can induce higher disturbances in mass discrimination, for instance, easily and/or hardly ionizable elements (*e.g.*, Na and Cl – ionization energies of 5.14 and 12.97 eV, respectively) are able to produce changes in the plasma conditions, and therefore in the extent of mass discrimination, while also elements with a high level of oxide ion formation (*e.g.*, Ce) may significantly affect the mass bias.**[30]** For evaluating the actual effect of possible concomitant elements on Hg isotope ratio results, Ba, Cl, Ce, Cs, Na and Sb were selected as to cover a broad range of ionization potentials,

and the effect of their presence in the plasma on the extent of mass discrimination was assessed. Therefore, six artificial matrices were prepared *via* addition of these elements to the in-house standard solution of Hg previously characterized as reported on in section 3.3.

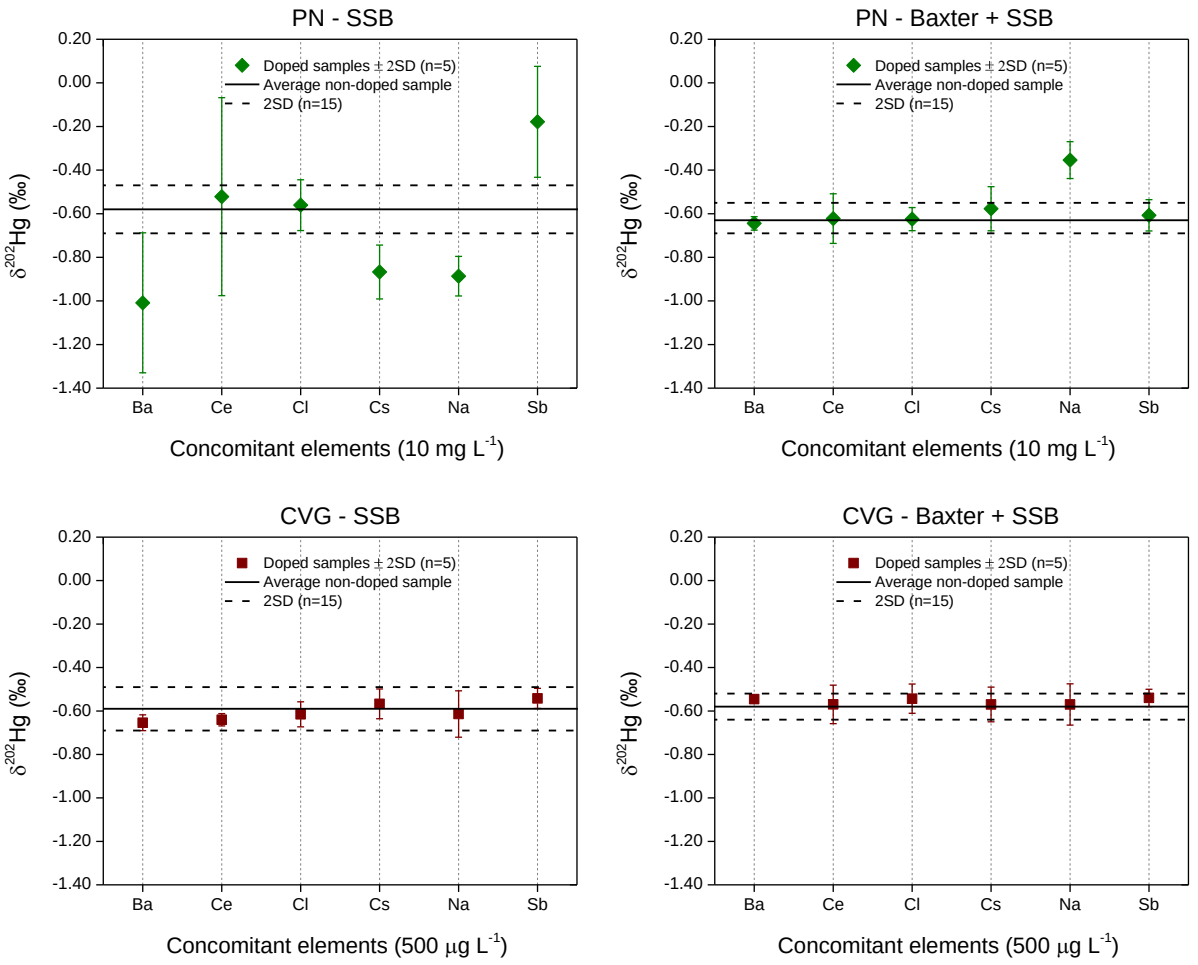

Figure 3-8. Evaluation of the effect of concomitant elements on the δ^{202}Hg (‰) values obtained using both introduction systems, PN (200 µg L^{-1}) and CVG (10 µg L^{-1}), and corrected for mass discrimination *via* SSB and double correction (Baxter + SSB).

The concentrations were selected in order to keep the Hg / concomitant element ratio constant at a ratio of 1:50, which corresponds to 10 mg L^{-1} of the concomitant elements for PN, and 500 µg L^{-1} for CVG. To check for and avoid possible remaining effects after the introduction of a synthetic matrix solution, the in-house standard solution of Hg was measured in-between two doped solutions. The measurements were otherwise performed in a random sequence. The results for δ^{202}Hg (‰) are shown as an example in **Figure 3-8**. The experiment was carried out for PN and CVG, and the results were corrected for mass discrimination using both, SSB and the combination of the Baxter approach followed by SSB, as indicated in section 3.3. As can be seen, with CVG, there are no significant differences between the δ^{202}Hg (‰) values obtained for the non-doped in-house standard solutions *via* any of the selected approaches, except for a slight degradation in the precision when only the SSB approach was used instead of the double correction. Additionally, the δ^{202}Hg (‰) values in the solutions containing the concomitant elements did not deviate significantly from the reference value with CVG, which further confirms the absence of additional fractionation coming from possible changes in the formation of Hg^0, induced by the concomitant elements studied. This illustrates the capabilities of this approach for the isotopic analysis of Hg without the necessity of prior isolation of the analyte element. With PN as a means of sample introduction, important deviations from the correct δ^{202}Hg (‰) value were observed when the SSB approach was used to correct for mass discrimination effects: a bias of -0.42, -0.28, -0.30 and +0.40 ‰ was found in the presence of Ba, Cs, Na and Sb, respectively. The combination of the Baxter approach and SSB, however, allows one to adequately correct for mass discrimination in all cases, except in the case of Na, where the application of the double correction method results in a bias of +0.23‰ with respect to the reference δ^{202}Hg (‰) value. These differences between results obtained *via* SSB and *via* the double correction approach with PN can be explained by the different matrix composition for standard and sample solutions in the case of external standardization, while in the double correction approach, the internal standard (Tl) is of course measured under exactly the same (matrix) conditions, thus providing accurate results, with the exception of the case of Na as concomitant element.

Table 3-7. Determination of the Hg isotopic composition in a variety of reference materials *via* CVG-MC-ICP-MS. The results of 3 different digestion replicates (average ± 2SD) are reported in delta notation (δ^{xxx}Hg ‰) *versus* NIST SRM 3133 and capital delta notation (Δ^{xxx}Hg ‰). Mass bias was corrected for using double mass bias correction (Baxter + SSB).

	δ^{199}Hg	δ^{200}Hg	δ^{201}Hg	δ^{202}Hg	Δ^{199}Hg	Δ^{200}Hg	Δ^{201}Hg
	NIST SRM 2704						
Gantner *et al.*[21]	-0.18 ± 0.05	-0.24 ± 0.06	-0.40 ± 0.05	-0.43 ± 0.03	-0.05 ± 0.06	-0.05 ± 0.05	-0.07 ± 0.03
This study	**-0.15 ± 0.10**	**-0.22 ± 0.14**	**-0.42 ± 0.19**	**-0.48 ± 0.19**	**-0.03 ± 0.04**	**0.02 ± 0.04**	**-0.09 ± 0.06**
	NRC-CNRC DORM-1						
Gantner *et al.* [21]	1.24 ± 0.11	0.16 ± 0.15	1.08 ± 0.20	0.19 ± 0.43	1.20 ± 0.14	0.05 ± 0.08	0.94 ± 0.14
This study	**1.17 ± 0.08**	**0.16 ± 0.12**	**0.96 ± 0.20**	**0.09 ± 0.19**	**1.15 ± 0.12**	**0.11 ± 0.09**	**0.89 ± 0.09**
	NRC-CNRC DORM-2						
Bergquist *et al.* [61]	1.11 ± 0.05	0.14 ± 0.06	1.02 ± 0.11	0.18 ± 0.08	1.07 ± 0.03	0.05 ± 0.02	0.88 ± 0.05
Malinovsky *et al.* [62]	1.11 ± 0.04	0.08 ± 0.06	1.01 ± 0.08	0.11 ± 0.16	1.08*	0.02*	0.93*
Mead *et al.* [42]	1.15 ± 0.08	0.13 ± 0.05	1.07 ± 0.11	0.18 ± 0.08	1.11 ± 0.07	0.04*	0.94 ± 0.05
This study	**1.04 ± 0.15**	**0.13 ± 0.17**	**1.00 ± 0.22**	**0.16 ± 0.29**	**1.00 ± 0.12**	**0.05 ± 0.06**	**0.88 ± 0.08**
	NRC-CNRC DORM-4						
This study	**1.66 ± 0.18**	**0.20 ± 0.12**	**1.53 ± 0.23**	**0.26 ± 0.14**	**1.59 ± 0.16**	**0.08 ± 0.10**	**1.34 ± 0.22**

Continued on next page

Continued from previous page

	NRC-CNRC TORT – 2						
Masbou *et al.* [24]	0.73 ± 0.11	0.03 ± 0.21	0.42 ± 0.14	-0.33 ± 0.16	0.82 ± 0.07	0.20 ± 0.018	0.67 ± 0.12
Hintelmann [8]	0.65*		0.45*	-0.18 ± 0.04	0.70 ± 0.03		0.59 ± 0.01
Kwon *et al.* [63]	0.82*		0.65*	0.10	0.79		0.57
This study	**0.51 ± 0.04**	**-0.08 ± 0.06**	**0.15 ± 0.14**	**-0.41 ± 0.22**	**0.61 ± 0.10**	**0.13 ± 0.18**	**0.45 ± 0.08**
	NRC-CNRC TORT – 3						
This study	**0.57 ± 0.10**	**-0.17 ± 0.12**	**0.14 ± 0.10**	**-0.47 ± 0.18**	**0.68 ± 0.14**	**0.07 ± 0.16**	**0.50 ± 0.12**
	BCR CRM 464						
Epov *et al.* [53]	2.33 ± 0.11	0.37 ± 0.14	2.23 ± 0.18	0.59 ± 0.20	2.18 ± 0.08	0.07 ± 0.08	1.79 ± 0.08
Laffont *et al.* [22]	2.24 ± 0.07	0.19 ± 0.15	2.01 ± 0.06	0.27 ± 0.20	2.20 ± 0.03	0.04 ± 0.05	1.82 ± 0.05
Perrot *et al.* [23]	2.02 ± 0.27	0.33 ± 0.03	1.96 ± 0.21	0.55 ± 0.06	1.88 ± 0.26	0.05 ± 0.20	1.54 ± 0.20
Perrot *et al.* [64]	2.61 ± 0.03	0.46 ± 0.14	2.56 ± 0.11	0.77 ± 0.19	2.42*	0.07*	1.98*
Masbou *et al.* [24]	2.48 ± 0.08	0.50 ± 0.14	2.47 ± 0.14	0.73 ± 0.14	2.29 ± 0.09	0.13 ± 0.07	1.92 ± 0.04
Sherman *et al.* [65]	2.57 ± 0.08	0.43 ± 0.05	2.48 ± 0.03	0.68 ± 0.06	2.40 ± 0.02	0.09 ± 0.04	1.97 ± 0.07
This study	**2.09 ± 0.19**	**0.35 ± 0.20**	**2.05 ± 0.18**	**0.56 ± 0.20**	**1.95 ± 0.16**	**0.07 ± 0.10**	**1.63 ± 0.18**

*δ^{xxx}Hg and Δ^{xxx}Hg values (‰) have been calculated from the literature data.

3.3.6. Hg isotopic analysis of reference materials via CVG-MC-ICP-MS

To further proof the capabilities of the approach developed using the dual introduction system, the determination of the Hg isotopic composition in 7 reference materials of different origin and of environmental interest, was carried out *via* CVG-MC-ICP-MS. Three replicate digests were obtained for each reference material. The concentration of Hg was measured – using the Element XR SF-ICP-MS with Rh as an internal standard – to ensure quantitative Hg recovery after acid digestion (90 – 99 %). After elemental analysis, isotopic analysis using CVG-MC-ICP-MS (avoiding any chromatographic separation) was performed for each digest. The contribution of the blank was less than 1% of the total Hg intensity, leading to maximal deviations of ~ 0.01 ‰ (δ^{xxx}Hg), which is negligible within the precision attainable, and thus, no blank subtraction was performed.**[47]** The corresponding results are shown in **Table 3-7**, which represent the average δ^{xxx}Hg (‰) and Δ^{xxx}Hg (‰) values and accompanying 2SD (for N = 3 different digestion replicates). In general, good agreement was found between the results obtained in this work and the literature values available (t-test, $t_{exp} < t_{crit}$, p = 0.05). According to the best of the author's knowledge, no results for the Hg isotopic composition of DORM-4 (Fish protein) and TORT-3 (Lobster hepatopancreas) have been reported earlier. The results testify of mass-independent fractionation for the biological reference materials – DORM-1, 2 and 4, TORT-2 and 3, and BCR CRM 464 – affecting the odd-numbered Hg isotopes. For these materials, the $\Delta^{199,201}$Hg value (**Table 3-7**) is ≠ 0 (‰), which is not the case for the sediment reference material – NIST SRM 2704.

3.4. Conclusion

A systematic study, addressing the influence of various instrument settings on the figures of merit of Hg isotopic analysis *via* MC-ICP-MS was carried out. The capabilities and limitations of two different introduction systems, PN and CVG, were evaluated and the differences between both documented in detail. With the CVG approach, the internal standard Tl was added *via* mixing of a PN-produced wet aerosol with the dry Hg stream in a "T-piece". When using CVG instead of PN, the intensity was enhanced approximately 20-fold and the influence from the matrix

composition was avoided, enabling Hg isotopic analysis of samples with low analyte concentration without the requirement of prior isolation of the analyte element, in contrast to the situation with PN. At similar signal intensities (approx. 1.2 V for ^{202}Hg), there was no significant difference in long-term precision – ≤0.006% RSD (N = 250, 18 months) between both set-ups evaluated. Instrumental mass discrimination was adequately corrected for by using a combination of external and internal correction (admixed Tl, revised Russell law – Baxter approach). CVG-MC-ICP-MS was subsequently validated *via* successful Hg isotopic analysis of various reference materials. For the latest generations of some biological RMs, first Hg isotope ratio results were presented. The results obtained in this work also demonstrate the suitability of the approach developed in this work for a variety of real-life applications for which Hg isotopic analysis is of scientific interest.

References

[1] W.F. Fitzgerald, C.H. Lamborg, Geochemistry of mercury in the environment. In Treatise on Geochemistry. Elservier, New York, 9 (2003) 107 - 148.

[2] W.I. Ridley, S.J. Stetson, Appl. Geochem., 21 (2006) 1889 - 1899.

[3] National Research Council (1978) An Assessment of Mercury in the Environment, National Academy of Sciences, Washington DC.

[4] D. Mergler, H.A. Anderson, L.H.M. Chan, K.R. Mahaffey, M. Murray, M. Sakamoto, A.H. Stern, Ambio, 36 (2007) 3 - 11.

[5] P.A. Baya, M. Gosselin, I. Lehnherr, V.L. St.Louis, H. Hintelmann, Environ. Sci. Technol., 49 (2015) 223 - 232.

[6] W.F. Fitzgerald, D.R. Engstrom, R.P. Mason, E.A. Nater, Environ. Sci. Technol., 32 (1998) 1 - 7.

[7] J.D. Blum, Applications of stable mercury isotopes to biogeochemistry, In: Bskaran M (ed) Handbook of Environmental Isotope Geochemistry, Advances in Isotope Geochemistry, Springer, Berlin, (2011).

[8] H. Hintelmann, Use of stable isotopes in mercury research, In: Bank MS (ed) Mercury in the Environment, Univ. Cali. Press, Berkeley, (2012).

[9] J.D. Blum, L.S. Sherman, M.W. Johnson, Annu. Rev. Earth Planet. Sci., 42 (2014) 249 - 269.

[10] R. Yin, X. Feng, X. Li, B. Yu, B. Du, Trends Environ. Anal. Chem., 2 (2014) 1 - 10.

[11] F. Vanhaecke, L. Balcaen, D. Malinovsky, J. Anal. At. Spectrom., 24 (2009) 863 - 886.

[12] R. Yin, X. Feng, W. Shi, Appl. Geochem., 25 (2010) 1467 - 1477.

[13] E.D. Young, A. Galy, H. Nagahara, Geochim. Cosmochim. Acta, 66 (2002) 1095 - 1104.

[14] J. Bigeleisen, J. Am. Chem. Soc., 118 (1996) 3676 - 3680.

[15] A.L. Buchachenko, J. Phys. Chem. A, 105 (2001) 9995 - 10011.

[16] J. Chen, H. Hintelmann, X. Feng, B. Dimock, Geochim. Cosmochim. Acta, 90 (2012) 33 - 46.

[17] Z. Wang, J. Chen, X. Feng, H. Hintelmann, S. Yuan, H. Cai, Q. Huang, S. Wang, F. Wang, C. R. Geosci., 347 (2015) 358 - 367.

[18] M.H. Theimens, Science, 283 (1999) 341 - 345.

[19] J. Farqijar, H. Bao, e. M. Tjoe, Science, 289 (2000) 756 - 759.

[20] T. Zambardi, J.E. Sonke, J.P. Toutain, F. Sortino, H. Shinohara, Earh Planet. Sci. Lett., 277 (2009) 236 - 243.

[21] N. Gantner, H. Hintelmann, W. Zheng, D.C. Muir, Environ. Sci. Technol., 43 (2009) 9148 - 9154.

[22] L. Laffont, J.E. Sonke, L. Maurice, H. Hintelmann, M. Pouilly, Y.S. Bacarreza, T. Perez, P. Behra, Environ. Sci. Technol., 43 (2009) 8985 - 8990.

[23] V. Perrot, V.N. Epov, M.V. Pastukhov, V.I. Grebenshchikova, C. Zouiten, J.E. Sonke, S. Husted, O.F.X. Donard, D. Amouroux, Environ. Sci. Technol., 44 (2010) 8030 - 8037.

[24] J. Masbou, D. Point, J. Sonke, J. Anal. Atom. Spectrom., 28 (2013) 1620 - 1628.

[25] F. Albarède, P. Telouk, J. Blichert-Toft, M. Boyet, A. Agranier, B. Nelson, Geochim. Cosmochim. Acta, 68 (2004) 2725 - 2744.

[26] J. Meija, L. Yang, Z. Mester, R.E. Sturgeon, Correction of Instrumental Mass Discrimination for Isotope Ratio Determination with Multi-Collector Inductively Coupled Plasma Mass Spectrometry, In: Vanhaecke F and Degryse P. Isotopic analysis. Fundamentals and Applications Using ICP-MS, Wiley-VCH, Germany, (2012).

[27] L. Yang, Mass Spectrom Rev., 28 (2009) 990 - 1011.

[28] N. Kivel, H.-D. Potthast, I. Günther-Leopold, F. Vanhaecke, D. Günther, Spectrochim. Acta, Part B, 93 (2014) 34 - 40.

[29] J. Barling, D. Weis, J. Anal. At. Spectrom., 23 (2008) 1017 - 1025.

[30] J. Barling, D. Weis, J. Anal. At. Spectrom., 27 (2012) 653 - 662.

[31] P.D.P. Taylor, P.d. Bièvre, A.J. Walder, A. Entwistle, J. Anal. At. Spectrom., 10 (1995) 395 - 398.

[32] L. Yang, R.E. Sturgeon, J. Anal. At. Spectrom., 18 (2003) 1452 - 1457.

[33] V. Devulder, L. Lobo, K.V. Hoecke, P. Degryse, F. Vanhaecke, Spectrochim. Acta, Part B, 89 (2013) 20 - 29.

[34] F. Vanhaecke, H. Vanhoe, R. Dams, Talanta, 39 (1992) 737 - 742.

[35] F. Albarède, E. Albalat, P. Télouk, J. Anal. At. Spectrom., 30 (2015) 1736 - 1742.

[36] W.A. Russell, D.A. Papanastassiou, T.A. Tombrello, Geochim. Cosmochim. Acta, (1978) 1075 - 1090.

[37] T. Hirata, Analyst, 121 (1996) 1407 - 1411.

[38] W.M. White, F. Albarède, P. Télouk, Chem. Geol., 167 (2000) 257 - 270.

[39] J. Woodhead, J. Anal. At. Spectrom., 17 (2002) 1381 - 1385.

[40] D.C. Baxter, I. Rodushkin, E. Engström, D. Malinovsky, Revised exponential model for mass bias correction using an internal standard for isotope abundance ratio measurements by multi-collector inductively coupled plasma mass spectrometry, J. Anal. At. Spectrom., 21 (2006) 427 - 430.

[41] F. Wombacher, M. Rehkämper, J. Anal. At. Spectrom., 18 (2003) 1371 - 1375.

[42] C. Mead, T.M. Hohnson, Anal. Bioanal. Chem., 397 (2010) 1529 - 1538.

[43] R.D. Evans, H. Hintelmann, P.J. Dillon, J. Anal. At. Spectrom., 16 (2001) 1064 - 1069.

[44] J.E. Sonke, T. Zambardi, J.-P. Toutain, J. Anal. At. Spectrom., 23 (2008) 569 - 573.

[45] K. Leopold, M. Foulkes, P.J. Worsfold, TrAC, Trends Anal. Chem., 28 (2009) 426 - 435.

[46] H. Hintelmann, S. Lu, Analyst, 128 (2003) 635 - 639.

[47] D. Foucher, H. Hintelmann, Anal. Bioanal. Chem, 384 (2006) 1470 - 1478.

[48] F. Vanhaecke, M.V. Holderbeke, L. Moens, R. Dams, J. Anal. At. Spectrom., 11 (1996) 543 - 548.

[49] K. Kritee, J.D. Blum, M.W. Johnson, B.A. Bergquist, T. Barkay, Environ. Sci. Technol., 41 (2007) 1889 - 1895.

[50] D. Foucher, N. Ogrinc, H. Hintelmann, Environ. Sci. Technol., 43 (2009) 33 - 39.

[51] J.E. Sonke, J. Schäfer, J. Chmeleff, S. Audry, G. Blanc, B. Dupré, Chem. Geol., 279 (2010) 90 - 100.

[52] M. Aramendía, M. Resano, F. Vanhaecke, J. Anal. At. Spectrom., 25 (2010) 390 - 404.

[53] V.N. Epov, P. Rodriguez-Gonzalez, J.E. Sonke, E. Tessier, D. Amouroux, L.M. Bourgoin, O.F.X. Donard, Anal. Chem., 80 (2008) 3530 - 3538.

[54] L. Yang, Z. Mester, L. Zhou, S. Gao, R.E. Sturgeon, J. Meija, Anal. Chem., 83 (2011) 8999 - 9004.

[55] J.B. Blum, B.A. Bergquist, Anal. Bioanal. Chem, 388 (2007) 353 - 359.

[56] J. Meija, L. Yang, R.E. Sturgeon, Z. Mester, J. Anal. At. Spectrom., 25 (2010) 384 - 389.

[57] E.H. Evans, J.J. Giglio, J. Anal. At. Spectrom., 8 (1993) 1 - 18.

[58] C. Agatemor, D. Beauchemin, Anal. Chim Acta, 706 (2011) 66 - 83.

[59] M. Rehkämper, K. Mezger, J. Anal. At. Mass Spectrom., 15 (2000) 1451 - 1460.

[60] G.H. Fontaine, B. Hattendorf, B. Bourdon, D. Günther, J. Anal. At. Spectrom., 24 (2009) 637 - 648.

[61] B. A. Bergquist, J. D. Blum, Science, 218 (2007) 417 - 420.

[62] D. Malinovsky, R. E. Sturgeon, L. Yang, Anal. Chem., 80 (2008) 2548 - 2555.

[63] S. Y. Kwon, J. D. Blum, C. Y. Chen, D. E. Meattey, R. P. Mason, Environ. Sci. Technol., 48 (2014) 10089 - 10097.

[64] V. Perrot, M. V. Pastukhov, V. N. Epov, S. Husted, O. F. X. Donard, D. Amouroux, Environ. Sci. Technol., 46 (2012) 5902 - 5911.

[65] L. S. Sherman, J. D. Blum, Sci. Total Environ., 448 (2013) 163 - 175.

Chapter 4

Assessment of Hg pollution released from a WWII submarine wreck (U-864) by Hg isotopic analysis of sediments and *Cancer pagurus* tissues

Adapted from Rua-Ibarz et. al., Environ. Sci. Technol., 50 (2016) 10361 – 10369

4.1. Introduction

At the end of World War II (February 9th, 1945), the German submarine U-864 was torpedoed and sunk by the British submarine HMS Venturer in the proximity of Bergen (Norway) as it is shown in **Figure 4-1**. According to the cargo list, the U-boat was transporting 67 tons of metallic mercury (Hg) in almost 2000 steel containers in its keel. In 2003, the wreckage was discovered by the Royal Norwegian Navy at 150 m depth and 2 nautic miles (nmi) west of Fedje island. Some of the containers were broken and Hg has contaminated the surrounding sediments. This has aroused serious concern about the corresponding environmental impact.**[1]** Since 2004, the Hg levels in seafood have been monitored by the National Institute of Nutrition and Seafood Research (NIFES) on behalf of the Norwegian Coastal Administration to evaluate potential introduction of this Hg into the marine food chain.**[2, 3]**

Figure 4-1. U-864 submarine wreckage.

Hg is a highly toxic heavy metal that can be globally distributed due to its capacity for traveling long distances in the atmosphere, and it readily biomagnifies through the trophic chain.**[4, 5]** Hg toxicity strongly depends on its chemical form, and although both inorganic (IHg) and organic Hg have a deleterious effect on human health, methylmercury (MeHg) poses the greatest risk. This Hg species is prevalent in fish, the consumption of which is the primary source of human MeHg exposure.**[4, 6, 7]** Hg in the environment is mainly attributed to anthropogenic sources, *e.g.*, fossil fuel combustion, mining-related emissions, and industrial

activities;**[8-10]** although also natural sources, *e.g.*, volcanic emissions,**[11]** contribute. Hg deposition in aquatic systems and sediments enables the conversion of IHg into MeHg *via* microbial methylation,**[12]** thus favoring its bioaccumulation through the aquatic food web. Previous studies have found a strong correlation between the Hg levels in sediments and in biota,**[13, 14]** suggesting such processes as the main source of Hg in the aquatic food web. However, atmospheric deposition**[15]** and/or MeHg accumulation in the water column particles, have also been suggested as possible sources.**[16]**

Next to elemental and speciation analysis,**[17, 18]** determination of the isotopic composition of Hg has emerged as a key tool for providing a better understanding of the biogeochemical cycling of this element and for evaluating its environmental risk.**[19-22]** However, although its applicability has already been demonstrated in some real-life case-studies during the last years,**[8, 13, 23, 24]** important knowledge gaps concerning the chemical transformations that Hg can undergo in complex environmental systems and the corresponding effects on its isotopic composition remain. This remark is especially valid for the unusual context of this work, characterized by the presence of a massive amount of elemental Hg. In addition, Hg isotopic analysis is not free from challenges and multi-collector inductively coupled plasma-mass spectrometry (MC-ICP-MS) instrumentation is required due to the small range of natural variation in the isotopic composition of Hg. Cold vapor generation (CVG) of Hg(0) enables accurate and precise Hg isotopic analysis as a steady signal without isotope fractionation is generated *via* complete reduction of the Hg(II) in the sample digest using $SnCl_2$. Also, compared to conventional pneumatic nebulization, CVG provides a 20-fold improvement in Hg^+ signal intensity, allowing the measurement of environmental samples in which Hg concentrations tend to be low.**[25-27]**

Hg isotopes display fractionation as its isotopes may engage in physical processes and/or bio-geochemical reactions to a slightly different extent. In the case of mass-dependent fractionation (MDF), the observed change in the isotope ratio is linearly dependent on the difference in mass between nominator and denominator isotope.**[28, 29]** The resulting differences in the isotopic composition are typically reported as $\delta^{202}Hg$ and have already been measured in several sample types*, e.g.*, coal, soil, rock, lichen, peat, snow, rainfall, sediment and biological materials,**[19-21]** and many environmental processes and reactions, *e.g.*, evaporation, biotic

methylation and demethylation,**[30-32]** were shown to be accompanied by MDF. This renders Hg isotopic analysis a *via*ble tool for the identification of Hg pollution sources and for tracing Hg emitted into the environment.**[8, 33]**

In addition to MDF, the isotopic composition of Hg may also be affected by mass-independent fractionation (MIF),**[34, 35]** reported as Δ^{199}Hg and Δ^{201}Hg. Although the origin of MIF has not been fully understood yet, it has been tentatively explained in terms of nuclear volume and magnetic isotope effects.**[36, 37]** Berquist and Blum**[38]** and Malinovsky *et al.***[39]** reported MIF for the odd-numbered isotopes of Hg as a result of photochemical reduction in aqueous medium, while this "odd-MIF" was not observed when the reduction was carried out in dark abiotic conditions. Bergquist and Blum**[38]** showed that fish samples collected from three different lakes displayed a wide range of MIF (expressed as Δ^{199}Hg) and used these data to estimate the extent of MeHg photodegradation prior to MeHg uptake by organisms from the lowest level within the food web, assuming that MIF is not modified by trophic transfer to fish. Although this assumption has been experimentally documented in previous studies,**[13, 23, 40]** Jackson *et al.***[41]** and Das *et al.***[42]** suggested that Δ^{199}Hg values can be modified *in vivo*. Further indications for the absence of *in vivo* MIF are presented along this PhD manuscript and are based on experimental results obtained for different species along the food chain (see the results provided in this chapter and in chapters 5 and 6). In addition to "odd-MIF", recent studies have also reported MIF of the even-numbered isotopes of Hg. This "even-MIF" has been observed for samples of atmospheric origin, *e.g.*, rain water and snow; photo-initiated oxidation of Hg(0) in the tropopause has been suggested as the possible origin of this MIF.**[43-45]**

Clearly, the complementary information provided by MDF and MIF of Hg isotopes may help in understanding the chemistry of Hg in the environment and in tracking Hg sources. In this work, quantitative Hg determination and MeHg speciation have been combined with high-precision MC-ICP-MS Hg isotopic analysis of sediments and *Cancer pagurus* tissues with the aim of evaluating the degree of Hg pollution in the vicinity of the U-864 wreck and of assessing the potential introduction of metallic Hg released from the wreck into the marine food chain. Chapter 5 provides additional information on the introduction of the U-864 Hg into another level in the marine food chain as it focuses on a fish species (*Brosme brosme*) from the same geographic location.

4.2 Experimental section

4.2.1. Area of study and sample collection

Metallic Hg from the U-864 wreck was retrieved from an intact steel container found in the sediment near the wreckage (**Figure 4-2A**). Core sediments (n = 14, **Figure 4-2B**) were sampled in the immediate vicinity of the wreck at different depths (0 – 2.4 m) in January 2013 using an ROV (Solhjell & Lunne, 2013).

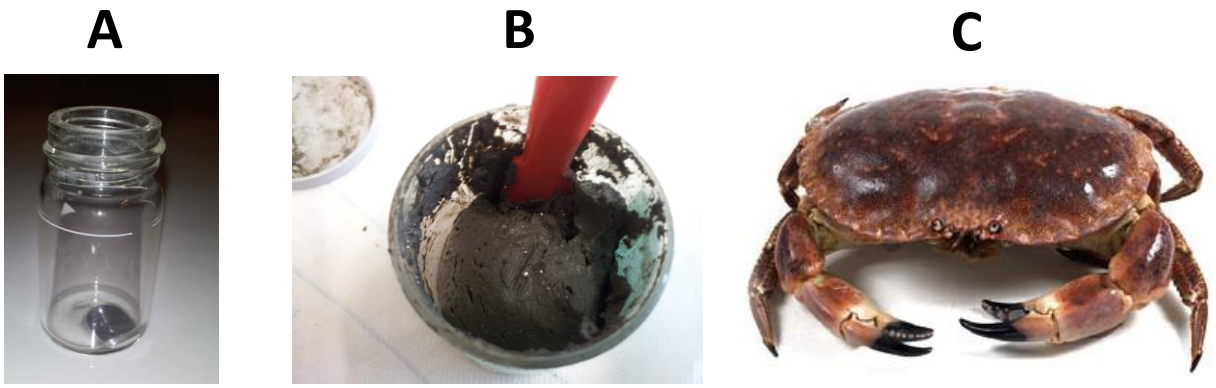

Figure 4-2. Samples analyzed in this work: metallic Hg (A), sediment samples (B) and *Cancer pagurus* tissues (C)

Cancer pagurus crabs (n = 74, **Figure 4-2C**) were caught in June 2014 at three sites – the wreck location and about 4 nmi north and 4 nmi south – from the M/K Vikingfjord H-1-A vessel using deep-water pots (**Figure 4-3** shows the sampling zones). Sample preparation at NIFES was done as described in detail by Julshanm *et al.***[46]** Claw meat (muscle) and brown meat (mainly hepatopancreas and gonads) were analyzed separately. From the complete set of samples, claw meat and brown meat from 13 individual crabs from each location were selected for the purpose of this work (n = 78). *C. pagurus*, also referred to as brown crab, is abundant in northern European coastal waters, is night active and known to prey on mussels, snails, barnacles, sea urchins and polychaetes that it can crush with its claws. It might also eat softer species like algae, jellyfish and ascidians.**[47, 48]** In Norway, *C. pagurus* is exploited for consumption both commercially and recreationally,**[49]** and both the claw meat and the brown meat are consumed.

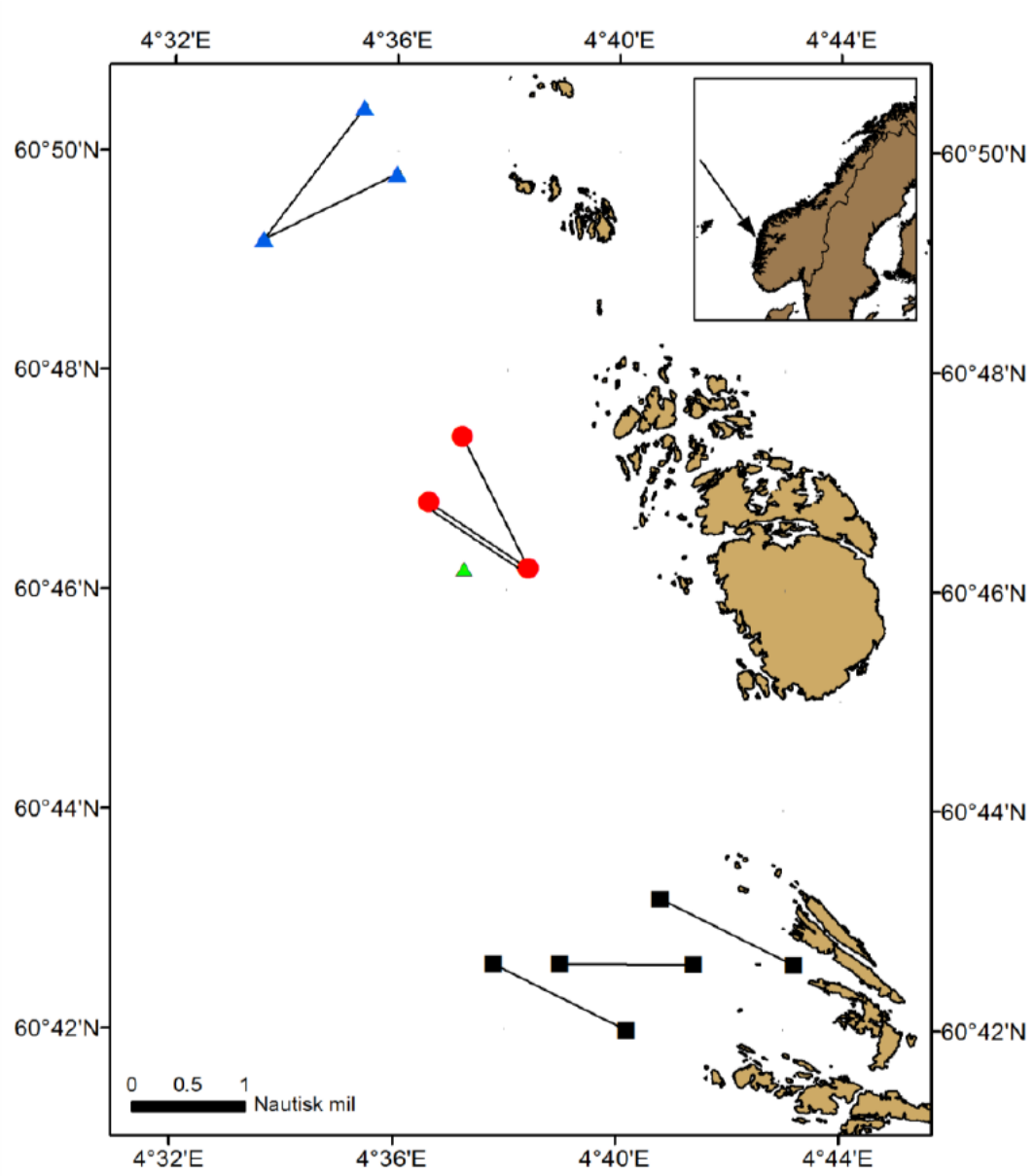

Figure 4-3. Map of the sampling locations. Location of the U-864 submarine wreck and sediment collection (green triangle), and of the three zones of crab collection: wreck location (red circles), 4 nautical miles north (blue triangles) and 4 nautical miles south (black squares).

4.2.2. THg and % of MeHg determination

The metallic Hg from the submarine was dissolved in 14 M HNO_3 (ChemLab, Belgium) and diluted appropriately for isotopic analysis (without prior

quantification) with high-purity water (resistivity > 18.2 MΩ.cm) obtained from a Milli-Q Element water purification system (Millipore, France). The total mercury (THg) concentration was determined in all sediment and crab tissue samples using a ThermoScientific (Germany) Element XR single-collector sector field ICP-MS (SF-ICP-MS) instrument, equipped with a 100 μL min^{-1} concentric nebulizer mounted onto a cyclonic spray chamber for sample introduction. Quantification was accomplished *via* external calibration with Rh (1 μg L^{-1}) as an internal standard and $KBrO_3$ (0.009 mM) for inhibiting Hg evaporation and minimizing memory effects. Acid digestion was accomplished with a 3:1 mixture of 14 M HNO_3 and 9.8 M H_2O_2 (Fluka, Belgium) and of 7 M HNO_3 and 9.8 M H_2O_2, for sediment and crab tissue samples, respectively. It needs to be pointed out, though, that a complete mineralization of the sediment samples was not achieved using this mixture. However, all Hg was extracted from the sediment samples, it was demonstrated by the results obtained for NIST SRM 2704 – Buffalo river sediment, a certified reference material with matrix composition similar to that of the samples of interest (*vide infra*). The digestion was carried out in closed Teflon® Savillex Beakers, pre-cleaned with HNO_3 and HCl (ChemLab, Belgium) and subsequently rinsed with Milli-Q water. The samples were heated on a hot plate at 110 °C overnight to complete the digestion and diluted subsequently for ICP-MS analysis. For the sediment samples, multiple digestion replicates were obtained (n = 2 – 3), whereas for the crab tissue samples, only one digestion was possible due to the limited sample mass, low Hg concentration and subsequent high sample intake required for isotopic analysis. The entire procedure was validated using the following certified reference materials (CRMs) with a matrix composition similar to that of the samples of interest: BCR CRM 464 (tuna fish), NIST SRM 2704 (Buffalo river sediment), NRC-CNRC DORM-1, DORM-2 and DORM-4 (fish protein), and NRC-CNRC TORT-2 and TORT-3 (lobster hepatopancreas). The results thus obtained are summarized in **Table 4-1**. In addition to THg determination, MeHg speciation was performed for the crab tissue samples *via* isotope dilution gas chromatography ICP-MS (GC-ICP-IDMS). The method was validated in a previous work with the CRMs ERM CE 464 (tuna fish), NIST SRM 1566B (oyster tissue) and NIST SRM 2977 (blue mussel), NRC-CNRC DOLT-4 (dogfish liver), DORM-3 and TORT-2, as reported by Valdersnes *et al.***[50]**

Table 4-1. Results obtained for quantification and isotopic analysis of Hg in various certified reference materials (average ± SD – 3 digestion replicates)

	Recoveries (%)	δ^{202}Hg (‰)	Δ^{199}Hg (‰)	Δ^{201}Hg (‰)
		NIST SRM 2704		
Gantner *et al.* [13]		-0.43 ± 0.02	-0.05 ± 0.03	-0.07 ± 0.02
Rua-Ibarz *et al.* [27]		-0.48 ± 0.09	-0.03 ± 0.02	-0.09 ± 0.03
This study	**98.2 ± 3.0**	**-0.48 ± 0.02**	**-0.03 ± 0.01**	**-0.11 ± 0.02**
		NRC-CNRC DORM-1		
Gantner *et al.* [13]		0.19 ± 0.21	1.20 ± 0.07	0.94 ± 0.07
Rua-Ibarz *et al.* [27]		0.09 ± 0.09	1.15 ± 0.06	0.89 ± 0.05
This study	**96.0 ± 5.4**	**0.06 ± 0.03**	**1.16 ± 0.05**	**0.88 ± 0.01**
		NRC-CNRC DORM-2		
Bergquist *et al.* [38]		0.18 ± 0.04	1.07 ± 0.02	0.88 ± 0.03
Malinovsky *et al.* [51]		0.11 ± 0.08	1.08*	0.93*
Mead *et al.* [52]		0.18 ± 0.04	1.11 ± 0.04	0.94 ± 0.03
Rua-Ibarz *et al.* [27]		0.16 ± 0.14	1.00 ± 0.06	0.88 ± 0.04
This study	**98.8 ± 5.5**	**0.17 ± 0.06**	**1.04 ± 0.05**	**0.87 ± 0.05**
		NRC-CNRC DORM-4		
Rua-Ibarz *et al.* [27]		0.26 ± 0.07	1.59 ± 0.08	1.34 ± 0.11
This study	**98.5 ± 2.7**	**0.23 ± 0.07**	**1.63 ± 0.04**	**1.34 ± 0.07**
		NRC-CNRC TORT-2		
Masbou *et al.* [53]		-0.33 ± 0.08	0.82 ± 0.04	0.67 ± 0.06
Hintelmann [54]		-0.18 ± 0.02	0.70 ± 0.02	0.59 ± 0.01
Kwon *et al.* [55]		0.10	0.79	0.57
Rua-Ibarz *et al.* [27]		-0.41 ± 0.11	0.61 ± 0.05	0.45 ± 0.04
This study	**95.8 ± 3.5**	**-0.38 ± 0.10**	**0.66 ± 0.03**	**0.48 ± 0.01**
		NRC-CNRC TORT-3		
Rua-Ibarz *et al.* [27]		-0.47 ± 0.09	0.68 ± 0.07	0.50 ± 0.06
This study	**95.9 ± 3.1**	**-0.30 ± 0.05**	**0.65 ± 0.01**	**0.49 ± 0.04**
		BCR CRM 464		
Epov *et al.* [56]		0.59 ± 0.10	2.18 ± 0.04	1.79 ± 0.04
Laffont *et al.* [57]		0.27 ± 0.10	2.20 ± 0.02	1.82 ± 0.03
Perrot *et al.* [23]		0.55 ± 0.03	1.88 ± 0.13	1.54 ± 0.10
Perrot *et al.* [58]		0.77 ± 0.09	2.42*	1.98*
Masbou *et al.* [53]		0.73 ± 0.07	2.29 ± 0.05	1.92 ± 0.02
Sherman *et al.* [24]		0.68 ± 0.03	2.40 ± 0.01	1.97 ± 0.04
Rua-Ibarz *et al.* [27]		0.56 ± 0.10	1.95 ± 0.08	1.63 ± 0.09
This study	**97.4 ± 6.6**	**0.63 ± 0.03**	**2.00 ± 0.05**	**1.68 ± 0.04**

4.2.3. Hg isotopic analysis

Hg isotopic analysis was carried out using a ThermoScientific (Germany) Neptune multi-collector ICP-MS (MC-ICP-MS) unit, equipped with nine Faraday cups (instrumental parameters are shown in **Table 4-2**).

Table 4-2. Cup configuration, instrument settings and data acquisition parameters for the Neptune MC-ICP-MS instrument

Neptune MC-ICP-MS						
Cup configuration						
L3	L2	L1	C	H1	H2	H3
^{198}Hg	^{199}Hg	^{200}Hg	^{201}Hg	^{202}Hg	^{203}Tl	^{205}Tl
Instrument settings						
RF power (W)				1250 – 1300		
Cool gas flow rate (L min^{-1})				13.00 – 13.50		
Auxiliary gas flow rate (L min^{-1})				0.67 – 0.72		
Nebulizer gas flow rate (L min^{-1})				0.70 – 0.75		
Carrier gas flow rate (L min^{-1})				0.19 – 0.21		
Additional gas flow rate (L min^{-1})				0.03 – 0.04		
Uptake rate sample – Hg (mL min^{-1})				0.7		
Uptake rate Tl (mL min^{-1})				0.17		
Uptake rate $SnCl_2$ (mL min^{-1})				0.7		
Uptake time (s)				100		
Wash time (s)				180		
Sensitivity ^{202}Hg (mV per µg L^{-1})				120 - 190		
Sampler cone				Ni Thermo Scientific		
Skimmer cone				Ni, H-type Thermo Scientific		
Resolution				Low resolution		
Mode				Static mode		
Data acquisition parameters						
Integration time (s)				4		
Blocks				5		
Cycles/block				10		
Total cycles				50		

The sample introduction system was based on the combination of CVG – using an HGX-200 Cold Vapor & Hydride Generation unit (Teledyne Cetac Technologies, US) – and pneumatic nebulization (PN) – using a concentric nebulizer (100 µL min^{-1}) fitted onto a dual (cyclonic and Scott-type) spray chamber – for Hg (analyte) and Tl (internal standard selected for mass discrimination correction purposes),

respectively.**[27]** Hg was reduced to Hg(0) by $SnCl_2$ (3% $SnCl_2.2H_2O$ in 1.2 M HCl) in the gas liquid separator (GLS) of the CVG unit, and the resulting Hg vapor was carried away with an Ar gas flow and admixed with the wet aerosol of the Tl standard solution produced by PN prior to its introduction into the plasma. Instrumental mass discrimination was corrected for by using Tl (NIST SRM 997) as an internal standard in the "Baxter approach",**[59]** followed by external correction relying on NIST SRM 3133, measured in a sample-standard bracketing (SSB) approach. External standard and sample solutions were matched in both the Hg (5 ± 0.5 µg L^{-1}) and acid (0.7 M HNO_3) concentration. Data acquisition was carried out using 5 blocks of 10 cycles and 4 s of integration time. Procedural blank solution intensities were less than 1 % of the sample intensities, and therefore, no blank subtraction was performed because its effect on the δ^{xxx}Hg results was demonstrated to be of the order of ~0.01 ‰ only, which was considered negligible within the precision attainable. MDF is reported in delta notation (δ^{xxx}Hg ‰), referring to NIST SRM 3133:

$$\partial^{xxx}Hg\ (‰) = \left(\frac{\left({}^{xxx}Hg/{}^{198}Hg\right)_{sample}}{\left({}^{xxx}Hg/{}^{198}Hg\right)_{NIST\ SRM\ 3133}} - 1\right) * 1000 \qquad \textbf{Equation 4 – 1}$$

where xxx = 199, 200, 201 or 202.

MIF signatures are expressed using the capital delta notation (Δ^{xxx}Hg ‰), as the difference between the measured δ^{xxx}Hg and the theoretically calculated value, assuming purely kinetic MDF:**[28]**

$$\Delta^{199}Hg = \partial^{199}Hg - \left(\partial^{202}Hg * 0.2520\right) \qquad \textbf{Equation 4 – 2}$$

$$\Delta^{200}Hg = \partial^{200}Hg - \left(\partial^{202}Hg * 0.5024\right) \qquad \textbf{Equation 4 – 3}$$

$$\Delta^{201}Hg = \partial^{201}Hg - \left(\partial^{202}Hg * 0.7520\right) \qquad \textbf{Equation 4 – 4}$$

Table 4-3. Hg isotopic composition of the in-house standard solution

In-house Hg standard solution							
	$\delta^{199}Hg$ (‰)	$\delta^{200}Hg$ (‰)	$\delta^{201}Hg$ (‰)	$\delta^{202}Hg$ (‰)	$\Delta^{199}Hg$ (‰)	$\Delta^{200}Hg$ (‰)	$\Delta^{201}Hg$ (‰)
	-0.18	-0.31	-0.48	-0.60	-0.02	0.00	-0.02
	-0.15	-0.24	-0.43	-0.53	-0.02	0.02	-0.03
	-0.17	-0.27	-0.37	-0.54	-0.03	0.00	0.03
	-0.07	-0.27	-0.45	-0.55	0.07	0.01	-0.04
	-0.23	-0.33	-0.43	-0.58	-0.09	-0.04	0.00
	-0.08	-0.29	-0.42	-0.52	0.05	-0.03	-0.03
	-0.13	-0.22	-0.41	-0.51	0.00	0.04	-0.03
	-0.07	-0.22	-0.36	-0.53	0.06	0.04	0.04
	-0.12	-0.33	-0.47	-0.65	0.04	-0.01	0.02
	-0.10	-0.21	-0.41	-0.57	0.04	0.07	0.01
	-0.14	-0.23	-0.38	-0.53	-0.01	0.04	0.02
	-0.16	-0.34	-0.47	-0.65	0.01	-0.02	0.02
	-0.16	-0.29	-0.48	-0.58	-0.02	0.00	-0.05
	-0.13	-0.22	-0.40	-0.51	0.00	0.03	-0.02
	-0.16	-0.30	-0.43	-0.54	-0.02	-0.03	-0.02
	-0.08	-0.25	-0.44	-0.64	0.08	0.07	0.04
	-0.09	-0.22	-0.37	-0.52	0.04	0.04	0.02
	-0.19	-0.33	-0.50	-0.64	-0.02	-0.01	-0.01
	-0.14	-0.27	-0.44	-0.53	0.00	0.00	-0.04
	-0.18	-0.36	-0.58	-0.66	-0.02	-0.03	-0.09
	-0.13	-0.24	-0.35	-0.50	-0.01	0.01	0.02
	-0.17	-0.36	-0.57	-0.61	-0.02	-0.06	-0.11
	-0.13	-0.28	-0.40	-0.53	0.00	-0.01	0.00
	-0.17	-0.28	-0.45	-0.62	-0.02	0.03	0.02
	-0.18	-0.27	-0.45	-0.51	-0.05	-0.01	-0.07
	-0.12	-0.22	-0.43	-0.53	0.02	0.05	-0.03
	-0.11	-0.30	-0.37	-0.58	0.03	-0.01	0.07
	-0.14	-0.29	-0.35	-0.55	0.00	-0.02	0.06
	-0.12	-0.32	-0.47	-0.61	0.04	-0.02	-0.02
	-0.11	-0.28	-0.39	-0.56	0.03	0.01	0.03
	-0.09	-0.29	-0.46	-0.68	0.08	0.05	0.05
	-0.16	-0.28	-0.46	-0.51	-0.03	-0.02	-0.08
	-0.07	-0.28	-0.36	-0.55	0.07	0.00	0.06
	-0.14	-0.39	-0.50	-0.63	0.02	-0.07	-0.03
	-0.06	-0.20	-0.35	-0.52	0.07	0.07	0.04
	-0.17	-0.27	-0.41	-0.58	-0.02	0.03	0.03
	-0.12	-0.23	-0.46	-0.55	0.01	0.04	-0.05
	-0.18	-0.32	-0.45	-0.66	-0.02	0.01	0.05
	-0.08	-0.26	-0.50	-0.55	0.06	0.01	-0.08
	-0.13	-0.26	-0.43	-0.55	0.01	0.02	-0.02
Average	**-0.13**	**-0.28**	**-0.43**	**-0.57**	**0.01**	**0.01**	**-0.01**
SD	**0.04**	**0.05**	**0.06**	**0.05**	**0.04**	**0.03**	**0.04**

An in-house Hg standard solution (Inorganic Ventures, The Netherlands, Lot: F2-HG02105)**[27]** was measured approximately every five samples as a measurement quality control sample (**Table 4-3**). Its associated uncertainty – expressed as standard deviation (SD, n = 40) – can be used as the uncertainty in those cases in which the SD calculated for the sample is smaller than that associated to the in-house Hg standard solution. In addition, the same CRMs selected for validation of the Hg quantification were also used to validate the isotopic analysis of Hg in the samples of interest. The isotopic compositions obtained for these CRMs are provided **in Table 4-1**, in which δ^{202}Hg and $\Delta^{199,201}$Hg are compared to values reported in literature. The entire procedure was also validated in chapter 3, in which an in-depth evaluation of accuracy and precision in Hg isotopic analysis was performed.**[27]**

4.3. Results and discussion

4.3.1. THg concentration in sediments

The THg concentration in sediments collected close to the submarine wreck as a function of depth (n = 2 – 3 at each depth) ranged from ~60 to ~24,000 mg Kg^{-1} (wet weight – w.w.). The complete data set is provided in **Table 4-4**. Previous studies have documented THg concentrations in marine sediments coming from, *e.g.*, the Gulf of Trieste (0.1 – 23.3 mg Kg^{-1}),**[8]** the central Portuguese Margin (0.018 – 0.594 mg Kg^{-1}),**[60]** and the South China Sea (12 – 84 μg Kg^{-1}).**[61]** The THg background in ocean sediments is 20 – 100 μg Kg^{-1}.**[62]** Both the high THg concentration and the wider range obtained here indicate important Hg contamination, as was previously reported on by Uriansrud *et al.*,**[63]** who obtained IHg levels in surface sediments next to the U-864 wreck of up to 108,000 mg Kg^{-1}. The THg distribution as a function of depth, provided in **Figure 4-4** (left y-axis), demonstrates high heterogeneity, with peak values at 1 and 2.6 m depth, corresponding with samples containing visible metallic Hg droplets. The depth profile does not reveal information on origin (or timing) and/or changes in Hg pollution. The heterogeneity can be related to the explosion that occurred during the torpedoing/sinking, the possibility of metallic Hg sinking down through the sand and clay particles, and the fact that the location suffers from landslides,**[64]** preventing time-resolved information to be obtained from the variation in THg as a function of depth.

Table 4-4. THg concentration (mg Kg^{-1}) and Hg isotopic composition ($\delta^{xxx}Hg$ and $\Delta^{xxx}Hg$) of sediment samples collected at a location in the immediate vicinity of the U-864 submarine wreck at different depths

Sediment samples									
	Depth (m)	**THg (mg Kg^{-1})**	**$\delta^{199}Hg$ (‰)**	**$\delta^{200}Hg$ (‰)**	**$\delta^{201}Hg$ (‰)**	**$\delta^{202}Hg$ (‰)**	**$\Delta^{199}Hg$ (‰)**	**$\Delta^{200}Hg$ (‰)**	**$\Delta^{201}Hg$ (‰)**
S1	0.05	3522	-0.16	-0.24	-0.43	-0.44	-0.07	-0.01	-0.10
		1702	-0.12	-0.25	-0.40	-0.51	-0.02	0.00	-0.02
		7092	-0.18	-0.30	-0.47	-0.61	-0.05	0.01	-0.01
	Average	**2100**	**-0.16**	**-0.24**	**-0.41**	**-0.48**	**-0.06**	**0.00**	**-0.05**
	SD	**1300**	**0.03**	**0.01**	**0.02**	**0.03**	**0.04**	**0.01**	**0.04**
S2	0.15	7092	-0.18	-0.30	-0.47	-0.61	-0.05	0.01	-0.01
		7903	-0.18	-0.31	-0.43	-0.60	-0.06	-0.01	0.02
	Average	**7500**	**-0.18**	**-0.30**	**-0.45**	**-0.61**	**-0.05**	**0.00**	**0.01**
	SD	**570**	**0.00**	**0.00**	**0.03**	**0.01**	**0.00**	**0.01**	**0.02**
S3	0.25	1303	-0.16	-0.23	-0.41	-0.45	-0.07	-0.01	-0.08
		433	-0.14	-0.16	-0.28	-0.33	-0.07	0.00	-0.03
		796	-0.12	-0.20	-0.37	-0.53	-0.01	0.07	0.03
	Average	**670**	**-0.13**	**-0.19**	**-0.34**	**-0.36**	**-0.06**	**-0.01**	**-0.07**
	SD	**560**	**0.03**	**0.04**	**0.07**	**0.07**	**0.02**	**0.01**	**0.03**
S4	0.45	796	-0.12	-0.20	-0.37	-0.53	-0.01	0.07	0.03
		280	-0.11	-0.14	-0.25	-0.35	-0.04	0.03	0.01
	Average	**540**	**-0.11**	**-0.17**	**-0.31**	**-0.44**	**-0.02**	**0.05**	**0.02**
	SD	**360**	**0.01**	**0.04**	**0.08**	**0.13**	**0.02**	**0.02**	**0.01**
S5	0.5	2395	-0.13	-0.19	-0.35	-0.40	-0.05	0.01	-0.05
		1074	-0.12	-0.20	-0.33	-0.45	-0.03	0.02	0.01
		6025	-0.18	-0.26	-0.42	-0.54	-0.07	0.01	-0.01
	Average	**1550**	**-0.15**	**-0.23**	**-0.40**	**-0.48**	**-0.06**	**0.01**	**-0.05**
	SD	**740**	**0.05**	**0.06**	**0.11**	**0.09**	**0.03**	**0.01**	**0.05**
S6	0.6	6025	-0.18	-0.26	-0.42	-0.54	-0.07	0.01	-0.01
		2316	-0.21	-0.26	-0.52	-0.62	-0.08	0.05	-0.05
	Average	**4200**	**-0.19**	**-0.26**	**-0.47**	**-0.58**	**-0.08**	**0.03**	**-0.03**
	SD	**2600**	**0.02**	**0.00**	**0.07**	**0.06**	**0.00**	**0.03**	**0.03**
S7	0.7	883	-0.15	-0.26	-0.44	-0.48	-0.05	-0.02	-0.07
		1024	-0.18	-0.24	-0.39	-0.47	-0.08	0.00	-0.04
	Average	**950**	**-0.16**	**-0.25**	**-0.41**	**-0.48**	**-0.07**	**-0.01**	**-0.06**
	SD	**100**	**0.02**	**0.01**	**0.03**	**0.00**	**0.02**	**0.01**	**0.03**
S8	0.9	196	-0.12	-0.18	-0.39	-0.42	-0.03	0.03	-0.07
		260	-0.12	-0.19	-0.32	-0.34	-0.05	-0.01	-0.06
	Average	**228**	**-0.12**	**-0.18**	**-0.35**	**-0.38**	**-0.04**	**0.01**	**-0.07**
	SD	**45**	**0.00**	**0.00**	**0.05**	**0.05**	**0.01**	**0.03**	**0.01**
S9	1.0	24106	-0.19	-0.29	-0.49	-0.58	-0.07	0.00	-0.05
		8544	-0.17	-0.28	-0.45	-0.54	-0.06	0.00	-0.04
		1908	-0.19	-0.18	-0.42	-0.44	-0.10	0.04	-0.09
	Average	**12900**	**-0.18**	**-0.28**	**-0.46**	**-0.55**	**-0.06**	**0.00**	**-0.04**
	SD	**9800**	**0.01**	**0.01**	**0.03**	**0.03**	**0.01**	**0.00**	**0.01**
S10	1.2	1908	-0.19	-0.18	-0.42	-0.44	-0.10	0.04	-0.09
		1068	-0.15	-0.23	-0.35	-0.44	-0.06	-0.01	-0.02
	Average	**1490**	**-0.17**	**-0.21**	**-0.39**	**-0.44**	**-0.08**	**0.01**	**-0.05**
	SD	**590**	**0.03**	**0.04**	**0.05**	**0.00**	**0.03**	**0.04**	**0.05**

Sediments – *continued*									
S11	2.0	648	-0.04	-0.09	-0.24	-0.27	0.01	0.05	-0.04
		35	-0.05	-0.10	-0.13	-0.19	-0.02	0.00	0.02
	Average	**56**	**-0.05**	**-0.09**	**-0.18**	**-0.23**	**0.00**	**0.02**	**-0.01**
	SD	**54**	**0.01**	**0.00**	**0.08**	**0.06**	**0.02**	**0.03**	**0.04**
S12	2.2	214	-0.16	-0.25	-0.45	-0.49	-0.06	-0.01	-0.08
		451	-0.17	-0.31	-0.36	-0.50	-0.07	-0.05	0.02
	Average	**330**	**-0.16**	**-0.28**	**-0.41**	**-0.50**	**-0.06**	**-0.03**	**-0.03**
	SD	**170**	**0.01**	**0.04**	**0.06**	**0.01**	**0.01**	**0.03**	**0.07**
S13	2.4	108	-0.09	-0.12	-0.24	-0.23	-0.03	0.00	-0.07
		139	-0.07	-0.15	-0.26	-0.28	0.00	-0.01	-0.05
		104	-0.07	-0.08	-0.14	-0.15	-0.04	0.00	-0.02
	Average	**117**	**-0.08**	**-0.12**	**-0.21**	**-0.22**	**-0.02**	**-0.01**	**-0.05**
	SD	**19**	**0.01**	**0.04**	**0.07**	**0.06**	**0.02**	**0.01**	**0.02**
S14	2.6	5216	-0.17	-0.33	-0.44	-0.53	-0.07	-0.06	-0.04
		21646	-0.16	-0.30	-0.43	-0.59	-0.04	0.00	0.02
	Average	**13000**	**-0.17**	**-0.31**	**-0.43**	**-0.56**	**-0.05**	**-0.03**	**-0.01**
	SD	**12000**	**0.01**	**0.02**	**0.01**	**0.05**	**0.02**	**0.04**	**0.04**
Average		**3300**	**-0.14**	**-0.22**	**-0.37**	**-0.45**	**-0.05**	**0.00**	**-0.04**
SD		**5600**	**0.04**	**0.07**	**0.10**	**0.12**	**0.03**	**0.03**	**0.04**

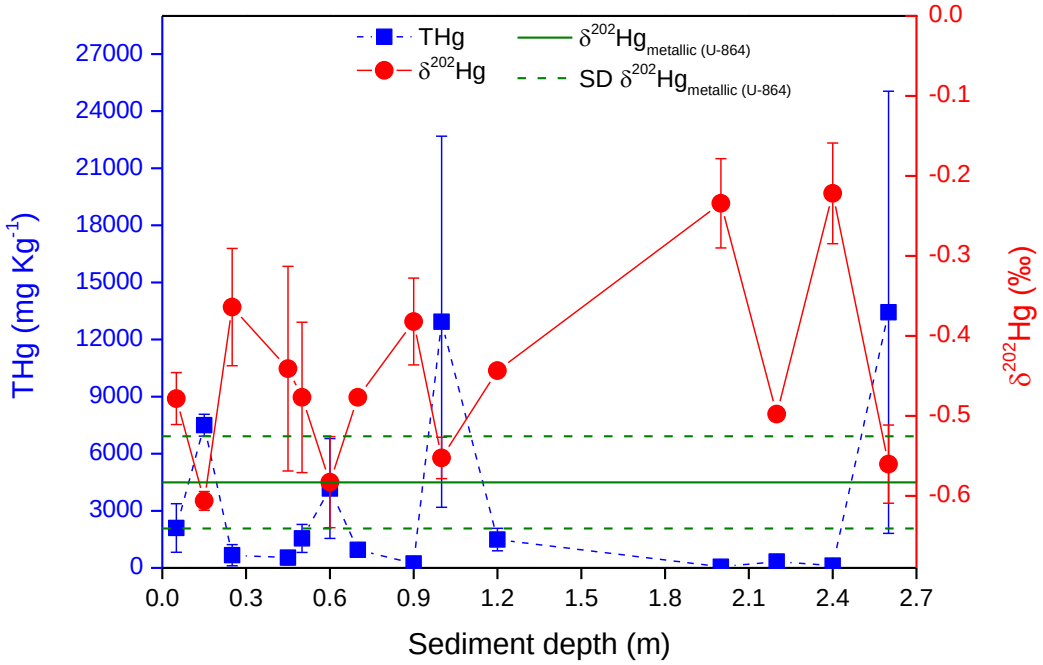

Figure 4-4. Total Hg concentration (THg, blue squares, left y-axis) and δ^{202}Hg (red circles, right y-axis) as a function of depth for sediment samples collected in the immediate vicinity of the U-864 submarine wreck. The error bars indicate the SD for 2 or 3 digestion replicates. The solid and dashed green lines show the δ^{202}Hg (average ± SD, n = 10) for the metallic Hg salvaged from the submarine wreck.

4.3.2. THg and MeHg concentration in crab tissue samples

THg and MeHg concentrations in the two types of tissues for the crab samples (n = 78), as well as the average and the SD for each type of meat are provided in **Table 4-5** for the three locations studied. Within the entire area, the THg concentration varied from 0.033 to 0.220 mg Kg^{-1} (w.w.) with a mean of 0.094 mg Kg^{-1} in brown meat and from 0.036 to 0.290 mg Kg^{-1} (w.w.) with a mean of 0.11 mg Kg^{-1} in claw meat. Previous results for *C. pagurus* caught along the entire Norwegian coast were in the range of 0.015 to 0.35 mg Kg^{-1} (mean of 0.067 mg Kg^{-1}) and 0.021 to 0.40 mg Kg^{-1} (mean of 0.095 mg Kg^{-1}) for brown and claw meat, respectively.**[65]** Concentrations of THg in brown meat of crabs were higher near the submarine wreck than background levels for the Norwegian coast. Claw meat, on the other hand, showed levels similar to background levels. In other studies using the same crab species in different marine ecosystems, the THg concentration determined ranged from 0.10 to 0.23 mg Kg^{-1} (dry weight – d.w.) for hepatopancreas and from 0.16 to 2.04 mg Kg^{-1} (d.w.) for muscle.**[66-68]** In agreement with literature values, the THg concentrations reported in this work are higher for the claw meat than for the brown meat (**Figure 4-5A** – average values), although the differences are not statistically significant ($t_{exp} = 1.81 < t_{crit} = 2.02$). In addition, the THg concentration was established to be slightly higher in samples from the north compared to samples from the two other locations, as indicated *via* ANOVA ($F_{exp} = 9.28 > F_{crit} = 3.12$), which could be tentatively explained by the North Atlantic oceanic current going from the south to the north in this region.

MeHg speciation was carried out to determine the fraction of THg present as MeHg (expressed as the MeHg fraction in %) in the two types of crab meat and at the three different locations. Clearly, the MeHg fraction (%) was distributed differently between the two tissue types ($t_{exp} = 2.01 < t_{crit} = 13.58$) with ranges of 53 to 62% and of 89 to 99% for brown and claw meat, respectively (see **Figure 4-5B** and **Table 4-5**). Such difference in bioaccumulation of IHg and of MeHg in different tissues has been documented in the literature and possible accumulation routes have been described. Previous studies concluded that the dominant input of Hg in marine organisms comes from the food, although also direct uptake from the water column contributes.**[69-71]** After Hg ingestion, both IHg and MeHg are rapidly transferred to the visceral organs, *i.e.* brown meat in crab, and from there, the Hg species are further distributed. In crustaceans, the hepatopancreas acts as the main reservoir

Table 4-5. THg concentrations (mg Kg^{-1}). % of MeHg and Hg isotopic composition ($\delta^{xxx}Hg$ and $\Delta^{xxx}Hg$) for both types of meat for the selected crab samples collected at the wreck location, 4 nautical miles north and 4 nautical miles south.

Crab Samples (*Cancer Pagurus*)									
	THg (mg Kg^{-1})	**% MeHg**	**$\delta^{199}Hg$ (‰)**	**$\delta^{200}Hg$ (‰)**	**$\delta^{201}Hg$ (‰)**	**$\delta^{202}Hg$ (‰)**	**$\Delta^{199}Hg$ (‰)**	**$\Delta^{200}Hg$ (‰)**	**$\Delta^{201}Hg$ (‰)**
North	0.120	59	0.30	0.09	0.37	0.17	0.26	0.00	0.23
Brown	0.120	83	0.37	0.05	0.25	-0.01	0.37	0.06	0.26
	0.100	65	0.22	0.01	0.08	-0.05	0.24	0.03	0.12
	0.160	38	0.23	0.18	0.26	0.24	0.17	0.06	0.08
	0.094	72	0.48	0.15	0.40	0.16	0.44	0.07	0.28
	0.130	75	0.40	0.10	0.34	0.10	0.38	0.05	0.27
	0.130	26	0.14	0.05	0.17	0.11	0.12	0.00	0.09
	0.077	60	0.21	0.04	0.05	-0.08	0.23	0.09	0.11
	0.130	29	0.17	-0.01	0.00	-0.07	0.18	0.02	0.06
	0.170	34	0.19	0.01	0.13	-0.03	0.19	0.02	0.15
	0.220	64	0.13	-0.02	0.10	-0.15	0.16	0.06	0.21
	0.068	31	0.28	0.11	0.21	0.01	0.28	0.11	0.20
	0.150	54	0.18	0.02	0.06	-0.08	0.20	0.05	0.11
Average	**0.128**	**53**	**0.25**	**0.06**	**0.19**	**0.02**	**0.25**	**0.05**	**0.17**
SD	**0.041**	**19**	**0.11**	**0.06**	**0.13**	**0.12**	**0.10**	**0.03**	**0.08**
Wreck	0.130	38	0.12	0.02	0.07	0.05	0.11	0.00	0.03
Brown	0.130	55	0.21	0.05	0.17	0.02	0.21	0.04	0.16
	0.052	65	0.17	0.02	0.08	-0.13	0.20	0.08	0.17
	0.160	45	0.12	-0.07	-0.04	-0.24	0.18	0.05	0.13
	0.130	38	0.16	-0.16	-0.24	-0.42	0.27	0.05	0.08
	0.150	36	0.26	0.05	0.14	-0.12	0.29	0.11	0.23
	0.046	70	0.15	0.01	0.21	0.04	0.14	-0.01	0.18
	0.076	36	0.04	-0.16	-0.10	-0.27	0.11	-0.02	0.11
	0.060	63	0.15	-0.09	0.05	-0.16	0.19	0.00	0.18
	0.042	62	0.21	-0.10	-0.01	-0.31	0.29	0.06	0.22
	0.042	64	0.30	-0.01	0.16	-0.12	0.33	0.05	0.25
	0.041	59	0.32	-0.04	0.13	-0.10	0.34	0.01	0.21
	0.049	67	0.25	0.05	0.19	0.02	0.24	0.04	0.18
Average	**0.085**	**54**	**0.19**	**-0.03**	**0.06**	**-0.13**	**0.22**	**0.03**	**0.16**
SD	**0.047**	**13**	**0.08**	**0.08**	**0.13**	**0.15**	**0.08**	**0.04**	**0.06**
South	0.033	73	0.43	0.05	0.32	0.06	0.42	0.02	0.28
Brown	0.096	49	0.30	0.14	0.33	0.20	0.25	0.04	0.18
	0.092	60	0.23	0.03	0.19	0.02	0.23	0.02	0.17
	0.072	54	0.34	0.03	0.30	0.09	0.32	-0.01	0.23
	0.097	70	0.13	-0.07	0.03	-0.09	0.15	-0.03	0.10
	0.062	60	0.19	0.01	0.13	-0.02	0.19	0.02	0.15
	0.078	73	0.44	0.11	0.50	0.20	0.38	0.00	0.35
	0.095	69	0.34	0.08	0.34	0.16	0.30	0.00	0.21
	0.066	50	0.12	-0.02	0.07	-0.06	0.13	0.01	0.12
	0.070	41	0.20	0.08	0.18	0.14	0.16	0.01	0.07
	0.043	67	0.22	0.02	0.24	0.00	0.22	0.02	0.24
	0.058	90	0.29	0.04	0.24	-0.01	0.29	0.04	0.25
	0.044	48	0.16	0.05	0.16	0.14	0.13	-0.02	0.06
Average	**0.070**	**62**	**0.26**	**0.04**	**0.23**	**0.07**	**0.24**	**0.01**	**0.18**
SD	**0.022**	**13**	**0.11**	**0.05**	**0.13**	**0.10**	**0.09**	**0.02**	**0.09**
Average	**0.094**	**56**	**0.23**	**0.02**	**0.16**	**-0.01**	**0.24**	**0.03**	**0.17**
SD	**0.045**	**16**	**0.10**	**0.08**	**0.15**	**0.15**	**0.09**	**0.03**	**0.08**

Crab Samples (*Cancer Pagurus*) – *continued*									
	THg (mg Kg^{-1})	**% MeHg**	**δ^{199}Hg (‰)**	**δ^{200}Hg (‰)**	**δ^{201}Hg (‰)**	**δ^{202}Hg (‰)**	**Δ^{199}Hg (‰)**	**Δ^{200}Hg (‰)**	**Δ^{201}Hg (‰)**
North	0.170	106	0.61	0.36	0.87	0.70	0.43	0.01	0.35
Claw	0.100	95	0.31	0.10	0.34	0.08	0.29	0.06	0.28
	0.100	95	0.48	0.30	0.55	0.46	0.36	0.07	0.21
	0.180	100	0.56	0.33	0.68	0.51	0.44	0.08	0.30
	0.290	100	0.89	0.42	1.12	0.72	0.71	0.06	0.58
	0.160	113	0.60	0.30	0.79	0.57	0.46	0.01	0.36
	0.078	94	0.49	0.22	0.54	0.31	0.41	0.06	0.31
	0.074	95	0.35	0.10	0.41	0.11	0.33	0.04	0.32
	0.072	88	0.38	0.18	0.52	0.41	0.28	-0.02	0.21
	0.140	100	0.56	0.23	0.58	0.31	0.49	0.08	0.35
	0.240	96	0.52	0.32	0.63	0.59	0.37	0.02	0.19
	0.046	107	0.44	0.19	0.55	0.31	0.36	0.03	0.32
	0.110	100	0.28	0.17	0.37	0.24	0.22	0.05	0.19
Average	**0.135**	**99**	**0.50**	**0.25**	**0.61**	**0.41**	**0.40**	**0.04**	**0.31**
SD	**0.068**	**6**	**0.16**	**0.10**	**0.22**	**0.20**	**0.12**	**0.03**	**0.10**
Wreck	0.071	89	0.49	0.34	0.82	0.61	0.34	0.03	0.37
Claw	0.140	93	0.67	0.19	0.72	0.32	0.59	0.04	0.48
	0.110	72	0.37	0.11	0.44	0.20	0.32	0.01	0.29
	0.140	93	0.53	0.21	0.68	0.46	0.41	-0.02	0.34
	0.052	88	0.49	0.11	0.51	0.18	0.44	0.02	0.37
	0.140	86	0.52	0.26	0.74	0.38	0.42	0.07	0.45
	0.100	93	0.56	0.31	0.70	0.56	0.42	0.03	0.27
	0.071	89	0.55	0.29	0.69	0.50	0.43	0.04	0.31
	0.075	92	0.35	0.08	0.33	-0.01	0.35	0.08	0.33
	0.090	88	0.51	0.20	0.50	0.28	0.44	0.06	0.29
	0.056	98	0.47	0.20	0.63	0.32	0.39	0.04	0.38
	0.075	89	0.60	0.29	0.71	0.45	0.48	0.07	0.38
	0.100	91	0.42	0.10	0.41	0.20	0.37	0.00	0.26
Average	**0.094**	**89**	**0.50**	**0.21**	**0.61**	**0.34**	**0.42**	**0.04**	**0.35**
SD	**0.030**	**6**	**0.09**	**0.09**	**0.15**	**0.17**	**0.07**	**0.03**	**0.07**
South	0.036	86	0.63	0.15	0.68	0.36	0.54	-0.03	0.41
Claw	0.110	91	0.71	0.39	0.91	0.70	0.54	0.04	0.39
	0.087	91	0.64	0.25	0.78	0.44	0.53	0.03	0.45
	0.120	100	0.69	0.22	0.86	0.54	0.55	-0.05	0.45
	0.150	93	0.66	0.33	0.81	0.60	0.51	0.02	0.36
	0.086	90	0.37	0.22	0.58	0.45	0.26	0.00	0.24
	0.130	100	0.46	0.08	0.53	0.07	0.45	0.04	0.48
	0.180	89	0.64	0.34	0.89	0.67	0.47	0.01	0.38
	0.067	85	0.63	0.14	0.71	0.32	0.55	-0.03	0.47
	0.065	95	0.38	0.28	0.63	0.55	0.24	0.00	0.22
	0.069	90	0.58	0.25	0.70	0.53	0.44	-0.02	0.30
	0.092	99	0.37	0.04	0.33	0.06	0.35	0.01	0.29
	0.047	91	0.31	0.05	0.27	0.10	0.28	0.00	0.20
Average	**0.095**	**92**	**0.54**	**0.21**	**0.67**	**0.41**	**0.44**	**0.00**	**0.36**
SD	**0.040**	**5**	**0.14**	**0.11**	**0.20**	**0.22**	**0.12**	**0.03**	**0.10**
Average	**0.108**	**94**	**0.51**	**0.22**	**0.63**	**0.39**	**0.42**	**0.03**	**0.34**
SD	**0.053**	**7**	**0.13**	**0.10**	**0.19**	**0.20**	**0.10**	**0.03**	**0.09**

for IHg when contamination comes from the food. IHg remains in the brown meat, whereas MeHg is accumulated in muscle tissue (claw meat), which is characterized by high MeHg storage capacity and low depuration rates.**[18]** In addition, the Assimilation Efficiency (AE) is considerably higher for MeHg than for IHg,**[17]** while the excretion is favorable for the latter,**[72]** which is in good agreement with the results reported in this work.

In contrast to the differences in THg concentration, ANOVA indicates no significant variations in the MeHg fraction (%) between the 3 locations studied (F_{exp} = 0.46 < F_{crit} = 3.12), as is shown in **Figure 4-5B** and **Table 4-5**. However, neither the THg concentration, nor the MeHg fraction (%), provides any insight into origin of the Hg pollution, thus necessitating Hg isotopic analysis.

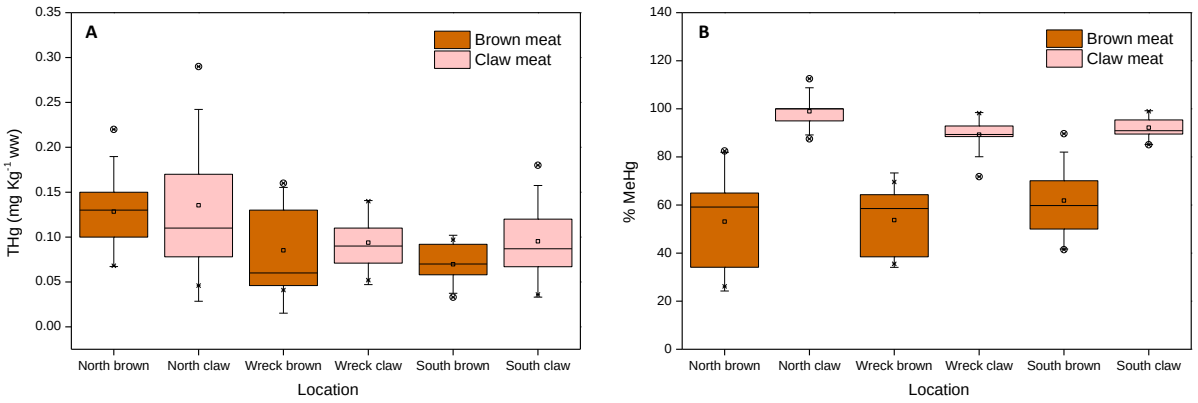

Figure 4-5. Total mercury (THg) concentration (as determined by ICP-MS) and fraction of the THg present as MeHg (% of MeHg, as determined *via* GC-ICP-IDMS) expressed as average of the selected individuals (n = 13 for each location) for both crab meat types and for the three locations studied.

4.3.3. Isotopic composition of metallic Hg

Isotopic analysis of metallic Hg salvaged from the submarine wreck was carried out aiming to elucidate whether this contamination source could be correlated with the Hg pollution observed in the surrounding area. The resulting isotopic composition reported as delta (δ^{xxx}Hg ‰) and capital delta (Δ^{xxx}Hg ‰) notation (average ± SD, n = 10) is shown in **Table 4-6**. The δ^{202}Hg value is -0.58 ± 0.06 ‰ and the isotopic composition seems to be affected by a slight extent of MIF (Δ^{199}Hg = -0.06 ± 0.04 ‰

and Δ^{201}Hg = -0.07 ± 0.04 ‰). These values are similar to those reported in literature for UM-Almaden metallic Hg (δ^{202}Hg = -0.58 ± 0.08 ‰ and Δ^{199}Hg = -0.01 ± 0.01 ‰),**[27, 73]** although with a slightly higher degree of negative MIF. This low-extent MIF (<0.2‰) is most likely caused by the nuclear volume effect (NVE) potentially accompanying metallic Hg vaporization.**[74]** In literature, NVE was reported to accompany Hg^0 evaporation/condensation,**[31]** Hg^{2+} reduction in the dark,**[75, 76]** and equilibrium Hg^{2+} – thiol complexation.**[77]** In the case of Hg^0 evaporation, the lighter isotopes with higher nuclear charge density are enriched in the vapor phase as a result of their weaker metallic bond and higher vapor pressure, while the heavier isotopes preferably remain in the metallic fraction. MIF caused by the NVE is characterized by a Δ^{199}Hg/Δ^{201}Hg ratio of ~1.6, a value that can be used to identify the presence of covalent Hg species, such as metallic Hg.**[78]** However, the low $\Delta^{199,201}$Hg values and their corresponding uncertainties in the metallic Hg studied do not enable to reliably calculate their ratio.

Table 4-6. Hg isotopic composition of metallic Hg salvaged from the U-864 submarine wreck

	Metallic Hg						
	δ^{199}Hg (‰)	**δ^{200}Hg (‰)**	**δ^{201}Hg (‰)**	**δ^{202}Hg (‰)**	**Δ^{199}Hg (‰)**	**Δ^{200}Hg (‰)**	**Δ^{201}Hg (‰)**
	-0.22	-0.31	-0.56	-0.65	-0.06	0.01	-0.07
	-0.18	-0.29	-0.55	-0.62	-0.02	0.02	-0.08
	-0.21	-0.36	-0.57	-0.68	-0.04	-0.02	-0.06
	-0.16	-0.24	-0.52	-0.57	-0.02	0.04	-0.09
	-0.20	-0.29	-0.52	-0.58	-0.06	0.00	-0.08
	-0.20	-0.26	-0.52	-0.57	-0.06	0.03	-0.09
	-0.20	-0.31	-0.48	-0.57	-0.06	-0.03	-0.06
	-0.19	-0.26	-0.39	-0.49	-0.07	-0.02	-0.02
	-0.22	-0.34	-0.51	-0.60	-0.07	-0.04	-0.06
	-0.23	-0.29	-0.45	-0.51	-0.10	-0.03	-0.06
Average	**-0.20**	**-0.30**	**-0.51**	**-0.58**	**-0.06**	**0.00**	**-0.07**
SD	**0.02**	**0.04**	**0.06**	**0.06**	**0.02**	**0.03**	**0.02**

4.3.4. Hg isotopic composition of sediment samples

The isotopic composition of Hg in the sediment samples collected in the immediate vicinity of the U-864 submarine as a function of depth is shown in **Table 4-4**. δ^{202}Hg ranged from -0.62 to -0.15 ‰ within the depth profile (0 – 2.6 m). **Figure 4-4** shows the THg content (left y-axis) and δ^{202}Hg value (right y-axis) as a function of depth. Interestingly, an opposite trend was found for the two parameters, *i.e.*, the higher the THg concentration, the lower the δ^{202}Hg and *vice versa*. In **Figure 4-4**, also the δ^{202}Hg value (solid green line) ± SD (dashed green lines) for the metallic Hg from the submarine wreck has been indicated. As can be seen, the lowest δ^{202}Hg sediment values are within the range for the metallic Hg. To further evaluate the correlation between concentration and isotopic composition, the δ^{202}Hg results for all sediments and digestion replicates were plotted as a function of the THg concentration using a linear (**Figure 4-6A**) and a logarithmic abscissa scale (**Figure 4-6B**). A strong negative correlation ($r = 0.762$, $p = 0.000$) was found between δ^{202}Hg and log(THg), with δ^{202}Hg values for sediment samples approaching that of the submarine Hg at high THg concentrations. This strongly suggests that the isotopic composition of sediments with the highest contamination levels are completely dominated by the isotopic composition of the metallic Hg from the U-864 (same isotopic signature).

Also the extent of MIF is of interest from an environmental point of view. **Figure 4-7** shows three-isotope plots for δ^{199}Hg vs δ^{202}Hg (A), δ^{200}Hg vs δ^{202}Hg (B) and δ^{201}Hg *vs* δ^{202}Hg (C) for the sediment samples. As can be seen in **Figure 4-7B** (δ^{200}Hg), the results plot perfectly on the theoretical mass-dependent fractionation line (absence of MIF for the even-numbered isotopes of Hg). In **Figure 4-7A** and **4-7C** (with data for δ^{199}Hg and δ^{201}Hg, respectively), on the other hand, the values show a slight deviation from the fractionation line, suggesting that MIF has possibly affected the odd-numbered isotopes of Hg.

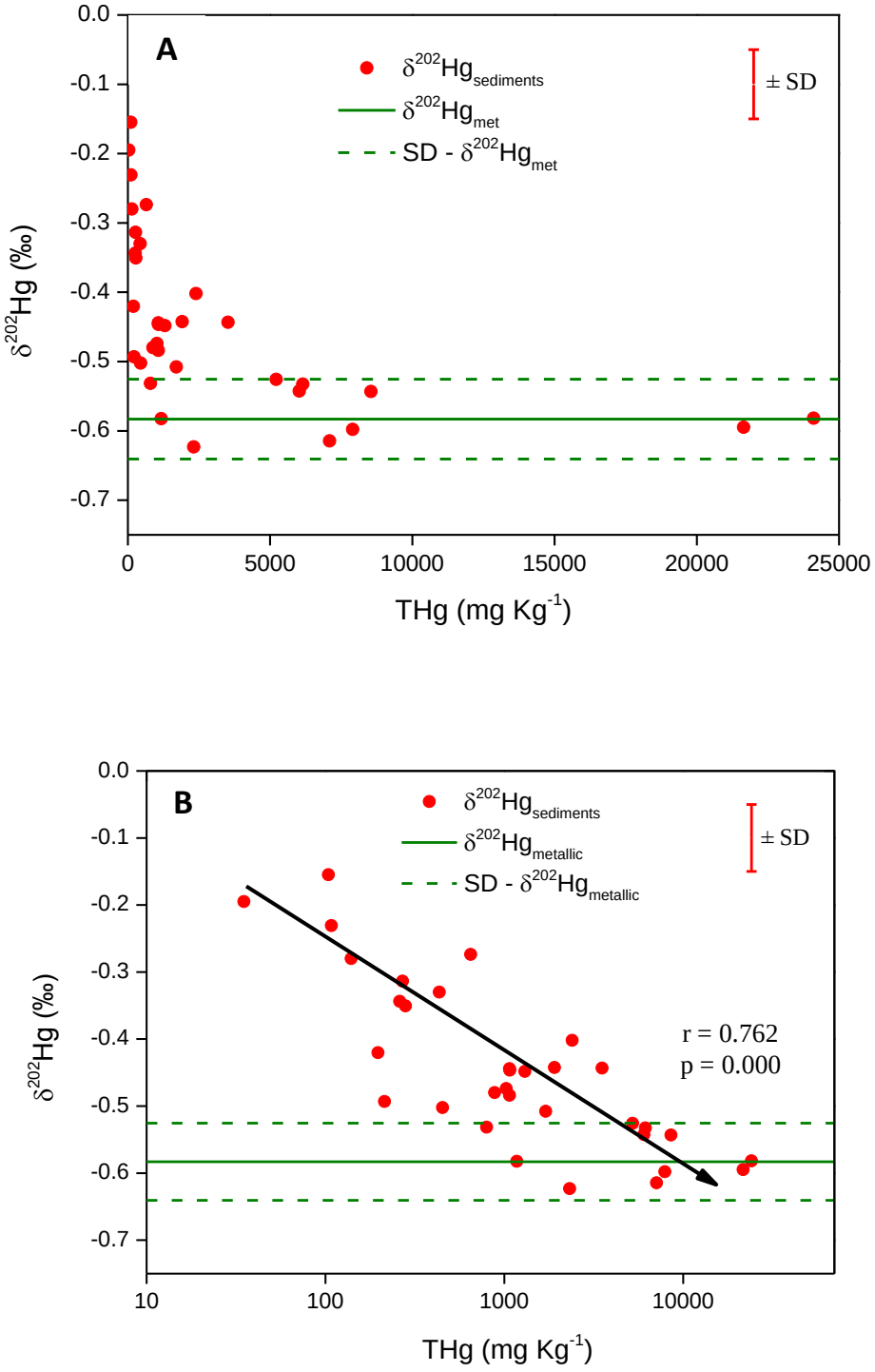

Figure 4-6. δ^{202}Hg vs THg for sediment samples (all digestion replicates) collected in the immediate vicinity of the U-864 submarine using (A) a linear scale and (B) a logarithmic scale for the abscissa. The solid and dashed green lines show the δ^{202}Hg (average ± SD, n = 10) for metallic Hg salvaged from the submarine wreck.

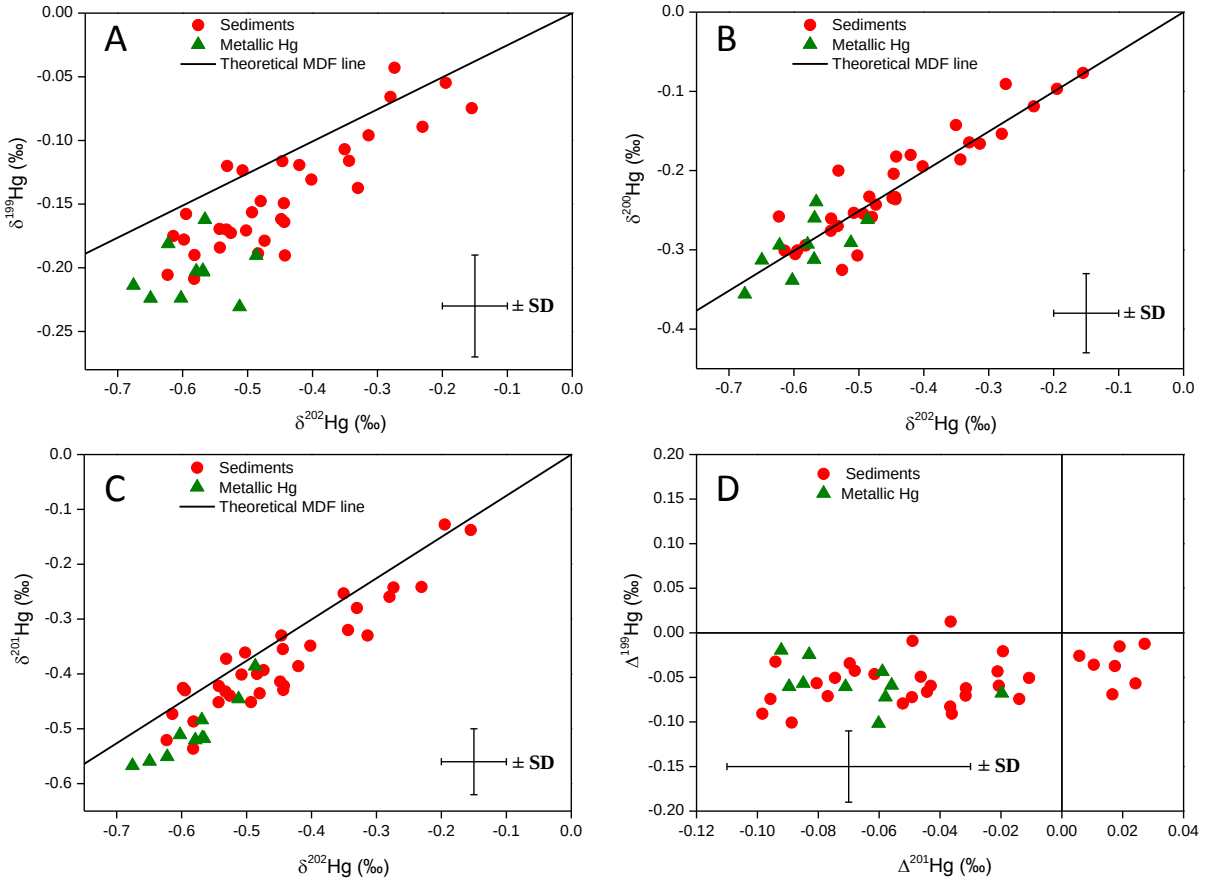

Figure 4-7. Three-isotope plots δ^{199}Hg vs δ^{202}Hg (A), δ^{200}Hg vs δ^{202}Hg (B) and δ^{201}Hg vs δ^{202}Hg (C) for sediments samples (all digestion replicates, red circles) and metallic Hg (green triangles). Theoretical MDF-lines are shown in black. (D) Δ^{199}Hg vs Δ^{201}Hg for sediment samples and metallic Hg.

The degree of MIF for sediments was reported as Δ^{199}Hg and Δ^{201}Hg (-0.05 ± 0.04 and -0.04 ± 0.04 ‰, respectively – see **Table 4-4**) and they were plotted one versus another in **Figure 4-7D**. These results can be interpreted as low negative MIF or absence of MIF, which can be attributed to the low extent of photochemical reduction at 150 m depth, and is in agreement with results reported in previous studies for sediment samples.**[19, 79]** The results also agree with the degree of MIF reported for the metallic Hg from the U-864 submarine, thus also rendering MIF signatures a useful tool to track the source of Hg contamination.

4.3.5. Hg isotopic composition of crab tissue samples

Isotope ratios of Hg in *C. pagurus* tissue samples are compiled in **Table 4-5**. These results, expressed as the average δ^{202}Hg value as a function of location and tissue type, ranged from -0.13 to 0.07‰ for brown meat and from 0.34 to 0.41‰ for claw meat. Generally speaking, significant differences were found between the two tissues (t_{exp} = 10.17 > t_{crit} = 1.99), which is attributed to the smaller fraction of Hg present as MeHg (%) in brown meat compared to claw meat, due to the capacity of the latter as reservoir of MeHg.**[80]** **Figure 4-8** (A, B and C) shows three-isotope plots of δ^{199}Hg vs δ^{202}Hg, δ^{200}Hg vs δ^{202}Hg and δ^{201}Hg vs δ^{202}Hg. The isotopic composition of Hg varies profoundly across the different sample types *i.e.*, metallic Hg, sediments, brown meat and claw meat. Moreover, in contrast to metallic Hg and sediments, both tissue types demonstrate a clear effect of MIF on the odd-numbered Hg isotopes, that is more remarkable for the claw meat than for the brown meat (*vide infra*).

The δ^{202}Hg values follow the trend: metallic Hg (-0.58 ± 0.06 ‰) < sediments (-0.45 ± 0.12 ‰) < brown meat (-0.01 ± 0.15 ‰) < claw meat (0.39 ± 0.20 ‰). Such differences in δ^{202}Hg between sediments and aquatic biota have already been reported in the literature, and sediments have been suggested as the dominant source of Hg in the aquatic food web.**[13, 14, 41, 55]** This Hg isotopic variation seems to be related with the differences in isotopic composition between MeHg and IHg, and the different extent of MeHg bioaccumulation across the trophic chain. This is related to MDF accompanying equilibrium sorption of the aqueous Hg species,**[77]** microbial Hg methylation and demethylation **[30, 81, 82]** and abiotic redox reactions,**[76]** prior to trophic transfer across the food web. Gehrke *et al.***[14]** and Kwon *et al.***[55]** reported δ^{202}Hg offsets of 0.73 ± 0.16 ‰ and 0.64 ± 0.38 ‰ between sediments and aquatic biota, *i.e.* forage fish and green crab, respectively. In this work, δ^{202}Hg offsets of 0.44 ± 0.10 and 0.84 ± 0.04 ‰ were observed between the sediment and the two tissue types *i.e.* brown and claw meat, respectively.

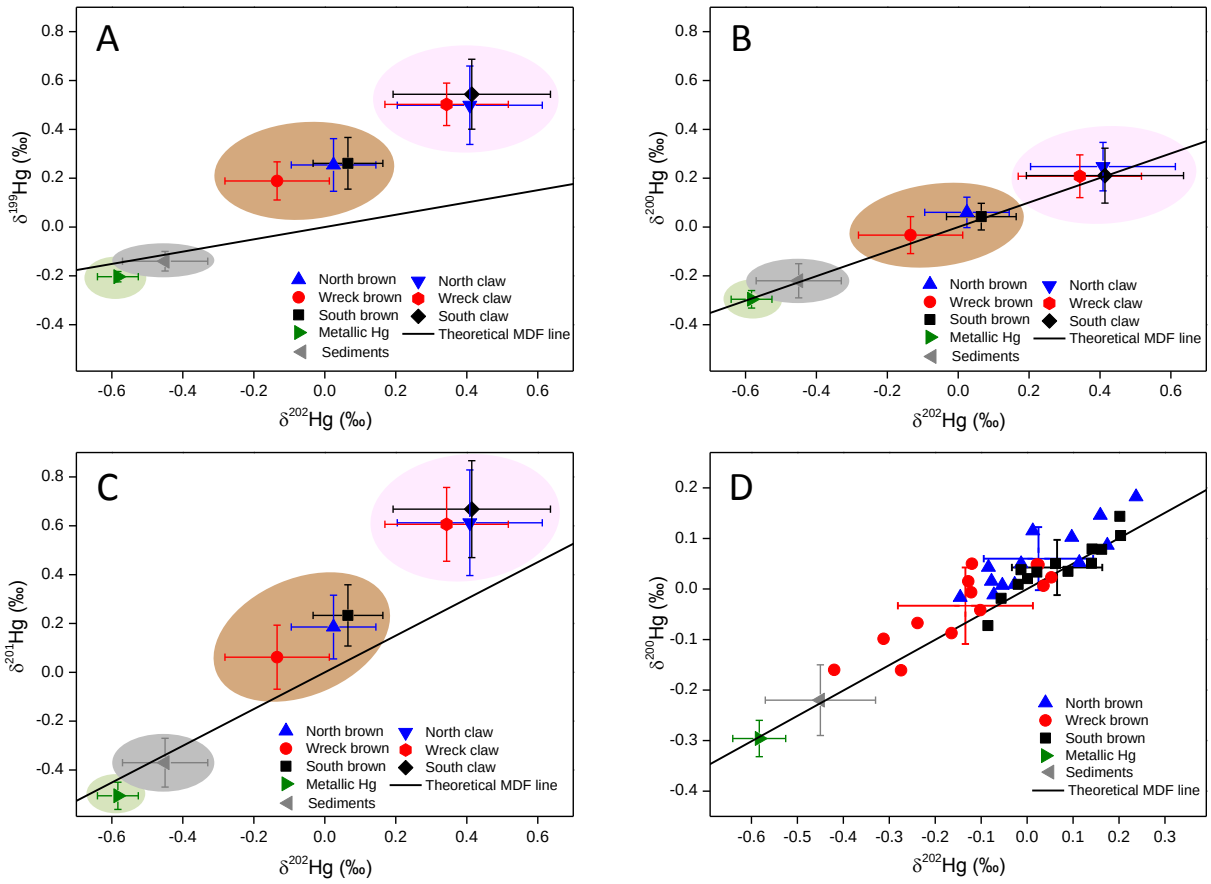

Figure 4-8. Three-isotope plots $\delta^{199}Hg$ vs $\delta^{202}Hg$ (A), $\delta^{200}Hg$ vs $\delta^{202}Hg$ (B) and $\delta^{201}Hg$ vs $\delta^{202}Hg$ (C) for metallic Hg from the U-864 wreck (green, n = 10), sediments from the wreck location (grey field, n = 14) and *C. pagurus* tissues – averages for brown (brown field) and claw meat (pink field) , n = 78 in total – from the three sampling zones: north (blue), south (black) and wreck (red). The error bars indicate the SD for each group of samples. **Figure 4-8D** shows the three-isotope plot $\delta^{200}Hg$ vs $\delta^{202}Hg$ for the brown meat from the three locations (one point per individual, n = 39) and the average values for sediment samples (n = 33) and the metallic Hg from the U-864 wreck (n = 10).

These differences are related with the extent of IHg and MeHg in both tissues. A significant correlation (r = 0.679, p = 0.000) was observed between %MeHg and $\delta^{202}Hg$ within the entire data set (n = 78), which is in good agreement with the values reported in previous works. Thus, we hypothesize that also in the context of this study, the sediments are the primary source of MeHg, although the

contribution of other sources of MeHg with a different isotopic composition cannot be ruled out. However, as a result of the massive presence of elemental Hg in the unusual context of this work and the high Hg heterogeneity observed in the sediments, this tentative conclusion has to be handled with care.

An in-depth evaluation of the isotopic signature for both crab tissues at the three locations studied shows the following results. For claw meat, ANOVA indicates no significant variations within the three sampling zones ($F_{exp} = 0.50 < F_{crit} = 3.26$). However, the isotopic composition of the brown meat (the main reservoir of IHg), seems to be a better vector for tracking Hg pollution coming from a specific contamination source as significant differences were found between the three sampling zones ($F_{exp} = 9.54 > F_{crit} = 3.26$). **Figure 4-8D** shows δ^{200}Hg as a function of δ^{202}Hg for the complete brown meat data set. As can be seen, no significant differences were found between the locations north and south of the wreck ($t_{exp} = 0.95 < t_{crit} = 2.06$), whereas statistically significant differences were observed between these two locations on the one hand and the wreck location on the other ($t_{exp} = 3.03 > t_{crit} = 2.06$ and $t_{exp} = 4.07 > t_{crit} = 2.06$ for north-of-wreck and south-of-wreck, respectively). Also, it is clearly shown that the isotopic signatures of brown tissue for the individual crabs collected at the wreck location are shifted in the direction of that of the submarine Hg and the sediments (see **Figure 4-8D**), which suggests that they are affected by metallic Hg from the U-864. Due to the feeding habits of this crab species (see experimental section),**[48]** we hypothesize that this difference most likely stems from the direct intake of metallic Hg by *C. Pagurus*, demonstrating that the determination of Hg isotopic signatures of visceral organs from *C. pagurus* is a valuable tool for tracking Hg pollution in the marine ecosystem studied and for evaluating the corresponding environmental risk.

As previously indicated, the isotopic composition of Hg in the crab tissue samples testify of MIF (expressed as Δ^{xxx}Hg notation). **Figure 4-9** shows the Δ^{199}Hg (A) and Δ^{201}Hg (B) *vs* δ^{202}Hg. Significant differences were found between the two tissue types ($t_{exp} = 8.64 > t_{crit} = 1.99$), with Δ^{199}Hg values ranging from 0.22 to 0.25 ‰ for brown meat and from 0.40 to 0.44 ‰ for claw meat (average Δ^{199}Hg as a function of location and tissue type).

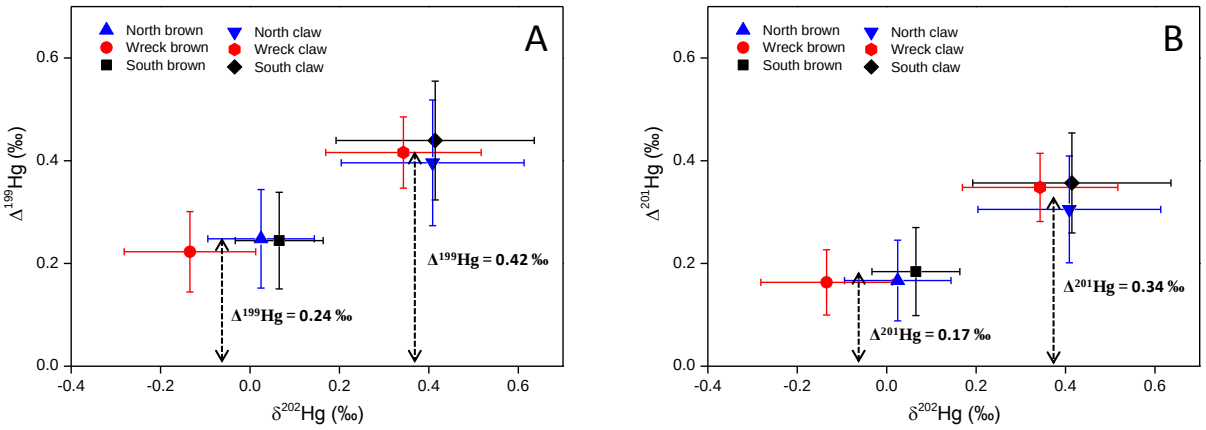

Figure 4-9. $\Delta^{199}Hg$ (A) and $\Delta^{201}Hg$ (B) vs $\delta^{202}Hg$ for both *C. pagurus* tissues for the three locations studied: north (blue), south (black) and wreck (red). The error bars indicate the SD for n = 13.

These differences are also related with the MeHg fraction (%) and a significant correlation (r = 0.707, p = 0.000) was found between %MeHg and $\Delta^{199}Hg$ within the entire data set (n = 78). However, in contrast to $\delta^{202}Hg$, for $\Delta^{199}Hg$ ANOVA indicates no significant variation between the three sampling zones (F_{exp} = 0.34 < F_{crit} = 3.26 and F_{exp} = 0.55 < F_{crit} = 3.26, for brown and claw meat, respectively). $\Delta^{199}Hg$ has been used in many studies to discern specific processes, such as photochemical reduction of Hg(II) and MeHg,**[19]** and to study biogeochemical transformations of the bioavailable pools of Hg.**[14]** Das *et al.***[42]** suggested that MIF in fish from the first two trophic levels might occur during the bioaccumulation and biomagnification of Hg. However, several works to date reported on the photochemical reactions involving Hg(II) and MeHg as the only processes yielding MIF in aquatic organisms.**[38, 40, 55, 57]** Next to the NVE, the other mechanism for explaining MIF of Hg isotopes is the magnetic isotope effect (MIE). Bergquist and Blum**[38]** came to the conclusion that photochemical reduction of aqueous Hg(II) and of MeHg is most likely accompanied by MIE, and that the participation of either Hg(II) or MeHg can be distinguished based on the slope of the straight line obtained by plotting $\Delta^{199}Hg$ versus $\Delta^{201}Hg$ (slopes of 1.0 and 1.3 for Hg(II) and MeHg photoreduction, respectively). In this work, $\Delta^{199}Hg$ is plotted as a function of $\Delta^{201}Hg$ in **Figure 4-10** for the complete data set. A regression line (R^2 = 0.83) with a slope of 1.02 ± 0.05 was obtained. This value is not significantly different from that for

photochemical reduction of Hg(II), suggesting that the MIF evidenced in crab tissue samples can be mainly attributed to MIE accompanying photoreduction of the IHg in the aquatic ecosystem studied.

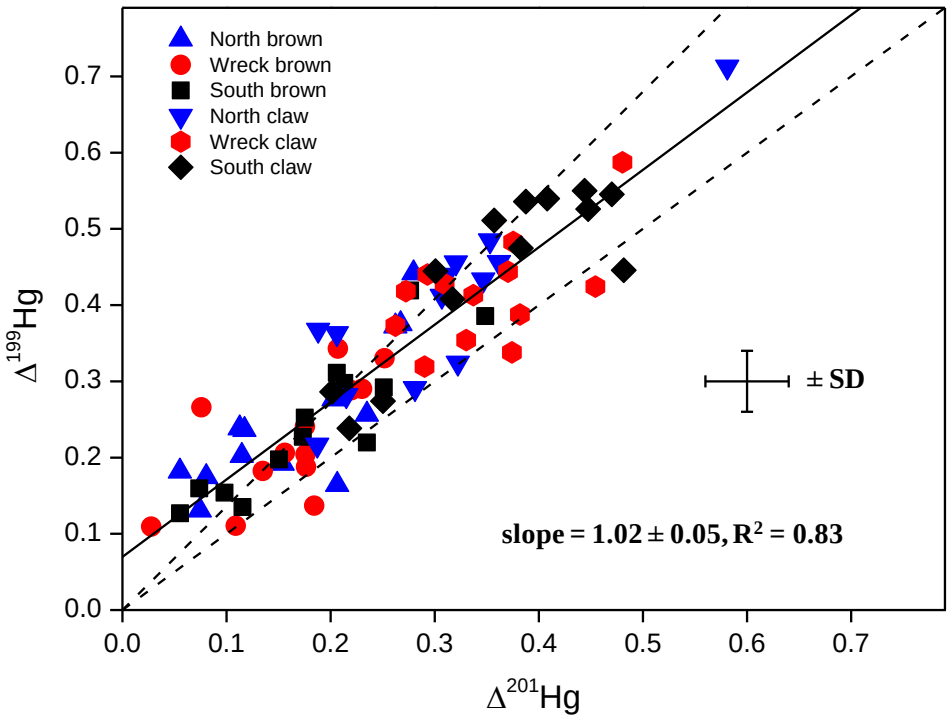

Figure 4-10. Δ^{199}Hg vs Δ^{201}Hg for the complete *C. pagurus* data set for both tissues from the three locations studied: north (blue), south (black) and wreck (red). The black solid line is the best-fitting straight line through the experimental data and its slope (1.02 ± 0.05) serves as an indicator of the type of mass-independent fractionation (MIF): the black dashed lines represent the slopes calculated by Bergquist and Blum **[38]** for MeHg (1.3) and Hg^{2+} photoreduction (1.0)

4.3.6. Environmental impact

Overall, the data obtained in this work provide an expected, but now undeniable link between the Hg pollution in the sediments and the metallic Hg leaking from the U-864 wreck. Due to the low content of organic matter in the sediments, there is little microbial methylation activity at the wreck location, suggesting that the Hg pollution from the U-864 submarine may predominantly remain in the form of

metallic Hg, which is characterized by a lower bioavailability than other Hg species. We hypothesize that the feeding habits of *Cancer pagurus* may allow for direct ingestion of this metallic Hg, and that the presence of metallic Hg in the digestive system (and thus, in the brown meat) of this crab species is most likely the responsible for the differences observed at the wreck place. However, except for this variation, the Hg isotope ratio results do not offer any proof for the introduction of the submarine Hg into the marine food chain.

References

[1] P.A. Olsvik, M. Brattås, K.K. Lie, A. Goksøyr, Chemosphere, 83 (2011) 552 - 563.

[2] S. Frantzen, A. Maage, D. Furevik, K. Julshamn, Mercury content in fish and seafood by the wreck of U864 west of Fedje - New analysis in 2009 and comparison with data from the time period 2004 to 2008. Kvikksølvinnhold i fisk og sjømat ved vraket av U864 vest av Fedje - Nye analyser i 2009 og sammenligning med data fra perioden 2004 til 2008, In Norwegian, (2010).

[3] K. Kvangarsnes, S. Frantzen, K. Julshamn, L.J. Sæthre, K. Nedreaas, A. Maage, J. Food Sci. Eng., 2 (2012) 603 - 615.

[4] W.F. Fitzgerald, C.H. Lamborg, C.R. Hammerschmidt, Chem. Rev., 107 (2007) 641 - 662.

[5] C.T. Driscoll, R.P. Mason, H.M. Chan, D.J. Jacob, N. Pirrone, Environ. Sci. Technol., 47 (2013) 4967 - 4983.

[6] F.M.M. Morel, A.M.L. Kraepiel, M. Amyot, Annu. Rev. Ecol. Syst., 29 (1998) 543 - 566.

[7] E.M. Sunderland, Environ. Health Perspect., 115 (2007) 235 - 242.

[8] D. Foucher, V. Ogrinc, H. Hintelmann, Environ. Sci. Technol., 43 (2009) 33 - 39.

[9] R. Sun, J.E. Sonke, L.-E. Heimbürger, H.E. Belkin, G. Liu, D. Shome, E. Cukrowska, C. Liousse, O.S. Pokrovsky, D.G. Streets, Environ. Sci. Technol., 48 (2014) 7660 - 7668.

[10] J.G. Wiederhold, U. Skyllberg, A. Drott, M. Jiskra, S. Jonsson, E. Björn, B. Bourdon, R. Kretzschmar, Environ. Sci. Technol., 49 (2015) 177 - 185.

[11] T. Zambardi, J.E. Sonke, J.P. Toutain, F. Sortino, H. Shinohara, Earth Planet. Sci. Lett., 277 (2009) 236 - 243.

[12] J.M. Benoit, C.C. Gilmour, A. Heyes, R.P. Mason, C.L. Miller, Geochemical and biological controls over methylmercury production and degradation in aquatic ecosystems. In *Biogeochemistry of Environmentally Important Trace Elements*; Cai, Y., Braids, O. C., Eds.; American Chemical Society: Washington DC, 835 (2003) 262 - 297.

[13] N. Gantner, H. Hintelmann, W. Zheng, D.C. Muir, Environ. Sci. Technol., 43 (2009) 9148 - 9154.

[14] G.E. Gehrke, J.D. Blum, D.G. Slotton, B.K. Greenfield, Environ. Sci. Technol., 45 (2011) 1264 - 1270.

[15] C.R. Hammerschmidt, W.F. Fitzgerald, Environ. Sci. Technol., 40 (2006) 7764 - 7770.

[16] C.Y. Chen, M.E. Borsuk, D.M. Bugge, T. Hollweg, P.H. Balcom, D.M. Ward, J. Williams, R.P. Mason, Plos One, 9 (2014) 1 - 11.

[17] W.-X. Wang, R.S.K. Wong, Mar. Ecol.: Prog. Ser., 261 (2003) 257 - 268.

[18] M.-B. Régine, D. Gilles, D. Yannick, B. Alain, Sci. Total Environ., 368 (2006) 262 - 270.

[19] B.A. Bergquist, J.D. Blum, Elements, 5 (2009) 353 - 357.

[20] J.D. Blum, L.S. Sherman, M.W. Johnson, Annu. Rev. Earth Planet. Sci., 42 (2014) 249 - 269.

[21] R. Yin, X. Feng, X. Li, B. Yu, B. Du, Trends Environ. Anal. Chem., 2 (2014) 1 - 10.

[22] Z. Pedrero, O.F.X. Donard, D. Amouroux, Anal. Bioanal. Chem., 408 (2016) 2641 - 2648.

[23] V. Perrot, V.N. Epov, M.V. Pastukhov, V.I. Grebenshchikova, C. Zouiten, J.E. Sonke, S. Husted, O.F.X. Donard, D. Amouroux, Environ. Sci. Technol., 44 (2010) 8030 - 8037.

[24] L.S. Sherman, J. D.Blum, Sci. Total Environ., 448 (2013) 163 - 175.

[25] R.D. Evans, H. Hintelmann, P.J. Dillon, J. Anal. At. Spectrom., 16 (2001) 1064 - 1069.

[26] D. Foucher, H. Hintelmann, Anal. Bioanal. Chem., 384 (2006) 1470 - 1478.

[27] A. Rua-Ibarz, E. Bolea-Fernandez, F. Vanhaecke, Anal. Bioanal. Chem., 408 (2016) 417 - 429.

[28] E.D. Young, A. Galy, H. Nagahara, Geochim. Cosmochim. Acta, 66 (2002) 1095 - 1104.

[29] F. Vanhaecke, L. Balcaen, D. Malinovsky, J. Anal. At. Spectrom., 24 (2009) 863 - 886.

[30] P. Rodríguez-González, V.N. Epov, R. Bridou, E. Tessier, R. Guyoneaud, M. Monperrus, D. Amouroux, Environ. Sci. Technol., 43 (2009) 9183 - 9188.

[31] N. Estrade, J. Carignan, J.E. Sonke, O.F.X. Donard, Geochim. Cosmochim. Acta, 73 (2009) 2693 - 2711.

[32] K. Kritee, T. Barkay, J.D. Blum, Geochim. Cosmochim. Acta, 73 (2009) 1285 - 1296.

[33] X. Feng, D. Foucher, H. Hintelmann, H. Yan, T. He, G. Qiu, Environ. Sci. Technol., 44 (2010) 3363 - 3368.

[34] D. Malinovsky, F. Vanhaecke, Anal. Bioanal. Chem., 400 (2011) 1619 - 1624.

[35] V.N. Epov, D. Malinovsky, F. Vanhaecke, D. Bégué, O.F.X. Donard, J. Anal. At. Spectrom., 26 (2011) 1142 - 1156.

[36] J. Bigeleisen, J. Am. Chem. Soc., 118 (1996) 3676 - 3680.

[37] A.L. Buchachenko, J. Phys. Chem. A, 105 (2001) 9995 - 10011.

[38] B.A. Bergquist, J.D. Blum, Science, 318 (2007) 417 - 420.

[39] D. Malinovsky, K. Latruwe, L. Moens, F. Vanhaecke, J. Anal. At. Spectrom., 25 (2010) 950 - 956.

[40] S.Y. Kwon, J.D. Blum, M.J. Carvan, N. Basu, J.A. Head, C.P. Madenjian, S.R. David, Environ. Sci. Technol., 46 (2012) 7527 - 7534.

[41] T.A. Jackson, D.M. Whittle, M.S. Evans, D.C.G. Muir, App. Geochem., 23 (2008) 547 - 571.

[42] R. Das, V.J. Salters, A.L. Odom, Geochem. Geophys. Geosys., 10 (2009) 1 - 12.

[43] L.E. Gratz, G.J. Keeler, J.D. Blum, L.S. Sherman, Environ. Sci. Technol., 44 (2010) 7764 - 7770.

[44] J. Chen, H. Hintelmann, X. Feng, B. Dimock, Geochim. Cosmochim. Acta, 90 (2012) 33 - 46.

[45] Z. Wang, J. Chen, X. Feng, H. Hintelmann, S. Yuan, H. Cai, Q. Huang, S. Wang, F. Wang, C. R. Geosci., 347 (2015) 358 - 367.

[46] K. Julshamn, S. Valdersnes, A. Duinker, K. Nedreaas, J.H. Sundet, A. Maage, Food Chem., 167 (2015) 409 - 417.

[47] G. Søvik, Taskekrabbe, Fisken og havet særnummer I, (2016) 186 (In Norwegian).

[48] A. Woll, The edible crab - biology, grading, handling live crabs. Handbook, Møreforsking, Norway, pp. 1 - 32 (Last accessed on September 2016 at www.moreforsk.com), (2005).

[49] A.K. Woll, G.I.V.d. Meeren, I. Fossen, ICES J. Mar. Sci., 63 (2006) 421 - 433.

[50] S. Valdersnes, A. Maage, D. Fliegel, K. Julshamn, J. AOAC Int., 95 (2012) 1189 - 1194.

[51] D. Malinovsky, R.E. Sturgeon, L. Yang, Anal. Chem., 80 (2008) 2548 - 2555.

[52] C. Mead, T.M. Johnson, Anal. Bioanal. Chem., 397 (2010) 1529 - 1538.

[53] J. Masbou, D. Point, J.E. Sonke, J. Anal. At. Spectrom., 28 (2013) 1620 - 1628.

[54] H. Hintelmann, Use of stable isotopes in mercury research. In: Mercury in the environment. M. S. Bank. Ed: University of California Press, Berkeley, (2012).

[55] S.Y. Kwon, J.D. Blum, C.Y. Chen, D.E. Meattey, R.P. Mason, Environ. Sci. Technol., 48 (2014) 10089 - 10097.

[56] V.N. Epov, P. Rodriguez-Gonzalez, J.E. Sonke, E. Tessier, D. Amouroux, L.M. Bourgoin, O.F.X. Donard, Anal. Chem., 80 (2008) 3530 - 3538.

[57] L. Laffont, J.E. Sonke, L. Maurice, H. Hintelmann, M. Pouilly, Y.S. Bacarreza, T. Perez, P. Behra, Anomalous Environ. Sci. Technol., 43 (2009) 8985 - 8990.

[58] V. Perrot, M.V. Pastukhov, V.N. Epov, S. Husted, O.F.X. Donard, D. Amouroux, Environ. Sci. Technol., 46 (2012) 5902 - 5911.

[59] D.C. Baxter, I. Rodushkin, E. Engström, D. Malinovsky, J. Anal. At. Spectrom., 21 (2006) 427 - 430.

[60] M. Mil-Homens, J. Blum, J. Canário, M. Caetano, A.M. Costa, S.M. Lebreiro, M. Trancoso, T. Richter, H.d. Stigter, M. Johnson, V. Branco, R. Cesário, F. Mouro, M. Mateus, W. Boer, Z. Melo, Chem. Geol., 336 (2013) 62 - 71.

[61] R. Yin, X. Feng, B. Chen, J. Zhang, W. Wang, X. Li, Environ. Sci. Technol., 49 (2015) 1347 - 1355.

[62] O. Lindqvist, A. Jernelov, K. Johansson, H. Rohde, Mercury in the Swedish Environment. Global and Local Sources; National Swedish Environmental Protection Board: Stockholm, Sweden, (1984).

[63] F. Uriansrud, J. Skei, M. Schøyen, Miljøkonsekvensvurdering av kvikksølv

ved sunket ubåt U-864, Fedje i Hordaland.Fase 1. Kvikksølvkartlegging. NIVA

Report No. 5022-2005 (in Norwegian), (2005).

[64] G. Tiwari, R. Tiwari, Pharm. Methods, 1 (2010) 25 - 38.

[65] K. Julshamn, B. Nilsen, S. Valdersnes, S. Frantzen, Årsrapport 2011 Mattilsynets program: Fremmedstoffer i villfisk med vekt på kystnaere farvann: Delrapport I: Undersøkelser av miljøgifter i taskekrabbe, (2012).

[66] J.L. Andersen, M.H. Depledge, Mar. Environ. Res., 44 (1997) 331 - 350.

[67] S. Barrento, A. Marques, B. Teixeira, M.L. Carvalho, P. Vaz-Pires, M.L. Nunes, Food Chem. Toxicol., 47 (2009) 150 - 156.

[68] T. Chouvelon, J. Spitz, F. Caurant, P. Mèndez-Fernandez, J. Autier, A. Lassus-Débat, A. Chappuis, P. Bustamante, Deep Sea Res., Part I, 65 (2012) 113 - 124.

[69] M. Canli, R.W. Furness, Environ. Toxicol. Chem., 14 (1995) 819 - 828.

[70] J.M. Laporte, J.P. Truchot, F. Ribeyre, A. Boudou, Mar. Pollut. Bull., 34 (1997) 880 - 893.

[71] P.C. Pickhardt, M. Stepanova, N.S. Fisher, Environ. Toxicol. Chem., 25 (2006) 2132 - 2142.

[72] M. Trudel, J.B. Rasmussen, Environ. Sci. Technol., 31 (1997) 1716 - 1722.

[73] R. Sun, D.G. Streets, H.M. Horowitz, H.M. Amos, G. Liu, V. Perrot, J.-P. Toutain, H. Hintelmann, E.M. Sunderland, J.E. Sonke, Elementa: Science of the Anthropocene, doi:10.12952/journal.elementa.000091 (2016).

[74] E.A. Schauble, Geochim. Cosmochim. Acta, 71 (2007) 2170 - 2189.

[75] W. Zheng, H. Hintelmann, Geochim. Cosmochim. Acta, 73 (2009) 6704 - 6715.

[76] W. Zheng, H. Hintelmann, J. Phys. Chem. A, 114 (2010) 4238 - 4245.

[77] J.G. Wiederhold, C.J. Cramer, K. Daniel, I. Infante, B. Bourdon, R. Kretzschmar, Environ. Sci. Technol., 44 (2010) 4191 - 4197.

[78] H. Hintelmann, W. Zheng, Tracking geochemical transformations and transport of mercury through isotope fractionation, In Environmental Chemistry and Toxicology of Mercury, Liu, G., Cai, Y., O'Driscoll, N. Eds.; John Wiley & Sons, Inc.: Hoboken, New Jersey 2012; pp 293 - 327.

[79] J. Liu, X. Feng, R. Yin, W. Zhu, Z. Li, Chem. Geol., 287 (2011) 81 - 89.

[80] S.G. Downs, C.L. MackLeod, J.N. Lester, Water, Air, Soil Pollut., 108 (1998) 149 - 187.

[81] K. Kritee, J.D. Blum, M.W. Johnson, B.A. Bergquist, B. T, Environ. Sci. Technol., 41 (2007) 1889 - 1895.

[82] K. Kritee, J.D. Blum, J.R. Reinfelder, T. Barkay, Chem. Geol., 336 (2013) 13 - 25.

Chapter 5

Tracing Hg pollution along the Norwegian coast *via* elemental and isotopic analysis of deep-water marine fish (*Brosme brosme*)

Adapted from Rua-Ibarz et. al., Environ. Sci. Technol. (Submitted)

5.1. Introduction

Mercury (Hg) is one of the most important global pollutants and both wildlife and humans are exposed to the harmful effects of this highly toxic heavy metal and its compounds. Methylmercury (MeHg) is the most toxic Hg species and it can be biomagnified and bioaccumulated across food chains,**[1]** making seafood consumption the prime source of human Hg intake. Norway is the world's second largest exporter of seafood and the related industry is one of the most important pillars of the country's economy.**[2]** Given its toxicity, there is increasing attention for Hg contamination in seafood, an issue requiring proper attention from the health and food safety authorities. Different monitoring programs, aiming at documenting the Hg levels in different Norwegian marine ecosystems and at identifying the main sources of Hg are being carried out. Nowadays, anthropogenic Hg emissions, resulting from a variety of processes, such as coal combustion, metal refining and manufacturing, cement production and waste incineration, are the main contributors to the increasing Hg levels around the world. However, also natural sources, such as volcanic activity and hydrothermal systems, can strongly affect the biogeochemical Hg cycle.**[3]** Hg can undergo various processes, and direct atmospheric emission, atmospheric transport, deposition to land and aquatic media, and re-volatilization occur, while also chemical transformations, based on oxidation, reduction, methylation and demethylation complicate the biogeochemical behavior of Hg.**[4]** It is this complexity of the Hg cycle in combination with the aforementioned toxicity that necessitates the development of new tools for monitoring Hg exposure with the final aim of minimizing the risks associated with seafood consumption.

Several aquatic/marine species, in different trophic positions, have been used over the years for tracing Hg pollution and for improving the understanding of the different pathways of Hg across aquatic/marine food chains.**[5]** A group of special interest comprises common seafood species that do not migrate over large distances. Tusk (*Brosme brosme*) is such a type of species. It is a benthic gadoid fish species that is distributed widely in Norwegian waters, both in fjords, along the coast and in open ocean areas. It can be found at depths ranging from 100 to 1000 m. In 2016, the catch of the Norwegian fisheries amounted to approximately two million tons of fish, 14,800 tons of which being tusk.**[6, 7]** It has been reported that this fish species tends to accumulate higher Hg levels than other fish species

living in the same area, *e.g.,* cod.**[8, 9]** As a result, tusk may be considered as a key species for present and future Hg monitoring programs.**[10]** In order to control Hg levels in marine ecosystems, the identification of the contributing Hg sources and the unraveling of the exposure pathways is of the utmost importance. Therefore, in addition to elemental and speciation analysis, also Hg isotopic analysis can contribute to an improved insight into the biogeochemical Hg cycle.**[11]** It has been demonstrated that the isotopic composition of Hg varies between different sources, and that different physical and/or (bio)chemical processes are accompanied by Hg isotope fractionation.**[12]** Mass-dependent fractionation (MDF) was shown to accompany various environmentally relevant processes, such as sorption,**[13, 14]** equilibrium evaporation,**[15, 16]** microbial methylation and demethylation,**[17, 18]** and photochemical reduction.**[19-21]** In addition to MDF, the isotopic composition of Hg can also be affected by mass-independent fractionation (MIF), exhibited primarily by the odd-numbered Hg isotopes (^{199}Hg and ^{201}Hg). MIF has been explained by the nuclear volume effect (NVE) and the magnetic isotope effect (MIE).**[22, 23]** The photoreduction of Hg(II) and the photodegradation of MeHg have been considered as the main processes yielding "odd-MIF".**[19]** However, MIF affecting the even-numbered Hg isotopes has recently also been observed and was attributed to an atmospheric photo-initiated oxidation of Hg(0) in the tropopause.**[24, 25]** As both MDF and MIF of Hg isotopes occur, Hg isotopic analysis provides a "multi-dimensional" tracer and a powerful tool for enhancing our understanding of the biogeochemical Hg cycle.

In this work, the possibility of using tusk as a widely consumed deep-water marine fish species for tracing Hg pollution along the Norwegian coast has been assessed by means of the determination, speciation and isotopic analysis of Hg in its liver and muscle tissues.

5.2. Materials and methods

5.2.1. Sample collection and sample preparation

A total of 137 tusk fish (*Brosme brosme*) were caught at eight different locations along the Norwegian coast by various fishermen on behalf of the National Institute of Nutrition and Seafood Research (NIFES), during various sampling campaigns

between September 2013 and June 2016 (see **Figure 5-1** and **Table 5-1** for further information on the sampling zones). Three of the locations are located in fjords: Sørfjord (7 fish), Steinstøberget (25 fish) and Lusterfjord (14 fish). The remaining five locations are spread along the Norwegian coast (south to north): Ryvingen fyr (25 fish), U-864 (6 fish), Nordøyan (25 fish), Landegode (25 fish) and Lofoten (7 fish). "U-864" refers to a location where a WWII submarine wreck carrying 70 tons of metallic Hg has contaminated the local bottom sediment.**[26]** The fish was caught with long-lines, deep-sea pots or gillnets.

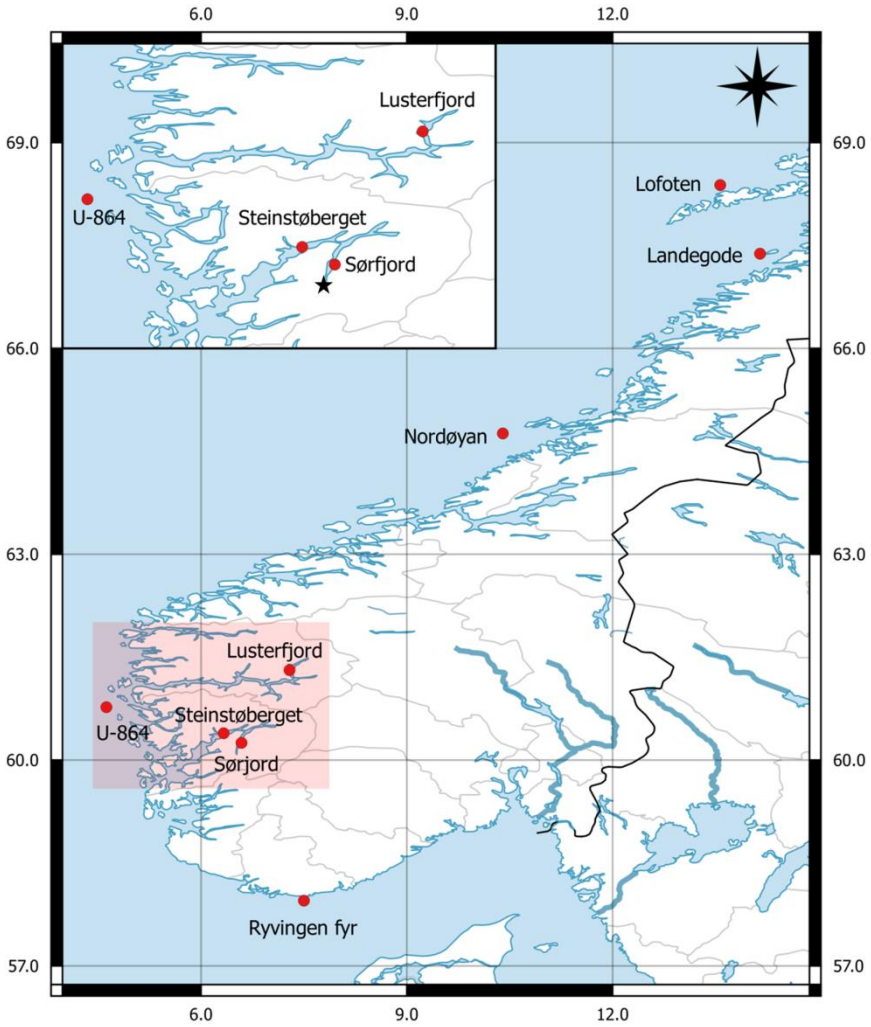

Figure 5-1. Map of Western Norway showing the sampling locations where the tusks (*Brosme brosme*) were collected. Fjords: Sørfjord, Steinstøberget and Lusterfjorden. Coastal locations: Ryvingen fyr, U-864, Nordøyan, Landegode and Lofoten. The star marks the location of the Zn smelter in Odda.

Table 5-1. Information on the sampling zones and tusk fish (*Brosme brosme*) studied in this work.

Sampling zones	Location	Sampling period	N° individuals (N)	Average length (cm)	Average age (years)	Latitude	Longitude	Depth (m)
Sørfjord (Sf)	Fjord	May 2015	8	51.8	9.9	60°15'N	63°6'E	< 350
Steinstøberget (St)	Fjord	April 2014	25*	55.5	8.6	60°23'N	61°9'E	150
Lusterfjorden (Lt)	Fjord	June 2016	14*	61.4	11.9	61°22'N	7°22'E	250 – 500
Ryvingen fyr (Ry)	Coast	September 2013	25*	88.1	15.8	57°57'N	7°30'E	130 – 300
U-864	Coast	July 2015	8	49.1	N.A.	60°46'N	43°7'E	150
Nordøyan (Ny)	Coast	July 2014	25*	62.7	11.3	64°45'N	10°24'E	60 – 250
Landegode (Ld)	Coast	September 2013	25*	75.6	13.8	67°26'N	14°10'E	< 350
Lofoten (Lf)	Coast	June 2014	7*	51.2	9.0	68°22'N	13°34'E	54 – 162

*Pool of samples

From each fish, liver and muscle tissues were manually separated and homogenized (thus resulting in 274 samples). For the Sørfjord and U-864 locations, the tissues of the individual fish (*i.e.* 26 tissue samples) were measured separately (both for elemental and isotopic analysis). For the other 6 locations, samples of liver and muscle of individual fish were analyzed for total Hg and MeHg, but for the isotopic analysis the liver samples or muscle samples from each location were homogenized as to obtain 12 pooled samples. After processing, all samples were stored frozen (< -20 °C) until analysis.

Prior to elemental and isotopic analysis, 0.5 – 1.2 g of sample or certified reference material (CRM) were acid-digested with a 3:1 mixture of 7 M HNO_3 and 9.8 M H_2O_2 in closed microwave vessels using a Milestone (Italy) Ethos One High-Performance Microwave Digestion System. The following microwave program was used: step 1: room temperature to 90 °C, 10 min; step 2: 90 °C, 5 min; step 3: 90 °C to 120 °C, 10 min; step 4: 120 °C, 5 min; step 5: 120 °C to 150 °C, 10 min; step 6: 150 °C, 10 min. After complete mineralization, the resulting solutions were appropriately diluted for ICP-MS measurement.

5.2.2. Reagents and standards

Pro-analysis 14 M HNO_3 and 12 M HCl (ChemLab, Belgium), further purified by sub-boiling distillation in PFA equipment, 9.8 M H_2O_2 (Fluka, Belgium) and high-purity water obtained from a Milli-Q Element water purification system (Millipore, France) were used for sample digestion and subsequent dilution.

Appropriate dilutions of 1000 mg L^{-1} stock solutions of As, Cd, Cr, Cu, In, Ni, Pb, Rh, Se and Zn (Inorganic Ventures, The Netherlands) were used as calibration standards for elemental analysis. For isotopic analysis, a standard solution of the Hg isotopic reference material NIST SRM 3133 and one of the NIST SRM 997 Tl isotopic reference material were used for mass bias correction. An in-house standard solution with well-characterized Hg isotopic composition (Inorganic Ventures, The Netherlands) was used for quality control purposes.

Analyte introduction was accomplished *via* a Teledyne Cetac Technologies (US) HGX-200 cold vapor and hydride generation unit, whereby Hg^{2+} was reduced into elemental Hg by selective reaction with $SnCl_2$ in a reaction vessel. Pro-analysis $SnCl_2.2H_2O$ (Sigma-Aldrich, UK) was prepared freshly every measurement day (3%

$SnCl_2$ in 1.2 M HCl) and the resultant solution was bubbled with purified Ar during approximately thirty minutes to avoid possible Hg contamination. The elemental Hg produced in the reaction vessel was carried into the ICP using an Ar carrier gas.**[27]**

Three CRMs – BCR CRM 464 tuna fish, NRC-CNRC DORM-4 fish protein and TORT-3 lobster hepatopancreas – with a matrix composition similar to that of the samples of interest were used to validate the analytical procedure.

5.2.3. Elemental analysis

A ThermoScientific (Germany) Element XR single-collector sector-field ICP-MS instrument (SF-ICP-MS) equipped with a 100 μL min^{-1} concentric nebulizer mounted onto a cyclonic spray chamber was used for elemental analysis. As, Cd, Cr, Cu, Hg, Ni, Pb, Se and Zn were quantified relying on external calibration (calibration curves with concentrations ranging from 0 to 25 μg L^{-1}) with In and Rh as internal standards correcting for potential matrix effects and instrumental instability. The ICP-MS instrument was operated at different resolution modes (see **Table 5-2** for a description of the instrument settings) and it was tuned prior to every measurement session, aiming at obtaining maximum sensitivity without compromising the interference-free conditions for each of the target nuclides.

In addition, MeHg speciation was performed at NIFES *via* isotope dilution gas chromatography ICP-MS (GC-ICP-IDMS) using an Agilent (Santa Clara, CA) 6890N gas chromatograph coupled to an Agilent Technologies (Japan) 7500a ICP-MS instrument, following the procedure described by Valdersnes *et al.***[28]**

The results obtained upon elemental analysis are expressed as their average ± standard deviation in the case of the pooled samples. For the Sørfjord and U-864 locations (for which individual fish were measured instead of pooled samples), however, median and minimum and maximum concentrations are reported throughout the manuscript.

Table 5-2. Instrument settings and data acquisition parameters for the Thermo Element XR high resolution sector field ICP-MS (HR-SF-ICP-MS) instrument.

Element XR SF-ICP-MS	
Instrument settings	
RF power (W)	1250
Cool gas flow rate (L min^{-1})	15
Auxiliary gas flow rate (L min^{-1})	0.85
Nebulizer gas flow rate (L min^{-1})	0.97 – 1.05
Resolution	Low, medium, high
Scan type	EScan
Data acquisition parameters	
Mass window (%)	150
Search window (%)	150
Integration window (%)	80
Sample time (s)	0.01
Samples/peak	30
Total analysis time/sample (s)	90
Nuclides monitored	
Low resolution	^{82}Se, ^{103}Rh, ^{114}Cd, ^{202}Hg, ^{208}Pb
Medium resolution	^{52}Cr, ^{60}Ni, ^{63}Cu, ^{66}Zn, ^{115}In
High resolution	^{75}As, ^{115}In

5.2.4. Hg isotopic analysis

A ThermoScientific (Germany) Neptune multi-collector ICP-MS (MC-ICP-MS) instrument equipped with nine Faraday cups was used for Hg isotopic analysis (instrument settings are described in **Table 5-3**). A combination of cold vapor generation (CVG) by using an HGX-200 cold vapor & hydride generation unit (Teledyne Cetac Technologies, US) and pneumatic nebulization (PN) by using a 100 µL min^{-1} concentric nebulizer mounted onto a dual (cyclonic and Scott-type) spray

chamber was used for the introduction of Hg and Tl, respectively (this setup is described in detail in Rua-Ibarz *et al.*).**[27]** Hg(0) is generated *via* the reduction of Hg^{2+} with 3% of $SnCl_2.2H_2O$ in 1.2 M HCl in the gas liquid separator (GLS) of the CVG unit and is mixed in a 'T' piece with the wet aerosol of Tl coming from the spray chamber prior to introduction into the plasma.

Table 5-3. Cup configuration, instrument settings and data acquisition parameters for the Thermo Scientific Neptune multi-collector ICP-MS (MC-ICP-MS) instrument.

Neptune MC-ICP-MS						
Cup configuration						
L3	L2	L1	C	H1	H2	H3
^{198}Hg	^{199}Hg	^{200}Hg	^{201}Hg	^{202}Hg	^{203}Tl	^{205}Tl
Instrument settings						
RF power (W)	1300					
Cool gas flow rate (L min^{-1})	13.00 – 14.00					
Auxiliary gas flow rate (L min^{-1})	0.65 – 0.75					
Nebulizer gas flow rate (L min^{-1})	0.65 – 0.70					
Carrier gas flow rate (L min^{-1})	0.19 – 0.21					
Additional gas flow rate (L min^{-1})	0.03 – 0.04					
Sampling cone	Ni					
Skimmer cone	Ni, H-type					
Resolution	Low resolution					
Mode	Static mode					
Data acquisition parameters						
Integration time (s)	4					
Blocks	5					
Cycles/block	10					
Total cycles	50					

Instrumental mass discrimination was corrected for by using the combination of the 'Baxter approach' – using Tl (NIST SRM 997) as an internal standard – and external correction in a sample-standard bracketing (SSB) approach using the Hg isotopic reference material NIST SRM 3133.**[27, 29]** Standard and sample solutions were matrix-matched within ± 10%. No blank correction was done as the influence of the blank on the final isotope ratio data is negligible within the precision attainable (< 0.01‰).**[27]** An in-house standard solution of Hg with a well-characterized Hg isotopic composition and the aforementioned CRMs with similar matrix composition were included in every measurement session (one such solution approximately every 3 – 5 sample measurements) for quality control and validation purposes, as described in previous works.**[26, 27]**

Mass-dependent fractionation (MDF) and mass-independent fractionation (MIF) are reported in delta (δ^{xxx}Hg ‰ – Equation 5-1) and capital delta (Δ^{xxx}Hg ‰ – Equation 5-2 –5-4) notation, respectively.

$$\partial^{xxx}Hg\ (‰) = \left(\frac{\left(^{xxx}Hg/^{198}Hg\right)_{sample}}{\left(^{xxx}Hg/^{198}Hg\right)_{NIST\ SRM\ 3133}} - 1\right) * 1000 \qquad \textbf{(Equation 5-1)}$$

where xxx = 199, 200, 201 or 202.

$$\Delta^{199}Hg = \partial^{199}Hg - \left(\partial^{202}Hg * 0.2520\right) \qquad \textbf{(Equation 5-2)}$$

$$\Delta^{200}Hg = \partial^{200}Hg - \left(\partial^{202}Hg * 0.5024\right) \qquad \textbf{(Equation 5-3)}$$

$$\Delta^{201}Hg = \partial^{201}Hg - \left(\partial^{202}Hg * 0.7520\right) \qquad \textbf{(Equation 5-4)}$$

5.3. Results and discussion

5.3.1. Hg and MeHg in tusk

Concentrations of THg and MeHg in liver and muscle tissues of tusks collected along the Norwegian coast are shown in **Table 5-4** and **Figure 5-2**. Total Hg (THg) concentrations ranged from 0.11 (Lofoten) to 27 (Sørfjord) mg Kg^{-1} in liver tissue and from 0.20 (Lofoten) to 2.6 (Sørfjord) mg Kg^{-1} in muscle tissue. There was a strong positive correlation between the Hg levels in both tissue types, although a clear deviation from the general behavior is observed for the Sørfjord location *i.e.*, the most polluted area, for which liver concentrations were particularly high

Table 5-4. Element concentrations in liver and muscle tissues of tusk (*Brosme brosme*).

Tusk samples (*Brosme brosme*)											
Tissue	**Location**	**Hg (mg Kg^{-1})**	**MeHg (mg Kg^{-1})**	**As (mg Kg^{-1})**	**Cd (mg Kg^{-1})**	**Cr (mg Kg^{-1})**	**Cu (mg Kg^{-1})**	**Ni (mg Kg^{-1})**	**Pb (mg Kg^{-1})**	**Se (mg Kg^{-1})**	**Zn (mg Kg^{-1})**
Muscle	Sørfjord	0.89 (0.38 - 2.55)	0.89 (0.10 - 1.60)	2.3 (1.0 - 9.6)	< LOQ*	0.014 (0.005 - 0.293)	< LOQ*	0.003 (<LOQ – 0.028)	0.0038 (0.0024 - 0.0146)	0.58 (0.44 - 0.66)	2.6 (2.3 - 3.3)
	Steinstøberget	0.62 ± 0.03	0.62 ± 0.37	10.8 ± 1.7	< LOQ*	0.094 ± 0.009	< LOQ*	0.036 ± 0.007	0.0017 ± 0.0007	0.35 ± 0.24	3.7 ± 0.3
	Lusterfjorden	1.17 ± 0.17	1.15 ± 0.46	21.0 ± 1.2	< LOQ*	0.015 ± 0.006	0.027 ± 0.044	0.006 ± 0.004	0.0087 ± 0.0011	0.40 ± 0.01	2.5 ± 0.4
	Ryvingen fyr	0.62 ± 0.02	0.69 ± 0.33	7.6 ± 0.3	< LOQ*	0.066 ± 0.007	0.006 ± 0.004	0.028 ± 0.009	< LOQ*	0.47 ± 0.01	4.3 ± 0.3
	U-864	0.26 (0.23 - 0.51)	0.32 (0.23 - 0.53)	9.9 (5.4 - 19.0)	< LOQ*	0.007 (0.003 – 0.013)	0.033 (0.008 - 0.052)	< LOQ*	0.0020 (0.0012 - 0.0618)	0.47 (0.39 - 0.56)	3.5 (2.8 - 4.4)
	Nordøyan	0.27 ± 0.01	0.32 ± 0.15	2.9 ± 0.1	< LOQ*	0.005 ± 0.003	0.049 ± 0.016	< LOQ*	< LOQ*	0.32 ± 0.04	3.8 ± 0.2
	Landegode	0.64 ± 0.09	0.76 ± 0.37	1.93 ± 0.02	< LOQ*	0.008 ± 0.002	< LOQ*	0.004 ± 0.001	0.0188 ± 0.0262	0.33 ± 0.07	3.2 ± 0.3
	Lofoten	0.20 ± 0.04	0.18 ± 0.08	2.9 ± 0.1	< LOQ*	0.039 ± 0.002	0.063 ± 0.001	0.010 ± 0.004	0.0005 ± 0.0004	0.34 ± 0.05	3.5 ± 0.3
Liver	Sørfjord	3.79 (0.21 - 27.4)	0.62 (0.26 - 3.50)	4.3 (4.2 - 5.9)	0.122 (<LOQ - 0.487)	0.022 (0.005 - 0.096)	4.4 (1.6 - 11.6)	0.070 (<LOQ - 0.206)	0.2547 (0.0128 - 1.3000)	9.1 (4.6 - 21.7)	30.3 (9.4 - 44.9)
	Steinstøberget	1.16 ± 0.12	0.27 ± 0.21	9.9 ± 0.6	0.211 ± 0.006	0.010 ± 0.008	2.1 ± 0.2	0.016 ± 0.001	0.0504 ± 0.0023	4.0 ± 0.4	18.0 ± 0.4
	Lusterfjorden	2.12 ± 0.24	0.50 ± 0.32	13.7 ± 2.1	0.444 ± 0.005	0.037 ± 0.017	5.0 ± 0.1	0.073 ± 0.007	0.0475 ± 0.0048	8.2 ± 1.0	17.0 ± 0.8
	Ryvingen fyr	0.79 ± 0.18	0.17 ± 0.10	5.3 ± 0.5	0.353 ± 0.039	0.011 ± 0.006	1.8 ± 0.1	0.017 ± 0.002	0.0436 ± 0.0238	3.8 ± 0.3	12.7 ± 0.3
	U-864	0.23 (0.14 - 0.86)	0.08 (0.06 - 0.18)	6.4 (3.7 - 23.3)	0.105 (0.015 - 1.050)	0.018 (0.005 - 0.034)	1.3 (1.2 - 2.8)	0.030 (0.007 - 0.061)	0.0195 (0.0074 - 0.0467)	4.3 (3.3 - 7.4)	17.9 (14.8 - 29.4)
	Nordøyan	0.29 ± 0.02	0.09 ± 0.05	3.4 ± 1.1	0.559 ± 0.039	0.008 ± 0.002	1.3 ± 0.3	0.014 ± 0.004	0.0075 ± 0.0016	2.3 ± 0.5	15.7 ± 0.2
	Landegode	0.92 ± 0.12	0.32 ± 0.19	2.7 ± 0.2	0.260 ± 0.029	0.017 ± 0.001	2.4 ± 0.1	0.033 ± 0.005	0.0425 ± 0.0071	3.7 ± 0.2	17.4 ± 0.1
	Lofoten	0.11 ± 0.01	0.05 ± 0.02	4.3 ± 1.4	0.191 ± 0.018	0.048 ± 0.003	2.5 ± 0.1	0.034 ± 0.008	0.0115 ± 0.0047	3.0 ± 0.4	20.6 ± 0.6

*LOQ (Cd) = 0.002 mg Kg^{-1}, LOQ (Cu) = 0.004 mg Kg^{-1}, LOQ (Ni) = 0.003 mg Kg^{-1}, LOQ (Pb) = 0.0003 mg Kg^{-1}

compared to the muscle concentrations (Spearman's correlation excluding the Sørfjord data point, ρ = 0.964, p = 0.000 – **Figure 5-3A**). Overall, liver and muscle tissues of tusk collected in the fjords show higher THg concentrations than those from coastal locations. This observation can most likely be attributed to the higher effect of local anthropogenic Hg sources on fjord ecosystems and/or the poorer water circulation in comparison to open ocean areas. The specific morphology of the fjords gives rise to higher accumulation of pollutants, such as Hg and other heavy metals, that can potentially be trapped at great depths and for longer periods within the fjord.**[30]**

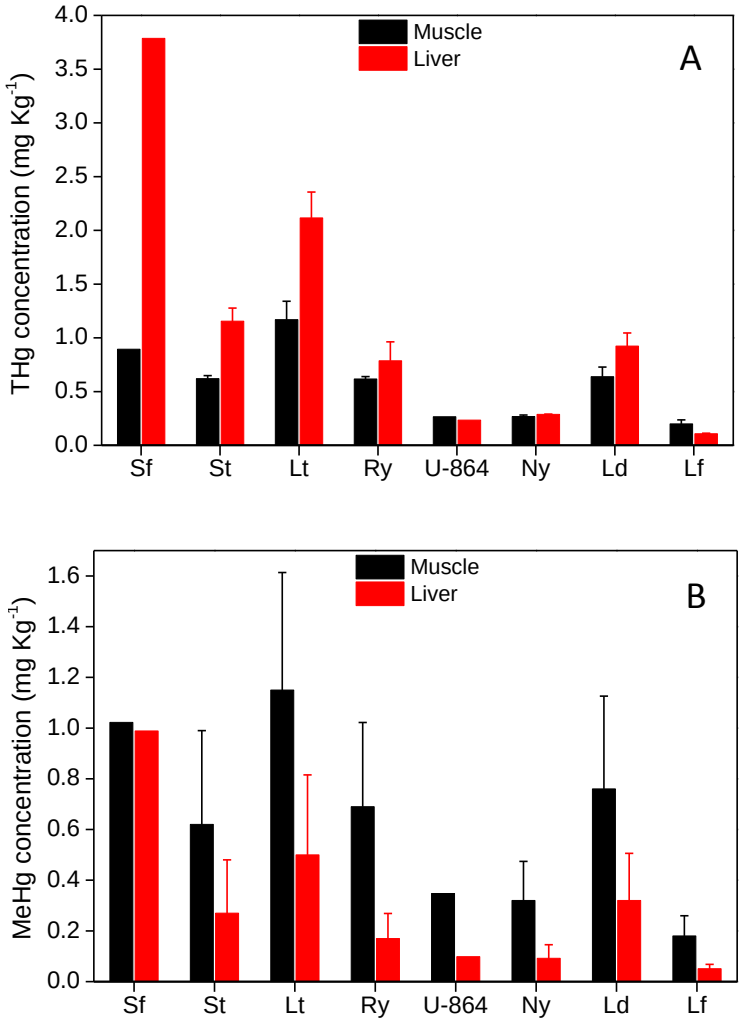

Figure 5-2. THg (A) and MeHg (B) concentrations in liver and muscle tissues of tusk for the eight locations studied. The results are expressed as average ± SD in the case of pooled samples and as median in the case of measurements of individual tusk fish (Sørfjord and U-864 locations).

Additionally, THg concentrations were found to be significantly higher in liver than in the corresponding muscle tissue for tusk from the three fjord locations (THg_{liver}/THg_{muscle} ratio ranging from 1.8 to 4.3), while for tusk from the coastal locations, the THg concentrations in muscle were rather similar to or higher than in liver (THg_{liver}/THg_{muscle} ratio ranging from 0.55 to 1.4). The THg concentrations observed in the fjords may indicate an unusually high Hg intake for this fish species, greatly affecting the liver owing to the key metabolic role of this organ in, *e.g.*, excretion and/or detoxification mechanisms.**[31]**

For both tissue types, the highest THg concentrations were found in the Sørfjord (inner part of the Hardangenfjord), while the lowest THg concentrations were observed in Lofoten (the northernmost coastal location). The European maximum level for THg in most fish species is established at 0.5 mg Kg^{-1} (w.w.).**[32]** The level of THg in tusk muscle tissue (the edible part) exceeded the maximum level in five of the eight locations studied in this work, *i.e.* in all of the fjord locations and in two of the five coastal locations (Ryvingen fyr and Landegode). For U-864, Nørdøyan and Lofoten, the THg concentrations were below the maximum level. The elevated concentrations of Hg in the three fjords could be attributed to the fjord topography and the possible contribution of local anthropogenic sources of Hg, as indicated above. Previously, high Hg concentrations have already been reported for the Sørfjord location.**[33, 34]** These previous observations are in good agreement with the high Hg levels found in liver and muscle tissues of tusk in this work. This high Hg pollution has mainly been attributed to the impact of the Zn smelter located in Odda, a small town situated at the southern end of the Sørfjord. Hg contamination may stem from ore roasting (atmospheric emission and subsequent deposition) and/or (accidental) release of contamination into the fjord water, *e.g.*, during unloading of Zn ore material at the dock.**[35-38]** Elevated concentrations of Hg have been reported in fish and soils from the vicinity of and further away from the Odda Zn smelter.**[8, 39, 40]** In the case of Steinstøberget (outer part of the Hardangenfjord), the relatively high Hg concentrations could be related to the strong pollution observed in the Sørfjord, but elemental analysis of Hg does not enable one to distinguish different sources (see section 3.3 for isotopic analysis of Hg).

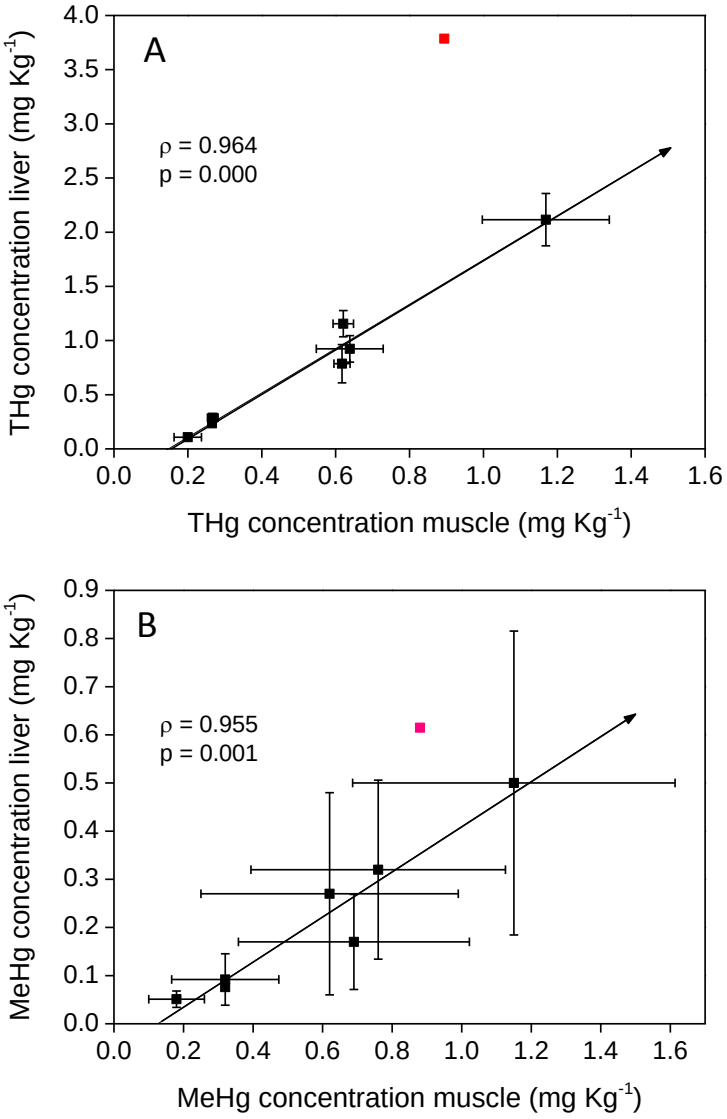

Figure 5-3. Relationship between THg concentrations (A) and MeHg concentrations (B) in tusk liver and muscle, respectively, for all locations studied. The data for Sørfjord are indicated in red.

In addition to the three fjords, the two coastal locations of Ryvingen fyr and Landegode were found to testify of relatively high Hg pollution. The differences between these two locations and the other three locations displaying Hg concentrations below the limits may be related to the higher input of Hg coming from various Hg sources and subsequent transport by sea currents. For instance, Hg carried by sea currents coming from the areas of Denmark and Oslo could elevate the level of Hg at Ryvingen fyr, while at Landegode, Hg could accumulate as

a result of geographical constraints, limiting the circulation of water and hampering the removal of discharged waste (see **Figure 5-1**).

It needs to be pointed out that one of the three areas studied that did not show a high level of Hg pollution is the U-864 location. The U-864 is a German submarine that was carrying 67 tons of metallic Hg in its keel when it was torpedoed and sunk in the proximity of Bergen (Norway) at the end of World War II.**[26, 41]** However, although the U-864 Hg has contaminated the surrounding sediments with metallic Hg,**[42]** the Hg concentrations measured in tusk collected in this area were not found to be elevated compared to tusk sampled in other areas along the west coast of Norway.**[8, 9]**

In addition to the THg concentration, the speciation of Hg is of special relevance due to the higher toxicity of MeHg and its high capacity for bioaccumulation. In this work, MeHg concentrations ranged from 0.050 (Lofoten) to 3.5 (Sørfjord) mg Kg^{-1} in liver tissue and from 0.18 (Lofoten) to 1.6 (Sørfjord) mg Kg^{-1} in muscle tissue (see **Table 5-4** and **Figure 5-2B**). MeHg concentrations in liver and muscle tissues correlated with the corresponding THg concentrations (Spearman's correlation, ρ = 0.976 and 0.970, p = 0.000 for liver and muscle, respectively – **Figure 5-4**). Approximately 100% of the Hg in muscle tissue of tusk was in the form of MeHg,**[31]** while in liver only 14 to 52% of the Hg was in the form of MeHg. Similarly to the situation described above for the THg concentration, a clear correlation was also established between MeHg concentrations in liver and muscle tissue for tusk from the different locations studied. However, the data point for the Sørfjord location clearly deviates from this general trend (Spearman's correlation excluding the Sørfjord data point, ρ = 0.955, p = 0.001 – see **Figure 5-3B**), as was also the case for the THg concentration (see **Figure 5-3A**). This could be attributed to a significant Hg pollution at this location, as the low % MeHg in liver tissues (14%) could point to anthropogenic Hg present as iHg. In addition, it needs to be noted that the highest % MeHg in liver tissue of tusk was found for Lofoten, the least polluted area. Thus, the % MeHg in liver tissues of tusk individuals appears to be a good indicator of anthropogenic iHg contamination and it seems to be more sensitive than muscle tissue to input from anthropogenic Hg (see section 3.3).

Although THg and MeHg levels already provide valuable information on anthropogenic Hg exposure, isotopic analysis of Hg can provide added value aiding an enhanced understanding of the biogeochemical Hg cycle.

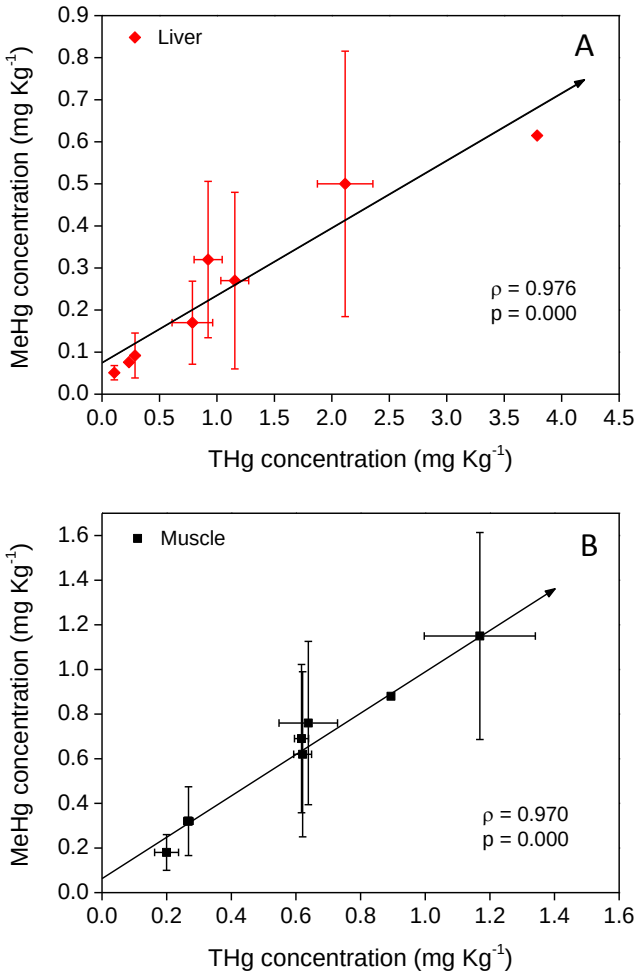

Figure 5-4. MeHg concentration *vs* THg concentration for tusk liver (A) and muscle (B) for all locations studied.

5.3.2. Determination of other environmentally relevant metals in tusk

In addition to THg and MeHg concentrations, also those of other environmentally relevant metals were determined to evaluate possible links with the occurrence of Hg in fish tissues. The concentrations of five essential elements (Cr, Cu, Ni, Se and Zn) and three toxic ones (As, Cd and Pb) were determined. The corresponding results are provided in **Table 5-4** and **Figure 5-5**. Only for Cd and Pb, maximum allowable levels in fish have been defined by the EU. For the other harmful elements no such maximum levels are set, but tolerable weekly intake levels (TWI; EFSA) or provisional tolerable weekly intake levels (PTWI; JECFA) have been established for

several elements by organizations such as the European Food Safety Authority (EFSA) and/or the Joint FAO/WHO Expert Committee on Food Additives (JECFA).**[43, 44]**

Overall, significant differences were found between both tissue types, with liver tissue generally showing much higher concentrations than muscle tissue (with only a few exceptions in the case of As, Cr and Ni at some of the locations studied). Additionally, for the majority of the target elements, the concentrations were found to be higher in tusk from the fjords than in those from coastal waters.

Cu, Ni and Se levels were significantly higher in tusk from the Sørfjord and the Lusterfjord (both inner parts of a fjord), which are also characterized by higher Hg concentrations. This finding is especially interesting for Se, as it has been demonstrated that this element plays an important role in Hg detoxification due the well-known antagonistic Hg-Se effect.**[45]** However, it needs to be noted that Hg-Se interactions are of high complexity, as they are affected by the specific Se- and Hg-containing compounds involved, the Se/Hg elemental ratio, etc (see Chapter 6 for further information on Hg detoxification as a result of Hg-Se interaction).**[46-48]** For Zn, very similar concentrations were observed for all locations, with the exception of the Sørfjord, where the concentration was found to be approximately two-fold higher. This higher Zn concentration is likely due to discharge from the Zn smelter located in Odda, which supports the hypothesis that the Hg pollution within the Sørfjord may also be linked to the Zn smelter.

None of the muscle tissues (*i.e.* tusk fillet) analyzed in this work showed a Cd or Pb level exceeding the European maximum levels of 0.05 and 0.3 mg Kg^{-1}, respectively.**[32, 49]** However, significant concentrations of these toxic elements were found in the liver tissue of tusk, which could serve as an indicator of metal contamination.

The levels of As, Cd and Pb did not seem to correlate with those of Hg in liver and muscle tissues of tusk, although previous works reported on in literature have suggested the possibility of such a relation in liver tissues, *e.g.*, Hg-Cd.**[8]** For the Sørfjord, tusk livers showed significantly higher concentrations of Pb than for the other locations (5 – 10-fold higher), illustrating the anthropogenic pollution affecting this area. In the case of As, the concentrations in liver and muscle tissues of tusk

were found to be similar in most of the locations, and even higher in muscle than in liver tissue in the areas with the highest levels. Suñer *et al.***[50]** reported higher

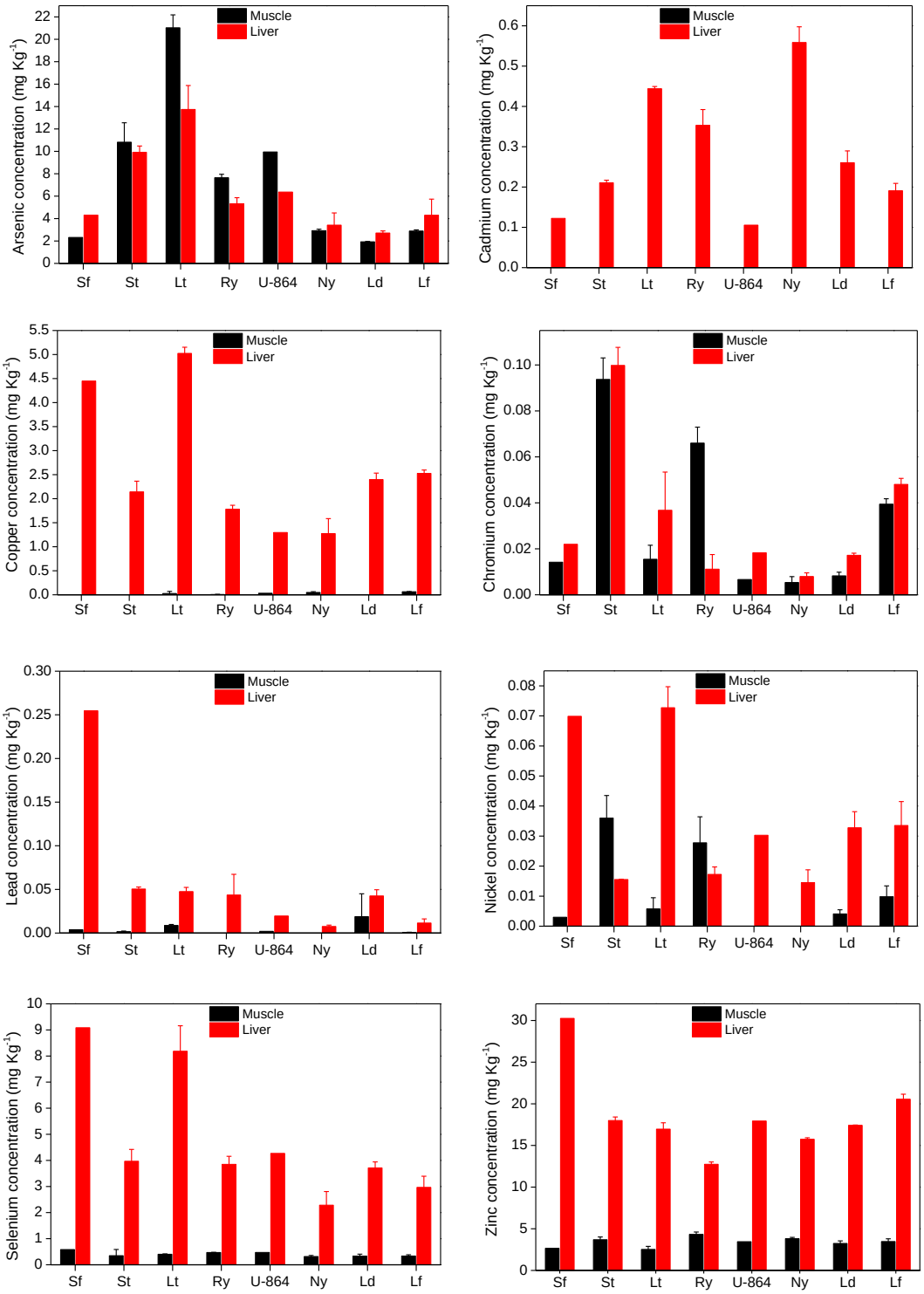

Figure 5-5. Concentrations of other environmentally relevant metals: As, Cd, Cu, Cr, Pb, Ni, Se and Zn in tusk liver (red) and muscle (black) for all locations studied.

concentrations of As in fish liver compared to muscle due to the occurrence of detoxification mechanisms taking place mainly in the liver, similarly as in mammals. However, De Gieter *et al.***[51]** did not support this hypothesis, as in half of the cases studied, As concentrations were higher in muscle than in liver of North Sea fish, which is in better agreement with the results obtained in this work. However, As in tusk is not to be considered as a food safety issue, as it has previously been shown that only a very low portion of the As present in muscle tissue of tusk is in the form of inorganic As, the most toxic As species.**[52]**

5.3.3. Hg isotopic analysis in tusk

5.3.3.1. Mass-dependent fractionation (MDF) of Hg isotopes

The isotopic compositions ($\delta^{199,200,201,202}$Hg and $\Delta^{199,200,201}$Hg) of Hg in tissues of tusk collected from different locations along the Norwegian coast have been summarized in **Table 5-5**. In addition, **Figure 5-6** shows the three-isotope plots (δ^{199}Hg, δ^{200}Hg, and δ^{201}Hg *vs* δ^{202}Hg) obtained for all locations and tissue types. The results indicate a clear deviation from the theoretical MDF line in the case of δ^{199}Hg and δ^{201}Hg, thus indicating that the isotopic composition of Hg was affected by MIF for the odd-numbered isotopes.**[53]** The extent of MIF and the corresponding conclusions that can be derived from this observation will be discussed below (see section 3.3.2).

Figure 5-7 shows how δ^{202}Hg varied between the different locations and between the two tissue types, with values ranging from -1.32 to 0.17 ‰ for liver tissue (average of -0.65 ‰) and from -0.54 to 1.00 ‰ for muscle tissue (average of 0.35 ‰). Overall, significant variations were observed between the different locations studied in this work, with liver tissue always showing a more negative δ^{202}Hg (a lighter isotopic composition of Hg) than the corresponding muscle tissue. In earlier literature, the differences in Hg isotopic composition between liver and muscle tissues have been linked to a difference in Hg speciation between the two tissue types.**[54]** Inorganic Hg and MeHg are the two Hg species present in organisms and these two species show a different Hg isotopic composition. Therefore, the speciation of Hg in both tissue types affect the corresponding bulk Hg isotopic signatures.

Table 5-5. Overview of Hg isotopic compositions ($\delta^{199,200,201,202}$Hg and $\Delta^{199,200,201}$Hg – ‰) of tusk fish (*Brosme brosme*) tissues collected at different locations along the Norwegian coast.

Tusk samples (*Brosme brosme*)								
Tissue	**Location**	**δ^{199}Hg (‰)**	**δ^{200}Hg (‰)**	**δ^{201}Hg (‰)**	**δ^{202}Hg (‰)**	**Δ^{199}Hg (‰)**	**Δ^{200}Hg (‰)**	**Δ^{201}Hg (‰)**
Muscle	Sørfjord	0.06 ± 0.09	-0.27 ± 0.07	-0.24 ± 0.12	-0.54 ± 0.13	0.19 ± 0.08	0.00 ± 0.03	0.17 ± 0.08
	Steinstøberget	0.31 ± 0.05	-0.18 ± 0.07	0.08± 0.07	-0.37 ± 0.06	0.40 ± 0.06	0.00 ± 0.05	0.35 ± 0.05
	Lusterfjord	0.65 ± 0.02	0.21 ± 0.04	0.66 ± 0.06	0.32 ± 0.04	0.57 ± 0.02	0.05 ± 0.03	0.42 ± 0.04
	Ryvingen fyr	0.56 ± 0.02	0.27 ± 0.06	0.72 ± 0.06	0.47 ± 0.07	0.45 ± 0.01	0.03 ± 0.03	0.37 ± 0.02
	U-864	0.45 ± 0.09	0.20 ± 0.07	0.61 ± 0.13	0.36 ± 0.13	0.36 ± 0.07	0.02 ± 0.02	0.34 ± 0.05
	Nordøyan	0.93 ± 0.10	0.50 ± 0.08	1.29 ± 0.10	1.00 ± 0.06	0.68 ± 0.09	-0.01 ± 0.06	0.54 ± 0.10
	Landegode	1.01 0.03	0.43 ± 0.04	1.26 ± 0.07	0.81 ± 0.05	0.80 ± 0.04	0.02 ± 0.03	0.65 ± 0.03
	Lofoten	0.99 ± 0.02	0.39 ± 0.06	1.28 ± 0.06	0.76 ± 0.07	0.79 ± 0.03	0.01 ± 0.03	0.71 ± 0.04
Liver	Sørfjord	-0.21 ± 0.09	-0.68 ± 0.08	-0.88 ± 0.10	-1.32 ± 0.09	0.12 ± 0.08	-0.01 ± 0.04	0.12 ± 0.06
	Steinstøberget	0.04 ± 0.06	-0.60 ± 0.03	-0.64 ± 0.02	-1.23 ± 0.02	0.35 ± 0.06	0.01 ± 0.03	0.28 ± 0.03
	Lusterfjord	0.28 ± 0.06	-0.39 ± 0.05	-0.23 ± 0.09	-0.85 ± 0.06	0.49 ± 0.05	0.04 ± 0.03	0.41 ± 0.06
	Ryvingen fyr	0.18 ± 0.07	-0.40 ± 0.06	-0.34 ± 0.06	-0.88 ± 0.06	0.40 ± 0.07	0.04 ± 0.04	0.32 ± 0.05
	U-864	0.15 ± 0.07	-0.38 ± 0.07	-0.36 ± 0.09	-0.77 ± 0.10	0.36 ± 0.05	0.02 ± 0.03	0.22 ± 0.09
	Nordøyan	0.56 ± 0.03	-0.05 ± 0.06	0.42 ± 0.09	-0.20 ± 0.07	0.61 ± 0.04	0.06 ± 0.07	0.57 ± 0.13
	Landegode	0.64 ± 0.03	-0.19 ± 0.06	0.29 ± 0.06	-0.39 ± 0.07	0.74 ± 0.04	0.01 ± 0.06	0.59 ± 0.02
	Lofoten	0.82 ± 0.07	0.11 ± 0.03	0.78 ± 0.08	0.17 ±0.04	0.77 ± 0.07	0.03 ± 0.02	0.65 ± 0.08

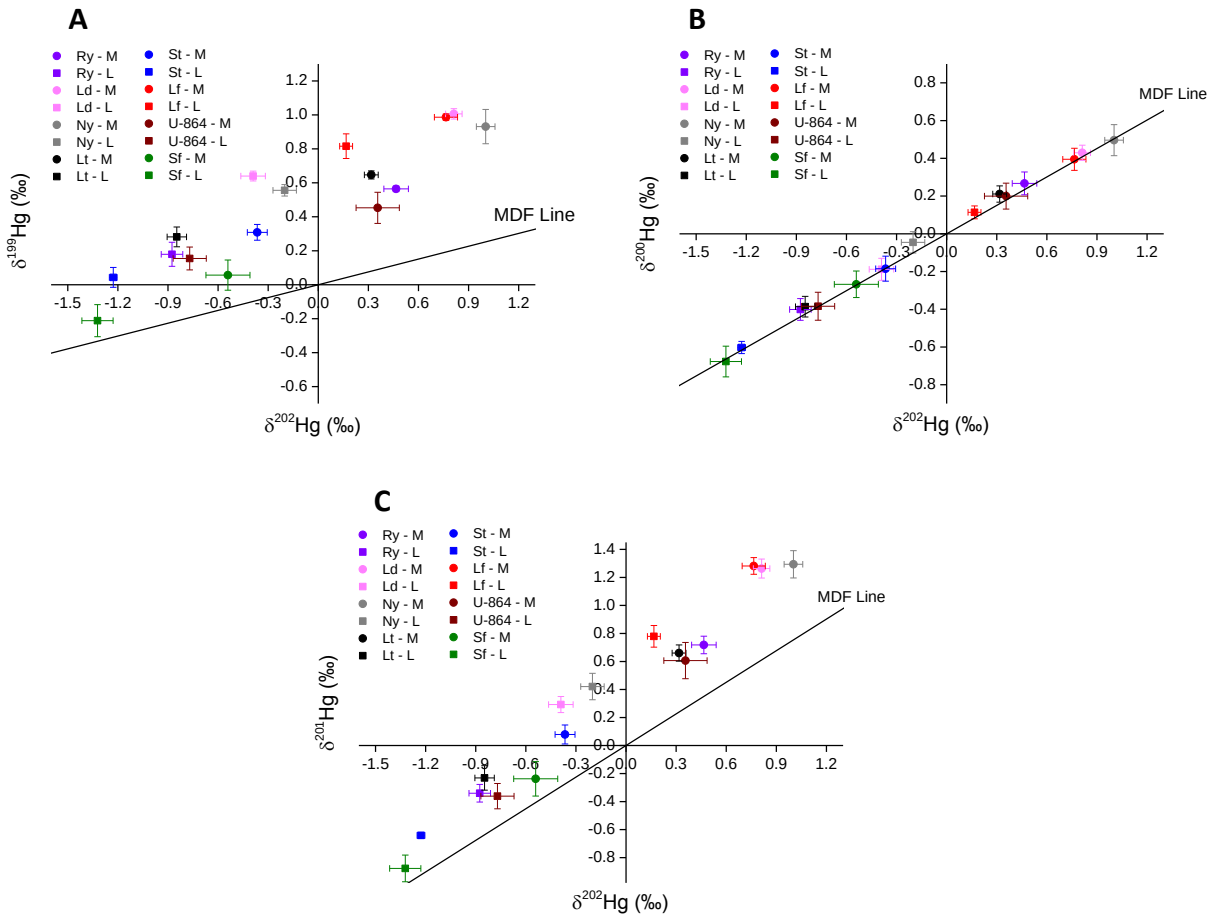

Figure 5-6. Three isotope plots – δ^{199}Hg *vs* δ^{202}Hg (A), δ^{200}Hg *vs* δ^{202}Hg (B), and δ^{201}Hg *vs* δ^{202}Hg (C) – for liver (L) and muscle (M) tissues of tusk (*Brosme brosme*) from different locations along the Norwegian coast.

Significant variations in Hg isotopic composition were observed between the different locations studied. These differences can be related to various Hg sources (*e.g.,* natural and anthropogenic) and to environmental conditions at each location (*e.g.,* fjords and coastal waters). The lowest δ^{202}Hg values for liver and muscle tissues were found in the Sørfjord (-1.32 ± 0.09 and -0.54 ± 0.13 ‰, respectively) although these values were not significantly different from those for tusk from Steinstøberget (-1.23 ± 0.02 and -0.37 ± 0.06 ‰, for liver and muscle respectively). These two locations are situated in the inner and outer parts of the Hardangerfjord, respectively (**Figure 5-1**). The highest δ^{202}Hg liver values were found in tusk from Lofoten (0.17 ± 0.04 ‰) and the highest δ^{202}Hg muscle values were found in tusk from Nordøyan (1.00 ± 0.06 ‰). These two locations are situated on the Norwegian

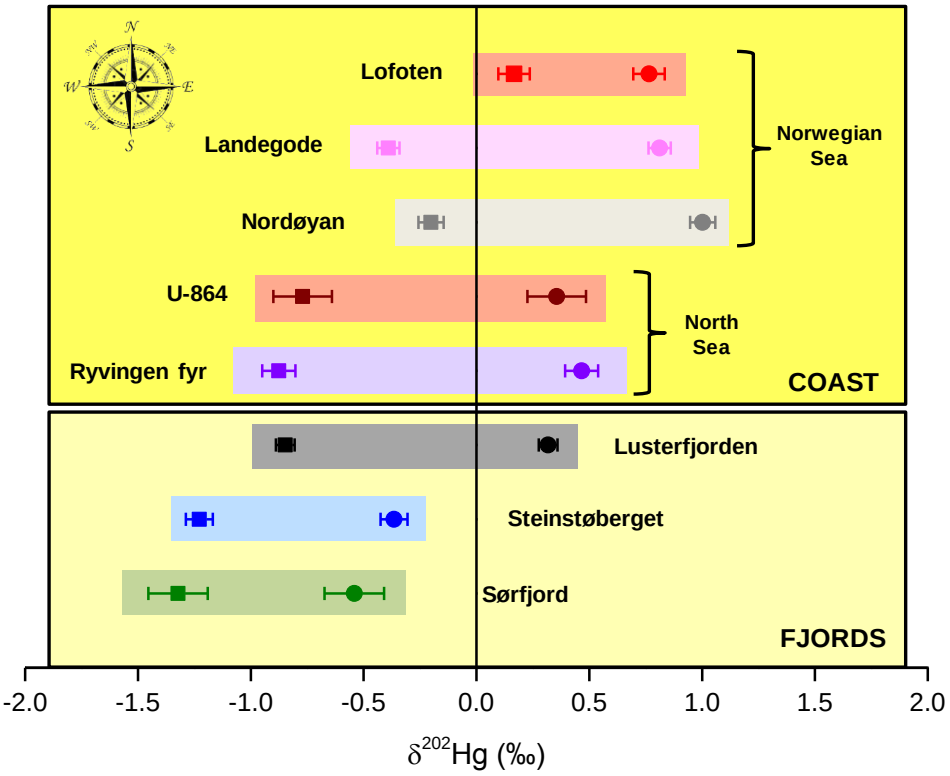

Figure 5-7. δ^{202}Hg values (‰) for liver (squares) and muscle (circles) tissues of tusk (*Brosme brosme*) for the different locations studied in this work.

Sea coast, where a high level of Hg accumulation is not expected as it is relatively remote from most sources of Hg pollution. As indicated in section 3.1, the highest Hg concentration of all locations studied was found in tusk from the Sørfjord, while the lowest concentrations were found in tusk from Lofoten and Nordøyan, respectively, suggesting a certain correlation between the THg concentration and the δ^{202}Hg value. The existence of a correlation between THg and δ^{202}Hg was indeed confirmed for liver tissue (Spearman's correlation, $\rho = -0.786$, $p = 0.021$), while such a correlation was not found for muscle tissue. The differences between the two tissue types may be explained in terms of Hg species distribution between the different organs of the tusk.**[31]** Marine fish primarily accumulate Hg *via* the diet, although some direct absorption *via* the gills, particularly in highly polluted areas, cannot be ruled out.**[55]** When the ingested Hg has been absorbed in the intestine, it is transported through the blood stream to vital organs, such as the liver. From there it is either distributed to other organs and tissues, such as muscle tissue,

where it is finally accumulated, and/or it is excreted.**[55]** Thus, the liver is more sensitive to immediate changes in Hg intake due to local anthropogenic Hg emissions, while the muscle may reflect the Hg accumulated over a longer period of exposure.

As indicated above, two well-established anthropogenic Hg sources were considered of special relevance in the context of this work. On the one hand, the high Hg concentrations reported for different environmental compartments of the Sørfjord have been confirmed for tusk collected at this location (see section 3.1). The particularities of a fjord ecosystem and the possible influence of the Zn smelter located in Odda merit further study using Hg isotopic analysis. Hg isotopic signatures of liver and muscle tissues of tusk from the Sørfjord are the result of mixing of Hg from multiple sources, such as direct release of pollution into the seawater, atmospheric deposition and freshwater runoff.

During Zn ore roasting, Hg present in the ore is fractionated, resulting in local atmospheric deposition of Hg characterized by a light isotopic composition or low δ^{202}Hg value. This is in good agreement with the results obtained in this work for the Sørfjord location.**[56]** Additionally, the same Hg isotopic signature has been imprinted in tusk located in Steinstøberget, which most likely can be attributed to the water current going from the inner to the outer part of the Hardangerfjord and to the predominant winds going from south to north in this area (*i.e.* following the direction of the fjord as shown in **Figure 5-1**).**[40]**

The so-called U-864 location still remains a special area of concern for the Norwegian authorities owing to the large amount of metallic Hg released from the WWII U-864 submarine wreckage.**[41]** In previous work from the same authors,**[26]** Hg isotopic analysis of crab (*Cancer pagurus*) tissues showed that δ^{202}Hg values in the brown meat (predominantly consisting of the digestive system and the gonads) of crabs from the wreck location were shifted towards the isotopic signature of the metallic Hg collected at the vicinity of the submarine wreckage, while such differences were not found for claw (muscle) meat. It was therefore hypothesized that the feeding habits of this crab species may allow for direct ingestion of metallic Hg, which could explain the difference in Hg isotopic composition in brown meat of crabs from the wreck location. It was further expected that the low bioavailability of metallic Hg and the absence of methylation of metallic Hg (due to the low level of microbial activity) did not allow for the introduction of the U-864 Hg into the marine

food chain.**[26]** The results obtained in this work seem to confirm this hypothesis, as no significant differences in δ^{202}Hg were found between tusk from the U-864 location and from Ryvingen fyr, the location further south in the North Sea, suggesting that, so far, the metallic Hg from the U-864 wreckage has not entered the food chain. **Figure 5-8** contains the results obtained for both crab (Chapter 4) and tusk tissues from the U-864 location. Clear differences were found between the regression lines obtained on the basis of the Hg isotope ratio results for different tissues of the two species. In the case of crab, this regression line connects the isotopic signatures of both tissues with that of the sediments and, thus, the metallic Hg from the U-864 submarine, while the regression line obtained based on the isotopic signatures of the tusk tissues shows a different slope and does not include the data point for the sediments/submarine Hg (**Figure 5-8A**). In addition, the Δ^{199}Hg values (see **Figure 5-8B**) obtained for liver and muscle tissue of tusk and claw meat from crabs are similar, while the Δ^{199}Hg value for brown meat of crab is lower. The latter is attributed to the intake of Hg from various sources, mainly MeHg from the diet and metallic Hg from the U-864 submarine. These observations are in agreement with the assumed low bioavailability of metallic Hg from the U-864 submarine.

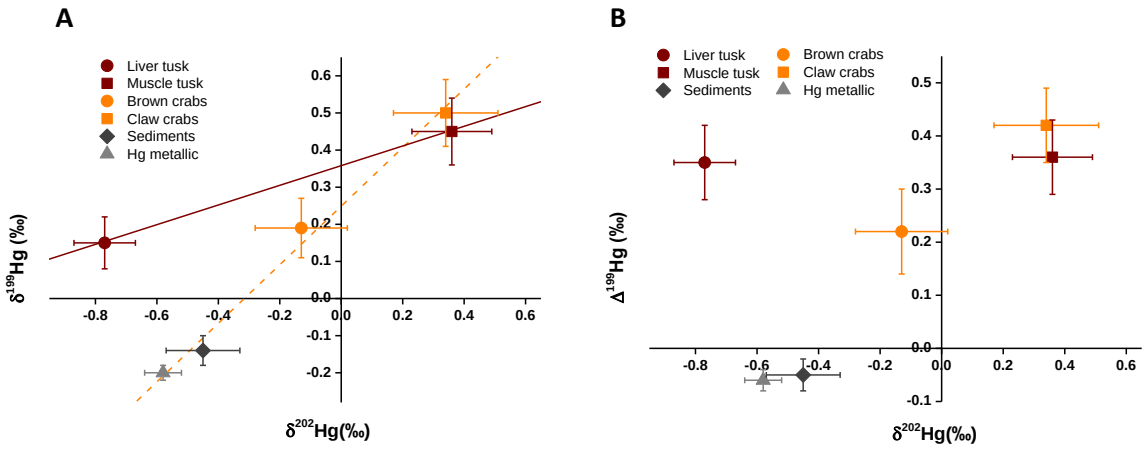

Figure 5-8. Comparison of the Hg isotopic compositions obtained for tissues of tusk (*Brosme brosme*) and brown crab (*Cancer pagurus* – Chapter 4) caught at the U-864 location.

A further evaluation of the MDF Hg isotopic signatures of tusk from the different locations seems to indicate the occurrence of three groups with $\delta^{202}Hg$ values increasing from south to north (see **Figure 5-7**). These groups correspond with the two locations of (*i*) the Hardangenfjorden (the Sørfjord and Steinstøberget), (*ii*) the two locations in the North Sea (U-864 and Ryvingen fyr) and (*iii*) the three locations in the Norwegian Sea (Nørdoyan, Landegode and Lofoten). In the case of the Lusterfjord, the $\delta^{202}Hg$ values were not significantly different from those observed for the two locations from the North Sea. In addition, the $\delta^{202}Hg$ values for muscle tissues were found to be more consistent within the same group than the $\delta^{202}Hg$ values for the liver tissues, which is especially visible for the locations from the Norwegian Sea. This could be attributed to the more sensitive behavior of the liver towards sudden changes in Hg concentrations due to anthropogenic sources, as indicated above. The same is valid for the % MeHg, as muscle tissues are characterized by ~100% MeHg, while the % MeHg in liver tissues is more variable.

Moreover, the differences in $\delta^{202}Hg$ values between the two tissues ($\delta^{202}Hg_{muscle}$ - $\delta^{202}Hg_{liver}$) were not constant for all locations, with values ranging from 0.60 to 1.34 ‰. The difference between $\delta^{202}Hg_{muscle}$ and $\delta^{202}Hg_{liver}$ showed a clear negative correlation with % MeHg in liver (**Figure 5-9**). This observation has already been reported on in the literature and is considered a result of a net positive MDF (fractionation in favor of the heavier Isotope) induced by different chemical and/or biological transformations, such as redox reactions, methylation and/or demethylation processes.**[15, 17, 19, 57]**

It can be seen, however, that the results obtained for the fjord locations were found to deviate from the line defined by the values obtained for the coastal locations; and this deviation was particularly relevant for the two locations from the Hardangerfjord (*i.e.* the Sørfjord and Steinstøberget). When tracing the best fitting straight line through the data for the coastal locations only, *i.e.* excluding the data for the three fjords, an R^2 coefficient of 0.9358 was obtained. This deviation from the trend at the fjord locations shows an unexpected behavior in comparison with tusk collected in coastal waters (see below).

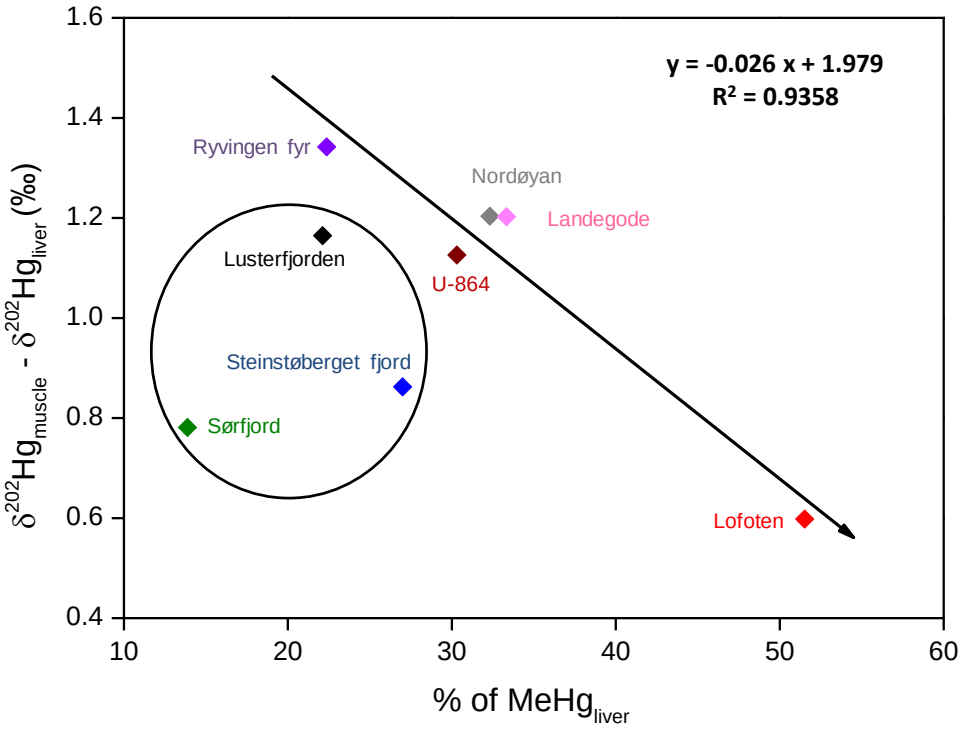

Figure 5-9. $\delta^{202}Hg_{muscle}$ - $\delta^{202}Hg_{liver}$ as a function of the % of MeHg for the eight locations studied in this work.

Careful consideration of the results also show that even at the same % MeHg for both tissue types, there is a slight and constant difference between the corresponding $\delta^{202}Hg$ values. This constant difference ($\delta^{202}Hg_{muscle}$ - $\delta^{202}Hg_{liver}$) can be calculated for an assumed value of 100% MeHg in liver tissue, by extrapolation of the regression line shown in **Figure 5-9** to 100% of $MeHg_{liver}$. We hypothesize that this deviation ($\delta^{202}Hg_{muscle}$ - $\delta^{202}Hg_{liver}$ = -0.62 ‰) may be attributed to differences in Hg metabolic pathways, resulting in an enrichment of the liver in the heavier isotopes. This enrichment in the heavier Hg isotopes in the liver could be the result of the net effect of different metabolic processes occurring in this organ, such as transport, excretion, methylation and demethylation.**[17, 58-61]** It is well known that lighter Hg isotopes are preferentially excreted and transported, leading to an enrichment of the heavier Hg isotopes in the liver.**[62]** The occurrence of *in-vivo* methylation and demethylation in fish still remains controversial and several studies based on feeding experiments have reported contradictory results.**[63-65]** A study based on the use of isotopically enriched tracers **[66]** suggested that *in-vivo*

methylation occurs in tilapia fish intestine *via* bacterial activity, and that the newly formed MeHg, which is enriched in the lighter Hg isotopes, goes first to the vital organs (*e.g.*, liver) from where it is distributed and finally deposited in the muscle. Additionally, a recent study of MeHg demethylation in marine fish **[67]** suggested that the intestine plays a predominant role in the *in-vivo* MeHg demethylation during MeHg exposure, pointing out that the intestine demethylation served as an important pathway for MeHg detoxification. The demethylation process leads to an enrichment of the iHg thus produced in lighter isotopes in comparison to the initial MeHg.

The deviations observed for the two locations in the Hardangenfjord could be related to a more direct Hg exposure owing to the occurrence of an important Hg anthropogenic source, which can be attributed to the proximity of the Zn smelter. This could lead to a more specific source-related Hg isotopic composition and a different isotopic pattern in liver and muscle tissues, not following the behavior established for coastal locations.

5.3.3.2. Mass-independent fractionation (MIF) of Hg isotopes

As indicated above, the three-isotope plots (**Figure 5-6**) showed that additional MIF has affected the odd-numbered isotopes of Hg. MIF values, expressed as Δ^{199}Hg as a function of location and tissue type, ranged from 0.12 to 0.77 ‰ in liver tissue and from 0.19 to 0.80 ‰ in muscle tissue (see **Figure 5-10** and **Table 5-5**). The lowest Δ^{199}Hg values were found in tusk from the Sørfjord and the highest in the two northernmost locations, Landegode and Lofoten. In contrast to MDF, only slight differences in Δ^{199}Hg values between liver and muscle tissues were observed, barely affected by the location studied. However, the Δ^{199}Hg value of muscle tissue was always found to be slightly higher than that of the corresponding liver tissue from the same area. The extents of MIF can be used to provide complementary information on physical and chemical transformations involved in the biogeochemical Hg cycle.**[68]** For biological processes, most of the studies conducted to date have concluded absence of *in-vivo* MIF,**[59, 69-71]** suggesting that the degree of MIF in fish species may reflect the MIF signature of Hg prior to its incorporation into the food web. Two tentative mechanisms have been proposed aiming at explaining the occurrence of MIF in the case of Hg, *i.e.* (*i*) the nuclear

volume effect (NVE) and (*ii*) the magnetic isotope effect (MIE).**[22, 23]** Moreover, it has been demonstrated that the MIE has a larger contribution than the NVE to the final extent of MIF.**[19, 20]** In aquatic organisms, the main processes yielding MIF are photo-mediated reactions, such as the photochemical reduction of Hg(II) and the photodegradation of MeHg in the presence of dissolved organic carbon (DOC), both specifically affecting the odd-mass numbered isotopes of Hg.**[19]**

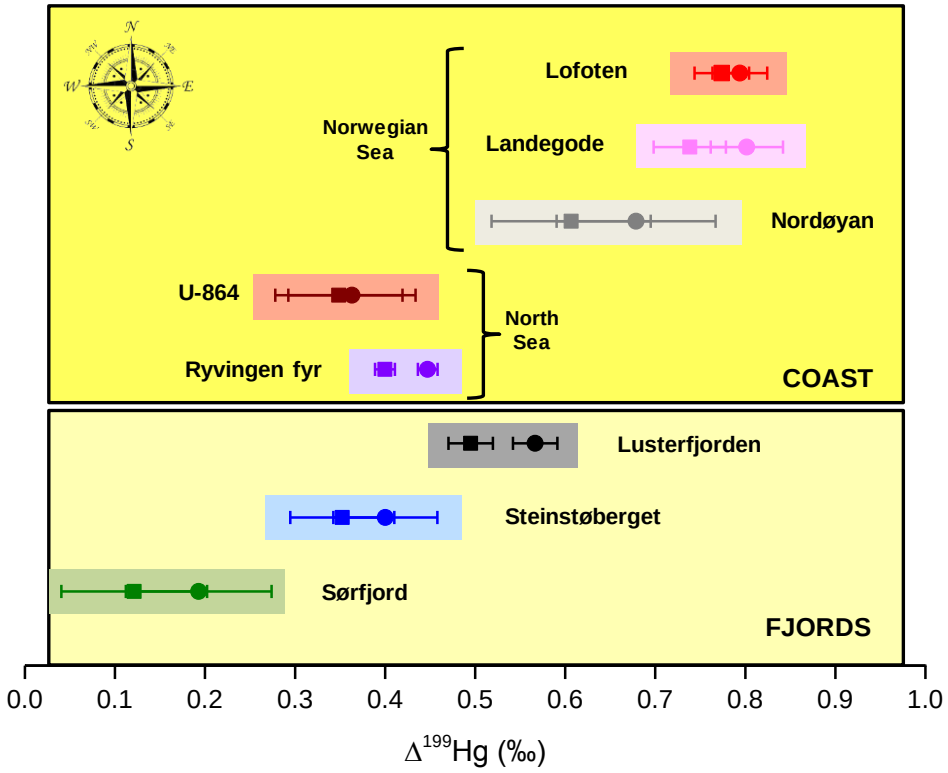

Figure 5-10. Δ^{199}Hg values (‰) for liver (squares) and muscle (circles) tissues of tusk (*Brosme brosme*) for the different locations studied in this work.

A further evaluation of the extent of MIF (Δ^{199}Hg) of Hg isotopes (**Figure 5-10**) pointed to the occurrence of different groups as a function of the location, as previously also indicated by the MDF (δ^{202}Hg) of Hg isotopes. However, in the case of MIF, significant differences were found between the three fjords studied, even between the two locations from within the Hardangerfjord, *i.e.* the Sørfjord and Steinstøberget. The lowest Δ^{199}Hg values (0.12 ± 0.08 and 0.19 ± 0.08 ‰ for liver and muscle, respectively) were found in the Sørfjord, while Steinstøberget showed a slightly higher degree of MIF (0.35 ± 0.06 and 0.40 ± 0.06 ‰ for liver and muscle,

respectively). MIF of Hg tends to be low in highly polluted areas owing to the large amount of anthropogenic iHg.**[72]** With the Zn smelter located in Odda as the main source of Hg pollution within the Hardangerfjord, tusk collected in the Sørfjord will most likely be affected to a higher extent due to the proximity of the contamination source and especially the Hg in the liver is thus indeed expected to display a lower level of MIF. In the case of Steinstøberget, MDF δ^{202}Hg points to the high Hg contamination level in the Sørfjord as the main source of Hg in the outer part of the Hardangerfjord, then MIF may be higher because Hg has taken longer time to reach there and thus MIF may have taken place on the way. In addition, Hg MIF in marine ecosystems has also been found to be strongly affected by depth, with lower Δ^{199}Hg values for shallower waters in comparison with deeper waters.**[73]** The effect of depth on the degree of MIF was found to be in good agreement with the different Δ^{199}Hg between the Sørfjord (with depths of ~ 350 m) and Steinstøberget (with depths of ~150 m).

For the coastal locations, however, Δ^{199}Hg values do not show significant differences between different locations from the same sea, which is in good agreement with the aforementioned hypothesis based on the results obtained for MDF (δ^{202}Hg). The highest extents of MIF (Δ^{199}Hg) of Hg isotopes were found at Lofoten and Landegode (~0.8 ‰), both locations from the Norwegian Sea, showing significant differences with the locations from the North Sea (~0.4 ‰ for the U-864 and Ryvingen fyr). Based on the relatively constant degree of MIF in tusk of different locations from the same sea, the effect of oceanic currents and water conditions, and the distance from the sources of pollution, seem to be the most likely explanation for these differences. Previous laboratory experiments have reported different extent of MIF as a function of the pH, the ionic strength of the water and the concentration of total dissolved solids (TDS).**[20]** The geographical trend – south (North Sea) to north (Norwegian Sea) – could also explain the results obtained for Nordøyan (Δ^{199}Hg = 0.61 – 068 ‰). Nordøyan is located in the Norwegian Sea, but the degree of MIF was found to be slightly lower in comparison with the other locations from the same sea, which could be related with the influence of the North Sea displaying two-fold lower MIF of Hg isotopes in tusk compared to the Norwegian Sea.

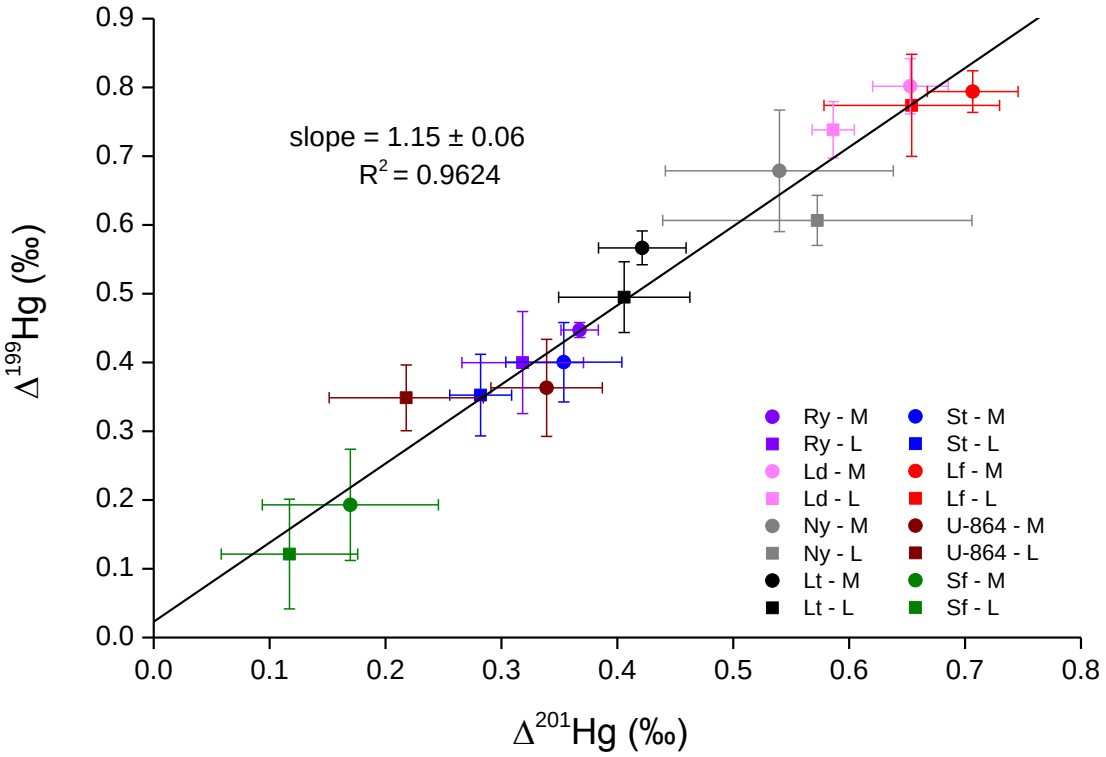

Figure 5-11. Δ^{199}Hg vs Δ^{201}Hg (‰) for the complete data set of liver (squares) and muscle (circles) tissues of tusk (*Brosme brosme*).

In addition to the extent of MIF, also the experimental $\Delta^{199}Hg/\Delta^{201}Hg$ ratio provides interesting information, as it can be used to discern between the two types of photochemical reductions, corresponding with a value of 1.00 and of 1.36 in the case of Hg(II) photoreduction and MeHg photodegradation, respectively. Most of the works reporting on the analysis of fresh water fish (*e.g.,* estuarine, lakes), have reported a $\Delta^{199}Hg/\Delta^{201}Hg$ ratio of ~1.3,**[74, 75]** while studies based on marine fish have reported a slope of ~1.2.**[76]** This difference has been attributed to different water conditions, mainly owing to the different amount of dissolved organic carbon (DOC), as the $\Delta^{199}Hg/\Delta^{201}Hg$ slope strongly depends on the organic ligands that Hg is bounded with.**[21]** Nevertheless, the values reported on in literature for both fresh water and marine fish species were found to be close to the value obtained for MeHg photodegradation, suggesting the bioaccumulation of the remaining MeHg as the main contributor to the MIF-affected Hg isotopic signature in fish, with a generally minor contribution of Hg(II) photoredution. **Figure 5-11** shows the linear regression obtained by plotting Δ^{199}Hg *vs* Δ^{201}Hg for the complete data set, leading

to a slope of 1.15 ± 0.06. It needs to be pointed out, though, that slight differences were observed by separately plotting the data for both tissue types, thus obtaining slopes of 1.11 ± 0.09 for liver and 1.20 ± 0.09 for muscle tissue. This difference between tissues can be attributed to the higher % iHg in the liver in comparison with the muscle.

Based on the assumption that MIF is mainly caused by processes that MeHg undergoes prior to its incorporation into the food web, the extent of MeHg loss *via* this MeHg photodegradation can be estimated according to the procedure described by Bergquist and Blum.**[19]** In this work, a MeHg photoreduction experiment was relied on for obtaining the relationship between the fraction of Hg remaining in solution and the Δ^{201}Hg, following a Rayleigh distillation model outlined by Mariotti *et al.***[77]** By using this approach, the fraction of MeHg remaining after photodegradation (f) can be calculated according to Equation 5-5, where S corresponds to the slope of the aforementioned relationship obtained by Bergquist and Blum and Δ^{201}Hg values are those obtained in this work for each location. Thereafter, the % MeHg photodegradated prior to its incorporation into the food web can be calculated according to Equation 5-6.**[19, 78]**

$$\text{Ln}(f) = [10^3 \times \ln (10^{-3} \times \Delta^{201}\text{Hg} + 1)]/S \qquad \textbf{(Equation 5-5)}$$

$$\%\ \text{of MeHg photodegradated} = 100 \times (1 - \exp[\ln(f)]) \qquad \textbf{(Equation 5-6)}$$

The values thus obtained were 6, 12, 16, 13, 11, 20, 22 and 24% for Sørfjord, Steinstøberget, Lusterfjord, Ryvingen fyr, U-864, Nordøyan, Landegode and Lofoten, respectively. These experimental results were found to be in good agreement (with the exception of the Sørfjord) with the values reported on in literature for coastal locations 10 – 34%.**[76, 78]** In the Sørfjord, however, the % MeHg loss was lower than the expected value (< 10%). Once more, this result points to the occurrence of an important anthropogenic Hg source greatly affecting the Sørfjord location and the surrounding marine ecosystem.

5.3.4. Environmental trends and perspectives

At the Minamata Convention on Mercury, urgent measures to avoid and/or minimize the mercury threat were approved. Exposure to Hg is an issue of growing concern that requires major attention. Efforts should include the development of reliable methods for evaluating the level of Hg exposure on a short and long term basis. Therefore, providing novel tools to be introduced in new and/or currently existing monitoring programs is of the utmost importance for an appropriate follow-up of the fate of Hg in nature. Fish consumption is the primary source of human Hg exposure. Monitoring Hg in appropriate seafood species may shed light onto the complex Hg cycle.

In this work, clear differences in the Hg isotopic composition of tusk (*Brosme brosme*) tissues were found between fjords and coastal locations, pointing to specific Hg contamination sources (*e.g.*, the Zn smelter located in Odda). Differences were also established between samples from (i) the fjords, from (ii) the North Sea and from (iii) the Norwegian Sea, respectively. This observation can most likely be attributed to different Hg contamination sources along the Norwegian coastal waters, thus demonstrating the potential of isotopic analysis of selected species for tracing Hg pollution in specific marine environments. In addition, isotopic analysis of different tissues (*i.e.*, liver and muscle) was found to provide different and thus, complementary information at some locations, which stresses the necessity of taking into account potential metabolic processes accompanied by Hg isotope fractionation within the fish body. The use of Hg isotopic analysis for tracing Hg sources may be hampered by the occurrence of such *in vivo* metabolic processes as they affect the Hg isotopic signature of the original source. However, at the same time, the monitoring of Hg in different tissues (*i.e.* liver and muscle) is also a powerful approach to provide additional information, potentially enhancing our understanding of the metabolic routes of Hg and its detoxification pathways.

Clearly, important knowledge gaps still remain in our understanding of the biogeochemical Hg cycle, but the combination of elemental, speciation and isotopic analysis of Hg in (i) different species collected at the same location, (ii) a given species collected at different locations and (iii) in different tissues of a selected species, offers a powerful approach for dealing with this important environmental and human threat.

References

[1] C.T. Driscoll, R.P. Mason, H.M. Chan, D.J. Jacob, N. Pirrone, Environ. Sci. Technol., 47 (2013) 4967 - 4983.

[2] M.G. Sandberg, G.H. Volden, I.J. Aarhus, M. Hofman, T. Olafsen, Betydningen av fiskeri- og havbruksnæringen for Norge i 2008 – en ringvirkningsanalyse (The importance of the fisheries and aquaculture sector for Norway in 2008 – An analysis of spillover effects). SINTEF, Trondheim., (2010).

[3] J.D. Blum, Chapter 12: Application of stable mercury isotopes to biogeochemistry. In Handbook of Environmental Isotope Geochemistry. M. Baskaran, Ed. Springer, Berlin., (2012) 229 - 245.

[4] R. Yin, X. Feng, X. Li, B. Yu, B. Du, Trends Environ. Anal. Chem., 2 (2014) 1 - 10.

[5] C. Chen, A. Amirbahman, N. Fischer, G. Harding, C. Lamborg, D. Nacci, D. Taylor, EcoHealth, 5 (2008) 399 - 408.

[6] W.R. Bowering, K.H. Nedreaas, Sarsia, 86 (2001) 53 - 68.

[7] P. Sandberg, A.K. Steinseide, Economic and biological figures from Norwegian fisheries - 2016, (2017) 38.

[8] K. Kvangarsnes, S. Frantzen, K. Julshamn, L.J. Sæthre, K. Nedreaas, A. Maage, J. Food Sci. Eng., 2 (2012) 603 - 615.

[9] S. Frantzen, A. Maage, Fremmedstoffer i villfisk med vekt på kystnære farvann. Brosme lange og bifangstarter. Gjelder tall for prøver samlet inn i 2013 - 2015. NIFES. Bergen, (2016) 115.

[10] A. Maage, O. Bjell;and, P. Olsvik, B. Nilsen, K. Julshamn, Contaminants in fish and seafood products 2011. Miljøgifter i fisk og fiskevarer 2011: Kvikksølv i djupvassfisk og skaldyr frå Hardangerfjorden samt miljøgifter i marine oljer. NIFES report. In: Norwegian, Summary in English, Bergen, (2012) 1 - 31.

[11] R. Yin, X. Feng, W. Shi, Appl. Geochem., 25 (2010) 1467 - 1477.

[12] J.D. Blum, L.S. Sherman, M.W. Johnson, Annu. Rev. Earth Planet. Sci., 42 (2014) 249 - 269.

[13] J.G. Wiederhold, C.J. Cramer, K. Daniel, I. Infante, B. Bourdon, R. Kretzschmar, Environ. Sci. Technol., 44 (2010) 4191 - 4197.

[14] M. Jiskra, J.G. Wiederhold, B. Bourdon, R. Kretzschmar, Environ. Sci. Technol., 46 (2012) 6654 - 6662.

[15] N. Estrade, J. Cargnan, J.E. Sonke, O.F.X. Donard, Geochim. Cosmochim. Acta, 73 (2009) 2693 - 2711.

[16] S. Ghosh, E.A. Schauble, G.L. Couloume, J.D. Blum, B.A. Bergquist, Chem. Geol., 336 (2013) 5 - 12.

[17] P. Rodríguez-González, V.N. Epov, R. Bridou, E. Tessier, R. Guyoneaud, M. Monperrus, D. Amouroux, Environ. Sci. Technol., 43 (2009) 9183 - 9188.

[18] V. Perrot, R. Bridou, Z. Pedrero, R. Guyoneaud, M. Monperrus, D. Amouroux, Environ. Sci. Technol., 49 (2015) 1365 - 1373.

[19] B.A. Bergquist, J.D. Blum, Science, 318 (2007) 417 - 420.

[20] D. Malinovsky, K. Latruwe, L. Moens, F. Vanhaecke, J. Anal. At. Spectrom., 25 (2010) 950 - 956.

[21] W. Zheng, H. Hintelmann, J. Phys. Chem. A, 114 (2010) 4246 - 4253.

[22] J. Bigeleisen, J. Am. Chem. Soc., 118 (1996) 3676 - 3680.

[23] A.L. Buchachenko, J. Phys. Chem. A, 105 (2001) 9995 - 10011.

[24] L.E. Gratz, G.J. Keeler, J.D. Blum, L.S. Sherman, Environ. Sci. Technol., 44 (2010) 7764 - 7770.

[25] J. Chen, H. Hintelmann, X. Feng, B. Dimock, Geochim. Cosmochim. Acta, 90 (2012) 33 - 46.

[26] A. Rua-Ibarz, E. Bolea-Fernandez, A. Maage, S. Frantzen, S. Valdersnes, F. Vanhaecke, Environ. Sci. Technol., 50 (2016) 10361 - 10369.

[27] A. Rua-Ibarz, E.B. Fernandez, F. Vanhaecke, Anal. Bioanal. Chem., 408 (2016) 417 - 429.

[28] S. Valdersnes, A. Maage, D. Fliegel, K. Julshamn, J. AOAC Int., 95 (2012) 1189 - 1194.

[29] D.C. Baxter, I. Rodushkin, E. Engström, D. Malinovsky, J. Anal. At. Spectrom., 21 (2006) 427 - 430.

[30] S. Manzetti, J.H.V. Stenersen, Mar. Pollut. Bull., 60 (2010) 2167 - 2174.

[31] M.-B. Régine, D. Gilles, D. Yannick, B. Alain, Sci. Total Environ., 368 (2006) 262 - 270.

[32] E. Commission, Setting maximum levels for certain contaminants in food stuffs, Commission Regulation (EC) No 466/2001, (2001).

[33] A. Ruus, N.W. Green, Monitoring the envrionmental quality in the Sørfjord 2006. Contaminants in organisms. Overvåking av miljøforholdene i Søfjorden 2006, Delrapport 3, Miljøgifter i organismer, Norsk institutt for vannforskning. In: Norwegian, Summary in English, Oslo, (2007) 23 - 24.

[34] A. Ruus, J. Skeí, N. Green, M. Schøyen, Monitoring the envrionmental quality in the Sørfjord 2009. Contaminants in organisms. Overvåking av miljøforholdene i Søfjorden 2009. Metaller i vannmassene, Miljøgifter i organismer. Rapport til KLIF, NIVA-rapport 6018 - 2010. In: Norwegian, Summary in English, Oslo, (2010) 1 - 92.

[35] L.D. Hylander, R.B. Herbert, Environ. Sci. Technol., 42 (2008) 5971 - 5977.

[36] J.E. Sonke, J. Schäfer, J. Chmeleff, S. Audry, G. Blanc, B. Dupré, Chem. Geol., 279 (2010) 90 - 100.

[37] S.X. Wang, J.X. Song, G.H. Li, Y. Wu, L. Zhang, Q. Wan, D.G. Streets, C.K. Chin, J.M. Hao, Environ. Pollut., 158 (2010) 3347 - 3353.

[38] J. Masbou, D. Point, J.E. Sonke, Application of a selective extraction method for methylmercury compound specific stable isotope analysis (MeHg-CSIA) in biological materials, J. Anal. At. Spectrom., 28 (2013) 1620 - 1628.

[39] P.A. Olsvik, M. Lindgren, A. Maage, Aquat. Toxicol., 144 - 145 (2013) 172 - 185.

[40] M.L. Svendsen, E. Steinnes, H.A. Blom, Soil Sediment Contam., 16 (2007) 585 - 603.

[41] P.A. Olsvik, M. Brattås, K.K. Lie, A. Goksøyr, Chemosphere, 83 (2011) 552 - 563.

[42] E. Solhjell, T. Lunne, U-864 2013 Soil survey, NGI, Oslo, (2013) 199.

[43] A.C. Bosch, B. O'Neill, G.O. Sigge, S.E. Kerwath, L.C. Hoffman, J. Sci. Food Agric. , 96 (2016) 32 - 48.

[44] JECFA, Evaluations of the Joint FAO/WHO Expert Committee on Food Additives (JECFA). Database: http://apps.who.int/food-additives-contaminants-jecfa-database/search.aspx?fcc=2 (Accessed October 2017).

[45] M.A. Lourdes, A. Cuvin-Aralar, R.W. Furness, Ecotoxicol. Environ. Saf., 21 (1991) 348 - 364.

[46] H.E. Ganther, C. Goudie, M.L. Sunde, M.J. Kopecky, P. Wagner, Science, 175 (1972) 1122 - 1124.

[47] N. Belzile, G.J. Wu, Y.W. Chen, V.D. Appanna, Sci. Total. Environ., 367 (2006) 704 - 714.

[48] M.A. García-Sevillano, G. Rodríguez-Moro, T. García-Barrera, F. Navarro, J. Gómez-Ariza, Chem.-Bio. Interact., 229 (2015) 82 - 90.

[49] E. Commission, Setting maximum levels for certain contaminants in food stuffs, Commission regulation (EC) No 1881/2006, Official Journal of the European Union 364 (2006) 5 - 24.

[50] M.A. Suñer, V. Devesa, O. Muñoz, F. López, R. Montoro, A.M. Arias, J. Blasco, Sci. Total. Environ., 242 (1999) 261 - 270.

[51] M.D. Gieter, M. Leermakers, R.V. Ryssen, J. Noyen, L. Goeyens, W. Baeyens, Arch. Environ. Contam. Toxicol., 43 (2002) 406 - 417.

[52] K. Julshamn, B.M. Nilsen, S. Frantzen, S. Valdersnes, A. Maage, K. Nedreaas, J.J. Sloth, Food Addit. Contam., Part B, 5 (2012) 229 - 235.

[53] J.D. Blum, B.A. Bergquist, Anal. Bioanal. Chem., 388 (2007) 353 - 359.

[54] V. Perrot, J. Masbou, M.V. Pastukhov, V.N. Epov, D. Point, S. Bérail, P.R. Becker, J.E. Sonke, D. Amouroux, Metallomics, 8 (2016) 170 - 178.

[55] P.C. Pickhardt, M. Stepanova, N.S. Fisher, Environ. Toxicol. Chem, 25 (2006) 2132 - 2142.

[56] L.S. Sherman, J.D. Blum, G.J. Keeler, J.D. Demers, J.T. Dvonch, Environ. Sci. Technol., 46 (2012) 382 - 390.

[57] K. Kritee, T. Barkay, J.D. Blum, Geochim. Cosmochim. Acta, 73 (2009) 1285 - 1296.

[58] R. Yin, X. Feng, B. Meng, Environ. Sci. Technol., 47 (2013) 2238 - 2245.

[59] S.Y. Kwon, J.D. Blum, M.A. Chirby, E.J. Chesney, Environ. Toxicol. Chem., 32 (2013) 2322 - 2330.

[60] J.L.A.V. Walleghem, P.J. Blanchfield, H. Hintelmann, Environ. Sci. Technol., 41 (2007) 5895 - 5901.

[61] C.C. Brombach, Z. Gajdosechova, B. Chen, A. Brownlow, W.T. Corns, J. Feldmann, E.M. Krupp, Anal. Bioanal. Chem., 407 (2015) 973 - 981.

[62] L.S. Sherman, J.D. Blum, A. Franzblau, N. Basu, Environ. Sci. Technol., 47 (2013) 3403 - 3409.

[63] A. Pennacchioni, R. Marchetti, C.F. Gaggion, J. Environ. Qual., 5 (1976) 451 - 454.

[64] J.W.M. Rudd, A. Furutani, M.A. Turner, Appl. Environ. Microbiol., 40 (1980) 777 - 782.

[65] A.E. Collin, T.A. Joshua, Y. Julie, L.A. Terrence, Environ. Toxicol. Chem., 28 (2009) 568 - 577.

[66] R. Wang, X.-B. Feng, W.-X. Wang, Environ. Sci. Technol., 47 (2013) 7949 - 7957.

[67] X. Wang, F. Wu, W.-X. Wang, Environ. Sci. Technol., 51 (2017) 6441 - 6451.

[68] J.E. Sonke, Geochim. Cosmochim. Acta, 75 (2011) 4577 - 4590.

[69] S.Y. Kwon, J.D. Blum, M.J. Carvan, N. Basu, J.A. Head, C.P. Madenjian, S.R. David, Environ. Sci. Technol., 46 (2012) 7527 - 7534.

[70] K. Kritee, J.D. Blum, T. Barkay, Environ. Sci. Technol., 42 (2008) 9171 - 9177.

[71] L. Laffont, J.E. Sonke, L. Maurice, S.L. Monroy, J. Chincheros, D. Amouroux, P. Behra, Environ. Sci. Technol., 45 (2011) 9910 - 9916.

[72] S.Y. Kwon, J.D. Blum, C.Y. Chen, D.E. Meattey, R.P. Mason, Environ. Sci. Technol., 48 (2014) 10089 - 10097.

[73] J.D. Blum, B.N. Popp, J.C. Drazen, C.A. Choy, M.W. Johnson, Nature Geoscience, 6 (2013) 879 - 884.

[74] N. Gantner, H. Hintelmann, W. Zheng, D.C. Muir, Environ. Sci. Technol., 43 (2009) 9148 - 9154.

[75] L.S. Sherman, J.D. Blum, Sci. Total Environ., 448 (2013) 163 - 175.

[76] D.B. Senn, E.J. Chesney, J.D. Blum, M.S. Bank, A. Maage, J.P. Shine, Environ. Sci. Technol., 44 (2010) 1630 - 1637.

[77] A. Mariotti, J.C. Germon, P. Hubert, P. Kaiser, R. Letolle, A. Tardieux, P. Tardieux, Plant Soil, 62 (1981) 413 - 430.

[78] V. Perrot, M.V. Pastukhov, V.N. Epov, S. Husted, O.F.X. Donard, D. Amouroux, Environ. Sci. Technol., 46 (2012) 5902 - 5911.

Chapter 6

Unraveling Hg exposure of long-finned pilot whales (*Globicephala melas*) *via* isotopic analysis with multi-collector ICP-mass spectrometry

Adapted from Rua-Ibarz et. al. (in preparation)

6.1. Introduction

Mercury (Hg) is a toxic heavy metal that is ubiquitously present in the environment. There are different forms of Hg, such as elemental (or metallic) Hg, inorganic Hg (iHg) and organic Hg compounds. Hg toxicity strongly depends on its chemical form, methylmercury (MeHg) being the most toxic Hg species.**[1]** Due to the high volatility of elemental Hg and other Hg compounds, Hg is globally distributed through the atmosphere, in which Hg has a residence time of up to 1 year.**[2]** Atmospheric Hg is predominantly deposited in oceans, one of the major reservoirs of Hg on Earth; between 60,000 and 80,000 tons of Hg are present in the global ocean according to recent estimations.**[3]** In aquatic environments, inorganic Hg species are converted into the more toxic organic MeHg compound, a process that proceeds *via* biotic or abiotic methylation occurring in sediment and/or in the water column.**[4, 5]** MeHg exposure of aquatic biota occurs mainly *via* the diet, resulting in the bioaccumulation and biomagnification of MeHg across food webs. This leads to high Hg levels in predatory animals (this means that the Hg level in biota is a function of their position within the trophic chain), thus making the consumption of these species the primary source of human MeHg exposure. Thus, marine and/or aquatic ecosystems are considered of utmost relevance within the biogeochemical Hg cycle and their study is of high scientific interest.

As predatory species located at the top of the aquatic food web and with a long lifespan, marine mammals accumulate high amounts of Hg in their tissues.**[6-8]** This is still an issue of great concern in terms of seafood safety, as despite of the potential health risks, these marine species are consumed by humans at some locations around the world. However, the study of marine mammals is even more relevant owing to the similarities these species share with humans in terms of metabolic pathways. Different studies carried out for marine mammals (and seabirds) have shown that despite of the high Hg concentrations present in their tissues, they do not show the toxic effects observed in humans, suggesting the existence or the development of effective Hg detoxification mechanisms.**[9]** Thus, the study of the Hg metabolic pathways (*e.g.*, uptake, transport, distribution and excretion) in marine mammals may aid at improving our understanding of the behavior of Hg in humans and at developing new strategies aiming to avoid and/or minimize the toxic effects induced by Hg and its related compounds, such as neurological damage and cardiovascular problems.**[10]**

So far, some authors have reported a species-specific Hg distribution in different organs of marine mammals,**[11]** and have pointed out the high affinity of Hg for biomolecules containing Se, and thus, suggested the formation of less toxic or inert iHg-Se compounds, such as HgSe particles, as a possible Hg detoxification mechanism.**[12, 13]** However, important knowledge gaps remain in our understanding of the metabolic pathways of Hg in marine mammals, thus necessitating the development of novel tools aiming at elucidating the complex biochemistry of Hg.

The measurement of Hg isotope ratios is to be considered a promising approach to shed light onto the biogeochemical Hg cycle in nature.**[14-16]** Hg is one of the few elements that display not only mass-dependent (MDF), but also mass-independent fractionation (MIF). As the $\Delta^{199}Hg/\Delta^{201}Hg$ ratio provides additional information, Hg isotopic analysis constitutes a multi-dimensional approach.**[17, 18]** MDF has been documented for most of the transformations that Hg undergoes in the environment, such as methylation, demethylation, volatilization, liquid-vapor evaporation and reduction.**[19-23]** MIF, however, has only been observed in photomediated reactions and is affecting the odd-numbered Hg isotopes only.**[24, 25]** A low extent of MIF has been reported on in literature for the even-numbered Hg isotopes ($\Delta^{200}Hg \neq 0$) also, but always in atmospheric samples.**[26-28]** In aquatic biota, MIF affects the odd-numbered Hg isotopes as a result of the photoreduction of Hg(II) and/or the photodegradation of MeHg in the presence of dissolved organic matter (DOM). These two photoreduction mechanisms can be distinguished based on the $\Delta^{199}Hg/\Delta^{201}Hg$ ratio.**[24]** Additionally, the extent of this odd-MIF depends on (*i*) the pH, (*ii*) the ionic strength, (*iii*) the concentration of total dissolved solids (TDS) of the water, (*iv*) the ratios Hg/DOM, MeHg/DOM, and the type of Hg-DOM binding ligand, and (*v*) most likely, also on the intensity and wavelength of sunlight.**[25, 29-32]** Several laboratory experiments and field studies have indicated that Hg trophic transfer and most of the biological processes (*e.g.*, excretion, transport between organs, methylation, demethylation,...) can produce *in vivo*-MDF. However, these processes have been characterized by the absence of *in vivo*-MIF, therefore suggesting that the MIF signatures of aquatic animals located at the top of the trophic chain may reflect the MIF of the residual Hg present in the water prior to its incorporation into the food web.**[24, 33-37]**

In this work, different tissues and biological fluids (liver, kidney, muscle, blood and milk) of stranded long-finned pilot whales have been analyzed for their THg concentration, MeHg content and Hg isotope ratios, aiming at obtaining a more profound insight into the metabolic processes that Hg undergoes in these marine mammals, such as uptake, storage, distribution, excretion, methylation and demethylation.

6.2. Materials and methods

6.2.1. Sample collection and sample preparation

On the 12th of September 2012, 31 long-finned pilot whales (*Globicephala melas*) stranded on a beach between Ansturther and Pittenween in Scotland, United Kingdom (**Figure 6-1**). From the complete pod, 10 whales were refloated, while 21 whales died at the stranding site, where the autopsy of each animal was carried out and their organs were dissected and stored for research purposes.**[9]** In the context of this work, 73 samples comprising 21 samples of liver, 20 samples of kidney, 15 samples of muscle, 15 samples of blood and 2 samples of milk, were provided by the University of Aberdeen (Scotland). The age of the whales was determined by Gajdosechova *et al.***[9]** following the method described by Lockyer.**[38] Table 6-1** provides the overall information (age, gender and length) of the set of animals analyzed in this work.

Figure 6-1. Mass stranding event of long-finned pilot whales.**[39]**

All tissue samples, biological fluids and certified reference materials (see section 6.2.2. for a list of the CRMs measured in this work) were acid-digested (0.2 – 1.2 g)

in pre-cleaned closed microwave vessels using a Milestone (Italy) Ethos One High-Performance Microwave Digestion System using a mixture of 7 M HNO_3 and 9.8 M H_2O_2 (see section 6.2.2. for a list of reagents). The microwave program is given in **Table 6-2**. After digestion, the samples were kept at 3 – 5 °C until analysis. In addition, HgSe particles were extracted and isolated from some liver tissues following an enzymatic digestion, as described in Gajdosechova *et al.***[13]**

Table 6-1. Information on the pod of whales analyzed in this work

Whale ID	Age (years)	Gender	Length (cm)
1	2.5	F	291
2	25.5	F	420
3	17	F**	389
4	25*	F**	420
5	20	F**	411
6	1*	F	192
7	1*	F	191
8	1*	F	194
9	6*	M	333
10	4	F	291
11	29	F**	445
12	3	F	315
13	9	F	360
14	2.5	M	296
15	35.5	F	462
16	4	M	318
17	2	M	287
18	25	F	440
19	15	M	444
20	28	F	435
21	16	M	538

*Age estimated based on body length
**Lactating mothers

6.2.2. Reagents and standards

High-purity water (resistivity > 18.2 MΩ cm) obtained from a Milli-Q Element water purification system (Millipore, France), pro-analysis 14 M HNO_3 and 12 M HCl (ChemLab, Belgium), further purified by sub-boiling distillation; and 9.8 M H_2O_2 (Fluka, Belgium), were used for digestion and subsequent dilution prior to ICP-MS measurements.

For quantification purposes, single-element standard solutions of Hg and Rh (1 gL^{-1}, Instrument solutions, The Netherlands) were appropriately diluted with 0.35 M

HNO_3. $KBrO_3$ (1 mM in 0.12 M HCl) was prepared freshly every day from $KBrO_3$ (≥ 99%, Sigma Aldrich, USA).

For isotopic analysis, NIST SRM 3133 (isotopic reference material of Hg) and NIST SRM 997 (isotopic reference material of Tl) were dissolved in a mixture of 0.7 M HNO_3 and 0.6 M HCl, and in 0.35 M HNO_3, respectively. Both isotopic reference materials were used for instrumental mass discrimination correction purposes. Additionally, an in-house standard solution of Hg (Inorganic Ventures, The Netherlands, Lot: F2-HG02105) with known Hg isotopic composition **[40]** was diluted in the same acid mixture as the Hg isotopic reference material, and it was used throughout the work for instrument optimization and quality control of the measurements.

A solution of 3% $SnCl_2.2H_2O$ in 1.2 M HCl was prepared freshly every day from pro-analysis $SnCl_2.2H_2O$ (≥ 98 %, Sigma Aldrich, USA) and it was bubbled with purified Ar during approximately 30 minutes before its use, aiming at removing possible traces of Hg.

For validation of the entire analytical procedure, three CRMs with a similar matrix composition as those of the samples of interest in this work, were used: BCR CRM 464 (tuna fish), NRC-CNRC DORM-4 (fish protein) and TORT-3 (lobster hepatopancreas).

Table 6-2. Microwave program used for microwave-assisted acid digestion in a Milestone Ethos One High-Performance Microwave Digestion System.

Step	Temperature (°C)	Time (min)
1	Room temperature to 70	5
2	70 to 90	7
3	90	5
4	90 to 120	7
5	120	5
6	120 to 150	7
7	150	5

6.2.3. Elemental analysis

The total Hg (THg) concentration was determined using a ThermoScientific (Germany) Element XR single-collector sector-field ICP-MS instrument (SF-ICP-MS) working at low resolution mode. The instrument was equipped with a 100 μL min^{-1}

concentric nebulizer mounted onto a cyclonic spray chamber. The quantification of Hg was carried out relying on external calibration (calibration curve based on standard solutions with Hg concentrations of 0, 0.5, 1, 2.5 and 5 μg L^{-1}) using Rh (1 μg L^{-1}) as an internal standard to correct for instrument instability, signal drift and possible matrix effects. 1 mM $KBrO_3$ in 0.12 M HCl was added to all samples, standards and wash solutions (final concentration of 0.01mM of $KBrO_3$) to avoid Hg volatilization and to reduce memory effects.

Additionally, Hg speciation was performed at the University of Aberdeen using a HP-6890 GC-unit (Agilent Technologies, Japan) coupled to an Agilent 7500 ICP-MS instrument (Agilent Technologies, Japan), as was previously described by Gajdosechova *et al.***[9]**

6.2.4. Hg isotopic analysis

Hg isotopic analysis was carried out using a ThermoScientific (Germany) Neptune multi-collector ICP-MS (MC-ICP-MS) instrument equipped with nine Faraday cups. Hg was introduced as Hg(0) generated *via* the reduction of Hg^{2+} with 3% $SnCl_2.2H_2O$ in 1.2 M HCl in an HGX-200 cold vapor & hydride generation unit (Teledyne Cetac Technologies, US). The Hg(0)-loaded carrier gas coming from the CVG unit was admixed in a 'T' piece with a wet aerosol of Tl (used for internal mass discrimination correction purposes) generated by using a 100 μL min^{-1} concentric nebulizer mounted onto a dual (cyclonic and Scott-type) spray chamber. A complete description of this set-up can be found in a previous manuscript from the same authors and in Chapter 3.**[40]**

For instrumental mass discrimination correction, a combination of internal correction using the "Baxter approach" (with NIST SRM 997 Tl as internal standard) and external correction in a sample standard bracketing (SSB) approach (with NIST SRM 3133 Hg as external standard) was relied upon.**[40, 41]**

An in-house standard solution of Hg and the CRMs selected in this work were measured in-between the samples (approximately every five samples) for quality control of the measurements and validation of the entire analytical procedure (*i.e.*, MW acid digestion, storage, dilution and subsequent MC-ICP-MS measurement).

The Hg concentration and acid content of all samples, standards and CRMs were matched within ± 10 % as to avoid inaccurate results. Moreover, no blank subtraction was applied because the effect of the blank was demonstrated to be negligible within the precision attainable in this work.

The Hg isotopic composition is reported in delta (δ^{xxx}Hg) and capital delta (Δ^{xxx}Hg) notation – in per mil units (‰) – for mass-dependent (MDF) and mass-independent (MIF) fractionation, respectively.**[42]**

6.3. Results and discussion

6.3.1. Hg and MeHg quantification in long-finned pilot whales

THg concentrations and MeHg fractions (% MeHg) for all tissue samples analyzed in this work are provided in **Table 6-3** (liver), **6-4** (kidney), and **6-5** (muscle). Overall, the highest Hg accumulation was found in the liver, with THg concentrations ranging between 0.98 to 608 mg kg^{-1}. THg concentrations of kidney and muscle tissues ranged from 0.42 to 21.8 mg kg^{-1} and from 0.50 to 4.72 mg kg^{-1}, respectively. A positive correlation was observed between the age of long-finned pilot whales and the THg concentrations in liver, kidney, and muscle (Spearman's correlation r = 0.984, 0.947, 0.953, respectively), thus suggesting that Hg is accumulated in these tissues over the lifespan of the whales. The THg concentration trend observed for the different tissues of long-finned pilot whales (THg_{Liver} > THg_{Kidney} > THg_{Muscle}) was found to be in good agreement with previous data reported on in literature for marine mammal studies.**[7, 9, 43]**

MeHg speciation indicates that in muscle tissue, Hg is predominantly present as MeHg *i.e.* the most toxic Hg species, with values ranging from 65.3 to 100 %. However, in liver and kidney, the majority of the Hg is present in its inorganic form (iHg), with % MeHg values ranging from 1.0 to 32.1 % and from 4.7 to 46.5 %, respectively. Analysis of the stomach content of the same long-finned pilot whales previously showed that their predominant prey species are cephalopods, and that Hg is mainly present as MeHg in these species.**[9]** Based on the assumption that the Hg intake by marine mammals occurs mainly from the diet, MeHg is expected to be the major Hg species in the different tissues and biological fluids of long-finned pilot whales. However, as indicated above, the major Hg species in liver and kidney

is iHg, thus suggesting that the MeHg ingested *via* the diet must be demethylated *in vivo* and converted into the less toxic form iHg present in these organs, while the remaining MeHg is bioaccumulated in the muscle tissue, which acts as a reservoir of MeHg.

It also needs to be noted that for all samples studied (*i.e.*, liver, kidney and muscle), THg concentration values increase as a function of the age, while the MeHg fraction decreases (see **Figure 6-2**). In other words, the higher the THg concentrations, the higher the extent of demethylation. This trend was found to be more significant for the liver compared to kidney and muscle tissues, suggesting that liver could be a key organ for MeHg demethylation. In a recent study of *in vivo* Hg demethylation in marine fish,**[44]** the authors reported that the intestinal tract seems to be the major site for demethylation when the fish is directly exposed to MeHg, while during the depuration stage (*i.e.* no exposure to MeHg), the liver plays the major role.

An in-depth evaluation of the concentrations of the Hg species in the liver shows a clearly more pronounced decrease of the MeHg fraction (% MeHg) at an early age, especially for individuals ranging from 1 to 5 years old. These results may be related with differences in diet and Hg metabolism between juvenile and adult long-fined pilot whales. The Hg intake *via* the diet in juvenile marine mammals is expected to be strongly affected by lactation *i.e.*, it depends on the mother's milk. In a previous study of bottlenose dolphins (*Tursiops truncates*), it was found that Hg concentrations in mother milk are higher than those in the prey fish of adult dolphins.**[45]** In addition, high MeHg concentrations have been reported for breast milk from lactating women exposed to MeHg *via* the diet,**[46-48]** and for rats and mice (Holtzman rat and Balb/c CUM mice) **[49, 50]** and dolphins (*Stenella coeruleoalba* and *Sotalia guianensis*) **[51, 52]** that were exposed to high MeHg amounts *via* the placenta. Thus, the high MeHg fraction shown in long-fined pilot whales at young age could most likely be attributed to MeHg intake *via* mother milk and/or *in utero* MeHg exposure.

However, the development of detoxification mechanisms developed in an attempt to mitigate the toxic effects of Hg cannot be discarded as a potential explanation for the fast decrease in the MeHg fraction, *i.e.*, in comparison with the increase in THg concentrations, as a function of age.

Table 6-3. THg, % MeHg and Hg isotopic composition measured in liver tissues of long-finned pilot whales.

Whale ID	Age (years)	THg (mg Kg^{-1})	% MeHg	$\delta^{199}Hg$ (‰)	$\delta^{200}Hg$ (‰)	$\delta^{201}Hg$ (‰)	$\delta^{202}Hg$ (‰)	$\Delta^{199}Hg$ (‰)	$\Delta^{201}Hg$ (‰)
6	1	0.98 ± 0.10	32.1	0.89 ± 0.05	-0.32 ± 0.07	0.34 ± 0.04	-0.65 ± 0.10	1.05 ± 0.04	0.83 ±0.05
7	1	1.33 ± 0.26	28.2	0.98 ± 0.05	-0.29 ± 0.02	0.46 ± 0.07	-0.57 ± 0.04	1.12 ± 0.05	0.89 ± 0.09
8	1	0.98 ± 0.15	28.3	0.89 ± 0.11	-0.10 ± 0.07	0.70 ± 0.06	-0.23 ± 0.13	0.94 ± 0.10	0.87 ± 0.05
1	2.5	5.9 ± 1.0	18.6	0.81 ± 0.07	-0.40 ± 0.06	0.17 ± 0.05	-0.97 ± 0.04	1.05 ± 0.08	0.89 ± 0.06
12	3	8.7 ± 1.1	14.9	0.79 ± 0.05	-0.43 ± 0.03	0.18 ± 0.03	-0.97 ± 0.06	1.04 ± 0.05	0.91 ± 0.07
10	4	27.4 ± 4.7	5.9	0.70 ± 0.05	-0.55 ± 0.04	-0.03 ± 0.04	-1.12 ± 0.02	0.98 ± 0.05	0.81 ± 0.04
13	9	57.7 ± 8.2	4.8	0.78 ± 0.02	-0.44 ± 0.02	0.16 ± 0.07	-0.91 ± 0.03	1.00 ± 0.02	0.84 ± 0.07
3	17	147 ± 18	3.6	0.88 ± 0.07	-0.29 ± 0.03	0.31 ± 0.04	-0.65 ± 0.02	1.04 ± 0.07	0.80 ± 0.05
5	20	148 ± 21	2.2	0.92 ± 0.01	-0.24 ± 0.01	0.44 ± 0.06	-0.57 ± 0.05	1.06 ± 0.03	0.87 ± 0.06
18	25	243 ± 36	2.6	0.82 ± 0.05	-0.30 ± 0.02	0.34 ± 0.08	-0.65 ± 0.06	0.99 ± 0.05	0.84 ± 0.07
4	25	208 ± 10	2.4	0.73 ± 0.04	-0.36 ± 0.02	0.19 ± 0.06	-0.81 ±0.07	0.93 ± 0.06	0.80 ± 0.01
2	25.5	234 ± 27	2.5	0.98 ± 0.03	-0.21 ± 0.03	0.49 ± 0.01	-0.58 ± 0.04	1.13 ± 0.02	0.93 ± 0.03
20	28	472 ± 88	0.9	0.96 ± 0.04	-0.13 ± 0.06	0.55 ± 0.03	-0.35 ± 0.08	1.05 ± 0.02	0.81 ± 0.05
11	29	415 ± 26	1.2	0.94 ± 0.04	-0.08 ± 0.03	0.66 ± 0.02	-0.29 ± 0.05	1.01 ± 0.03	0.87 ± 0.03
15	35.5	608 ± 71	1.0	1.01 ± 0.03	-0.01 ± 0.04	0.78 ± 0.03	-0.15 ± 0.03	1.05 ± 0.02	0.89 ± 0.04
17	2	2.61 ± 0.44	22.6	0.95 ± 0.02	-0.36 ± 0.02	0.39 ± 0.04	-0.74 ± 0.03	1.13 ± 0.02	0.95 ± 0.06
14	2.5	6.14 ± 0.55	15.4	0.78 ± 0.07	-0.44 ± 0.09	0.10 ± 0.08	-0.95 ± 0.11	1.02 ± 0.05	0.82 ± 0.01
16	4	8.6 ± 1.2	14.2	0.77 ± 0.04	-0.47 ± 0.02	0.10 ± 0.07	-0.98 ± 0.03	1.02 ± 0.03	0.84 ± 0.05
9	6	43.9 ± 3.5	6.3	0.71 ± 0.04	-0.60 ± 0.03	-0.03 ± 0.09	-1.23 ± 0.07	1.02 ± 0.04	0.89 ± 0.08
19	15	58.2 ± 11	4.0	0.80 ± 0.05	-0.45 ± 0.04	0.13 ± 0.04	-0.92 ± 0.06	1.03 ± 0.07	0.82 ± 0.02
21	16	214 ± 28	1.6	0.83 ± 0.04	-0.33 ± 0.05	0.25 ± 0.07	-0.69 ± 0.05	1.00 ± 0.03	0.77 ± 0.04

Table 6-4. THg, % MeHg and Hg isotopic composition measured in kidney tissues of long-finned pilot whales.

Whale ID	Age (years)	THg (mg Kg^{-1})	% MeHg	$\delta^{199}Hg$ (‰)	$\delta^{200}Hg$ (‰)	$\delta^{201}Hg$ (‰)	$\delta^{202}Hg$ (‰)	$\Delta^{199}Hg$ (‰)	$\Delta^{201}Hg$ (‰)
6	1	0.60 ± 0.25	32.8	0.89 ± 0.07	-0.33 ± 0.08	0.32 ± 0.07	-0.76 ± 0.13	1.08 ± 0.05	0.89 ± 0.03
7	1	0.54 ± 0.08	41.9	0.94 ± 0.08	-0.33 ± 0.05	0.34 ± 0.11	-0.64 ± 0.11	1.11 ± 0.07	0.83 ± 0.03
8	1	0.42 ± 0.09	32.2	0.92 ± 0.08	-0.14 ± 0.04	0.51 ± 0.05	-0.33 ± 0.01	1.00 ± 0.08	0.76 ± 0.06
1	2.5	1.07 ± 0.10	46.5	1.00 ± 0.06	-0.09 ± 0.02	0.68 ± 0.11	-0.29 ± 0.05	1.07 ± 0.06	0.90 ± 0.10
12	3	1.31 ± 0.58	40.9	0.88 ± 0.04	-0.17 ± 0.04	0.52 ± 0.09	-0.39 ± 0.06	0.98 ± 0.03	0.81 ± 0.05
10	4	1.8 ± 1.0	33.7	0.89 ± 0.04	-0.24 ± 0.03	0.50 ± 0.05	-0.47 ± 0.03	1.01 ± 0.04	0.86 ± 0.05
13	9	6.3 ± 1.3	13.2	0.77 ± 0.06	-0.54 ± 0.04	0.02 ± 0.07	-1.10 ± 0.05	1.05 ± 0.07	0.85 ± 0.03
3	17	5.15 ± 0.74	28.7	0.75 ± 0.07	-0.32 ± 0.02	0.31 ± 0.04	-0.62 ± 0.05	0.91 ± 0.08	0.78 ± 0.01
5	20	9.8 ± 3.8	10.4	0.89 ± 0.03	-0.24 ± 0.05	0.45 ± 0.03	-0.52 ± 0.07	1.02 ± 0.02	0.84 ± 0.04
18	25	15.0 ± 5.5	10.5	0.83 ± 0.04	-0.41 ± 0.06	0.33 ± 0.10	-0.82 ± 0.09	1.03 ± 0.05	0.95 ± 0.03
4	25	4.31 ± 1.2	11.7	0.89 ± 0.05	-0.32 ± 0.04	0.25 ± 0.11	-0.63 ± 0.04	1.05 ± 0.06	0.73 ± 0.09
2	25.5	10.6 ± 0.9	12.8	0.90 ± -0.02	-0.32 ± 0.03	0.29 ± 0.04	-0.76 ± 0.03	1.09 ± 0.02	0.86 ± 0.03
20	28	20.7 ± 1.3	4.7	0.86 ± 0.03	-0.33 ± 0.10	0.38 ± 0.08	-0.67 ±0.11	1.03 ± 0.01	0.88 ± 0.07
11	29	21.8 ± 2.8	7.6	0.84 ± 0.03	-0.33 ± 0.05	0.35 ± 0.10	-0.72 ± 0.04	1.02 ± 0.03	0.88 ± 0.09
15	35.5	N.A.	N.A.	N.A.	N.A.	N.A.	N.A.	N.A.	N.A.
17	2	1.22 ± 0.21	24.6	0.76 ± 0.04	-0.50 ± 0.07	0.11 ± 0.12	-1.02 ± 0.13	1.02 ± 0.04	0.87 ± 0.06
14	2.5	1.93 ± 0.44	26.1	0.85 ± 0.05	-0.31 ± 0.07	0.36 ± 0.07	-0.71 ± 0.07	1.03 ± 0.04	0.89 ± 0.03
16	4	2.99 ± 0.49	24.2	0.87 ± 0.05	-0.33 ± 0.01	0.34 ± 0.04	-0.73 ± 0.07	1.06 ± 0.07	0.89 ± 0.02
9	6	2.80 ± 0.10	34.2	0.98 ± 0.01	-0.25 ±0.05	0.46 ± 0.04	-0.55 ± 0.03	1.12 ± 0.02	0.87 ± 0.02
19	15	6.03 ± 0.62	26.2	0.89 ± 0.02	-0.35 ± 0.02	0.34 ± 0.04	-0.73 ± 0.06	1.07 ± 0.01	0.89 ± 0.04
21	16	7.0 ± 1.4	11.1	0.85 ± 0.03	-0.41 ± 0.01	0.29 ± 0.06	-0.78 ± 0.06	1.05 ± 0.03	0.88 ± 0.05

N.A. = not available

Table 6-5. THg, % MeHg and Hg isotopic composition measured in muscle tissues of long-finned pilot whales.

Whale ID	Age (years)	THg (mg Kg^{-1})	% MeHg	δ^{199}Hg (‰)	δ^{200}Hg (‰)	δ^{201}Hg (‰)	δ^{202}Hg (‰)	Δ^{199}Hg (‰)	Δ^{201}Hg (‰)
6	1	0.51 ± 0.15	89.7	1.38 ± 0.10	0.57 ± 0.10	1.70 ± 0.08	1.03 ± 0.03	1.12 ± 0.11	0.93 ± 0.06
7	1	0.61 ± 0.06	100.0	1.39 ± 0.06	0.59 ± 0.04	1.71 ± 0.04	1.05 ± 0.10	1.13 ± 0.08	0.92 ± 0.05
8	1	0.50 ± 0.09	78.7	1.23 ± 0.09	0.54 ± 0.01	1.58 ± 0.02	0.98 ± 0.03	0.99 ± 0.10	0.84 ± 0.04
1	2.5	0.95 ± 0.05	100.0	1.28 ± 0.04	0.48 ± 0.03	1.60 ± 0.03	0.98 ± 0.03	1.04 ± 0.05	0.86 ± 0.04
12	3	1.51 ± 0.25	N.A.	1.37 ± 0.05	0.68 ± 0.04	1.84 ± 0.06	1.31 ± 0.08	1.04 ± 0.05	0.85 ± 0.02
10	4	1.51 ± 0.21	86.1	1.35 ± 0.03	0.62 ± 0.03	1.72 ± 0.08	1.13 ± 0.08	1.07 ± 0.04	0.87 ± 0.02
13	9	3.15 ± 0.63	99.0	1.34 ± 0.06	0.53 ± 0.06	1.68 ± 0.07	1.07 ± 0.02	1.07 ± 0.06	0.87 ± 0.05
3	17	4.2 ± 0.65	89.6	1.32 ± 0.06	0.55 ± 0.01	1.62 ± 0.04	0.98 ± 0.06	1.08 ± 0.07	0.88 ± 0.02
5	20	4.2 ± 0.65	87.2	1.33 ± 0.02	0.47 ± 0.01	1.53 ± 0.03	0.80 ± 0.03	1.13 ± 0.01	0.93 ± 0.04
18	25	N.A	N.A.	N.A.	N.A.	N.A.	N.A.	N.A.	N.A.
4	25	3.84 ± 0.38	75.4	1.17 ± 0.05	0.34 ± 0.08	1.43 ± 0.05	0.71 ± 0.03	0.99 ± 0.06	0.89 ± 0.07
2	25.5	3.82 ± 0.9	67.5	1.15 ± 0.08	0.29 ± 0.03	1.29 ± 0.01	0.55 ± 0.04	1.01 ± 0.09	0.87 ± 0.02
20	28	N.A.	N.A.	N.A.	N.A.	N.A.	N.A.	N.A.	N.A.
11	29	4.72 ± 0.35	65.3	1.19 ± 0.02	0.16 ± 0.03	1.09 ± 0.09	0.20 ± 0.09	1.14 ± 0.02	0.94 ± 0.03
15	35.5	N.A.	N.A.	N.A.	N.A.	N.A.	N.A.	N.A.	N.A.
17	2	1.04 ± 0.15	87.2	1.36 ± 0.06	0.58 ± 0.02	1.67 ± 0.03	1.05 ± 0.04	1.10 ± 0.07	0.88 ± 0.05
14	2.5	N.A.	N.A.	N.A.	N.A.	N.A.	N.A.	N.A.	N.A.
16	4	1.26 ± 0.15	88.2	1.37 ± 0.05	0.57 ± 0.07	1.72 ± 0.12	1.01 ± 0.05	1.12 ± 0.04	0.96 ± 0.12
9	6	1.69 ± 0.34	93.7	1.37 ± 0.03	0.50 ± 0.06	1.72 ± 0.02	0.95 ± 0.07	1.13 ± 0.01	1.01 ± 0.06
19	15	N.A.	N.A.	N.A.	N.A.	N.A.	N.A.	N.A.	N.A.
21	16	N.A.	N.A.	N.A.	N.A.	N.A.	N.A.	N.A.	N.A.

N.A. = not available

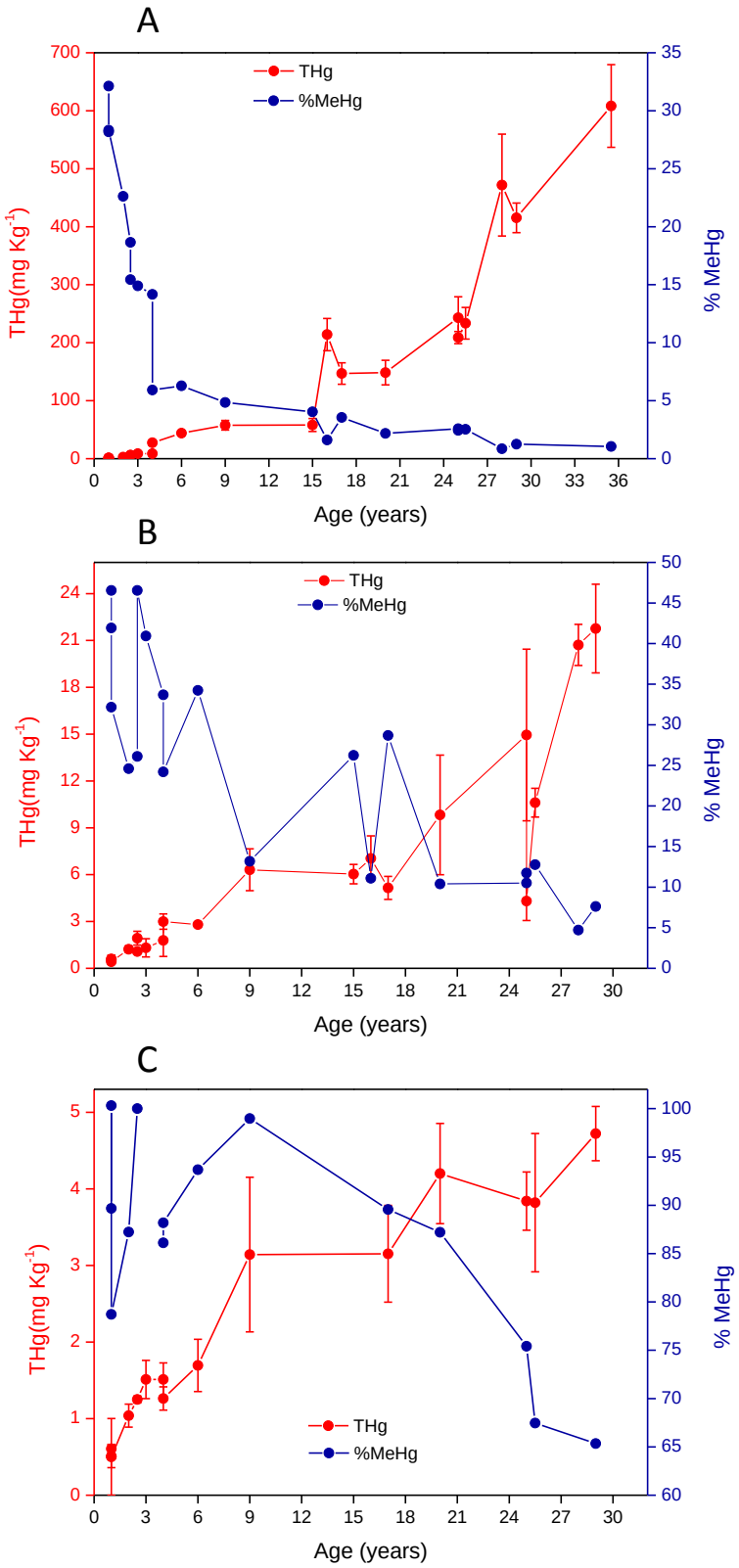

Figure 6-2. THg concentration (red) and % MeHg (blue) as a function of age for liver (A), kidney (B), and muscle (C) tissues of long-finned pilot whales.

It is well known that Se has a protective effect against Hg toxicity owing to the Hg-Se antagonism, and thus, this element could play an important role in the MeHg demethylation processes.**[53]** Sakamoto *et al.***[54]** reported a strong positive correlation between Hg and Se concentrations in muscle tissues of five different species of toothed whales. Moreover, this observation is in good agreement with the results obtained by Gajdosechova *et al.* based on elemental analysis of the same samples evaluated in this work,**[9]** for which also a strong positive correlation was found between Hg and Se in liver, kidney and muscle tissues. This correlation suggests that Se-mediated MeHg demethylation processes might take place in the liver, kidney and muscle of long-finned pilot whales. Additionally, in the work of Gajdosechova *et al.*,**[13]** an important fraction of the liver Hg was found to be present in the form of HgSe particles (tienmannite). The formation of these particles has been suggested as a potential Hg detoxification mechanism in marine mammals. Also the formation of HgS (cinnabar) has been proposed, but the affinity of Se for Hg is known to be higher than that of S.**[55]** The formation of the crystalline HgSe is mediated by Hg-metallothionein (Hg-MT) interaction and/or by the binding of Hg–Se complexes to high-molecular-weight substances.**[56, 57]** These mechanisms have been mainly observed in the liver of marine mammals, thus suggesting a key role of this organ in Se-mediated Hg detoxification. However, HgSe particles have also been found in other tissues, such as brain, kidney, lung, muscle, pancreas, pituitary and spleen.**[13, 55, 58]** Therefore, the so-called Hg-Se antagonistic effect might be responsible for the decrease of the MeHg fraction as a function of age, and for the increase in THg concentrations in liver, kidney and muscle tissues as a result of the formation of HgSe particles.

It needs to be pointed out, though, that despite of the high level of Hg accumulation in liver tissues, marine mammals typically do not show evidence of toxic effects. We can therefore hypothesize that HgSe particles may be considered as inert Hg compounds. However, the increased presence of micro- and nanoparticles could induce organ malfunction owing to their ability to traverse cell boundaries, while a high MeHg dietary intake has a direct impact on the biosynthesis of Se-proteins, which compromises other metabolic processes.**[13]** Thus, the formation of HgSe particles needs to be rather regarded as a short-term solution to high Hg, and especially MeHg, exposure.

6.3.2. Hg isotopic analysis in long-finned pilot whales

The results of Hg isotopic analysis ($\delta^{199,200,201,202}$Hg and $\Delta^{199,201}$Hg) of different tissues and biological fluids of long-finned pilot whales are displayed in **Table 6-3** (liver), **6-4** (kidney), **6-5** (muscle), and **6-6** (blood and milk). In addition, **Figure 6-3** shows the three-isotope plots of δ^{199}Hg (A), δ^{200}Hg (B) and δ^{201}Hg (C) *vs* δ^{202}Hg for all samples analyzed in this work. Overall, it needs to be stressed that the δ^{200}Hg *vs* δ^{202}Hg data fall along the theoretical mass-dependent fractionation (MDF) line, while the data for the odd-numbered Hg isotopes (^{199}Hg and ^{201}Hg) are clearly also influenced by additional mass-independent fractionation (MIF) (*vide infra*).

From the complete data set of MDF-Hg data (see **Figure 6-4**), it is clear that negative δ^{202}Hg values are found for liver (-1.23 to -0.15 ‰) and kidney (-1.10 to -0.29 ‰) tissues, and positive ones for muscle tissue (0.20 to 1.31 ‰) and for biological fluids, *i.e.* blood (-0.18 to 1.2 ‰) and milk (0.12 to 0.91 ‰). Broadly speaking, δ^{202}Hg values are similar for liver and kidney (lighter Hg isotopic compositions) and for muscle, blood and milk (heavier Hg isotopic compositions). These differences can be attributed to the species-specificity of the Hg isotopic signatures *i.e.*, different Hg isotopic compositions of MeHg and iHg. As indicated in the previous section, liver and kidney tissues are characterized by a mixture of both Hg species (predominantly iHg), while a larger fraction of the Hg present in muscle and biological fluids is in the form of MeHg. The differences in Hg speciation and the corresponding variations in the isotopic composition of Hg for different tissues and biological fluids of long finned pilot whales may be the result of *in vivo* demethylation of organic MeHg and the corresponding MDF of Hg accompanying this process. It has been documented that abiotic and biotic processes preferentially demethylate MeHg compounds containing the lighter isotopes of Hg, resulting in higher δ^{202}Hg values in the remaining MeHg fraction and in lower δ^{202}Hg values in the iHg produced.**[25, 59, 60]** Based on the assumption that *in vivo* demethylation of ingested MeHg may induce similar MDF in long-finned pilot whales, the results obtained in this work for MDF-Hg in muscle (mainly MeHg), and in liver and kidney (mainly iHg), seem to be in good agreement with the MDF observed for Hg in abiotic and biotic processes.

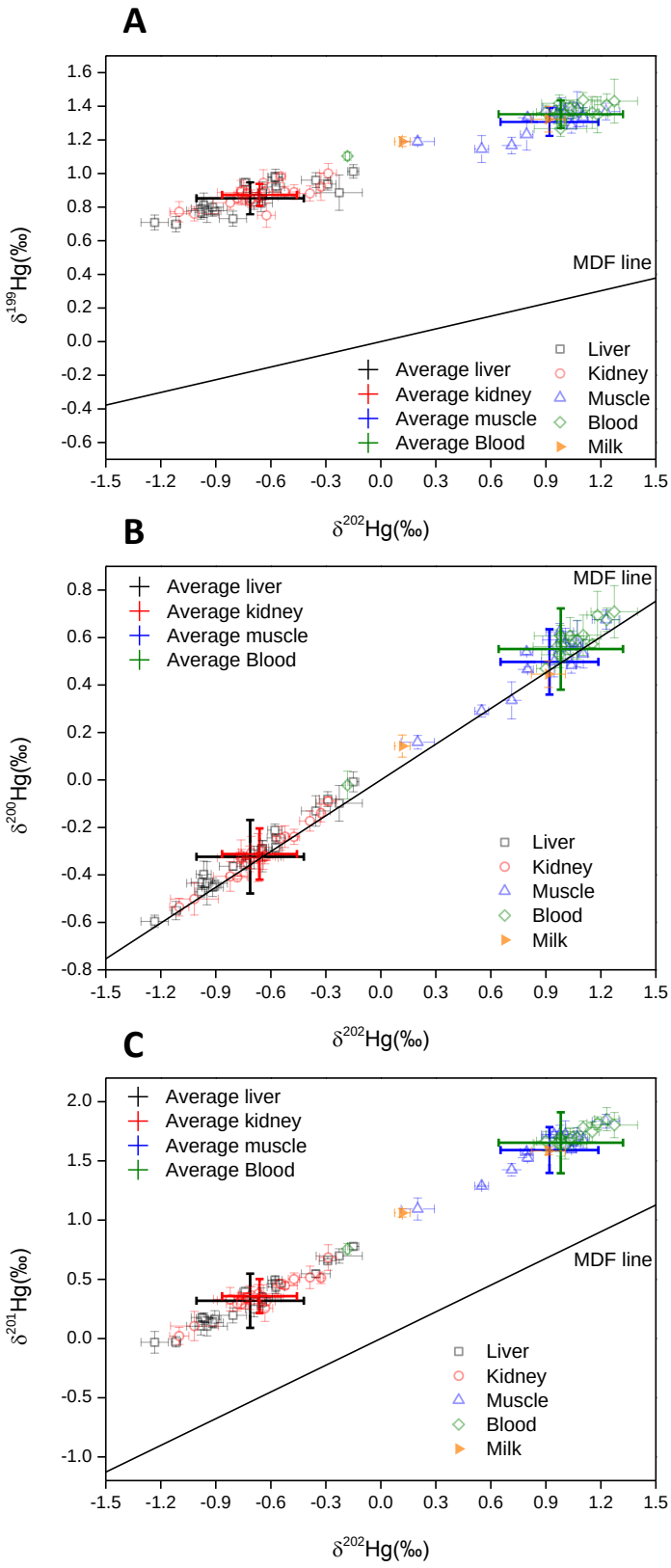

Figure 6-3. Three-isotope plots: δ^{199}Hg (A), δ^{200}Hg (B) and δ^{201}Hg (C) *vs* δ^{202}Hg for all the samples analyzed in this work.

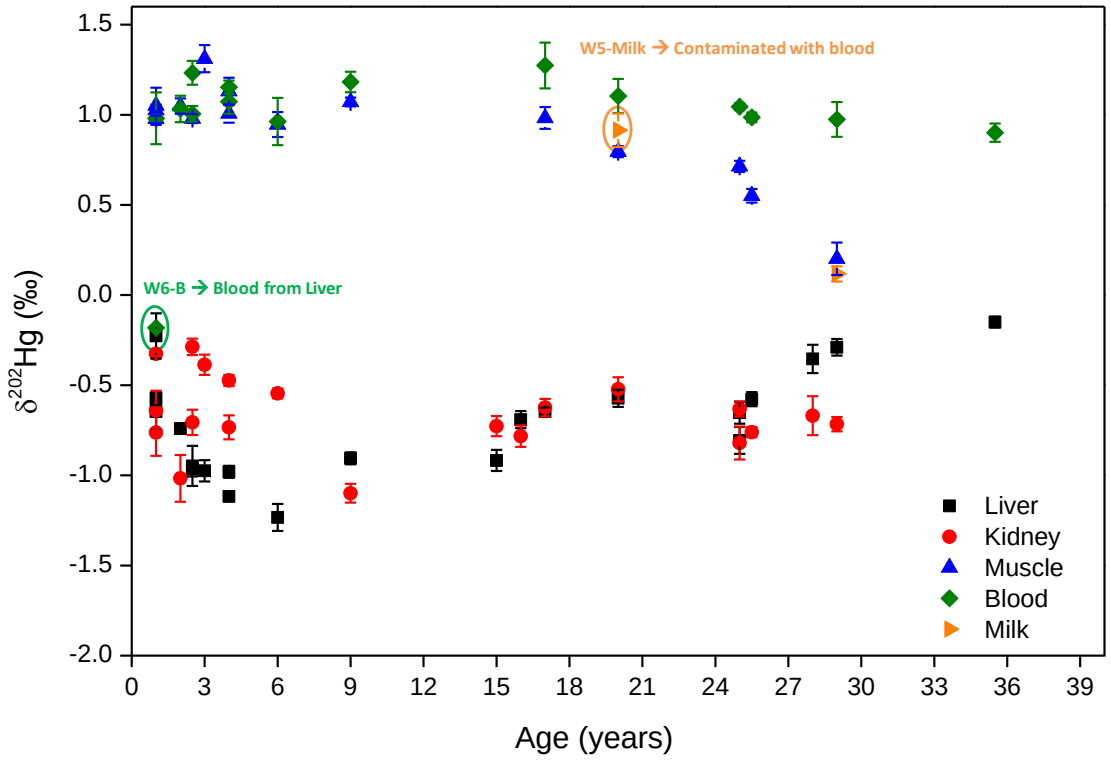

Figure 6-4. Overview of the MDF-Hg isotopic signatures (δ^{202}Hg) of different tissues of long-finned pilot whales as a function of age.

However, although the aforementioned behavior explains the Hg isotopic signatures of different tissues and biological fluids of long-finned pilot whales in general terms, some deviations are found when looking into more detail, thus providing additional information regarding specific Hg metabolic processes. **Figure 6-5** shows the results of Hg isotopic analysis (δ^{202}Hg) as a function of age for samples from female and male individuals (no gender-based differences were observed within the entire study).

Muscle tissue is characterized by a high MeHg fraction, and, as a consequence (*vide ante*), by a Hg isotopic signature generally enriched in the heavier Hg isotopes (high δ^{202}Hg values). It can be seen (**Figure 6-5A**) that for muscle tissues of juvenile whales *i.e.*, ≤ 6 years old, the relation between δ^{202}Hg values and the % MeHg is not clear. This could be related with the fact that the ages of younger individuals are subjected to a large uncertainty owing to the method used for estimation,**[9]** which could explain the random behavior at low ages. For adult whales ≥ 17 years old,

however, both δ^{202}Hg and % of MeHg decrease systematically as a function of the individual's age. This pattern is in agreement with the hypothesis that the lighter Hg isotopes are preferentially demethylated, *i.e.*, the remaining MeHg is enriched in the heavier Hg isotopes, thus resulting in lower δ^{202}Hg values accompanying the increase of the iHg fraction as a function of age. It needs to be noted that for the oldest whale for which muscle tissue was available (29 years old), δ^{202}Hg is lowered by ~0.8‰ regarding to whale individuals with ages ≤17 years old, while the MeHg fraction decreased from ~90 to 65% MeHg. Therefore, the decrease in the MeHg fraction and in the δ^{202}Hg value for muscle tissues of adult whales from certain ages may correspond with metabolic changes in the whale body. This may be attributed to the response towards a high Hg accumulation, thus increasing the extent of MeHg demethylation aiming to reduce the possible toxic effects of organic MeHg *via* conversion into less toxic iHg species.

In contrast to muscle, Hg in liver tissues is mainly present as iHg. In **Figure 6-5B**, it can be seen that at low ages (≤ 6 years old), both δ^{202}Hg and % of MeHg decrease following the same pattern, which is in agreement with the hypothesis that a decrease in the MeHg fraction is generally accompanied by an enrichment of the iHg fraction in the lighter Hg isotopes *i.e.*, lower δ^{202}Hg values. Interestingly, for whale individuals above 5 – 6 years old, an opposite trend between δ^{202}Hg and % MeHg as a function of age is observed for liver tissue of both female and male long finned pilot whales. It is noteworthy that an increase in δ^{202}Hg of ~1‰ was found between 5 – 6 and 35.5 years old, while the MeHg fraction still decreases as a function of age (from 32 to 1% approximately). To the best of the author's knowledge, this behavior has not been reported on in literature to date and cannot be explained by the preferential demethylation of lighter Hg isotopes. Thus, we hypothesize that the enrichment of the iHg fraction in the heavier Hg isotopes (higher δ^{202}Hg values) must be related with the key role of the liver in the biochemistry of Hg within the whale body. **Figure 6-6** shows the δ^{202}Hg values as a function of the THg concentration (A) and of the MeHg fraction (B). Clearly, both figures point to different Hg sources and metabolic pathways for juvenile and adult whales, respectively, corresponding with an increase in THg concentration and with a decrease in the MeHg fraction for liver tissues.

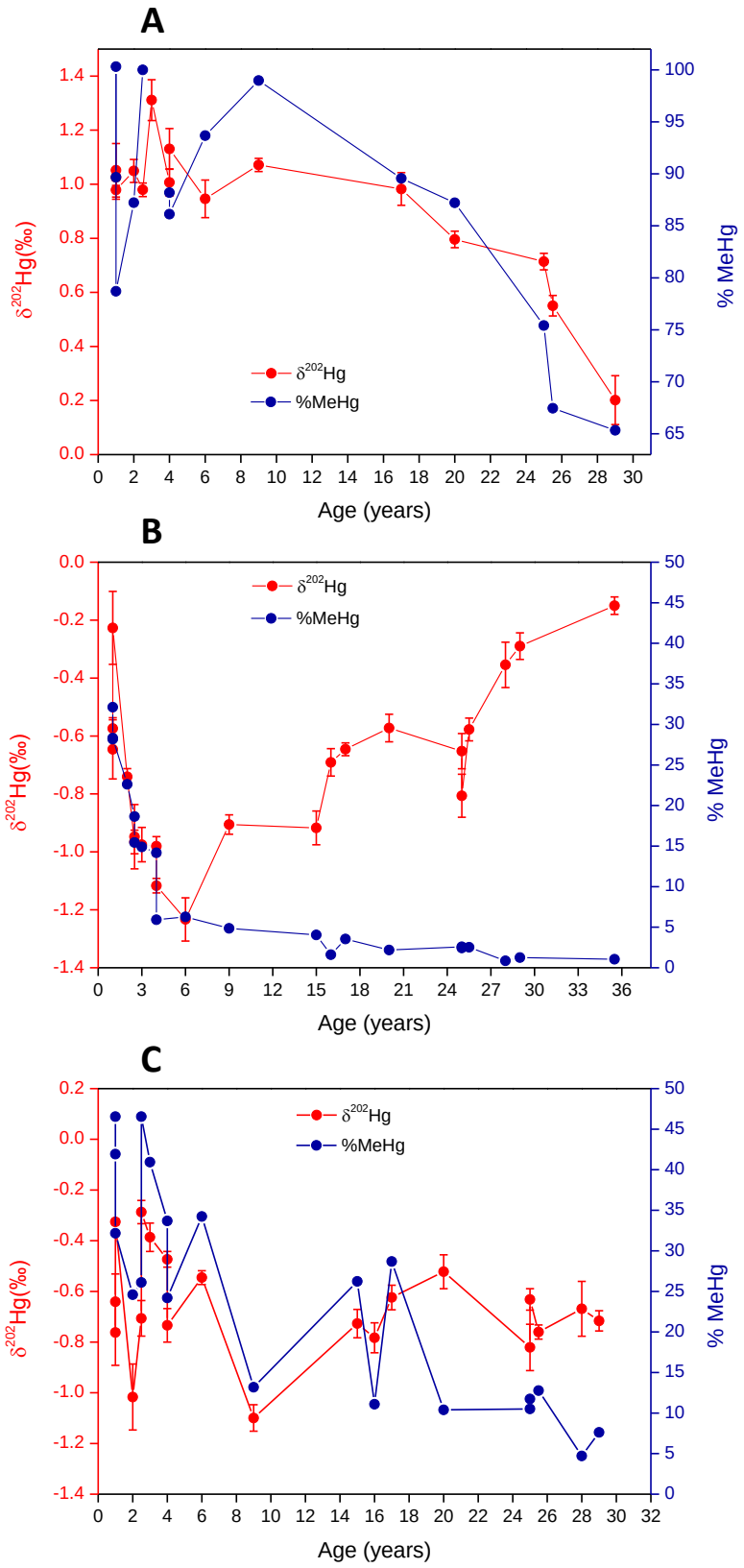

Figure 6-5. δ^{202}Hg (red – left y-axis) and MeHg fraction (% MeHg, blue – right y-axis) obtained for muscle (A), liver (B) and kidney (C) tissues as a function of age.

As was hypothesized in section 6.3.1, the high MeHg fraction in the liver of young long-finned pilot whales can be tentatively explained by a higher MeHg intake coming from the diet (ingestion of mother's milk during lactation) and/or from the placenta (during gestation). It needs to be noted that MeHg from the mother can be easily transported into the placenta *via* the blood stream, and that the Hg isotopic composition in the liver and blood of adult whales is characterized by higher δ^{202}Hg values. It needs to be stressed that constant and high δ^{202}Hg values (~1‰) were observed for all blood samples, except in the case of blood coming from the liver (W6) that was characterized by having approximately the same Hg isotopic signature as the corresponding liver tissue from the same individual. In order to demonstrate the influence of mother's milk on the Hg speciation and isotopic composition of young whales during lactation, milk samples from lactating whales were collected and analyzed for their Hg isotopic composition (see **Table 6-6**). Although it needs to be pointed out that the collection of milk during the autopsies of stranded long-finned pilot whales was found to be hampered by contamination issues with blood, two milk samples were finally obtained. One of the samples (whale ID 5) was found to be affected by blood contamination, which was reflected in its Hg isotopic composition *i.e.*, approximately the same Hg isotopic compositions were established for milk and blood (see **Figure 6-4**). For the other sample (whale ID 11), however, a clean sample was obtained and subsequently characterized for its Hg isotopic composition, resulting in a δ^{202}Hg value of 0.12 ± 0.03‰. This Hg isotopic signature was found to be significantly lower than that of the blood sample from the same whale, and similar to that of muscle tissue. Additionally, this Hg isotopic composition was found to be relatively close to those characteristic for the liver tissues of the youngest whales.

Table 6-6. Hg isotopic composition measured in blood and milk of long-finned pilot whales.

	Whale ID	Age (years)	δ^{199}Hg (‰)	δ^{200}Hg (‰)	δ^{201}Hg (‰)	δ^{202}Hg (‰)	Δ^{199}Hg (‰)	Δ^{201}Hg (‰)
Blood Females	6	1	1.10 ± 0.02	-0.02 ± 0.06	0.76 ± 0.05	-0.18 ± 0.01	1.15 ± 0.03	0.89 ± 0.05
	7	1	N.A.	N.A.	N.A.	N.A.	N.A.	N.A.
	8	1	1.27 ± 0.05	0.61 ± 0.04	1.64 ± 0.10	0.98 0.14	1.02 ± 0.05	0.90 ± 0.01
	1	2.5	1.35 ± 0.07	0.52 ± 0.03	1.63 ± 0.12	1.01 ± 0.04	1.10 ± 0.07	0.88 ± 0.09
	12	3	N.A.	N.A.	N.A.	N.A.	N.A.	N.A.
	10	4	1.36 ± 0.09	0.57 ± 0.01	1.75 ± 0.08	1.15 ± 0.04	1.07 ± 0.09	0.88 ± 0.06
	13	9	1.35 ± 0.11	0.69 ± 0.10	1.82 ± 0.06	1.18 ± 0.06	1.05 ± 0.12	0.93 ± 0.07
	3	17	1.43 ± 0.13	0.71 ± 0.11	1.80 ± 0.11	1.27 ± 0.13	1.11 ± 0.12	0.84 ± 0.04
	5	20	1.44 ± 0.04	0.61 ±0.09	1.78 ± 0.06	1.10 ± 0.09	1.16 ± 0.05	0.95 ± 0.07
	18	25	N.A.	N.A.	N.A.	N.A.	N.A.	N.A.
	4	25	1.37 ± 0.05	0.59 ±0.04	1.70 ± 0.04	1.04 ± 0.02	1.11 ± 0.05	0.92 ± 0.06
	2	25.5	1.31 ± 0.03	0.57 ± 0.05	1.68 ± 0.03	0.99 ± 0.03	1.06 ± 0.02	0.94 ± 0.01
	20	28	N.A.	N.A.	N.A.	N.A.	N.A.	N.A.
	11	29	1.42 ± 0.05	0.53 ± 0.06	1.69 ± 0.01	0.97 ± 0.10	1.17 ± 0.05	0.96 ± 0.07
	15	35.5	1.36 ± 0.04	0.47 ± 0.02	1.67 ± 0.08	0.90 ± 0.05	1.14 ± 0.04	0.99 ± 0.05
Blood Males	17	2	1.39 ± 0.04	0.61 ±0.08	1.68 ± 0.09	1.03 ± 0.07	1.13 ± 0.03	0.91 ± 0.05
	14	2.5	1.41 ± 0.07	0.67 ± 0.05	1.85 ± 0.10	1.23 ±0.07	1.10 ± 0.05	0.93 ± 0.05
	16	4	1.38 ± 0.04	0.59 ± 0.08	1.70 ± 0.06	1.07 ± 0.07	1.12 ± 0.03	0.96 ± 0.04
	9	6	1.35 ± 0.05	0.56 ± 0.07	1.65 ± 0.07	0.96 ± 0.13	1.11 ± 0.02	0.93 ± 0.04
	19	15	N.A.	N.A.	N.A.	N.A.	N.A.	N.A.
	21	16	N.A.	N.A.	N.A.	N.A.	N.A.	N.A.
	Whale ID	**Age (years)**	**δ^{199}Hg (‰)**	**δ^{200}Hg (‰)**	**δ^{201}Hg (‰)**	**δ^{202}Hg (‰)**	**Δ^{199}Hg (‰)**	**Δ^{201}Hg (‰)**
Milk	5	35.5	1.31 ± 0.06	0.45 ± 0.06	1.58 ± 0.03	0.91 ± 0.07	1.08 ± 0.04	0.90 ± 0.03
	11	29	1.18 ± 0.03	0.14 ± 0.05	1.06 ± 0.04	0.12 ± 0.03	1.15 ± 0.04	0.97 ± 0.03

N.A. = not available

Therefore, based on these results, it seems reasonable to think that during the first years of life, the isotopic composition of Hg in the liver may be affected by a strong contribution of MeHg from the mother. The mixing of two sources of MeHg, such as the direct intake *via* the placenta and *via* the mother's milk, may be related with the anomalously higher δ^{202}Hg in liver tissues of juvenile whales. MeHg from the placenta is mainly related with the mother's blood *i.e.*, high δ^{202}Hg (~1‰), while the influence of MeHg from milk was demonstrated to be characterized by lower δ^{202}Hg values (~0.10‰). The influence of MeHg from the placenta on the isotopic composition of Hg in the liver of young whales should be more relevant in the first period of their life and it should be progressively replaced by MeHg intake *via* mother's milk. Together with the slow introduction of solid food in the diet, this may explain the trend observed for δ^{202}Hg values in the liver tissues of juvenile long-finned pilot whales.

However, as indicated above, a clear change in the trend observed for juvenile whales was found at an age of approximately 6 years old. As of that age, the decrease in the MeHg fraction is accompanied by a progressive enrichment in the heavier isotopes. This intriguing trend cannot be explained by the aforementioned MeHg demethylation documented for biotic and abiotic processes; therefore, other mechanisms must be developed after certain ages, which are generally characterized by high Hg accumulation (see **Figure 6-6**). The development of Hg detoxification pathways aiming to avoid Hg poisoning can be the most likely explanation for this different behavior and for the Hg isotope fractionation towards higher δ^{202}Hg values. In previous works based on different species, including fish and humans, it was observed that only a fraction of the iHg generated by MeHg demethylation processes accumulates in liver, while another fraction is excreted *via* the urine or feces.**[61, 62]** We suggest that excretion processes, characterized by preferential removal of lighter Hg isotopes, thus leading to higher δ^{202}Hg values in the remaining iHg fraction in liver tissues of long-finned pilot whales, might be the responsible for the trend observed in adult whales.**[63, 64]** It needs to be noted that excretion could be used as a Hg detoxification mechanism by whales with a high Hg accumulation. The development of this mechanism could be related with the increase in Hg excretion rate as a function of THg concentrations, and hence, the whale's age.

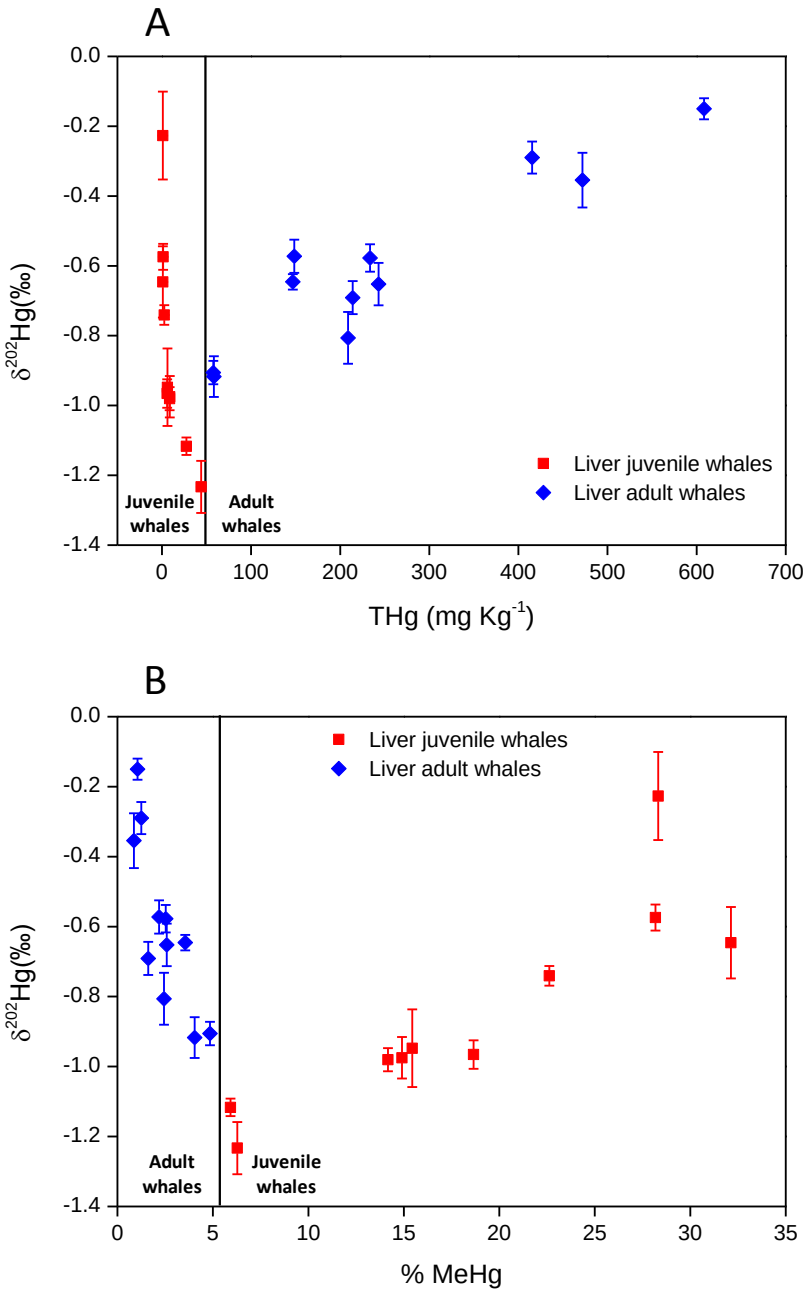

Figure 6-6. δ^{202}Hg *vs* THg (A) and δ^{202}Hg *vs* % MeHg (B) for liver tissues of long-finned pilot whales.

An additional Hg detoxification mechanism occurring mainly in liver tissues of marine mammals is related with the formation of HgSe particles, as indicated in the previous section.**[13]** A large fraction of the Hg accumulated in liver tissues is under the form of HgSe particles; this species is considered non-toxic compare to other Hg

species. However, the formation process of HgSe particles in liver tissues of marine mammals still remains poorly understood and important knowledge gaps, including the accompanying isotope fractionation, exist. However, based on the δ^{202}Hg results obtained in this work for liver tissue of adult long-finned pilot whales, we hypothesize that the formation of HgSe particles leads to higher δ^{202}Hg values in the accumulated particles, while the remaining iHg (enriched in the lighter Hg isotopes) is partially excreted. Therefore, the net effect of the overall process would be a liver tissue Hg isotopic composition enriched in the heavier Hg isotopes, owing to the accumulation of HgSe particles over the lifespan of these marine mammals. In order to further proof this hypothesis, HgSe particles were isolated from liver tissue of 5 long-finned pilot whales and analyzed for their Hg isotopic composition. The results obtained are shown in **Table 6.7**. **Figure 6.7** allows a comparison of the δ^{202}Hg values obtained for the HgSe particles and those obtained for bulk liver tissue from the same animal. It can be seen that in all cases, an enrichment in the heavier Hg isotopes is observed for the HgSe particles, thus demonstrating that the formation of HgSe particles as a MeHg detoxification mechanism in the liver of long-fined pilot whales can most likely be responsible for the trend observed for δ^{202}Hg in liver tissue as a function of age.

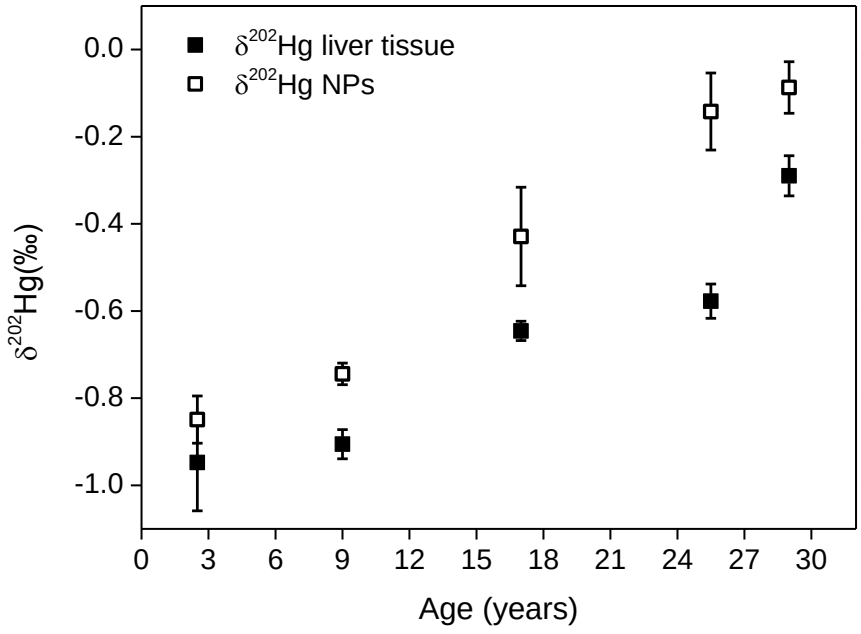

Figure 6-7. δ^{202}Hg *vs* age for five liver tissue and the corresponding isolated HgSe particles for 5 pilot whales.

Table 6.7. Hg isotope ratio date obtained for the isolated HgSe particles extracted from liver tissues.

Whale ID	Age (years)	δ^{199}Hg (‰)	δ^{200}Hg (‰)	δ^{201}Hg (‰)	δ^{202}Hg (‰)	Δ^{199}Hg (‰)	Δ^{201}Hg (‰)
14	2.5	0.68 ± 0.08	-0.38 ± 0.04	0.07 ± 0.03	-0.85 ± 0.05	0.89 ± 0.08	0.70 ± 0.02
13	9	0.75 ± 0.08	-0.32 ± 0.05	0.20 ± 0.07	-0.74 ± 0.02	0.94 ± 0.07	0.76 ±0.05
3	17	0.77 ± 0.10	-0.18 ± 0.07	0.38 ± 0.08	-0.43 ± 0.11	0.88 ± 0.08	0.71 ± 0.05
2	25.5	0.87 ± 0.06	-0.05 ± 0.04	0.71 ± 0.03	-0.14 ± 0.09	0.91 ± 0.07	0.81 ± 0.08
11	29	0.84 ± 0.06	-0.01 ± 0.06	0.70 ± 0.03	-0.09 ± 0.06	0.86 ± 0.06	0.76 ± 0.07

Based on the hypothesis that Hg is detoxified *via* excretion processes (*e.g.*, urine) and/or *via* the storage as HgSe particles in the liver, the kidney may also play an important role in the Hg metabolism within the whale body. **Figure 6-5C** shows the Hg isotopic composition and MeHg fraction as a function of age. Interestingly, the clear differences in tendency shown for δ^{202}Hg in liver between juvenile and adult whales were not found in the case of δ^{202}Hg in kidney, suggesting that liver indeed plays a major role compared to other organs in the Hg metabolism of marine mammals. However, it is important to note that until 17 years old, the variations of δ^{202}Hg values in kidney were found to be accompanied by the corresponding changes in the MeHg fractions *i.e.*, both δ^{202}Hg and % MeHg changed in the same direction. These variations in the isotopic composition can thus be explained by differences in the Hg speciation, as indicated above. After 17 years old, however, an increase in δ^{202}Hg values corresponded with a decrease in % MeHg and *vice versa*. As indicated in the case of liver, the development of Hg detoxification mechanisms may explain this different behavior as a function of age and THg concentration. Nevertheless, the "turning point" in the case of kidney seems to appear at a higher age in comparison with the liver, which could be tentatively explained by a higher rate of Hg elimination *via* excretion mechanisms at adult ages. Self-evidently, further investigation is required in order to elucidate the exact role of every organ/tissue in the development of Hg detoxification mechanisms. However, the use of δ^{202}Hg values in different tissues of long-finned pilot whales shown in this work has shed some light onto the complex Hg metabolic routes of Hg in marine mammals.

MIF of Hg can provide additional information aiding the identification of the different transformations that Hg undergoes in nature. The three-isotope plots (δ^{199}Hg (A), δ^{200}Hg (B) and δ^{201}Hg (C) *vs* δ^{202}Hg) for all the samples analyzed in this work (**Figure 6-3**) showed that only the odd-numbered Hg isotopes (^{199}Hg and ^{201}Hg) were affected by MIF. This odd-MIF has been tentatively explained in terms of nuclear volume effects (NVE) and magnetic isotope effects (MIE).**[65, 66]** The NVE has been reported to accompany Hg^0 liquid-vapor evaporation, Hg^{2+} abiotic reduction in the absence of light and distribution of Hg between dissolved Hg^{2+} and thiol-bound Hg,**[21, 25, 67]** while the MIE is the predominant effect accompanying reaction mechanisms involving radicals, such as photochemical reactions.**[17, 68]** Δ^{199}Hg and Δ^{201}Hg values obtained for the different tissues and biological fluids from the pod of long-finned pilot whales studied were found to be very constant, independent of the sample type (see **Figure 6-8**), with average values of 1.06 ± 0.06 and 0.88 ± 0.05 ‰, respectively.

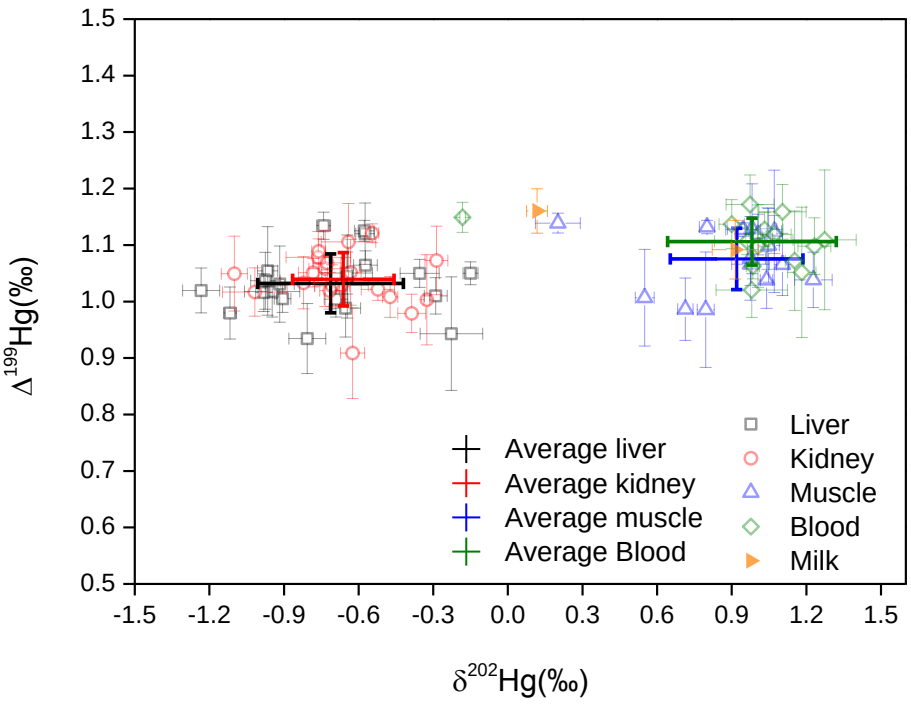

Figure 6-8. Δ^{199}Hg *vs* δ^{202}Hg values obtained for all the samples analyzed in this work.

These values suggest that, after Hg intake, there is not *in vivo* MIF accompanying the different Hg metabolic processes within the whale body, such as methylation, demethylation, transport and excretion. The absence of *in vivo* MIF is in good agreement with the previous literature for aquatic ecosystems. In previous works, photochemical reactions were identified as the only processes inducing MIF,**[24, 33]** and it was concluded that MIF does not occur during trophic transfer in fish, marine mammals and humans.**[36, 37, 61, 64, 69, 70]**

In addition, laboratory experiments carried out by Bergquist and Blum **[24]** indicated that photochemical reactions involving Hg^{2+} and MeHg can be distinguished based on the slope of the best-fitting straight line through the data points obtained by plotting $\Delta^{199}Hg$ *vs* $\Delta^{201}Hg$. The values thus obtained correspond to 1.0 and 1.36 for the photoreduction of Hg^{2+} and the photodegradation of MeHg in the presence of dissolved organic carbon (DOC), respectively. Several works based on actual fish samples have shown that a slight difference exists between the slopes obtained for samples from fresh and marine waters (~1.3 and 1.2, respectively);**[71-73]** these differences have been mainly attributed to the effect of water conditions, such as the amount of DOC.**[25]** However, in both cases, the values obtained are closer to that of the photodegradation of MeHg. This indicates that the main contributor to the $\Delta^{199}Hg$ and $\Delta^{201}Hg$ values in fish samples is the intake and further bioaccumulation of the remaining MeHg after photodegradation. The representation of the $\Delta^{199}Hg$ *vs* $\Delta^{201}Hg$ values (see **Figure 6-9**) obtained for the different tissues and biological fluids of long-finned pilot whales of this study, however, could not be considered as a representative slope owing to the small range of $\Delta^{199,201}Hg$ values covered by the complete data set. Therefore, the $\Delta^{199}Hg/\Delta^{201}Hg$ ratio has been calculated point by point and an average value of 1.21 ± 0.06 was obtained. This ratio is in agreement with previous works based on marine fish, marine mammals, and humans; and demonstrates that the main factor contributing to the MIF-Hg in long-finned pilot whales is due to the remaining MeHg after photodegradation prior to its incorporation into the base of the food web.**[24, 61]**

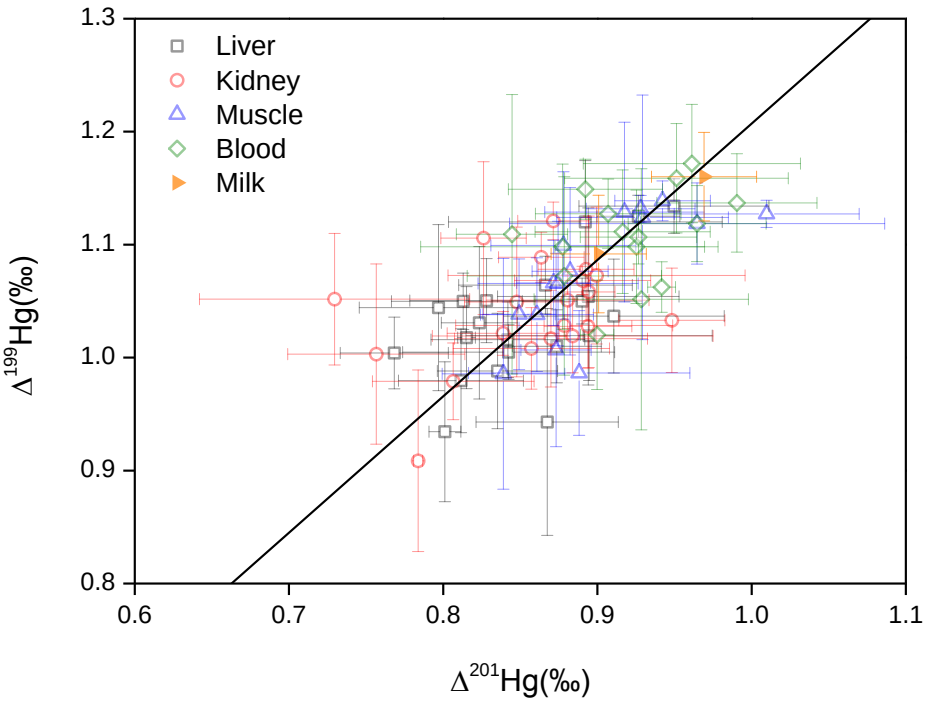

Figure 6-9. Δ^{199}Hg *vs* Δ^{201}Hg values obtained for all the samples analyzed in this work.

Because of the fact that Δ^{199}Hg and Δ^{201}Hg values ≠ 0 in marine mammals occurs mainly as a result of MeHg intake *via* the diet and that there is not MIF *in vivo*, the MIF-Hg isotopic signatures are unaltered through the food web. Thus, the Hg isotopic signatures can be used to distinguish between different species living in specific environments that are characterized by different parameters, such as total level of dissolved solids (TDS), ionic strength of water, pH and depth.**[30]** A recent work has demonstrated that the extent of photochemical demethylation in a specific ecosystem (*i.e.* the North Pacific Ocean) can be related with water depth.**[74]** The Δ^{199}Hg values obtained for the long-finned pilot whales of this work are comparable with those of deep-sea fish (>400 m) from the North Pacific Ocean, as reported in the aforementioned study (**Figure 6-10** has been adapted from Blum *et al.*).**[74]** This is in agreement with the feeding habits of pilot whales that can even reach depths of 800 m during short dives. Therefore, the magnitude of the Δ^{199}Hg and Δ^{201}Hg values in long-finned pilot whales may also serve as an indicator to provide

insight about the feeding habits of marine mammals, which could be of high interest for further biological studies.**[75, 76]**

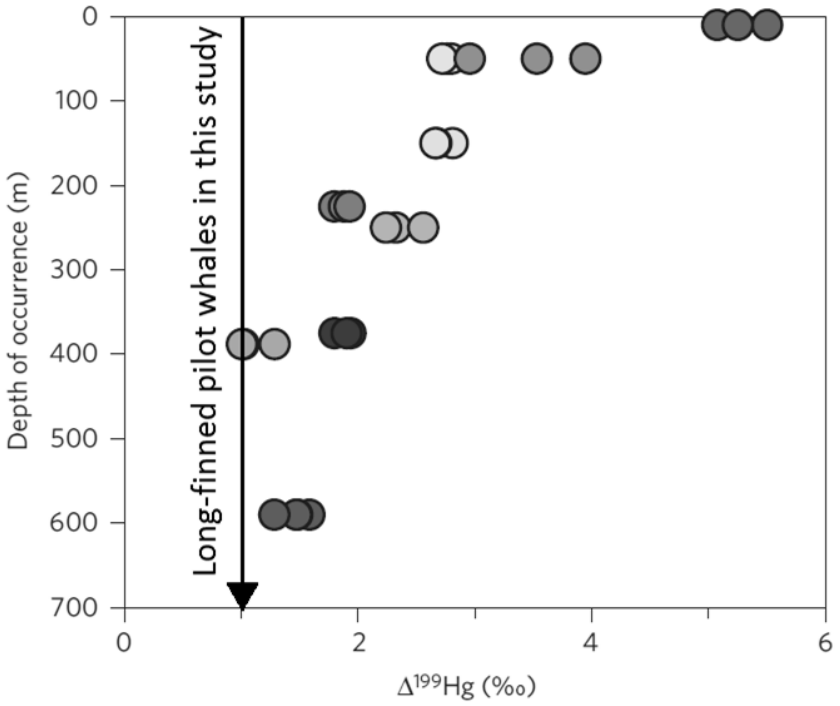

Figure 6-10. Δ^{199}Hg values (‰) obtained for pilot whales (black arrow) in this study, and nine species of marine fish that feed at different depths in the central North Pacific Ocean (adapted from Blum *et al.* 2013).**[74]**

6.4. Conclusion

In this work, THg quantification, MeHg speciation analysis, and Hg isotopic analysis have been carried out, aiming at obtaining a more profound insight into the Hg metabolism and possible detoxification mechanisms in long-finned pilot whales. It was found that Hg species accumulated differently and, to a different extent, as a function of (*i*) age and/or (*ii*) body compartment. Although the Hg isotopic signatures were found to be directly related with the Hg speciation (MeHg and iHg fractions), important deviations from a more general behavior were observed, and tentatively related to the development of Hg detoxification pathways. Interestingly, δ^{202}Hg values in liver of juvenile whales showed a fast decrease towards lighter Hg isotopic signatures during the first years, and it was possible to establish a

hypothetical link between this trend and the MeHg intake *via* the placenta and/or mother's milk. Most likely, a reversal in the trend observed for adult whales indicated the development of Hg detoxification mechanisms in order to avoid Hg poisoning. Hg excretion and the formation of Hg-Se particles in key organs, such as liver and kidney, have been proposed as hypotheses for explaining the aforementioned relation between δ^{202}Hg values and MeHg fractions. In addition, the Δ^{199}Hg and Δ^{201}Hg values were found to be constant between organs, suggesting the absence of *in vivo* MIF. Therefore, these Δ^{199}Hg and Δ^{201}Hg values could be suitable for the identification of the feeding habits of marine mammals.

References

[1] T.W. Clarkson, L. Magos, Crit. Rev. Toxicol. 36 (2006) 609 - 662.

[2] J.M. Pacyna, O. Travnikov, F.D. Simone, I.M. Hedgecock, K. Sundseth, E.G. Pacyna, F. Steenhuisen, N. Pirrone, J. Munthe, K. Kindbom, Atmos. Chem. Phys. 16 (2016) 12495 - 12511.

[3] C.H. Lamborg, C.R. Hammerschmidt, K.L. Bowman, G.J. Swarr, K.M. Munson, D.C. Ohnemus, P.J. Lam, L.-E. Heimbürger, M.J.A. Rijkenberg, M.A. Saito, Nature 512 (2014) 65 - 68.

[4] G.C. Compeau, R. Bartha, Appl. Environ. Microbiol. 50 (1985) 498 - 502.

[5] V. Celo, D.R.S. Lean, S.L. Scott, Sci. Total Environ. 368 (2006) 126 - 137.

[6] T. Ikemoto, T. Kunito, I. Watanabe, G. Yasunaga, N. Baba, N. Miyazaki, E.A. Petrov, S. Tanabe, Environ. Pollut. 127(83 - 97) (2004).

[7] R. Wagemann, E. Trebacz, G. Boila, W.L. Lockhart, Sci. Total Environ. 218 (1998) 19 - 31.

[8] V.M. Woshner, T.M. O'Hara, J.A. Eurell, M.A. Wallig, G.R. Bratton, R.S. Suydam, V.R. Beasley, Toxicol. Pathol. 30 (2002) 209 - 215.

[9] Z. Gajdosechova, A. Brownlow, N.T. Cottin, M. Fernandes, F.L. Read, D.S. Urgast, A. Raab, J. Feldmann, E.M. Krupp, Sci. Total Environ. 545 - 546 (2016) 407 - 413.

[10] H.H. Harris, I.J. Pickering, G.N. George, Science 301 (2002) 1203.

[11] Z.P. Zayas, L. Ouerdane, S. Mounicou, R. Lobinski, M. Monperrus, D. Amouroux, Anal. Bioanal. Chem. 406 (2014) 1121 - 1129.

[12] M.A.K. Khan, F. Wang, Chem. Res. Toxicol. 23 (2010) 1202 - 1206.

[13] Z. Gajdosechova, M.M. Lawan, D.S. Urgast, A. Raab, K.G. Scheckel, E. Lombi, P.M. Kopittke, K. Loeschner, E.H. Larsen, G. Woods, A. Brownlow, F.L. Read, J. Feldmann, E.M. Krupp, Sci. Rep. 6: 34361 (2016) 1 - 11.

[14] R. Yin, X. Feng, W. Shi, Appl. Geochem. 25 (2010) 1467 - 1477.

[15] J.D. Blum, L.S. Sherman, M.W. Johnson, Annu. Rev. Earth Planet. Sci. 42 (2014) 249 - 269.

[16] R. Yin, X. Feng, X. Li, B. Yu, B. Du, Trends Environ. Anal. Chem. 2 (2014) 1 - 10.

[17] B.A. Bergquist, J.D. Blum, Elements 5 (2009) 353 - 357.

[18] J.E. Sonke, Geochim. Cosmochim. Acta 75 (2011) 4577 - 4590.

[19] W. Zheng, D. Foucher, H. Hintelmann, J. Anal. At. Spectrom. 22 (2007) 1097 - 1104.

[20] K. Kritee, J.D. Blum, T. Barkay, Environ. Sci. Technol. 42 (2008) 9171 - 9177.

[21] N. Estrade, J. Carignan, J.E. Sonke, O.F.X. Donard, Geochim. Cosmochim. Acta 73 (2009) 2693 - 2711.

[22] P. Rodríguez-González, V.N. Epov, R. Bridou, E. Tessier, R. Guyoneaud, M. Monperrus, D. Amouroux, Environ. Sci. Technol. 43 (2009) 9183 - 9188.

[23] M. Jiménez-Moreno, V. Perrot, V.N. Epov, M. Monperrus, D. Amouroux, Chem. Geol. 336 (2013) 26 - 36.

[24] B.A. Bergquist, J.D. Blum, Science 318 (2007) 417 - 420.

[25] W. Zheng, H. Hintelmann, J. Phys. Chem. A 114 (2010) 4238 - 4245.

[26] L.E. Gratz, G.J. Keeler, J.D. Blum, L.S. Sherman, Environ. Sci. Technol. 44 (2010) 7764 - 7770.

[27] J. Chen, H. Hintelmann, X. Feng, B. Dimock, Geochim. Cosmochim. Acta 90 (2012) 33 - 46.

[28] Z. Wang, J. Chen, X. Feng, H. Hintelmann, S. Yuan, H. Cai, Q. Huang, S. Wang, F. Wang, C. R. Geosci. 347 (2015) 358 - 367.

[29] W. Zheng, H. Hintelmann, Geochim. Cosmochim. Acta 73 (2009) 6704 - 6715.

[30] D. Malinovsky, K. Latruwe, L. Moens, F. Vanhaecke, J. Anal. At. Spectrom. 25 (2010) 950 - 956.

[31] F.J. Black, B.A. Poulin, A.R. Flegal, Geochim. Cosmochim. Acta 84 (2012) 492 - 507.

[32] P. Chandan, S. Ghosh, B.A. Bergquist, Environ. Sci. Technol. 49 (2014) 259 - 267.

[33] T.A. Jackson, D.M. Whittle, M.S. Evans, D.C.G. Muir, Appl. Geochem. 23 (2008) 547 - 571.

[34] R. Das, V.J.M. Salters, A.L. Odom, Geochem. Geophys. Geosyst. 10 (2009) 1 - 12.

[35] D. Point, J.E. Sonke, R.D. Day, D.G. Roseneau, K.A. Hobson, S.S.V. Pol, A.J. Moors, R.S. Pugh, O.F.X. Donard, P.R. Becker, Nat. Geosci. 4 (2011) 188 - 194.

[36] V. Perrot, M.V. Pastukhov, V.N. Epov, S. Husted, O.F.X. Donard, D. Amouroux, Environ. Sci. Technol. 46 (2012) 5902 - 5911.

[37] S.Y. Kwon, J.D. Blum, M.J. Carvan, N. Basu, J.A. Head, C.P. Madenjian, S.R. David, Environ. Sci. Technol. 46 (2012) 7527 - 7534.

[38] C. Lockyer, Report of the International Whaling Commission 14 (1993) 137 - 161.

[39] A. Brownlow, J. Baily, M. Dagleish, N. Davison, R. Deaville, G. Foster, Z. Gajdosechova, S.-K. Jensen, P. Jepson, E. Krupp, B. McGovern, M. Morell, R. Penrose, M. Perkins, F. Read, Investigation into the long-finned pilot whale mass stranding event, Pittenweem, Fife, 2nd September 2012. Final report to Marine Scotland, Scottish Government (2014) 1 - 48.

[40] A. Rua-Ibarz, E. Bolea-Fernandez, F. Vanhaecke, Anal. Bioanal. Chem. 408 (2016) 417 - 429.

[41] D.C. Baxter, I. Rodushkin, E. Enström, D. Malinovsky, J. Anal. At. Spectrom. 21 (2006) 427 - 430.

[42] J.D. Blum, B.A. Bergquist, Anal. Bioanal. Chem. 388 (2007) 353 - 359.

[43] J.P. Frodello, M. Roméo, D. Viale, Environ. Pollut. 108 (2000) 447 - 452.

[44] X. Wang, F. Wu, W.-X. Wang, Environ. Sci. Technol. 51 (2017) 6441 - 6451.

[45] J.P. Frodello, D. Viale, B. Marchand, Mar. Pollut. Bull. 44 (2002) 551 - 554.

[46] S. Skerfving, Bull. Environ. Contam. Toxicol. 41 (1988) 475 - 482.

[47] P. Grandjean, P. Weihe, L.L. Needham, V.W. Burse, D.G.P. Jr, E.J. Sampson, P.J. Jørgensen, M. Vahter, Environ. Res. 71 (1995) 29 - 38.

[48] J. Sundberg, B. Ersson, B. Lönnerdal, A. Oskarsson, Toxicology 137 (1999) 169 - 184.

[49] M.M. Mansour, N.C. Dyer, L.H. Hoffman, A.R. Schulert, A.B. Brill, Environ. Res. 6 (1973) 479 - 484.

[50] N.-G. Ilbäck, Toxicology 67 (1991) 117 - 124.

[51] K. Honda, R. Tatsukawa, T. Fujiyama, Agric. Biol. Chem 46 (1982) 3011 - 3021.

[52] J. Lailson-Brito, R. Cruz, P.R. Dorneles, L. Andrade, A.d.F. Azevedo, A.B. Fragoso, L.G. Vidal, M.B. Costa, T.L. Bisi, R. Almeida, D.P. Carvalho, W.R. Bastos, O. Malm, PLoS One 7 (2012) 1 - 10.

[53] N.V.C. Ralston, L.J. Raymond, Toxicology 278 (2010) 112 - 123.

[54] M. Sakamoto, T. Itai, A. Yasutake, T. Iwasaki, G. Yasunaga, Y. Fujise, M. Nakamura, K. Murata, H.M. Chan, J.L. Domingo, M. Marumoto, Environ. Res. 143 (2015) 55 - 61.

[55] F.E. Huggins, S.A. Raverty, O.S. Nielsen, N.E. Sharp, J.D. Robertson, N.V.C. Ralston, Environ. Bioindic. 4 (2009) 291 - 302.

[56] T. Ikemoto, T. Kunito, H. Tanaka, N. Baba, N. Miyazaki, S. Tanabe, Arch. Environ. Contam. Toxicol. 47 (2004) 402 - 413.

[57] T. Ikemoto, T. Kunito, Y. Anan, H. Tanaka, N. Baba, N. Miyazaki, S. Tanabe, Environ. Toxicol. Chem. 23 (2004) 2008 - 2016.

[58] E. Nakazawa, T. Ikemoto, A. Hokura, Y. Terada, T. Kunito, S. Tanabe, I. Nakai, Metallomics 3 (2011) 719 - 725.

[59] K. Kritee, J.D. Blum, M.W. Johnson, B.A. Bergquist, T. Barkay, Environ. Sci. Technol. 41 (2007) 1889 - 1895.

[60] K. Kritee, J.D. Blum, J.R. Reinfelder, T. Barkay, Chem. Geol. 336 (2013) 13 - 25.

[61] L.S. Sherman, J.D. Blum, A. Franzblau, N. Basu, Environ. Sci. Technol. 47 (2013) 3403 - 3409.

[62] M. Trudel, J.B. Rasmussen, Environ. Sci. Technol. 31 (1997) 1716 - 1722.

[63] C. Feng, Z. Pedrero, S. Gentès, J. Barre, M. Renedo, E. Tessier, S. Berail, R. Maury-Brachet, N. Mesmer-Dudons, M. Baudrimont, A. Legeay, L. Maurice, P. Gonzalez, D. Amouroux, Environ. Sci. Technol. 49 (2015) 12984 - 12993.

[64] S.Y. Kwon, J.D. Blum, M.A. Chirby, E.J. Chesney, Environ. Toxicol. Chem. 32 (2013) 2322 - 2330.

[65] J. Bigeleisen, J. Am. Chem. Soc. 118 (1996) 3676 - 3680.

[66] A.L. Buchachenko, J. Phys. Chem. A 105 (2001) 9995 - 10011.

[67] J.G. Wiederhold, C.J. Cramer, K. Daniel, I. Infante, B. Bourdon, R. Kretzschmar, Environ. Sci. Technol. 44 (2010) 4191 - 4197.

[68] H. Hintelmann, W. Zheng, Tracking geochemical transforamtions and transport of mercury through isotope fractionation. In Environmental Chemistry and Toxicology of Mercury; G. Liu, Y. Cai, N. O'Discoll, Eds. John Willey & Sons, Inc, Hoboken, NJ. (2012) 293 - 327.

[69] L. Laffont, J.E. Sonke, L. Maurice, S.L. Monrroy, J. Chincheros, D. Amouroux, P. Behra, Environ. Sci. Technol. 45 (2011) 9910 - 9916.

[70] V. Perrot, J. Masbou, M.V. Pastukhov, V.N. Epov, D. Point, S. Bérail, P.R. Becker, J.E. Sonke, D. Amouroux, Metallomics 8 (2016) 170 - 178.

[71] N. Gantner, H. Hintelmann, W. Zheng, D.C. Muir, Environ. Sci. Technol. 43 (2009) 9148 - 9154.

[72] D.B. Senn, E.J. Chesney, J.D. Blum, M.S. Bank, A. Maage, J.P. Shine, Environ. Sci. Technol. 44 (2010) 1630 - 1637.

[73] L.S. Sherman, J.D. Blum, Environ. Sci. Technol. 448 (2013) 163 - 175.

[74] J.D. Blum, B.N. Popp, J.C. Drazen, C.A. Choy, M.W. Johnson, Nature Geoscience 6 (2013) 879 - 884.

[75] F. Visser, P.J.O. Miller, R.N. Antunes, M.G. Oudejans, M.L. Mackenzie, K. Aoki, F.-P.A. Lam, P.H. Kvadsheim, J. Huisman, P.L. Tyack, Behaviour 151 (2014) 1453 - 1477.

[76] L.D. Sivle, P.H. Kvadsheim, A. Fahlman, F.P.A. Lam, P.L. Tyack, P.J.O. Miller, Front. Aquat. Physiol. 3 (2012) Art. 400.

General conclusions

This PhD dissertation focuses on Hg isotopic analysis as a powerful tool for shedding light onto the complex biogeochemical Hg cycle. For this purpose, an accurate and precise method for the high-precision isotopic analysis of Hg in different sample matrices using cold vapor generation-inductively coupled plasma-mass spectrometry (CVG-MC-ICP-MS) has been successfully developed, validated and subsequently applied to various real-life study cases. In this context, Hg isotopic analysis has been used for studying the sources and fate of Hg in the environment and for unraveling the metabolic pathways of Hg in different marine species from different levels along the trophic chain. Aquatic ecosystems are considered of the utmost relevance, as they are the main site of MeHg production, bioaccumulation and biomagnification. In addition, fish and seafood consumption is the major source of human MeHg exposure.

The first chapter of this PhD dissertation describes the importance of Hg in the environment. Due to its unique physical and chemical properties, Hg is considered as one of the most important global pollutants and its biogeochemical cycle is complex. Hg is a highly toxic heavy metal and exposure to it can produce harmful effects to wildlife and humans. The main health implications related with Hg are neurological problems derived to MeHg exposure, the most toxic Hg species, although also other health problems have been described. In addition, this chapter also reviews the most important processes inducing Hg isotope fractionation. Hg is one of the few elements that is affected by both mass-dependent and mass-independent fractionation (MDF and MIF, respectively), and these fractionation processes accompany different processes, *i.e.* physical processes, methylation, reduction of Hg(II) and MeHg demethylation.

In Chapter 2, the basic principles of inductively coupled plasma-mass spectrometry (ICP-MS) are described. In addition, the specific instrumentation used for Hg isotopic analysis is covered into more detail. Multi-collector ICP-MS (MC-ICP-MS) is the technique of choice for isotopic analysis of Hg owing to the high precision required to see the small variations in the isotopic composition of Hg. The use of cold vapor generation (CVG) as a means of sample introduction into MC-ICP-MS is also reviewed. Hg introduction *via* CVG improves the sensitivity and avoids and/or minimizes matrix effects owing to the quantitative an selective reduction of Hg^{2+} by

$SnCl_2$. As a result of the separation of Hg from the concomitant matrix in the CVG unit, the usual chromatographic isolation of the analyte element prior to high-precision MC-ICP-MS analysis can be avoided. This chapter also comprises a description of different mass discrimination correction approaches, focusing especially on that finally used throughout this work.

Chapter 3 is focused on an in-depth evaluation of the accuracy and precision attainable in Hg isotopic analysis *via* pneumatic nebulization (PN) and cold vapor generation (CVG) MC-ICP-MS. This work was carried out in the context of the SIB-09 "Elements" project, funded by the EMRP (European Metrology Research Programme of EURAMET) with the aim to provide National Metrology Institutes (NMIs) with sufficient information as to which approach to use in the characterization of future Hg isotopic reference materials. Therefore, the capabilities and limitations of these two different introduction systems, and the effect of (*i*) instrument settings and acquisition parameters, (*ii*) concentrations of Hg and Tl, and (*iii*) mass bias correction approaches on the accuracy and precision of Hg isotope ratio results were evaluated. It was shown that the use of CVG increase the sensitivity approximately 20-fold compared to PN, while it also removes the effect of the matrix composition on the extent of instrumental mass discrimination. In contrast to PN, CVG enables Hg isotopic analysis of samples with relatively low Hg concentration and without the necessity of prior chromatographic isolation of the analyte from the sample matrix. No significant differences in long-term precision (≤ 0.006% RSD, N = 250, 18 months) were found between both introduction systems at similar signal intensities (approximately 1.2 V for ^{202}Hg). In addition, instrumental mass discrimination was adequately corrected for by either external correction or a combination of internal and external correction, although the precision was observed to be slightly better with the latter. Therefore, the use of CVG-MC-ICP-MS with a combination of internal (Baxter approach) and external (sample standard bracketing – SSB – approach) mass discrimination correction was validated *via* comparison of the Hg isotope ratio results obtained for various reference materials with values reported on in literature. The suitability of the method developed in this work was demonstrated and subsequently, it was deployed for real-life applications.

The next chapters of this PhD dissertation describe real-life applications, relying on the method for accurate and precise isotopic analysis of Hg, as described in Chapter 3.

In Chapter 4, the assessment of the potential introduction of metallic Hg pollution released from a WWII submarine wreck (U-864), which transported 67 tons of Hg in its keel when it was torpedoed and sunk, into a marine food chain was carried out. Hg salvaged from the U-864 submarine, sediments from the wreck location, and *Cancer pagurus* tissues (brown and claw meat) from the wreck location, and 4 nautic miles north and 4 nautic miles south of that location, were analyzed for their THg and MeHg concentrations, as well as for their Hg isotopic composition. The sediment pollution could be unequivocally linked with the metallic Hg transported in the submarine *via* the comparison of their Hg isotopic signatures. For the crab tissues, only the δ^{202}Hg values obtained for the brown meat (*i.e.*, mainly the hepatopancreas and gonads) of the individuals collected at the wreck location were shifted towards the isotopic signature of the sediments, and thus, the submarine Hg, suggesting that these individuals were affected by the metallic Hg released from the U-864 submarine. However, such differences were not found for the claw meat (*i.e.*, muscle). Therefore, the isotope ratio results suggest direct ingestion of metallic Hg by *Cancer pagurus*, but do not offer any proof for methylation of the submarine Hg and/or its further introduction into the marine food chain.

In Chapter 5, *Brosme brosme* (tusk fish) tissues from eight locations at the Norwegian coast, including fjords, were analyzed to identify the sources and fate of Hg in these marine ecosystems and to assess the suitability of using tusk in future monitoring programs. Tusks were also collected at the U-864 location, reported on in Chapter 4, and the results obtained confirmed the aforementioned hypothesis indicating that, so far, the metallic Hg from the submarine has not entered the food chain. The comparison of all locations studied in this work showed clear differences for THg concentrations and % MeHg values between different tissues and locations. At five of the eight locations, the Hg concentration in muscle tissue, *i.e.*, the edible part, exceeded the maximum allowable level of 0.5 mg Kg^{-1} w.w.. δ^{202}Hg values in both tissue types indicated that Hg speciation affects the bulk Hg isotopic signatures. Tusk liver seems to be more sensitive to immediate changes and to anthropogenic inorganic Hg, while the muscle rather reflects the Hg accumulated over a longer period of exposure. The δ^{202}Hg values also enabled different sources

and exposure pathways to be distinguished (*e.g.*, differences between fjords and locations from the North Sea and the Norwegian Sea). A clear correlation was found between $\delta^{202}Hg_{muscle}$ - $\delta^{202}Hg_{liver}$ with the % MeHg in liver for tusks from the coastal waters, but not for the fjords, thus suggesting an important source of anthropogenic iHg. No significant differences in $\Delta^{199}Hg$ values were found between both tissue types, indicating the absence of *in vivo* MIF. $\Delta^{199}Hg$ values also confirmed the existence of different groups depending on the location, with the lowest value in the most polluted area. This work demonstrated the suitability of using tusk as fish species in future Hg monitoring programs, while the added value of separated analysis of muscle and liver tissue was demonstrated.

Chapter 6 describes the Hg isotopic analysis of different tissues and biological fluids of long-finned pilot whales (*Globicephala melas*), a marine mammal located at the top of a marine trophic chain. It has been shown that, although these marine mammals accumulate high amounts of Hg over their lifespan, they do not show toxic effects, suggesting efficient Hg detoxification pathways, which is of high scientific interest. A pod of these whales stranded at a Scotland beach, and although a fraction could be refloated, 21 animals died on the stranding site. From the latter whales, different tissues (liver, kidney and muscle) and biological fluids (blood and milk) were analyzed for their THg concentration, MeHg speciation and Hg isotopic composition. The results obtained showed that Hg species accumulated differently and, to a different extent, as a function of age and/or body compartment. The Hg isotopic composition was linked with Hg speciation (levels of iHg and MeHg), although important deviations from the general behavior were observed. These differences were tentatively related with the occurrence of Hg detoxification pathways. The most striking trend was observed for liver tissue. $\delta^{202}Hg$ values in the livers of juvenile whales showed a fast decrease towards lighter Hg isotopic signatures during the first years, while a reversal in the trend was observed for adult whales, suggesting the development of new and/or different Hg detoxification mechanisms for avoiding Hg poisoning due to the bioaccumulation of Hg over the years. The hypothesis suggested for explaining this observation was the fractionation occurring during Hg excretion and/or the formation of Hg-Se particles in key organs (such as liver and kidney). The absence of *in vivo* MIF enables the use of $\Delta^{199}Hg$ an $\Delta^{201}Hg$ values for the identification of the feeding habits of marine mammals. This study demonstrated that the combination of elemental, speciation

and isotopic analysis of Hg can be used to obtain a more profound insight into the Hg metabolism and possible detoxification mechanisms in marine mammals, and this knowledge might be further translated into other species, and possibly also humans.

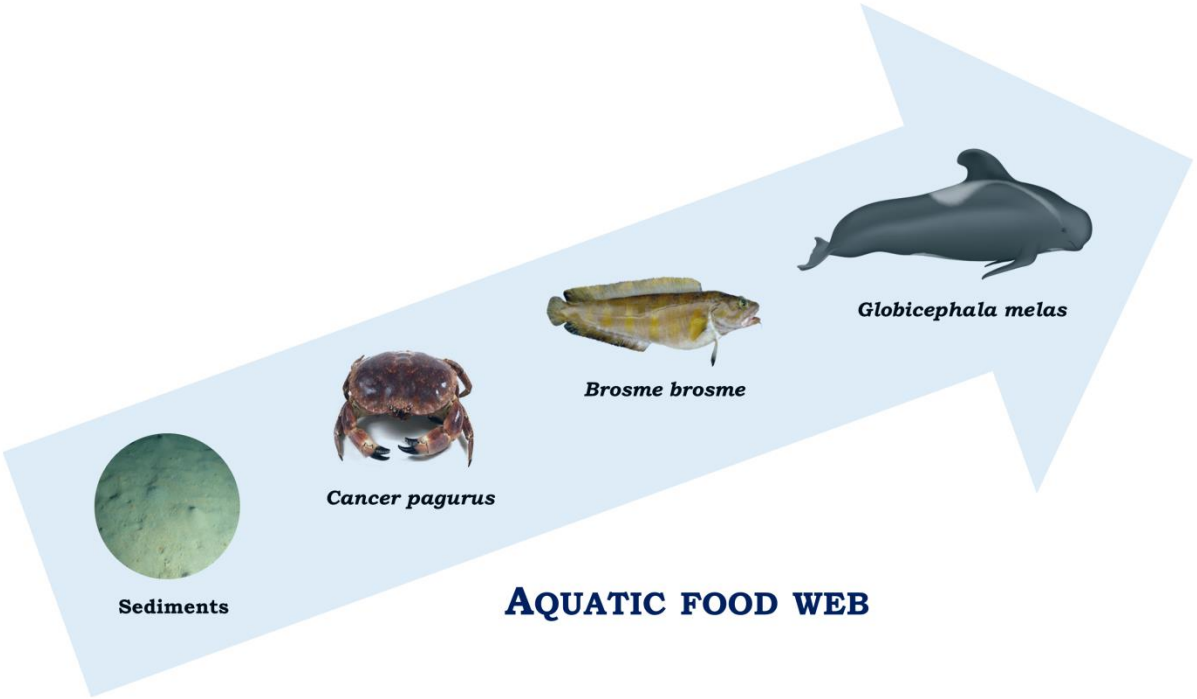

Overall, this PhD dissertation focuses on studying the fate of Hg in different environmentally relevant samples, with special attention to species from different levels within the aquatic food web. Aquatic ecosystems are of the utmost importance, as fish consumption is the main source of human MeHg exposure. In addition, the study of marine mammals may be considered of high relevance owing to the potential similarities with humans in terms of Hg detoxification mechanisms. In this work, the combination of determination of the THg concentration, MeHg speciation and Hg isotopic analysis of different tissues of various marine species (*i.e.*, brown crab, tusk fish and long-finned pilot whale) has been shown to be a powerful and versatile tool. It has been used for (i) both identifying the sources of Hg contamination and assessing their impact on the marine food chain, as well as for (ii) for elucidating *in vivo* Hg metabolic pathways. Suggestions has been made as to species that are suited for future monitoring campaigns and the use of different tissue types has been stressed.

Future perspectives

In this PhD, an accurate and precise method for the high-precision isotopic analysis of Hg in different sample matrices by CVG-MC-ICP-MS has been successfully developed and it has been applied in the context of real-life cases. However, important knowledge gaps still remain in our understanding of the processes that Hg undergoes in nature. Therefore, in addition to the urgent implementation of the measures adopted in the last Minamata Convention on Hg, further research is necessary to deal with this important human threat.

Clearly, THg quantification and speciation analysis, combined with isotopic analysis of Hg are capable of improving our understanding of the complex biogeochemical Hg cycle. Nevertheless, important efforts are still required in this context. Based on the experience gained during this work, several points have been identified as crucial for the future development and evolution of Hg isotopic analysis as a key tool for the study of Hg. On the one hand, it is clear that the success of such studies depends on the involvement of experts from different fields, as this is the only way to obtain a sufficient level of expertise as to obtain reliable data and interpret the complex results obtained correctly when dealing in the context of real-life cases. Within this PhD, collaborations were therefore established with NIFES and the University of Aberdeen. On the other hand, future work on isotopic analysis of Hg has to overcome current limitations, such as the relatively high concentrations of Hg required for obtaining accurate and precise Hg isotope ratio results and/or the limitation to the measurement of the bulk Hg isotopic signatures only *i.e.*, without species-specific Hg isotopic information. The use of off- and on-line pre-concentration approaches have already been reported on in literature, although their use significantly increases the complexity of the analytical method and could compromise the accuracy and the precision of the Hg isotope ratio results. These strategies are generally also applicable to a few sample matrix types only, thus limiting the wide applicability of such approaches in real-life applications. In the case of species-specific isotopic analysis, the hyphenation of gas chromatography (GC) to MC-ICP-MS has been used for the isotopic analysis of iHg and MeHg, although this type of analysis poses additional analytical challenges, such as a more laborious and challenging sample preparation and/or the necessity of dealing with transient signals. It needs to be taken into account, though, that every

additional step in the Hg isotopic analysis protocol may lead to potential chemical transformations, Hg losses and/or isotope fractionation.

Overall, it is clear that the isotopic analysis of Hg may aid our understanding of the complex biogeochemical Hg cycle, but there are still a number of pitfalls that need to be overcome. The required multidisciplinary character of such studies and the development of reliable approaches for pre-concentration and species-specific Hg isotopic analysis were already mentioned. In addition, the study of other environmental compartments, such as water and/or air, will shed further light onto the Hg biogeochemical cycle. However, the isotopic analysis of Hg in waters and/or in the atmosphere is still hampered by the very low concentrations of the target analyte and by the difficulty of sample collection, always taking into account the necessity of ensuring the traceability of the Hg isotopic signatures. Decreasing the minimum concentration required for successful Hg isotopic analysis will allow to study more species at a given location or more locations for a given species, thus providing a more comprehensive data set to evaluate. For metabolic studies, the analysis of different tissues and/or biological fluids of different species has demonstrated to be a key tool for understanding the biochemistry of Hg. Further research including those elements and/or biomolecules to which Hg binds can also provide additional insight of high scientific interest.

Acknowledgments

I would like to dedicate the last lines of my PhD dissertation to all the people who made it possible and I wish to thank you all for your input, help and support over the years.

It all started in January 2013 when I arrived in a cold winter evening in Belgium. I can still remember that moment, I was a little scared because of the big change in my life: new country and city, another language, unknown people, but also an important step of my scientific career. Starting from scratch is usually not easy, however, I must admit that my life in Ghent during these years has enriched me, both personally and professionally. This is definitely thanks to all the people that I have known during these years, this very nice city and its people. Gent will always be my home.

First, I would like to express my gratitude to my supervisors: Prof. Dr. Frank Vanhaecke & Prof. Dr. Martín Resano. Frank, I am very happy to say that it has been a pleasure for me to be part of your research team (A&MS) and to have you as my supervisor. You gave me the great opportunity of doing my PhD in Analytical Chemistry, and of being the person that I am today; I will always be grateful for that. I remember the moment that we met one each other in your office. I was really nervous because of the scientific challenge (isotopic analysis of mercury via CVG-MC-ICP-MS!!) and also because nobody in the lab was working on my topic. However, your confidence in me, your advice and your support have always motivated me to learn and to grow as scientist. Your close contact, your sense of humor and, of course, your scientific knowledge, make you a great team leader, and even a better person. Martín, thank you very much for saving me from the clutches of organic chemistry and for putting me back on the path of analytical chemistry again! I did not work with you in your lab, but you have always considered me as another member of your research group (MARTE). Your kind help and support (not only scientific) since the very beginning has been really important for me and I will always appreciate you.

The end of a PhD can sometimes be seen with lots of uncertainty, and it is in these moments when one realizes about the importance of having great people around you. Frank & Martín, you are definitely the type of people who help others without asking for anything in return. You have made possible that, during this acknowledgement section, I do not have to talk only about the past, but also about the future; and somehow, it is a future together. I want to say that I really appreciated that both of you helped me to continue with my scientific career. You thought of me for a postdoc position at VITO, and I am sure that your support during my application was decisive to achieve it. It is

well known that both of you are great scientist, but I also want to highlight that you are wonderful people.

Also related with my close future, I would like to briefly thank Kristof Tirez (member of the examination board) for your help and support during the selection process of the postdoc position at VITO. I look forward to working with you!

I also want to express my gratitude to all collaborators who have participated in different projects during this PhD. Many thanks to NIFES, especially to Prof. Dr. Amund Maage (also member of the examination board) and Dr. Sylvia Frantzen, as well as to the University of Aberdeen, especially Prof. Dr. Eva Krupp and Prof. Dr. Joerg Feldmann. My PhD thesis has benefited from your knowledge and contribution. I would also like to thank the other members of the examination board: Prof. Dr. Karel Strijckmans, Prof. Dr. Kerstin Leopold, Prof. Dr. Laszlo Vincze and Dr. Marta Costas Rodriguez for your input and comments to improve the quality of my PhD dissertation.

Thanks to all members of the MARTE research group (Miguel Angel, Ana Cris, Luis, Charo, Maite, Agueda, Raul, Flavio, and Diego) for always considering me as one of your colleagues. I must give a big thanks to Espe, for your always affectionate words and for taking care of us (siempre seremos "tus chicos"). Muchas gracias!

I want to especially thank all the members of the A&MS research group for your help, support and friendship during these years: Lieve (thanks for everything. I have a new task for you, please, take care of Eduardo ;-)), Sara, Karen, Tong, Carlos (7 meses no parece mucho tiempo, pero ha sido suficiente para empezar una bonita amistad), Edu, Yudi, Balazs, Stepan (my dear Russian friend, we have missed you a lot), Agustina, Veerle, Marieke, Lana, Sanwang, Yulia, Michaela, Yanwei, Marianela, Steven, Joke, Harry, Roger, Kris, Asha, Rosa, Andrei, Stijn, Thibaut, Jinxiang, Winfried, Charo (que buenos ratos durante las comidas y los cafés!), Claudia, Legna, Jefferson, and finally Lara & Marta (nuestra pequeña “Spanish Community”, sin vosotras todo hubiese sido mucho más duro. Muchas gracias por vuestra amistad desde el principio).

I also want to thank all members of the old Analytical Chemistry Department (S12 building), especially Chantal, Ingrid, Tine, Philip, Jorge and Karel for your help and support during this time. I do not want to forget about my students, mainly Alexander and Arnout, I have learnt from all of you.

También quería que aquí quedasen reflejadas unas palabras para personas importantes en mi vida.

Mis “Jennys”, vosotras ya sabéis lo mucho que os quiero y que a pesar de que con el tiempo nos hemos podido ir distanciando un poco todas por diferentes motivos, estoy muy orgullosa de teneros como amigas. Y como no, a todos los KAFRES, siempre me habéis hecho sentir como una más de vosotros desde el principio (hace ya muchos años…). Hemos pasado muy buenos momentos juntos (viajes, cenas, comidas, tardes de piscina,…) y los que nos quedan por vivir!!! Sois el mejor grupo de amig@s que cualquiera desearía, os quiero mucho!

Muchas gracias a toda mi familia: a mis tíos, mis primos, a mis abuelos y abuelas. Yaya Felisa y yaya Celi, a pesar de que ya no estáis conmigo, habéis sido muy importantes para mí. Gracias papa y mama (Rua y Ana), no hay palabras que puedan describir lo mucho que os quiero. Resultaría imposible agradeceros todo lo que habéis hecho por mí. Siempre estáis conmigo pase lo que pase y me habéis convertido en la persona que soy. Sobre todo muchas gracias por vuestro continuo apoyo y por vuestro amor incondicional. Sois los mejores padres del mundo! También quería dar las gracias a otra parte importante de mi familia, a Félix y Paquita por tratarme siempre tan bien, como a una hija más. A pesar de ser hija única, también puedo decir que tengo un hermano, German, que junto a Ana, nos han dado la oportunidad de poder disfrutar de nuestros sobrinos a pesar de la distancia, sobre todo de Marcos y tras aumentar la familia, también de Silvia y Lucia. Ahora nos tocara hablar por skype en pantalla grande para poder veros a todos juntos. A Marcos, como has crecido… Cuando llegamos a Gante todavía estabas en camino y ahora ya estas hecho todo un hombrecito! A pesar de haberte visto crecer desde la distancia, hemos tenido la gran suerte de poder compartir muchos momentos contigo durante estos años, y que tanto tu tío Edu como yo siempre recordaremos con mucha ilusión.

Y ya solo me queda un agradecimiento más, Edu. A pesar de ser el último no eres el menos importante como tú piensas, sino que lo mejor siempre se sirve al final, como el postre! Ya sabes que una parte de esta tesis es también tuya, porque sin tus consejos, tu apoyo y tu ayuda no hubiese sido posible. Cuando comenzamos esta aventura en un país diferente, no sabíamos que iba a pasar, pero afortunadamente siempre nos hemos tenido el uno al otro. Hemos compartido todos los momentos juntos, tanto los buenos como los malos y hemos aprendido muchas cosas que nos servirán para el resto de nuestra vida en común, porque como tú ya sabes, yo ya no me imagino una vida sin ti. Gracias por todo. Te quiero.